

©2018

Antoinette Gail Nelson

ALL RIGHTS RESERVED

THE DEVELOPMENT OF A NANO-BASED COLORECTAL PRE-EXPOSURE

PROPHYLAXIS FOR HIV

by

ANTOINETTE GAIL NELSON

A dissertation submitted to the

School of Graduate Studies

Rutgers, The State University of New Jersey

In partial fulfillment of the requirements

For the degree of

Doctor of Philosophy

Graduate Program in Biomedical Engineering

Written under the direction of

Patrick J. Sinko

And approved by

New Brunswick, New Jersey

May 2018

ABSTRACT OF THE DISSERTATION

THE DEVELOPMENT OF A NANO-BASED COLORECTAL PRE-EXPOSURE PROPHYLAXIS FOR HIV

By

Antoinette Gail Nelson

Dissertation Director:

Professor Patrick J. Sinko

The colorectal mucosa is a highly vulnerable site for Human Immunodeficiency Virus (HIV) transmission. The epithelium of this region is comprised of a thin single-cell layer that serves as a protective barrier, to prevent foreign pathogens from entering the body. Beneath the epithelial layer, the lamina propria provides direct access to an extensive population of immune cells that are highly susceptible to HIV infection. There is also access to the lymphatic system, which serves as an outlet for HIV to enter the systemic circulation, initiating permanent infection. To prevent HIV infection, it is important to achieve, and maintain, therapeutically effective concentrations of anti-HIV drugs within mucosal tissues. The objective of the current thesis is to fabricate and assess a nanoparticle (NP) platform, for use in a colorectal PrEP, with the goal to (1) deliver antiretroviral agents directly to the colorectal mucosa to minimize dosage requirements; (2) achieve high drug loading and sustained drug release; and (3) establish prolonged, therapeutically effective, drug concentrations within mucosal tissue to minimize dosing frequency to once-a-week. Based on average epithelial cell turnover rates in the colon of rodents and humans, 2-3 days in a murine model is considered equivalent to 5-8 days in humans.

The overall objective of this thesis is to design, fabricate, and evaluate a nanoparticle (NP) drug delivery system (DDS), for colorectal mucosal pre-exposure prophylaxis (mPrEP) of HIV. Within the first part of this thesis, the feasibility of a modified cell penetrating peptide (CPP) bactericin 7 (Bac7), to transport poly(ϵ -caprolactone)-poly(ethylene glycol) (PCL-PEG) NPs into, and across, a colorectal epithelial barrier, was evaluated. The hypothesis is that by functionalizing NPs with Bac7, NP transport across Caco-2 colonic cells will increase *in vitro*. Additionally, NPs of optimal architecture (dense PEG corona and effective Bac7 ligand density) will successfully traverse the colorectal mucus mesh lining *in vivo*. Bac7-labeled NPs with varied ligand densities resulted in a 163.2% to 384.6% increase in NP transport across a Caco-2 epithelial cell monolayer compared with plain NPs. NPs of 1% to 5% Bac7 surface coverage showed successful translocation across colorectal mucus to associate with the epithelial layer *in vivo* in a rat model.

In the second portion of this thesis, rilpivirine-loaded NPs were assessed for sustained drug release. The hypothesis that flash nanoprecipitation can be used to fabricate NPs with high RPV drug loading via *in situ* salt formation, and that NP formulations can be tuned to achieve sustained release for a minimum of 24 hours, was tested. RPV was successfully encapsulated within PCL-PEG NPs resulting in high encapsulation efficiencies (85% to 98%), and moderate to high drug loadings (10.9 % to 17.7%). Cumulative release over 24 hours was modulated to achieve between 20% and 40% extent of release. Poly(lactide)-poly(ethylene glycol) (PLA-PEG) NPs resulted in a greater extent of release (58% compared with 40% for PCL-PEG). However, PLA-PEG NPs achieved an approximately 10% lower encapsulation efficiency and 1% decrease in drug loading compared with PCL-PEG NPs, resulting in low cost-efficiency.

Furthermore, rilpivirine-loaded Bac7 NPs were evaluated as a long-acting PrEP platform *in vivo*. The postulation is that Bac7 labeling will increase NP residence within the mucosa to deliver

RPV to epithelial tissue and NPs will persist within mucosal tissue for 2 to 3 days *in vivo*. Greater than 13% and 26% RPV tissue association is reported for Bac7 NPs and plain NPs, respectively, after 2 hours. At this time, placebo Bac7 NPs showed 3-fold increase in mucosal tissue association compared with plain NPs (~1.7% and ~0.45%, respectively). However, Bac7 NPs were significantly cleared from tissue at 24 hours, although both plain NPs and Bac7 NPs were present at low levels past 48 hours. This project demonstrates the potential of a Bac7 NP platform for use as a colorectal mPrEP DDS. Further optimization is needed to achieve feasibility as a long-acting PrEP approach.

DEDICATION

To my family,

Jennifer M. Nelson, Lawrence B. Nelson and Marvin B. Nelson.

For without your love, support and encouragement,

I would never have realized how high I could soar.

TABLE OF CONTENTS

ABSTRACT OF THE DISSERTATION.....	ii
DEDICATION.....	v
LIST OF TABLES.....	xi
LIST OF FIGURES.....	xii
LIST OF SCHEMES.....	xv
CHAPTER 1: Acknowledgements.....	1
CHAPTER 2: Introduction and Specific Aims.....	4
2.1. Introduction.....	4
2.2. Specific Aims.....	10
2.3. References.....	12
CHAPTER 3: Drug Delivery Strategies and Systems for HIV/AIDS Pre-Exposure Prophylaxis (PrEP) and Treatment.....	14
3.1. Abstract.....	14
3.2. Introduction.....	15
3.3. Importance of Understanding HIV Pathogenesis to Enable Effective Anti-HIV Drug Delivery.....	17
3.4. Drugs for Prevention and Treatment of HIV Infection.....	20
3.5. Drug Delivery Strategies for HIV Prevention.....	21
3.5.1. Vaginal Gels.....	23
3.5.2. Intravaginal Rings (IVRs).....	25
3.5.3. Vaginal Films.....	27
3.5.4. Colorectal Microbicides.....	29
3.5.4.1. Administration methods as it relates to mucosal coverage.....	30
3.5.4.2. Patient acceptability and adherence as it relates to volume administered and retention.....	30
3.5.4.3. Coital dependence and persistence of therapeutic effect.....	30
3.5.4.4. Chronic safety/ toxicity of the DDS/formulation.....	31
3.6. Drug Delivery Systems for HIV Treatment.....	33
3.6.1. Gut Mucosa and Lymph Nodes: Targeting the critical sites of HIV infection.....	34
3.6.2. Targeting cell receptors on HIV infected T-cells and macrophages.....	37

3.6.3. Cell Depot-based DDS.....	38
3.7. Long-Acting/Extending-Release (LA/ER) Parenteral (Injectable) DDS for PrEP and Treatment.....	41
3.8. Future Perspectives, Gaps and Opportunities.....	44
3.9. Acknowledgements.....	46
3.10. Figures.....	47
3.11. References.....	50
CHAPTER 4: The Design, Characterization and Evaluation of Bac7-Labeled Nanoparticles as a Drug Delivery Platform for Colorectal HIV Pre-Exposure Prophylaxis (PrEP).....	58
4.1. Abstract.....	58
4.2. Introduction.....	59
4.3. Materials and Methods.....	62
4.3.1. Materials.....	62
4.3.2. Bac7 Molecular Modeling and <i>In Silico</i> Solubility Characterization.....	63
4.3.3. Bac7 Cell Penetrating Peptide Synthesis and Characterization.....	64
4.3.4. Bac7 Peptide Conjugation to PCL-PEG polymer.....	64
4.3.5. Fluorescent Dye Conjugation to PCL-PEG polymer.....	65
4.3.6. Carboxylic Acid Conjugation to PCL-PEG polymer.....	65
4.3.7. NP Synthesis and Characterization.....	65
4.3.8. Confocal Images of NPs.....	66
4.3.9. Cell Internalization of NPs in Caco-2 Cells Determined by Fluorescence-Activated Cell Sorting (FACS).....	66
4.3.10. Caco-2 Intestinal Epithelial Monolayer Translocation.....	68
4.3.11. Investigation of NP Tissue Association in a Rat Ligated Intestinal Loop Model.....	68
4.3.12. Statistical Analysis.....	69
4.4. Results.....	69
4.4.1. Characterization of Bac7 Peptide and Bac7-Labeled NP.....	69
4.4.2. Internalization of Bac7-labeled NPs in Caco-2 Cells.....	70
4.4.3. Effect of Ligand Density on Bac7-facilitated Nanoparticle Transport Across Caco-2 Cell Monolayers.....	71
4.4.4. NPs Travel Across Biological Barriers to Penetrate Colorectal Tissue <i>In Vivo</i>	71

4.4.5. NP Characterization and Mucosal Tissue Association After Ligand-Charge Balance <i>In Vivo</i>	72
4.5. Discussion.....	72
4.6. Authors Contributions.....	80
4.7. Figures.....	81
4.8. References.....	83
CHAPTER 5: Formulation, Characterization and Evaluation of Rilpivirine-Loaded Nanoparticles as a Long-Acting Platform for Colorectal HIV PrEP.....	97
5.1. Abstract.....	97
5.2. Introduction.....	98
5.3. Materials and Methods.....	100
5.3.1. Materials.....	100
5.3.2. NP Preparation.....	102
5.3.3. Determination of RPV Solubility in Distilled Water, DMEM and 0.1% Tween 80/DMEM	102
5.3.4. RPV Drug Loading and Release from NPs.....	103
5.3.5. Bac7 Cell Penetrating Peptide Synthesis.....	104
5.3.6. Bac7 Peptide Conjugation to PCL-PEG Polymer.....	105
5.3.7. Fluorescence Dye Conjugation to PCL-PEG Polymer.....	105
5.3.8. Rat Intestinal Sac Ligation Model.....	105
5.3.9. <i>In Vivo</i> NP Retention Studies.....	106
5.3.10. Validation of NP Surface Interactions and Fluorescence in Reaction Media.....	107
5.3.11. Statistical Analysis.....	108
5.4. Results.....	108
5.4.1. Optimization of Nanoparticle Hydrodynamic Diameter By Polymer Size Modifications.....	108
5.4.2. Rilpivirine Solubility in Release Media.....	109
5.4.3. Rilpivirine-NP Drug Loading and Characterization.....	109
5.4.4. Rilpivirine Release Kinetics.....	110
5.4.5. Ligated Loop Model - Analog Comparisons.....	110
5.4.6. Rilpivirine Tissue Extraction.....	111
5.4.7. <i>In Vivo</i> NP Retention Studies.....	112
5.5. Discussion.....	112

5.6. Authors Contributions.....	119
5.7. Figures.....	120
5.8. References.....	134
CHAPTER 6: Summary of the Dissertation and Future Directions.....	137
6.1. Summary.....	137
6.2. Recommendations of future directions for this project include.....	140
SUPPLEMENTAL MATERIALS.....	141
S1. Colorectal Delivery and Retention of PEG-Amprenavir-Bac7 Nanoconjugates – Proof of Concept for HIV Mucosal Pre-Exposure Prophylaxis.....	141
S1.1. Abstract.....	141
S1.2. Introduction.....	142
S1.3. Materials and Methods.....	146
S1.3.1. Materials.....	146
S1.3.2. Extraction of APV from Agenerase® capsules.....	147
S1.3.3. Preparation of APV-O-acetyl.....	147
S1.3.4. PEG _x -APV-O-acetyl and PEG _x -APV-OH.....	148
S1.3.5. APV-PEG _{3,4kDa} -FITC (APF).....	148
S1.3.6. Bac7 Cell Penetrating Peptide.....	149
S1.3.7. APV-PEG _{3,4kDa} -Bac7 (APB).....	149
S1.3.8. Bac7-PEG _{3,4kDa} -FITC (BPF).....	150
S1.3.9. Preparation of Stable Fluorescein Isothiocyanate Analog.....	150
S1.3.10. Stability of Amide Bonds in MT-2 CD4 ⁺ T-Cell Culture Medium Containing 10% Fetal Bovine Serum (FBS).....	150
S1.3.11. Cytotoxicity of NCs.....	150
S1.3.12. PR Inhibition Activity of PEG _x -APV-OH (x = 2, 5, 10, and 30 Da) in buffer.....	151
S1.3.13. Anti-HIV-1 Activity of APB and APF in MT-2 CD4 ⁺ T-Cells.....	151
S1.3.14. Flow Cytometry.....	152
S1.3.15. Confocal Microscopy.....	152
S1.3.16. APF and BPF penetration into mouse colorectal mucosa.....	153
S1.3.17. Statistical Analysis.....	153
S1.4. Results.....	154
S1.4.1. Synthesis and Characterization Studies.....	154
S1.4.2. Stability of Amide Linkage.....	154

S1.4.3. Cytotoxicity Studies.....	155
S1.4.4. Anti-HIV-1 PR activity of APV-PEG _x -OH NCs in buffer.....	155
S1.4.5. PEG conjugation ablated anti-HIV-1 activity in T-cells while further conjugation with Bac7 restored activity.....	157
S1.4.6. Flow cytometry and confocal microscopy.....	158
S1.4.7. NC penetration and retention in mouse colorectal mucosa.....	159
S1.5. Discussion.....	160
S1.6. Acknowledgements.....	166
S1.7. Figures.....	167
S1.8. References.....	182

LIST OF TABLES

Chapter 3

Table 1. Recent drugs in use or development.....	48
--	----

Chapter 4

Table 1. Molecular properties of Bac7 computed using pre-programmed Molinspiration software algorithms.....	82
Table 2. Effect of ligand type and density on NP properties.....	92

Chapter 5

Table 1. NP characterization of placebo NPs.....	122
Table 2. NP characterization of RPV-loaded NPs.....	124

Supplemental Materials

Table 1. HIV-1 PR inhibition activity of APV-PEG NCs.....	181
---	-----

LIST OF FIGURES

Chapter 3

Figure 1. Approximate timeline for establishing HIV infection after vaginal exposure to HIV.....	47
Figure 2. Colorectal Mucosal Barriers and HIV Transmission Pathway.....	49

Chapter 4

Figure 1. Predicted 3-D structure of Bac7 recapitulated in TASSER Software.....	83
Figure 2. Characterization of Bac7 peptide by High Performance Liquid Chromatography (HPLC).....	84
Figure 3. Characterization of Bac7 peptide by electrospray ionization–mass spectrometry.....	85
Figure 4. Confocal Microscopy of plain and Bac7-labeled NPs.....	88
Figure 5. Cell internalization of NPs in Caco-2 cells after 2 hour incubation.....	89
Figure 6. Translocation of NPs across Caco-2 intestinal monolayers.....	90
Figure 7. NP mucosal tissue association <i>in vivo</i> in Sprague-Dawley rats.....	91
Table 2. Effect of ligand type and density on NP properties.....	92
Figure 8. The effect of feces presence on NP tissue-interaction in the colon <i>in vivo</i> in Sprague-Dawley rats.....	93
Figure 9. NP mucosal tissue association after NP ligand-charge balance <i>in vivo</i> Sprague-Dawley rats.....	94

Chapter 5

Figure 1. NP size correlation with polymer hydrophilic-hydrophobic molecular weight block ratios for polymers.....	121
Table 1. NP characterization of placebo NPs.....	122
Figure 2. Measuring RPV solubility in 0.1% v/v Tween 80/DMEM, DMEM, and DI water.....	123
Table 2. NP characterization of RPV-loaded NPs.....	124
Figure 3. PRV release from PCL-PEG NPs with 5 kDa PEG coronas.....	125
Figure 4. RPV release from PCL-PEG NPs with 2 kDa PEG coronas.....	126
Figure 5. RPV release from PCL-PEG and PLA-PEG NPs with comparable block weights.....	127

Figure 6. RPV-NP Characterization for PCL-PEG NPs and PLA-PEG NPs.....	128
Figure 7. NP mucosal tissue association for wild-type (wt), inverso (I) and retroinverso (RI) Bac7 ligand analogs <i>in vivo</i> in Sprague-Dawley rats.....	129
Figure 8. RPV extraction from colorectal tissue after <i>in situ</i> treatment with RPV-loaded NPs (RPV-NPs) and RPV nanosuspensions in PEG 400 <i>in vivo</i> in male Sprague-Dawley rats.....	130
Figure 9. RPV extraction from colorectal tissue after intra-rectal treatment with RPV-loaded NPs and RPV nanosuspensions in PEG 400 <i>in vivo</i> in male CD-1 mice.....	131
Figure 10. Interaction of covalently-conjugated FITC dye on NP corona with serum proteins.....	132
Figure 11. NP tissue association of plain NPs and Bac7 I NPs over 48 hours <i>in vivo</i> in CD-1 mice.....	133

Supplemental Materials

Figure 1. Cleavage kinetics of HIV-1 PR FRET peptide substrate (5.0 μM) by recombinant HIV-1 PR (35.2 nM) at 37 °C in the assay buffer in the presence of different APV concentrations (0–5.0 μM).....	171
Figure 2. Plots of $\ln(F_{\infty} - F_t)$ vs. time for APV (0-5 μM). The plots were prepared using the data obtained from Figure 1.....	172
Figure 3. Plot of negative reciprocal of observed rate constant ($-1/k_{\text{obs}}$) vs. APV concentrations.....	173
Figure 4. Plots of $\ln(F_{\infty} - F_t)$ vs. time for APV, PEG-APV NCs and the two negative controls, all at 3.5 μM APV-equivalent concentrations.....	174
Figure 5. Effect of PEG size on the HIV-1 PR inhibition potency of APV-PEG NCs.....	175
Figure 6. Anti-HIV-1 activity of APV-PEG _{3.4kDa} - Bac7 CPP (APB), APV-PEG _{3.4kDa} -FITC (APF) and free APV.....	176
Figure 7. Total cell-associated fluorescence levels of NCs in Caco-2 and MT-2 cells as measured by flow cytometry.....	177
Figure 8. Intracellular levels of NCs in Caco-2 cells and MT-2 T-cells as measured by confocal microscopy.....	178

Figure 9. Confocal microscopic images of Caco-2 cells incubated with APF (left) or BPF (right) at 2.47 x magnification.....179

Figure 10. Retention of PEG-conjugated and Bac7 CPP-conjugated BPF in mouse colorectal mucosa.....180

LIST OF SCHEMES

Chapter 4

Scheme 1. Bac7 peptide synthesized in solid phase peptide synthesis.....	81
Scheme 2. Schematic of PCL-PEG-Bac7 conjugation.....	86
Scheme 3. Flash nanoprecipitation to fabricate NPs.....	87

Chapter 5

Scheme 1. Wild-type (wt), inverso (I) and retroinverso (RI) analogs of azido-PEG-linked Bac7 peptides synthesized by solid phase peptide synthesis.....	120
---	-----

Supplemental Materials

Scheme 1. Synthesis of PEG _x -APV-O-acetyl and PEG _x -APV-OH nanocarrier conjugates.....	167
Scheme 2. Synthesis of fluorescein-labeled APV-PEG (APF) and Bac7 CPP-PEG NCs (BPF): (A) APV-PEG _{3.4kDa} -FITC; (B) Structure of Bac7 analog; and (C) Bac7 CPP-PEG _{3.4kDa} -FITC.....	168
Scheme 3. Synthesis of APV-PEG _{3.4kDa} -Bac7 CPP (APB).....	169
Scheme 4. FRET-based PR activity inhibition assay.....	170

CHAPTER 1

Acknowledgements

This dissertation is the product of hard work, alongside the prayers of a village. I would like to, above all, thank God for the strength, courage and faith to complete this journey. My faith and connection to a purpose greater than myself provided me with the determination to continue on the days when my vision appeared blurry.

I would like to express my sincere gratitude to my dissertation advisor, Dr. Patrick J. Sinko for his guidance to complete this project. From your advisement, I have learned how to think independently as a scientist and have developed as a leader. I would also like to thank my committee members Dr. Bozena Michniak-Kohn, Dr. Stavroula Sofou, and Dr. Arash Hatefi for their time, kind insights, and encouraging words at various stages of this project. Additionally, I would like to thank Dr. Robert Prud'homme (Chemical and Biological Engineering, Princeton University) for his collaboration and input throughout the years.

I would like to acknowledge all members of the Sinko Research Group for their support and feedback that allowed for the completion of this work. The members that came before me, who laid the foundation for this project, are also owed thoughts of appreciation. Specifically, I would like to thank Dr. Xiaoping Zhang, Dr. Zoltan Szekeley, Dr. Li Shike, Dr. Dayuan Gao, and Jennifer Holloway for their expertise. Thank you to my friend Dan Myers, for sharing your knowledge with me. Thank you to Helen Wang who worked tirelessly to achieve the goals of this project. I will always remember our late nights and early mornings, preparing mucus samples and making nanoparticles. I also acknowledge George Kofi Marfo, for his friendship and support. Special acknowledgement is given to Mickerline Vilus for her love and pure spirit. I thank you

for your warm hugs and compassionate ear. Without your support, this would not be possible. Additionally, I would like to express my gratitude to the Biotechnology Training Program and in particular, Dr. Martin Yarmush and Dr. Ann Stock, for their constant support and encouragement.

Finally, to my family and external support team, you were my strength when I was weak, and words cannot express my gratitude. To my many aunts, uncles, cousins, and extended family, your love is immeasurable and a confidence builder. Thank you to Dr. Renea Faulknor and Dr. Brittany Taylor. You were the first black, female biomedical engineers I ever saw while I was still a young undergrad. You are rock stars and a continuous inspiration to me. To Joseanne Cudjoe, thank you for your big-sisterly love and care. These women were my cheerleaders on the field, and my coaches behind the scenes. Thank you to team PAK members, Paulina Krzyszczyk and Dr. Kamau Pierre. We started this journey together and it is beautiful to see how far we have come. I acknowledge all members of the Rutgers University Council of Black Graduates and our former advisor Dr. Prosper Godonoo. Dr. Godonoo showed a true selfless love for his students and was a champion for anyone in need. I thank him for the lessons he taught me about being a good human being and how to truly stand up for what I believe in.

Lastly, I want to express my gratitude to some of my best friends and soulmates including Omotoke Oloruntoba, Tonya Austin, Jendayi Hawkins, Dwight Gentle, and Ebony Anderson. Mark James, you fearlessly weathered the eye of the storm with me, for which I am so very grateful. Thank you all for your selfless love and gentle care. Special thanks are extended to my Brooklyn Technical High School and Stony Brook University families for their constant support. I also extend my gracious appreciation to members of the First Baptist Church of Lincoln Gardens, which served as a spiritual home-away-from-home during my time at Rutgers.

Without the love and devotion of the support system I was blessed with, this dissertation would not be possible. Their belief in me, gave me the motivation to push through on the most difficult days. I hope that my dedication and faith inspires those that come behind me. I want them to know that all of their dreams are possible and that I believe in them too.

CHAPTER 2

Introduction and Specific Aims

2.1. Introduction

In the year 2021 we approach the 40th anniversary of the first reported case of HIV/AIDS in 1981. Due to the global spread of HIV, it is now considered a pandemic. In 2016, the Joint United Nations Programme on HIV/AIDS (UNAIDS) estimated nearly 37 million people were living with HIV, with approximately one million mortalities due to AIDS related illnesses that year [1-3]. Fortunately, with the development of antiretroviral therapy (ART), there has been significant progress in controlling the spread of the virus. With chronic treatment, HIV infected individuals can now live normal lifespans. However, there is still no cure or vaccine available, making focus on prevention even more of a priority [2].

Sexual contact remains the predominant route of HIV transmission from infected to healthy individuals. Receptive anal intercourse is the most prevalent cause of new viral infections in developed countries. Men who have sex with men (MSM) represent the largest population of new infections in Australia, Western Europe and North America. Within the United States, only 4% of males identify as MSM, representing only 2% of the total population. However, this demographic group accounted for 78% of new infections amongst men and 63% of all new HIV infections in 2010 according to the Center for Disease Control and Prevention [4-6]. Although it is now clear that HIV disproportionately affects MSM within the developed world, women who engage in unprotected receptive anal intercourse (URAI) are also at a significantly higher risk of contracting HIV from an infected partner than those who participate in unprotected vaginal intercourse only (UVI). It is estimated that URAI results in 10-100 times more incidences per exposure than UVI.

Anal intercourse has been one of the most stigmatized forms of heterosexual behavior. Therefore, anal coitus within heterosexual relationships is often underreported although not uncommon practice. Within the United States, the absolute number of women who participate in URAI is ~7-fold higher than the absolute number of men who practice URAI. Additionally, it was reported that 75% of female study participants in a South African clinical trial site for microbicide testing, participate in URAI. This is important since nearly 70% of individuals currently living with HIV reside within Sub Saharan Africa [2, 7, 8].

Currently, the only FDA approved approach for HIV prevention, is the systemic pre-exposure prophylaxis (PrEP), Truvada. With this oral drug product, there are toxicity concerns since the entire body is being exposed to antiretrovirals and large dosages are required to achieve effective concentrations in mucosal tissues. Additionally, patient nonadherence is a critical challenge to PrEP efficacy. Therefore, alternative PrEP options are being explored. In particular, long-acting formulations may improve adherence, by conferring longer durations of protection, and avoiding the daily responsibility to adhere to medication [9-11]. A long-acting colorectal mucosal PrEP (mPrEP) drug delivery system (DDS) capable of delivering antiretrovirals directly to the colorectal mucosa, lowering the necessary dosage and frequency, and limiting systemic exposure, would be a major milestone for the PrEP field. While one strategy is unlikely to achieve universal acceptability, having a diverse array of options, to suit a range of user needs and preferences, can effectively enhance adherence and help to control viral spread [10, 12].

The development of new drug delivery strategies to achieve, and maintain, efficacious drug concentrations in mucosal tissues, remains a significant challenge. A number of biological and formulation barriers exist to DDSs. The gastrointestinal (GI) tract has several protective barriers that include the mucus layer and epithelial cell barrier. These physiological barriers limit the

delivery of therapeutic agents to the sites of action within the mucosa. In particular, the lamina propria, located beneath the epithelium, is a key target for prevention strategies. Ultimately, one of the primary rate-limiting steps is drug dissolution. More than 40% of new chemical entities (NCEs) are practically insoluble in water [13, 14]. The Biopharmaceutical Classification System (BCS) reports that most poorly soluble drugs belong to the BCS class II. Drugs within this class exhibit low water solubility and high membrane permeability [14]. Hence, sparse solubility and dissolution, within aqueous gastrointestinal fluids, are the primary cause of insufficient tissue absorption. Additionally, drugs in crystalline form require more energy for dissolution than the amorphous form and present additional challenges to permeability and bioavailability [13]. There are several strategies that have been employed to increase the drug dissolution of poorly soluble and crystalline drugs including solid dispersions, micronization and the addition of ionized salts. However, these techniques have faced limitations in drug-loading capacity, biodegradability, and toxicity. Nanotechnology has emerged as a promising alternative to address these challenges [13].

Nanoparticles (NPs) provide many advantages as DDSs. These carriers can be easily altered to fit the custom needs of a specific delivery system. They have the ability to increase therapeutic bioavailability and drug loading, actively and passively target tissues, as well as evade physical and immune barriers to delivery. These include members of the reticuloendothelial system or mucus that work to “detect” and remove foreign materials from the body [15]. For example, many NPs are coated with a layer of hydrophilic neutral polymers such as poly(ethylene glycol) (PEG), which enables them to travel through the body without detection by macrophages and other agents of the immune system. Additionally, for BCS Class II drugs, drug release from the dosage form is typically the rate-limiting step. NP fabrication processes also have the potential to modify NP structural properties and control drug release rates to meet therapeutic needs. Even with the enhanced benefits nanoparticles provide, penetration across the colonic epithelium remains a difficult task due to the low permeability of the epithelial cell membrane and tightly

connected cell layer [16]. It is especially difficult for materials of high molecular weights and/or hydrophilic properties to traverse the barrier by paracellular permeability [17]. To assist in the penetration of cargo through cell membrane, NP structure and/or surface properties may be altered. NPs may be functionalized with cell-penetrating peptides (CPPs), which are usually highly cationic or hydrophobic peptide sequences that have been used to facilitate in the transport of cargo across cell membranes.

NPs must also be able to successfully penetrate the mucus layer. Within the gastrointestinal tract, mucus lines the luminal surface and serves as a tenacious barrier to protect the epithelium from exposure to foreign particles and the external environment. Mucus is a semipermeable layer of viscoelastic gel that selectively enables the exchange of nutrients, water, gases, hormones and other necessary biological components while preventing the translocation of most bacteria and pathogens. It is 90-98% water with mucin, lipids, proteins, DNA, ions, and cells present throughout the matrix. Mucin fibers, secreted by goblet cells, are cross-linked and entangled to form a mesh-like system. These fibers are highly flexible and coated with a complex and diverse arrangement of proteoglycans mostly tipped with a carboxyl or sulfate group creating a net negative charge. These glycosylated regions are highly hydrophilic and separated by hydrophobic pockets. The flexible array of alternating regions in polarity allow for a variety of low-affinity hydrophilic and hydrophobic bonds to occur between the mucus gel and incoming particles. Additionally, spacing within the mesh range between 30-100 nm and may physically trap materials larger than the lower cut-off [15, 18-20].

Within the GI tract, there are two types of mucins structurally: secreted and cell attached. Additionally, secreted mucin, can be separated into two distinct layers, a loose outer layer and inner layer that is tightly adhered [15]. Some sections of the GI-tract are covered with either cell attached or secreted mucin [21]. The colon consists of both layers creating a more robust barrier

between 110-160 μm in thickness [19]. The inner mucus layer within the proximal colon has been shown to be partly penetrable to polystyrene beads about the size of bacteria (0.5-2 μm). The distal colon however, is largely impenetrable [21]. Mucus is also continuously secreted and shed, or digested and recycled, with a typical lifetime estimated to be about an hour for the inner mucus of the distal colon in rodents and humans [18, 22]. This relatively quick turnover makes it difficult for drugs and delivery systems to reach mucosal surfaces since they must travel “upstream” towards the epithelium and successfully penetrate the mucus lining before shedding occurs. It is common for mucus to adhere to particles along the way and essentially wrap itself around them to prevent them from coming in contact with epithelial cells. These particles are then removed with the shedding mucus [18, 19].

Therefore, to traverse the mucus layer, NPs must avoid adherence to the lipophilic or negatively charged regions of the mucin matrix. They must also be small enough to permeate the mucin fiber mesh. Therefore, carrier surface chemistry plays a major role in nanoparticle interaction with the mucus mesh and its ability to permeate across. NPs with cationic surface charges are more likely to adhere to the mucus layer, preventing their diffusion. Conversely, negatively charged particles may also be problematic resulting in electrostatic repulsion by the anionic barrier that may retard its diffusion. On the other hand, neutral NPs may be highly hydrophobic, causing hydrophobic interactions resulting in their sticking to mucus as well. These considerations highlight the intricacy of engineering nanocarriers to successfully traverse mucus and epithelial cells in series to deliver therapeutics as these two barriers are so vastly different in their physicochemical properties [15].

Once successfully past the mucus lining, intracellular delivery of most peptides, drugs and carriers is impeded by the cell membrane. To assist in the penetration of cargo through the cell membrane, cell-penetrating peptides (CPPs) have been utilized. These peptides are usually highly

cationic or hydrophobic. One family of CPPs, the bactenecin family, stems from a proline/arginine rich family of antimicrobials which function by inhibiting the intracellular protein synthesis machinery. In their native forms, bactenecins are present in the neutrophils of ruminants where they work to invade foreign microorganisms and kill microbes. Bactenecin 7, a member of this family, is a 59-residue protein rich in cationic charged amino acids [23]. The CPP Bac7 is a modified fragment of the region 15-24 which harbors the cell-penetrating properties of the native protein but not the microbial activity to influence the function of mammalian cells [24].

This dissertation thesis herein presents the design, fabrication, and evaluation of a nano-based DDS for colorectal mucosal HIV PrEP. The feasibility of the modified cell penetrating peptide (CPP), bactenecin 7 (Bac7), to transport poly(β -caprolactone-ethylene glycol) nanoparticles into, and across colorectal tissue, was evaluated. Nanoparticle encapsulation potential for a crystalline and BCS Class II drug, rilpivirine, was assessed. Drug release kinetics and flexibility in extent of release, by adjusting the physical properties of the NP copolymers, was investigated. Finally, NPs were evaluated *in vivo* to assess their translocation across mucus and cells, to maintain prolonged tissue retention.

A colorectal mucosal PrEP (mPrEP) DDS for HIV would deliver antiretrovirals directly to the colorectal region, a critical site of early HIV infection, to achieve and maintain effective mucosal drug concentrations, to minimize dose frequency, and to limit systemic toxicity. The current work establishes the feasibility of a NP DDS mPrEP platform labeled with Bac7, to be used in a mPrEP approach.

2.2. Specific Aims

Colorectal transmission of HIV plays a major role in the establishment of new infections. The anatomical structure of the colorectal mucosa makes it a vulnerable site for HIV. The colorectal epithelium is a thin single-cell layer that is much easier to penetrate than the multi-layer barrier found within the vagina. Once HIV traverses the epithelial layer and enters the lamina propria, it has direct access to an extensive population of activated CD4⁺ T cells, macrophages, and other lymphocytes that are highly susceptible to HIV infection. There is also access to the lymphatic system, which serves as a primary route for HIV to enter the systemic circulation. Currently, the only FDA approved approach for HIV prevention, Truvada, is an oral drug product, which requires strict adherence to a daily dosing regimen. In addition to toxicity concerns, patient non-adherence is a critical challenge to PrEP efficacy. Ideally, a long-acting/extended release pre-exposure prophylaxis approach, with sustained drug activity, would allow for more flexibility in application to increase adherence and efficacy. A long-acting colorectal mucosal PrEP (mPrEP) is likely to be effective if it (1) delivers antiretrovirals directly to the colorectal mucosa to lower the dosage requirements, (2) achieves high drug loading and sustained drug release capabilities, and (3) establishes prolonged therapeutically effective drug concentrations within mucosal tissue to minimize dosing frequency to once-a-week.

In this thesis, the above functional objectives were addressed through the design, fabrication, and evaluation of a nano-based drug delivery platform, for colorectal mucosal HIV PrEP. We evaluate the feasibility of the modified cell penetrating peptide (CPP) bactericidin 7 (Bac7) to transport poly(ϵ -caprolactone)-poly(ethylene glycol) nanoparticles into, and across a colorectal epithelial barrier. The encapsulation potential for a crystalline BCS Class II drug, rilpivirine, to be incorporated into NPs by flash nanoprecipitation, was assessed. We also investigated drug release kinetics and rate of release by modifying copolymers components prior to NP fabrication. Finally,

the NPs were evaluated *in vivo* to determine their capability to translocate across mucus and cells, and maintain prolonged tissue retention for 2-3 days in rodent models. The average epithelial cell turnover rate in the colon is 5-8 days in humans and 2-3 days in rodents [25]. Therefore retention that exceeds 2-3 days in a murine model indicates NP delivery to the lamina propria and is considered the rodent equivalent of a one-week duration.

This thesis is organized into two primary specific aims:

1. To design, characterize and evaluate Bac7-Labeled PCL-PEG nanoparticles as a drug delivery platform for colorectal HIV pre-exposure prophylaxis

Hypotheses: (a) The conjugation of a Bac7 CPP will increase NP uptake into/ or across Caco-2 colonic cells *in vitro*; and (b) NPs of optimal architecture (dense PEG corona and optimal Bac7 ligand density) will successfully traverse the colorectal mucus mesh lining *in vivo*.

2. To formulate, characterize and evaluate rilpivirine-loaded Bac7 nanoparticles as a long-acting platform for colorectal HIV PrEP

Hypotheses: (a) Flash nanoprecipitation can be used to fabricate NPs with high RPV drug loading via *in situ* salt formation, (b) RPV release rates can be tuned by modifying polymer block ratios to achieve sustained RPV release for a minimum of 24 hours; (c) Bac7 labeling will increase NP residence within the mucosa and deliver RPV to tissue *in vivo*. (d) NPs will maintain tissue persistence for 2 to 3 days *in vivo*.

2.3. References

- [1] UNAIDS, Fact Sheet - Latest statistics on the status of the AIDS epidemic. 2018).
- [2] A.G. Nelson, X. Zhang, U. Ganapathi, Z. Szekely, C.W. Flexner, A. Owen, P.J. Sinko, Drug delivery strategies and systems for HIV/AIDS pre-exposure prophylaxis and treatment, *Journal of Controlled Release* 219 (2015) 669-680.
- [3] M. Samizadeh, X. Zhang, S. Gunaseelan, A.G. Nelson, M.S. Palombo, D.R. Myers, Y. Singh, U. Ganapathi, Z. Szekely, P.J. Sinko, Colorectal Delivery and Retention of PEG-Amprenavir-Bac7 Nanoconjugates - Proof of Concept for HIV Mucosal Pre-Exposure Prophylaxis, *Drug delivery and translational research* 6(1) (2016) 1-16.
- [4] C.f.D.C.a. Prevention, HIV in the United States: At A Glance. <<http://www.cdc.gov/hiv/statistics/overview/ataglance.html>>).
- [5] A.E. Grulich, I. Zablotska, Commentary: Probability of HIV transmission through anal intercourse, *International Journal of Epidemiology* 39(4) (2010) 1064-1065.
- [6] L.J. Koenig, D. Hoyer, D.W. Purcell, S. Zaza, J. Mermin, Young People and HIV: A Call to Action, *American Journal of Public Health* (2016) e1-e4.
- [7] R.F. Baggaley, R.G. White, M.-C. Boily, HIV transmission risk through anal intercourse: systematic review, meta-analysis and implications for HIV prevention, *International Journal of Epidemiology* 39(4) (2010) 1048-1063.
- [8] D.T. Halperin, Heterosexual anal intercourse: prevalence, cultural factors, and HIV infection and other health risks, Part I, *AIDS patient care and STDs* 13(12) (1999) 717-730.
- [9] R.P. Walensky, M.M. Jacobsen, L.-G. Bekker, R.A. Parker, R. Wood, S.C. Resch, N.K. Horstman, K.A. Freedberg, A.D. Paltiel, Potential Clinical and Economic Value of Long-Acting Preexposure Prophylaxis for South African Women at High-Risk for HIV Infection, *The Journal of Infectious Diseases* 213(10) (2016) 1523-1531.
- [10] G.J. Greene, G. Swann, A.J. Fought, A. Carballo-Diéguez, T.J. Hope, P.F. Kiser, B. Mustanski, R.T. D'Aquila, Preferences for Long-Acting Pre-exposure Prophylaxis (PrEP), Daily Oral PrEP, or Condoms for HIV Prevention Among U.S. Men Who Have Sex with Men, *AIDS and Behavior* 21(5) (2017) 1336-1349.
- [11] W.C. Goedel, J.A. Schneider, H.R. Hambrick, N.T. Kreski, J.G. Morganstein, S.H. Park, O. Mgbako, D.T. Duncan, Are Anal Sex Roles Associated with Preferences for Pre-Exposure Prophylaxis Administration Modalities Among Men Who Have Sex with Men?, *Archives of Sexual Behavior* (2017).
- [12] J.M. Marrazzo, HIV Prevention: Opportunities and Challenges, *Topics in Antiviral Medicine* 24(4) (2016) 123-126.
- [13] S. Mazumder, A.K. Dewangan, N. Pavurala, Enhanced dissolution of poorly soluble antiviral drugs from nanoparticles of cellulose acetate based solid dispersion matrices, *Asian Journal of Pharmaceutical Sciences* 12(6) (2017) 532-541.
- [14] P. kommavarapu, A. Maruthapillai, K. Palanisamy, M. Sunkara, Preparation and characterization of rilpivirine solid dispersions with the application of enhanced solubility and dissolution rate, *Beni-Suef University Journal of Basic and Applied Sciences* 4(1) (2015) 71-79.
- [15] G. Aljayyousi, M. Abdulkarim, P. Griffiths, M. Gumbleton, Pharmaceutical Nanoparticles and the Mucin Biopolymer Barrier, *BioImpacts : BI* 2(4) (2012) 173-174.
- [16] S. Barua, S. Mitragotri, Challenges associated with penetration of nanoparticles across cell and tissue barriers: A review of current status and future prospects, *Nano Today* 9(2) (2014) 223-243.
- [17] F. Guo, M. Zhang, Y. Gao, S. Zhu, S. Chen, W. Liu, H. Zhong, J. Liu, Modified nanoparticles with cell-penetrating peptide and amphipathic chitosan derivative for enhanced oral colon absorption of insulin: preparation and evaluation, *Drug Delivery* (2015) 1-12.
- [18] S.K. Lai, Y.-Y. Wang, J. Hanes, Mucus-penetrating nanoparticles for drug and gene delivery to mucosal tissues, *Advanced drug delivery reviews* 61(2) (2009) 158-171.

- [19] R.A. Cone, Barrier properties of mucus, *Advanced Drug Delivery Reviews* 61(2) (2009) 75-85.
- [20] S.K. Lai, Y.-Y. Wang, D. Wirtz, J. Hanes, Micro- and macrorheology of mucus, *Advanced drug delivery reviews* 61(2) (2009) 86-100.
- [21] A. Ermund, A. Schütte, M.E.V. Johansson, J.K. Gustafsson, G.C. Hansson, Studies of mucus in mouse stomach, small intestine, and colon. I. Gastrointestinal mucus layers have different properties depending on location as well as over the Peyer's patches, *American Journal of Physiology - Gastrointestinal and Liver Physiology* 305(5) (2013) G341-G347.
- [22] M.E.V. Johansson, Fast Renewal of the Distal Colonic Mucus Layers by the Surface Goblet Cells as Measured by *In Vivo* Labeling of Mucin Glycoproteins, *PLoS ONE* 7(7) (2012) e41009.
- [23] K. Sadler, K.D. Eom, J.-L. Yang, Y. Dimitrova, J.P. Tam, Translocating Proline-Rich Peptides from the Antimicrobial Peptide Bactenecin 7, *Biochemistry* 41(48) (2002) 14150-14157.
- [24] R.I. Dmitriev, H.M. Ropiak, D.V. Yashunsky, G.V. Ponomarev, A.V. Zhdanov, D.B. Papkovsky, Bactenecin 7 peptide fragment as a tool for intracellular delivery of a phosphorescent oxygen sensor, *FEBS Journal* 277(22) (2010) 4651-4661.
- [25] M. Lipkin, *Proliferation and Differentiation of Normal and Diseased Gastrointestinal Cells*, Raven Press, New York, 1987.

CHAPTER 3

Note: This chapter was reproduced for this dissertation from the following publication:

Nelson, A. G.; Zhang, X; Ganapathi, U; Szekely, Z; Flexner, C. W.; Owen, A; Sinko, P. J. Drug Delivery Strategies and Systems for HIV/AIDS Pre-Exposure Prophylaxis (PrEP) and Treatment. *Journal of Controlled Release*. 219. 669-680.

Drug Delivery Strategies and Systems for HIV/AIDS Pre-Exposure Prophylaxis (PrEP) and Treatment

3.1. Abstract

The year 2016 marked an important milestone - the 35th anniversary of the first reported cases of HIV/AIDS. Antiretroviral Therapy (ART) including Highly Active Antiretroviral Therapy (HAART) drug regimens is widely considered to be one of the greatest achievements in therapeutic drug research having transformed HIV infection into a chronically managed disease. Unfortunately, the lack of widespread preventive measures and the inability to eradicate HIV from infected cells highlight the significant challenges remaining today. Moving forward there are at least three high priority goals for anti-HIV drug delivery (DD) research: (1) to prevent new HIV infections from occurring, (2) to facilitate a functional cure, i.e., when HIV is present but the body controls it without drugs and (3) to eradicate established infection. Pre-exposure Prophylaxis (PrEP) represents a significant step forward in preventing the establishment of chronic HIV infection. However, the ultimate success of PrEP will depend on achieving sustained antiretroviral (ARV) tissue concentrations and will require strict patient adherence to the regimen. While first generation long acting/extended release (LA/ER) DDS currently in development show considerable promise, significant DD treatment and prevention challenges persist. First, there is a critical need to improve cell specificity through targeting in order to selectively achieve

efficacious drug concentrations in HIV reservoir sites to control/eradicate HIV as well as mitigate systemic side effects. In addition, approaches for reducing cellular efflux and metabolism of ARV drugs to prolong effective concentrations in target cells need to be developed. Finally, given the current understanding of HIV pathogenesis, next generation anti-HIV DDS need to address selective DD to the gut mucosa and lymph nodes. The current review focuses on the DDS technologies, critical challenges, opportunities, strategies, and approaches by which novel delivery systems will help iterate towards prevention, functional cure and eventually the eradication of HIV infection.

3.2. Introduction

The year 2016 will mark an important milestone - the 35th anniversary of the first reported cases of HIV/AIDS. Antiretroviral Therapy (ART) drug regimens are widely considered to be one of the greatest achievements in therapeutic drug research. In fact, ART has transformed healthcare for HIV-infected people from a terminal illness where patients quickly progress from HIV infection to AIDS and serious opportunistic infections to today, where HIV infection is widely regarded as a chronic disease. Unfortunately, the discontinuation of ART or the development of drug resistance results in rapid viral rebound. The lack of widespread successful preventive measures and the inability to eradicate HIV from infected cells highlight the significant healthcare challenges and DD opportunities that remain today.

The World Health Organization (WHO) estimates that approximately 35.0 million people were living with HIV and 2.1 million people became newly infected in 2013 [1]. Due to the global spread of HIV/AIDS it is considered a pandemic with an estimated 39 million deaths from AIDS-related causes, including 1.5 million in 2013. Further, the impact of HIV/AIDS on society and the challenges of curing it are highlighted by two facts. First, the severity of the HIV/AIDS pandemic

is comparable to the plague (*Yersinia pestis* infection, over 75 million deaths) [1]. Second, the only infectious virus ever eradicated in humans is smallpox [2]. Fortunately, unlike past pandemics with high mortality rates, ART enables HIV-infected patients to have a near-normal lifespan and quality of life.

There is still no cure or vaccine available for HIV/AIDS. While ART regimens are considered to be highly successful, significant limitations to current approaches persist. These include the need for chronic administration, patient non-adherence to therapy, which is often exacerbated by side effects of current medications and the continued threat of drug resistance. Treating HIV during the early stages of infection is likely to be more effective than at later stages due to the vulnerability of the virus to drugs [3]. Early treatment of patients may limit the establishment of viral reservoirs and the emergence of resistant viral mutations, while preserving immune responses for controlling infection. Early treatment could move ART to the next level – a functional cure where the body is able to control the disease without drugs, despite the continued presence of the virus [4, 5]. Pre-Exposure Prophylaxis (PrEP), the treatment of non-infected individuals prior to HIV exposure, has become a high priority strategy/regimen that provides early treatment to prevent post-transmission establishment of HIV infection [6, 7]. PrEP was first used successfully in HIV-infected pregnant women undergoing ART thereby protecting the fetus from infection during pregnancy and labor/delivery [8]. Unfortunately, Truvada, the only drug product approved for chronic oral PrEP, suffers from the same limitations as chronic oral ART in terms of posology, adherence, side effects and the risk of resistance if an individual is infected in the intervening time. It is important to note that the goal of HIV eradication has thus far categorically not been met.

New DD systems and strategies are needed to facilitate a functional cure and/or enable HIV eradication. Achieving efficacious drug concentrations in HIV reservoir sites using targeting approaches and reducing cellular efflux and metabolism to prolong effective drug concentrations

in target cells remain significant DD challenges. In addition, the urgent need for long acting/extended release (LA/ER) treatments to reduce patient compliance issues and complement those technologies in late stage development has become clear. LA/ER strategies for PrEP have numerous desirable attributes that include infrequent dosing and long dosing intervals making administration convenient for patients; the possibility of directly observed therapy and better long-term adherence; use in difficult to treat populations such as adolescents or those with ongoing substance abuse; use in patients reporting pill fatigue; and protection of patient privacy by eliminating the risk of disclosing pill taking to family and co-workers. The current review focuses on DD technologies, critical challenges, opportunities, strategies, and approaches that will help iterate towards infection prevention, functional cure and eventually the eradication of HIV infection.

3.3. Importance of Understanding HIV Pathogenesis to Enable Effective Anti-HIV Drug Delivery

Unlike traditional pathogens that coevolved with mankind for millions of years, HIV is an exotic pathogen that crossed species from African primates to humans in at least five independent events (hence HIV-1 groups M, N, O and P and HIV-2) starting approximately a century ago [9]. Consequently, humans have not had sufficient time to develop an adequate immune response. While broadly neutralizing antibodies eventually develop in 10 to 30% of patients, the overwhelming majority of these antibodies (~ 99%) are not potent enough to stop the progression of disease. In addition, the induction of these antibodies through vaccination has been unsuccessful [10].

HIV is a member of the lentivirus genus in the retroviridae family. The high mutation rate allows HIV to evade destruction by host immune responses. The provirus form of HIV can hide in the genome of latently-infected CD4+ memory T cells for years without revealing any sign of infection to host immune surveillance. It also does not provide an obvious target for eradication

treatment. Natural eradication of any pathogen relies on host immunity. However, HIV is unique among retroviral pathogens because its main target is CD4⁺ helper T cells, which serve as key coordinators within the immune system. As the CD4⁺ T cell pool is progressively depleted, host immune function becomes weaker, making eradication increasingly difficult. Compounding the reduction in CD4⁺ T-cells is the establishment of cellular HIV reservoirs, defined in the context of eradication as a cell type or anatomical site that allows persistence of replication-competent HIV-1 on a timescale of years in patients on optimal ART [11-13]. Anatomically, HIV reservoirs are mainly located in the mucosa of the alimentary, respiratory and genital tracts, the brain/central nervous system (CNS), and some lymph nodes (LNs) [12, 14]. Cellular reservoirs include latently infected CD4⁺ memory T cells but may also include other infected cells such as hematopoietic stem cells and macrophages [11]. Some reservoir sites are also considered viral sanctuary sites where drug concentrations are suboptimal due to biological barriers (e.g., blood-brain barrier) that protect the anatomical sites (e.g., brain/CNS). This allows HIV to replicate unhindered [14].

HIV establishes persistent infection by two mechanisms: reservoir formation and ongoing replication. The gut mucosa plays a pivotal role in HIV pathogenesis. The gut mucosa harbors approximately 60% of the body's immune cells, including the majority of CD4⁺ T cells. Many of the CD4⁺ T cells are activated due to the bacteria present in the gut lumen, enabling viral replication. Furthermore, these CD4⁺ T cells express the HIV co-receptor CCR5, which is needed for HIV entry [15, 16]. Accordingly, at all stages of HIV infection, viral replication and CD4⁺ T cell depletion predominantly occurs in the gut mucosa, even under apparently successful ART [17, 18]. Following CD4⁺ T cell depletion, bacterial products breach the gut epithelial barrier. This leads to further local and systemic CD4⁺ T cell activation, and the acceleration of viral replication and immune cell depletion [19]. Very recently, whole-body immunoPET scans of simian immunodeficiency virus (SIV)-infected macaques confirmed that persistent viral replication occurs in strategic mucosal sites, such as the gut, irrespective of ART [20]. Thus, ART

cannot suppress low level, persistent viral replication in mucosal sites, making them high priority targets for DD.

Targeting HIV mucosal transmission earlier is likely to be more effective than treating at later stages of infection [3]. CD4⁺ T-cells are scattered throughout the colorectal and vaginal submucosa in small numbers. Innate immunity suppresses initial infection, resulting in a small founder population of infected cells that is highly vulnerable to ART [21]. During the first few days after transmission, there is a dynamic balance between the shrinkage of the infected founder cells resulting from viral and host innate immunity killing and expansion of these cells by spreading of infection to uninfected cells. The basic reproductive rate of the founder cells is the ratio of expansion to shrinkage and when the ratio falls below 1 the founder population of the infected cells shrinks, resulting in aborted infection. Once locally expanded HIV spreads to the draining LNs, systemic infection is established. The viral vulnerability creates prevention opportunities since it would not be necessary to completely inactivate all HIV or kill all infected cells. Rather, reducing the founder population to below the critical threshold value may suffice. This window of opportunity lasts about one week from the time of vaginal exposure to the establishment of HIV infection whereas after colorectal exposure, it may be significantly shorter (**Fig. 1**) [3]. Although this estimate is based on data from non-human primates and vaginal SIV challenge, the mechanism provides a logical basis and rationale for the concept of a window for establishing HIV infection in humans, post exposure to HIV, and an opportunity for PrEP DDS to deliver ART and prevent the establishment of HIV infection.

In a critical proof-of-concept study, Li et al [22] demonstrated that inhibition of the recruitment of CD4⁺ T cells alone was sufficient to prevent vaginal transmission in a SIV–macaque model. They found that mucosal inflammatory signaling in conjunction with the innate immune responses to infection greatly fueled CD4⁺ T cell recruitment. The signaling involves macrophage inflammatory protein-3 α cytokine, plasmacytoid dendritic cells (pDC) and pDC-

produced CCR51 chemokine. The surfactant glycerol monolaurate is an antimicrobial compound that has no effect on the SIV life cycle per se but is known to inhibit immune activation and chemokine/cytokine production *in vitro*. Topical application of glycerol monolaurate to the vaginal mucosa protected rhesus macaques from acute infection despite repeated intra-vaginal exposure to high doses of SIV. The data thus suggest that limiting local expansion to below a critical threshold alone can be effective in preventing viral infection. The concept of early treatment for prevention has also been supported in other studies using non-human primate models. For example, agents that block viral binding, co-receptor-mediated entry and reverse transcription have been shown to protect against SHIV and SIV vaginal and rectal challenges in the rhesus macaque model [3]. The implications for DD are clear: (1) constant, therapeutically effective drug concentrations need to be maintained in the vaginal or colorectal mucosa of high risk individuals prior to viral exposure, (2) methods to inactivate HIV prior to mucosal entry may have value, and (3) approaches to control the number and rate of responding immune cells to the colorectal and vaginal mucosa after HIV exposure are warranted.

3.4. Drugs for Prevention and Treatment of HIV Infection

There are currently 37 Food and Drug Administration (FDA)-approved ARV drug products used clinically in the US for the treatment of HIV/AIDS [23]. Although a myriad of highly potent drugs have been approved and widely used, the HIV drug pipeline still shows robust growth in volume as well as in molecular target diversity [24]. Existing ARVs can be classified by the site of action (i.e., extracellularly in the vaginal/colorectal lumen or mucosa or intracellularly in HIV-susceptible immune cells). Extracellular acting ARVs, which interfere directly with the entry process, target either the HIV co-receptor (CCR5) [25, 26] on host cells or gp41, the viral transmembrane glycoprotein on HIV. The vast majority of ARVs act inside host cells by preventing viral proliferation. Four classes of intracellular acting ARVs have been introduced including Nucleoside/nucleotide Reverse Transcriptase Inhibitors (NRTI), Non-nucleoside

Reverse Transcriptase Inhibitors (NNRTI), Protease Inhibitors (PI), and HIV Integrase Strand Transfer Inhibitors (InSTI). The vast majority of ARVs have solubility, stability and/or permeability limitations that ultimately lead to a high degree of pharmacokinetic (PK) variability in humans [27-31]. National Institute of Allergy and Infectious Diseases (NIAID) -supported researchers established ART regimens, a combination of at least two drugs, in order to reduce the incidence and rate of viral resistance. These treatment regimens are multi-class drug combination products. Truvada, an orally administered fixed combination drug product containing tenofovir disoproxil fumarate (TDF) and emtricitabine, represents the first potent combination drug product approved for preventing HIV infection.

Intensive ARV research has resulted in drugs with high potency and the discovery of new mechanisms of action (Table 1). Besides introducing newer generations of NRT, NNRT InSTI and protease inhibitors, novel mechanisms of action are being explored, e.g. therapeutic reclamation of apoptotic proficiency-based (TRAP) are moving to the clinical trials stage. As of today, 59 HIV PrEP clinical trials are listed in the AVAC database (avac.org). However, most trials involve Truvada. Even though new potent ARVs are needed, it appears that a paradigm shift from drug discovery to drug delivery is occurring in the field of HIV therapy.

3.5. Drug Delivery Systems for HIV Prevention

Currently, there are few options for preventing HIV infection. PrEP DDS in development are administered either locally through rectal or vaginal administration, or systemically by means of oral or parenteral administration, providing therapeutically relevant drug concentrations in vaginal and colorectal tissues [7, 40-45]. By any route of administration, the key requirements are the delivery and maintenance of effective ARV concentrations at vulnerable mucosal sites during periods of HIV exposure since HIV transmission through the colorectal and vaginal mucosae is responsible for the vast majority of new HIV infections [46, 47].

In 1995, Tsai et al. [48] published a seminal paper demonstrating that subcutaneous administration of TFV could prevent SIV transmission in macaques. Following this report, the use of vaginally- and orally-administered TFV and TDF, the orally bioavailable prodrug of TFV [49], to prevent HIV infection in high-risk populations became the focus of many investigations [42]. To date, numerous clinical trials have been conducted investigating TDF and other ARVs as potential oral PrEP agents. Of these studies, one treatment regimen was successful, leading to the only FDA-approved and licensed treatment for HIV prevention. This product, Truvada, consists of two drugs, TDF and emtricitabine (FTC) in a once a-day oral dose form [42].

One early investigation involving Truvada was the Partner's PrEP study where it was found to reduce HIV acquisition with a 75% rate of effectiveness. However, in the FEM-PrEP and VOICE (Vaginal and Oral Interventions to Control the Epidemic) clinical trials that followed, it was not found to be effective. A lack of patient compliance was determined to be one of the primary factors in the failure of these studies. Similar results were seen in other clinical trial including the iPrex study in which Truvada reduced HIV transmission by only 42% overall [42, 50]. It was determined that only 18% of patients were taking the drug at the prescribed daily regimen [42]. When the analysis was narrowed to only patients with high adherence to the regimen (i.e., where patients steady-state plasma TFV concentrations > 40 ng/mL), the therapies were found to be 88% and 91% effective for the groups that received TDF and TDF/FTC, respectively [51]. Therefore, while a number of trials have reported that systemic oral PrEP is only 39% to 75% effective, subsequent correction of the data for medication regimen adherence, as indicated by measureable drug blood levels, showed that effectiveness was greater than 90% in patients that took their medication consistently [40, 41, 43, 52, 53]. This and other pharmacokinetic (PK) studies show a clear relationship between PrEP efficacy and patient adherence as well [42, 52]. For rectal and vaginal PrEP formulations there is also a relationship between the size, texture and

color of a formulation, perceptibility (user sensory perceptions including leakiness/messiness) and patient adherence [54, 55].

This body of work highlights the two major challenges influencing patient adherence to PrEP regimens: the chronic nature of administration/frequency of use (oral, rectal and vaginal) and perceptibility (rectal and vaginal). Chronic oral PrEP also raises concerns of toxicity and the potential for ARV resistance due to widespread systemic exposure. Finally, additional studies have also revealed suboptimal drug concentrations in the target mucosal tissues even though relatively high drug concentrations are found in the blood [56]. Alternatively, microbicides are applied topically to the vagina or rectum and act locally to prevent HIV transmission. Therefore, the development of DD strategies and DDS for colorectal and vaginal mucosal PrEP that maximize local tissue drug concentrations and minimize systemic exposure are a high priority.

Microbicides have been extensively investigated as potential preventative options in numerous DDS/dose forms such as gels, creams, films, foams, quick-dissolving tablets and intravaginal rings (IVR) [41, 42, 44, 57-59]. Highlights of significant microbicide/local PrEP DDS are described below.

3.5.1. Vaginal Gels

Microbicides were first explored as a means of offering broad protection against most or all sexually transmitted infections in the early 1990's. The first generation of microbicides, were membrane solubilizing surfactants including the nonionic spermicide nonoxynol-9 (N-9), an OTC vaginal contraceptive known to destroy the membrane of cells [7, 40, 44]. Unfortunately, N-9 failed at the clinical trial stage where it was found to increase HIV transmission due to the development of inflammatory genital tract lesions in the epithelial layer of the vagina. Additionally, the product did not adequately cover the vaginal mucosa evenly, pointing to major formulation challenges for the future for vaginal PrEP products [41, 43, 52]. Since the publication

of these reports, N-9 and similar surfactants have been excluded, with few exceptions, from the developmental pipeline [41].

Second generation microbicides incorporated polymers into the application design. Early formulations of this period were aimed at reducing the toxicity of nonoxynol-9. Polymers were used to minimize mucosal irritation and prevent environmental changes in the vagina that may increase risk of infection. However, sufficient efficacy was not achieved. Thus with the widely accepted dismissal of surfactants, efforts focused on polyanionic compounds. This group of polymers was specifically chosen because of their ability to act as entry inhibitors to prevent HIV from entering target immune cells in the vagina [7]. Several polyanionic polymer-based microbicides advanced to clinical trials including Carraguard, Cellulose Sulfate and PRO2000. Unfortunately, all were proven ineffective [60].

Third generation topical PrEP focused on microbicides using intracellularly acting ARVs to prevent HIV infection [42]. Karim et al. [61] presented the results of a study (CAPRISA 004), which was carried out to assess the safety and effectiveness of a 1% TFV gel for HIV prevention. They demonstrated that the gel, if applied both before and after sex, reduced HIV incidence by 39% overall and by greater than 54% for those who used the gel consistently [57]. TFV was the first ARV found to be effective as a microbicide. However, although it was found to be safe and effective in preventing HIV infection, patient adherence was once again an obvious concern with these treatments [61].

Haaland et al. [62] reported another clinical trial studying an ARV microbicide candidate, UC781. UC781 is a NNRTI with poor oral bioavailability. Although it was unsuccessful as a potential oral agent, it was believed to be a promising choice as a topically applied microbicide. A carbopol gel formulation of 0.1% UC781 was found to be effective *in vitro* and *in vivo* in a macaque model. When evaluated in a phase III clinical trial, the study was quickly terminated due to the insolubility and instability of UC781; similar limitations were reported after oral

administration. This study showed the importance of evaluating microbicide effectiveness after exposure to the human female genital tract and to semen. It is possible that semen may inhibit the antiviral activity of UC781 *in vivo* albeit this interaction with semen plasma was investigated *in vitro* during preclinical studies and found to have no significant effect.

3.5.2. Intravaginal Rings (IVR)

In order to overcome patient adherence issues, IVRs have been proposed to deliver LA/ER ART [42, 59]. IVRs are typically formed from elastically deformable polymers such as thermostat silicones, poly(ethylene-co-vinyl acetate), or polyurethanes. The drug is usually mixed or dissolved in the polymer matrix during the formulation process and incorporated into the injection molding or hot-melt extrusion. Once the DDS is exposed to the vaginal lumen, a concentration gradient is initiated, allowing for the surface drug to diffuse into the contacting tissue. The rate of drug release depends on numerous factors such as drug solubility, partition coefficient, and diffusion coefficient of drug in IVR polymer and of drug in vaginal fluid.

Nel, et al. [63] reported a clinical trial investigating the safety and PK of an IVR that delivered the NNRTI dapivirine. Twenty-four women were treated with dapivirine (25 mg) silicone elastomer matrix IVR, dapivirine (25 mg) silicone elastomer reservoir IVR, or a silicone elastomer placebo IVR. IVRs were used for 28 consecutive days and plasma and vaginal fluid samples were collected on day 1 and day 28 of the trial. The matrix IVR and reservoir IVR were able to achieve significant drug levels in vaginal fluid with maximum drug levels of 6 mM and 42 μ M respectively. This data is encouraging because the reported vaginal fluid and mucosal tissue drug levels surrounding the IVR location were more than 1000-times the *in vitro* 50% effective concentration (EC_{50}) against the wild-type HIV-1. This suggests that the IVR investigated may be able to achieve sufficient drug concentrations within vaginal mucosal tissue to prevent HIV infection [59, 63].

Several other studies have been conducted investigating IVRs incorporating dapirivine [64-66]. Nel et al. presented results of a clinical trial for the Dapivirine Vaginal Ring-004 (25 mg dapivirine) at the 22nd Conference on Retroviruses and opportunistic infections. Patients wore the IVR for periods between 4 to 12 weeks at a time. For patients that wore the IVR for 12 weeks consistently, mean vaginal fluid concentrations were found to be more than 4000-times the *in vitro* IC₉₉ in cervical tissues at the end of the study. This ring is currently being evaluated for safety and efficacy in phase III clinical trials (International Partnership for Microbicides website: last accessed May 30, 2015).

Recently, a 90-day TFV reservoir ring inspired by the success of the 1% TFV gel was investigated [67]. They hypothesized that the IVR would be able to provide a more controlled and sustained vaginal drug concentrations in the cervicovaginal area. Polyurethane tubings of various hydrophobicities were filled with high densities semisolid paste of TFV, glycerol and water. *In vitro*, a more rapid release of TFV was found with increasing polyurethane hydrophilicity allowing for systematic control of drug release. IVRs were evaluated in two 90-day *in vivo* sheep studies where pharmacokinetics and safety of TFV was evaluated. The polyurethane IVR was found to be capable of delivering 10 to 30 mg of TFV daily for up to 90 days consistently. Previous matrix IVRs typically had high fractions of undissolved drug that was never released from the ring. They also commonly showed a decrease in drug release rates with time as well as a decrease in material stiffness as a result of drug release. This study is significant because it highlights a tunable membrane that can be controlled to achieve and maintain a desired TFV loading, release rate and ring stiffness by altering material properties. The polyurethane TFV IVR also showed no significant toxicological effects. However, in comparison to the control, there was slight to moderate increase in inflammatory infiltration within vaginal epithelium. Although clinical studies are needed to confirm the safety and potential efficacy of this therapy, it shows promising results for the future of IVR for HIV PrEP [67].

Patient adherence to PrEP regimens remain a concern and developing better ways of determining adherence are needed. Boyd et al. [68] describes the development of a technology to address the pivotal issue of inaccurate self-reporting of patient adherence during clinical trials. They report a temperature-monitoring microbicide-releasing vaginal ring that uses DST nano-T temperature loggers to monitor user adherence. While still in the pre-clinical stages, the IVR was tested in macaques where it showed high sensitivity to fluctuations in vaginal temperatures and the ability to detect periods of IVR removal with accuracy. This introduces the concept of multipurpose IVR to treat patients as well as monitor their use and significant events that may affect efficacy such as sexual arousal, vaginal intercourse, and menstrual cycle). Such technologies would markedly enhance the accuracy of product evaluation during clinical testing.

3.5.3. Vaginal Films

Another type of mucosal PrEP DDS being explored is the use of vaginal films for local mucosal PrEP [66, 67, 69, 70]. Polymeric vaginal films are a solid dosage form that offers several additional advantages over other microbicide dose forms such as gels and creams. Some of these advantages are (1) accuracy of dose administration in the absence of an applicator; (2) rapid drug release upon exposure to vaginal fluid; (3) discreet use and minimal product volume; (4) improved drug stability; (5) convenient storage; and (6) minimal leakage. In addition, when compared to soft-gel capsules and tablets (not discussed in this review), an acceptability study reported that greater than 80% of participants surveyed, found the films to be acceptable forms of treatment. 77% to 91% of women in the study also stated that they would definitely use any of these products if they were confirmed to be effective at preventing HIV transmission [6, 69, 70].

Until recently, most published studies proved the feasibility of formulating polymeric vaginal films containing a single anti-HIV drug candidate. For example, a vaginal film reported by Akil et al. [71] comprised of only dapivirine was shown to be effective in blocking HIV-1 both *in vitro* using P4/R5 and MT-2 cells as models of HIV infection. The film was also shown to be effective *ex vivo* in polarized and cervical explant models. Recently, research has given increased focus on developing films capable of co-delivering multiple drugs [70, 72]. Another paper by Akil et al. [70] describes the utilization of vaginal films to deliver different combinations of dapivirine, maraviroc, and TFV. Films were manufactured by a solvent casting method and solid phase solubility was used to select appropriate polymers to be used in the formulation. Cellulose polymers and polyvinyl alcohol were used in the development of three combinational film products. These vaginal films were determined to be stable for up to 12 months at ambient temperatures with rapid drug release reported (>50% of each drug) within the first 30 minutes *in vitro*. The results from this study show the potential of vaginal films to incorporate multiple antiretroviral agents, which is of great importance considering the prevalence in use of ART for both prevention and eradication. The vaginal films were also well tolerated by both the women and their partners, which makes them promising candidates for microbicide therapies.

A comprehensive summary of clinical trials for topical vaginal microbicides can be found in a recent paper by Antimisiaris et al. [73]. To date, there have not been any products approved for use in humans. This demonstrates a great need for new technologies and innovative ideas moving forward. Recently, there has been an increased interest in LA/ER ARV drug combinations for microbicides to enhance efficacy and user adherence. Nanotechnology-based drug delivery systems are a promising option to advance the field of microbicides by their ability to (1) facilitate drug/virus interactions, (2) increase synergy for drug cocktails (3) penetrate mucosa tissue, (4) provide sustained and triggered drug release, (5) target HIV susceptible cells, (6) improve drug solubility and permeability, and (7) serve as a drug barrier along the epithelial cell

lining [74-76]. Recent review articles published earlier this year discuss the benefits and potential drawbacks of exploring nanotechnology-based solutions to improve the efficacy of vaginal microbicides [73, 77].

3.5.4. Colorectal Microbicides

Until recently, most efforts at microbicide development and initiated clinical trials focused on vaginal microbicides despite the major role colorectal transmission plays in the establishment of new infections. Men and women who practice unprotected receptive anal intercourse (RAI) are at a much higher risk of contracting HIV from an infected partner than those who engage in unprotected vaginal sex. Unprotected RAI is estimated to result in 10-100 times more incidences per exposure than unprotected vaginal intercourse [78]. A major cause of this is the structure of the colorectal mucosa (shown in **Fig 2**) [79]. The colorectal epithelial barrier is a thin single-cell columnar layer above the lamina propria that is much easier to penetrate than the multi-layer barrier found within the vagina. Once HIV traverses the epithelial layer and enters the lamina propria, it has direct access to an extensive population of activated resident CD4⁺ T cells, macrophages, dendritic cells, and other lymphocytes that are highly susceptible to HIV. There are also individual LNs that serve as a primary route for HIV to enter the systemic circulation [56]. Due to distinct anatomical differences between the vagina and colorectum, microbicide technologies developed specifically for one route of administration cannot be incautiously translated to an application for the other.

Since colorectal microbicides were recently reviewed in this journal, a summary of the formulation factors, DDS issues and challenges will be presented and the reader is referred elsewhere for a more general discussion of broader issues [56]. Colorectal microbicide dose forms commonly include gels, enemas and suppositories. The use of these traditional dose forms present numerous delivery challenges to PrEP treatment and this is an area that would greatly benefit from the development of new DDS technologies and techniques. The challenges can be

generally categorized as follows: (1) administration methods as it relates to mucosal coverage, (2) patient acceptability and adherence as it relates to volume administered and retention, (3) coital dependence and persistence of therapeutic effect, and (4) chronic safety/toxicity of the DDS/formulation.

Administration methods as it relates to mucosal coverage – Complete coverage of the colorectal mucosa is important for providing protection from HIV transmission. It is suggested that a colorectal microbicide should cover the entire rectum, sigmoid colon and descending colon to up to the splenic flexure to provide sufficient protection. Careful consideration must be taken to choose the ideal delivery vehicle and applicator to ensure the spread of therapeutic agent to all areas that may become exposed to the virus [80-82].

Patient acceptability and adherence as it relates to volume administered and retention – While there is no standard volume of product that is used for colorectal treatments, the volume should be sufficient enough to cover the entire area that may become exposed to HIV during intercourse. One study [83] reported that participants tolerated up to 35 mL of a rectal microbicide gel, and once this volume was exceeded, there is increased anal leakage and discomfort. The smallest effective volume for treatment is preferred [56, 83]. As has been proven many times, patient acceptability will have a major influence on efficacy [54, 56].

Coital dependence and persistence of therapeutic effect – Coital dependence of an application (requiring dosing close to the time of sexual intercourse) may be a disadvantage when it relates to adherence. It requires that the users anticipate when they will have sex and be able to privately apply the treatment in advance. If the therapy is only active for a few hours, this may place a limitation on the timespan in which a person has to use the application. Ideally, a LA/ER PrEP approach with sustained drug activity would allow for more flexibility in application and increase adherence and efficacy [44].

Chronic safety/toxicity of the DDS/formulation – Microbicide formulations need to preserve the activity and stability of drugs while also ensuring that the excipient concentrations used pose no significant toxicity. Product acceptability is strongly dependent on the safety and comfort so it is important that products are nontoxic especially for chronic treatment.

In parallel to these four primary challenges, the physicochemical properties of the delivery vehicle play a key role in addressing these overcoming these challenges and increasing overall therapeutic efficacy. The ideal delivery vehicle will differ depending on the route of administration and vehicle type. In order to achieve sufficient levels of coverage, retention, safety, drug release and therapeutic efficacy, many properties of the formulation have to be optimized to compliment the biological environment that is being treated. Important properties to consider include pH, viscosity, osmolality, mucoadhesivity, yield stress and shear rate [56, 84, 85].

Although it has not always been a main focus of PrEP research, interest in colorectal PrEP has existed since the development of the first generation of microbicides. Nonionic surfactant N-9 was one of the first microbicides tested for colorectal application. Similarly to the results for vaginal administration, N-9 was found to cause significant epithelial sloughing and a potential increase in the risk of infection [56, 86]. Since then, five ARV phase 1 clinical trials have been completed for rectal microbicides. Most of these trials have also focused on TFV gel formulations and one study investigated the UC781 gel that was also explored as a vaginal application [42]. Anton, et al. [86] described the first phase 1 double-blind, placebo-controlled randomized clinical trial for UC781 gel as a rectal microbicide. Men and women were treated rectally with two concentrations of UC781 (0.1% and 0.25%) in gels formulated with Carbomer 974P, methylcellulose, glycerin, purified water and paraben preservatives. This class of gels is similar to thickened solutions with a limited ability to spread evenly or be retained on the mucosa. Both

dosages were found to be safe with no epithelial sloughing from rectal lavage and no changes in histology.

Another gel investigated as a rectal microbicide was the vaginal formula of the 1% TFV gel used in the CAPRISA 004. This gel was evaluated in a phase 1 rectal study [RMP-02/MTN-006] where it was shown to induce mild to moderate gastrointestinal side effects such as pain, bloating and diarrhea. These symptoms were believed to be caused by the osmolality of the vaginal formulation (3111 mOsmol/kg) [87, 88]. Following this study, a second gel was developed to address the osmolality of the 1% TFV gel. The gel formulation included a reduced amount of glycerin compared to the 1% TFV vaginal formulation and was studied in the MTN-007 phase 1 rectal microbicide trial. With a lower osmolality (836 mOsmol/kg), it was determined to be better tolerated by the participants of the trial [58, 88]. Recently, McGowan et al. [88] reported a randomized phase 1 clinical trial comparing the safety, acceptability, PK, pharmacodynamics of the 1% TFV gel, the reduced glycerin gel, and a third gel never tested before in a phase 1 rectal study (Charm-01). The third gel was a rectal-specific formulation made with an even lower concentration of glycerin than the already reduced glycerin formulation. An additional carbopol was also added to create a nearly iso-osmolar product (479 mOsmol/kg). After a single dose of each treatment, all three gels were found to be safe and acceptable to participants. *Ex vivo* colorectal studies were also performed and all formulations were found to result in a significant suppression of HIV-1 viral replication. However, due to low participation and limited product availability, Charm-01 was not fully enrolled and significant conclusions regarding which product should advance to later stage trials as a rectal microbicide could not be made. Currently the reduced glycerin gel is being evaluated in an International Phase 2 expanded safety study expected to be completed by early 2016.

Nano-sized DDS are showing promise for colorectal microbicide development. The majority of information published involves Vivagel® (Starpharma Pty Ltd). Vivagel is a carbomer-based gel

loaded with SPL7013, a dendrimer reported to have inhibitory activity against both X4 and R5 strains of HIV-1. A 5% SPL703 gel reduced HIV-1 infection by greater than 85% in colorectal explants *ex vivo* but it was also shown to cause epithelial shedding. The toxicity of the treatment was attributed to the vehicle and not the dendrimer [56, 89]. Das Neves et al. reports the use of poly(ethylene oxide)-modified poly(ϵ -caprolactone) (PEO-PCL)-based nanoparticles (NPs) as a potential nanocarrier (NC) for the NNRTI dapivirine. 200 nm PEO-PCL NPs loaded with dapivirine were shown to increase drug uptake into Caco-2 intestinal cells *in vitro* [56, 90, 91]. The development of colorectal microbicides is in the very early stages. An editorial published by Sarmiento and das Neves called for more research in this area and describes the growing field in more detail [92].

There are numerous rectally administered products and excipients that have been collectively approved for human use for literally hundreds of years. However, given the unique application to rectal microbicides, the use of traditional rectal products is not very promising. A technology covering the concept of a colorectal dose form/DDS that could spread uniformly along the descending colon from the splenic flexure to the rectum and be retained for a reasonable period of time is virtually nonexistent. Even if such a technology existed, the coital dependence of efficacy due to physical abrasion of the colorectal tissue and the persistence of effect would be questionable. The obvious modifications to traditional rectal dose forms/administration such as large volume enemas to deliver adequate volumes to ensure initial complete colorectal mucosal coverage would not be well received by patients. This will certainly result in unacceptable leakage volume and extremely poor patient use/adherence no less a transient effect due to poor mucosal retention. Hence, the dependence on old, approved rectal formulations that were not designed for the purpose of rectal microbicides is a critical issue facing the DD field.

3.6. Drug Delivery Systems for HIV Treatment

Although a variety of DDSs have been explored for treating HIV/AIDS, they have been, for the most part extensively covered in previous reviews [76, 93-97]. In the following sections, DDSs that focus on resolving the remaining DD challenges are highlighted.

3.6.1. Gut Mucosa and Lymph Nodes: Targeting the critical sites of HIV infection

The current understanding of HIV pathogenesis informs future DD strategies for eradicating HIV infection from the gut and LNs. Viral replication and CD4⁺ T cell depletion predominantly occurs in the gut mucosa at all stages of HIV infection even under apparently successful ART making DD to the gut mucosa a high priority [17, 18]. In a 2012 study [98], 30 acute HIV infected patients (viremia⁺/HIV IgG⁻) were identified/recruited from screening 24,430 high-risk persons and treated with mega-HAART (five drugs at the entry, RT and integration steps) for 24 weeks. The mega-HAART regimen resulted in a viral reservoir reduction and partial CD4⁺ T cell count recovery in the gut mucosa. However, even in these patients, the viral reservoir persisted emphasizing the need for a gut-targeted DDS to achieve a functional cure for early diagnosed patients.

The mucosal mucus layer is the first barrier that a DDS will encounter. Mucus properties, function, barrier to NP delivery and mucoadhesive and mucopenetrating polymeric NPs have been extensively reviewed [99]. The mucus layer covering the alimentary and reproductive tracts consists of interwoven fibers and water-filled spaces in between. NPs must penetrate through this layer to reach the mucosa. The Saltzman group has found that certain polymers (e.g., PEG and PVP) are capable of altering the mucus structure to facilitate polymeric NP, or even monocytes, penetration of the mucus layer [100]. While the Hanes group reported that short (~ 2 kDa) PEG polymers displayed on NPs are able to penetrate mucus layer, apparently mimicking the surface property of viruses that infect human epithelia (reviewed in [99]), the Sinko group demonstrated size dependence of particle translocation through mucus [101, 102]. Mucoadhesive NPs can be

used in HIV topical PrEP while mucopenetrating NPs are more suitable for oral DD. In the latter case, however, mucopenetrating alone is not sufficient; the NP must be able to penetrate the gut epithelial barrier. In this regard, an oral NP targeting the neonatal Fc receptor has achieved some degree of success [103].

Lipid-formulated DDS that exploit the gut lymphatic route for absorption are becoming increasingly popular [104]. Lipids are cost effective in comparison to synthetic polymers and the relative ease of manufacture, which avoids the use of organic solvents and collectively this makes this technology worthy of further investigation [105]. In separate rats dosed intraduodenally with a solid lipid NP formulation of lopinavir, cumulative lopinavir concentrations in lymph fluid were 9.68 μg for the nanoformulation compared to 1.97 μg for the conventional formulation 6 hours after administration [106]. Negi et al reported similar observations using another solid lipid NP of lopinavir that was fabricated using a hot self nano-emulsification technique [107, 108]. Although the gut lymphatic-targeting mechanism of lipid-formulated drugs is not clear, it is believed to be similar to dietary fat absorption. Dietary fats translocate across the gut in the form of nano-sized chylomicrons and since the chylomicrons are too big to enter the blood microvasculature they by default enter the close-ended/one way terminal capillary lymphatics (i.e., the lacteals) through endothelial intercellular gaps. This also suggests that lymphatic-targeted NPs have the potential to be retained in gut lamina propria if their size exceeds the size of the chylomicrons. Solid lipid NPs have been reported to exhibit low drug loading capacity and low lipid chemical stability, which may limit their use for some drug delivery applications [109]. Other technologies that result in the formation of micellar suspensions have also been shown to improve the plasma concentrations of various ARVs after oral administration but lymph penetration was not assessed as the potential mechanism [110, 111].

Since LNs are an important immune induction site, a HIV replication site and a reservoir, DD to LNs is also a high priority. Unfortunately, with the exception of a very early attempt in 2001 [112], literature reports suggesting or proving the feasibility of specifically targeting the gut mucosa using DDS are lacking. This 2001 study achieved a four-fold higher AZT gut mucosa concentrations 90 minutes after oral dosing in rat using a poly(isohexylcyanoacrylate) NP formulation compared to free AZT. The enhancement mechanism was proposed to be mucoadhesion. DD to the LNs has proven to have a disproportionately larger effect on controlling HIV as compared to the blood compartment (i.e., systemic therapy). Critical progress made in targeting LNs is described in the following sections.

The Ho lab pioneered LN targeted HIV DD. They found that in HIV-1 positive patients, indinavir (IDV) concentrations in LN mononuclear cells were about 25–35% that of mononuclear cells in blood. LN targeting enhanced IDV delivery in a HIV-2-infected macaque model [113]. The DDS consisted of a lipid-associated IDV complex NP (50–80 nm in diameter). The subcutaneously (SC) injected lipid/drug NPs became trapped in the draining and systemic LNs where they were taken up by resident macrophages. The LN macrophages served as a drug depot slowly releasing IDV. IDV concentrations in both peripheral and mesenteric LNs were 250–2270% higher than plasma while in humans soluble lipid-free drug administration reached a concentration <35% compared to the plasma. SC injection at IDV-equivalent 20 mg/kg daily for 30–33 weeks resulted in significantly reduced viral RNA load and increased CD4⁺ T-cell counts. Although the exact fate of SC-injected lipid-associated IDV NPs is not well characterized, it is likely that lipid-IDV NPs were trapped in LNs throughout the lymphatic system. The Ho group further optimized a lipid NP formulation [114]. Compared to previous formulations, new lipid-IDV NP provided 6-fold higher IDV concentrations in LNs of the macaque/SIV model and enhanced drug exposure in blood. Recently, they reported that they had further developed a lipid NP formulation incorporating newer HIV drugs [115]. With the new generation of lipid-drug formulation, they

reported a lipid-drug NP containing a combination of lopinavir, ritonavir, and TFV [116]. These NPs produced over 50-fold higher intracellular lopinavir, ritonavir and TFV concentrations in LNs compared to free drug. Enhanced plasma and intracellular drug levels persisted for 7 days after a single SC dose, exceeding that achievable with current oral therapies. These results underscore the benefit of targeting an anatomic site critical in HIV infection as compared to systemic administration.

3.6.2. Targeting cell receptors on HIV infected T-cells and macrophages

As evidenced by the lack of progress in HIV vaccine development, targeting HIV proteins has been difficult. Host cell surface receptors are more readily targeted regardless of HIV infection status. The major roadblock for targeting CD4⁺ T cells and macrophages is the limited availability of targeting ligands. Most potential targeting ligands are small molecule chemicals whereby conjugation to a DD carrier tends to reduce the ability of the ligand to bind to a target cell receptor. In addition, there is a tendency to “decorate” rather than engineer NC surfaces. Ligand display configuration (spacing, linker dimensions, density, etc.) will impact NC-receptor binding and cellular uptake. Little has been published in this area in general and specifically as it relates to HIV/AIDS. A priority must be put on the discovery of new cell targeting ligands for NCs, their optimal display on drug-loaded NCs. In addition, techniques to avoid endosomal entrapment and the avoidance of off-target uptake and effects will have to be carefully considered. While there have been some reviews regarding active DDS targeting in HIV/AIDS, this area remains largely undeveloped and, from a critical *in vivo* perspective, feasibility is largely unproven [93, 96, 117].

There are numerous potential cell targets on CD4⁺ T-cells and macrophages. However, only a few have been exploited due to concerns about the potential inference with host immune function or the lack of suitable ligands that can be conjugated to NCs. Most targeting ligands have been peptides as the peptidyl nature makes it amenable to conjugation to a NC. DV3 is a 10-mer, D

peptide derived from a natural CXCR7 ligand vMIP-II. It has been shown to be able to bind to CXCR4 and to exhibit an anti-HIV activity of EC_{50} 0.439 μ M [118]. Recently, a derivative of DV3 named DV1-K-(DV3) was reported [119]. It was created by chemically linking DV1 (a 21-mer peptide also derived from vMIP-II) and DV3. This peptidyl ligand of CXCR4 shows an anti- EC_{50} 4 nM, which is more potent than the natural CXCR4 ligand SDF-1a. T140 is a 14-mer peptide derived from a horseshoe crab protein named polyphemusin that is a CXCR4 antagonist with anti-HIV activity of EC_{50} 3.3 nM [120]. Remarkably, a cyclic pentapeptide derivative of T140 named FC131 retains most T140's potency and one of FC131 analogs is even more potent than T140 with an EC_{50} 1.4 nM [121]. Floudas' group has identified a few short (10 to 15 residue) peptides as HIV CXCR4 entry and HIV fusion inhibitors, respectively [122, 123]. New and better performing derivatives of these peptides are being tested in our lab (to be published). Tuftsin is a tetrapeptide with the sequence of TKPR that utilizes an unidentified receptor on macrophages. It was displayed on efaviranz-packed dendrimers and the resultant dendrimer demonstrated macrophage targeting specificity and moderate anti-HIV activity [124]. Other potential ligands for NCs have also been explored, including a three-residue short peptide fMLF [125] and the monosaccharide mannose [126, 127].

3.6.3. Cell Depot-based DDS

Significant progress has been made in using human cells as DD depot sites. These approaches have utilized macrophages as drug carriers. HIV drugs were first loaded into NCs [128] or red blood ghost cells [129] that become engulfed by macrophages *ex vivo* or *in vivo*. The macrophages then migrated to LNs or additionally to other reticuloendothelial system (RES) tissues, acting as a cellular depot in these critical sites of HIV infection where the drugs slowly diffuse out over a period of days to weeks resulting in sustained high local drug concentrations in the LNs or other RES tissue.

In a feline immunodeficiency virus (FIV) model [129], the membrane-impermeable HIV drug zalcitabine-TP was first loaded *ex vivo* into autologous red blood cells and the plasma membrane of these red blood cells was then chemically modified so macrophages would recognize and engulf them. In a 7-month experimental FIV infection, zalcitabine-loaded erythrocytes protected the majority of peritoneal macrophages and reduced the infection of circulating lymphocytes. The Gendelman group has developed LA/ER nanoformulations of ritonavir (RTV), indinavir (IDV) and efavirenz (EFV) (nanoART) [128]. They reasoned that circulating macrophages traveling across the blood-brain barrier could enhance nanoART brain delivery [130]. An HIV-1 encephalitis (HIVE) rodent model was used. IDV NPs (a nanoART) were loaded into murine bone marrow macrophages (BMM, IDV-NP-BMM) *ex vivo* and the IDV-NP-BMM was administered intravenously. Rhodamine-labeled IDV-NP showed up in areas of HIVE. Continuous IDV release was observed for 14 days. IDV-NP-BMM treatment led to reduced HIV-1 replication in HIVE brain regions. Mechanistic studies [131] showed that nanoART-macrophage interactions enhanced phagocytosis, secretory functions, and cell migration, which could be exploited to increase macrophage nanoART loading capacity. Aouadi et al. [132] studied anti-inflammatory siRNA delivery utilizing yeast ghost cells. Yeast ghost cells were made by chemically treatment of yeast cell wall so that the cell surface was left with only beta1 3-D-glucan, for which macrophages have a special receptor. siRNA was then loaded into the ghost cells. The ghost cells can be efficiently absorbed orally through M-cells and, once crossed M-cells, avidly phagocytosed by macrophages in the Peyer's Patches. Interestingly, macrophages in the Peyer's Patches were able to migrate into blood circulation and settle at various LNs. Oral gavage of mice with the siRNA-loaded ghost cells containing as little as 20 $\mu\text{g}/\text{kg}$ of siRNA directed against tumor necrosis factor alpha (TNF- α) depleted its messenger RNA in macrophages recovered from the peritoneum, spleen, liver and lung, and lowered serum TNF- α .

levels. Although not developed an HIV application, this approach is readily translatable to the delivery siRNA against HIV infection.

In addition to treating HIV/AIDS using pharmacotherapy, vaccination and even gene delivery have been attempted. Steinbach has extensively reviewed protein and oligonucleotide DDSs for vaginal microbicides against viral sexually transmitted diseases [133]. These biological agents include antibodies for passive immunization in the vagina, various proteins or plasmid DNA encoding viral proteins as antigens for induction of vaginal immunity, siRNA to downregulate the expression of viral and host proteins involved in infection, and other proteins and peptides as antagonists in virus-host interactions. Often, these agents are non-covalently or covalently complexed/linked to polymers or other molecules in vaginal formulations and the formulations are incorporated into various vaginal devices. These studies are generally at the early stages but they have established proof-of-concept. Typically, natural infection is the most effective vaccination. The fact that not a single patient among millions infected with HIV has spontaneously recovered, underlines the inefficiency of a conventional vaccination strategy for HIV. Current vaccine development focuses on new approaches, such as broadly neutralizing antibodies and unconventional vaccines with recombinant DNA technology [134, 135]. In 2009, a report of a cure in the so-called “Berlin Patient” by using bone marrow transplantation of stem cells homozygous for a deletion in the CCR5 gene proved for the first time that eradication of HIV is possible [136]. Unfortunately, this strategy has proven to be unrealistic for most patients leading to efforts to develop gene therapy based strategies to disrupt the gene encoding CCR5 or other host proteins, as well as to disrupt the provirus [137]. Another strategy being explored involves purging the latent reservoir by activating latent provirus while eliminating new infections with ART [138, 139]. So far none of these strategies has achieved eradication in patients.

3.7. Long-Acting/Extended-Release (LA/ER) Parenteral (Injectable) DDS for PrEP and Treatment

The development of LA/ER injectable ARV DDS that could be administered infrequently (i.e., monthly or less), either in the clinic or at home represents an important potential solution to many of the problems associated with chronic ART and PrEP. There are numerous challenges facing LA/ER injectable DDS including identifying the optimal dosing interval, number and volume of injections per visit, the classes and properties of drugs that can be combined, and what to do if a patient becomes pregnant after the drug is administered. However, benefits to patients include infrequent dosing and long dosing intervals making administration convenient; the possibility of directly observed therapy and better long-term adherence; use in difficult to treat populations such as adolescents or those with ongoing substance abuse; use in patients reporting pill fatigue; and protection of patient privacy by eliminating the risk of disclosing pill taking to family and co-workers. There is also a clear rationale for the benefit of using LA/ER ARV formulations in pregnant women, postpartum women (including those who are breast feeding), and infants/children who cannot take typical adult oral formulations. In fact, patient surveys disclose great enthusiasm for trying LA/ER injectable nanoformulations for treatment. One recently published survey found that 84% of patients currently taking oral therapy definitely or probably would try such an intervention if the dosing frequency was once-monthly or less frequent [140]. Additional applications that would benefit from LA/ER ARV formulations include their possible temporary use as parenteral ART for those unable to take oral medications. This could include patients requiring gastrointestinal surgery, those who are comatose and/or intubated, those with significant nausea and vomiting, patients developing severe mucositis from cancer chemotherapy, and very young pediatric patients unable to reliably swallow pills. Treatment options for such patients are extremely limited at present, resulting in significant risk of treatment failure as a consequence of intercurrent illness [141].

Injectable nanoformulation technologies previously applied to approved LA/ER treatments for chronic schizophrenia, such as paliperidone [142] or LA/ER injectable contraception, are now being evaluated for treating HIV [143]. The LA/ER formulation consists of a solid drug particle nanosuspension produced by wet bead milling of large fragments of drug in aqueous solution in the presence of a surfactant until the particles are within the nanometer size range. Since these NPs are composed of pure drug and not a mixed matrix including polymers and other excipients, which typically comprise 50% or more of the NP formulation, higher loading into the formulation of up to 200 mg/ml is possible along with a reduced injection volume. A formulation of the nanosuspension is administered to form an IM depot. Given typical IM injection volumes once monthly dosing is feasible for potent drugs. Due to the physicochemical and dosing limitations as well as insufficient antiviral potency of currently used ARVs, it was not feasible to apply this approach until the development of two potent ARVs, rilpivirine and cabotegravir (S/GSK1265744). Both compounds are poorly water-soluble but possess sufficient potency and favorable PK properties to support once monthly dosing. The combination subnanomolar potency and a plasma elimination half-life of approximately 40 hours makes cabotegravir an ideal candidate for this approach. One concern with IM depots of poorly soluble drugs is the relatively high variability in bioavailability that has been observed in other applications. This would be a concern if the lower end of the deviation in blood/tissue concentrations falls below the IC_{90} of HIV-1.

Two formulations, a LA/ER injectable NNRTI rilpivirine (LA-RPV), and an InSTI, LA/ER injectable cabotegravir (LA-744), have been developed and are currently undergoing clinical testing [45, 144, 145]. The target-dosing interval for LA-RPV, based on its PK properties, is once monthly, and for LA-744 is once every three months for prevention applications and once monthly if combined with LA-RPV. Although LA-RPV and LA-744 represent important first steps in developing LA/ER ARV's, they are not well matched in terms of PK properties.

Differences in half-life mean that missed dosing may negatively impact resistance since LA-RPV has a shorter half-life.

In the first study [146] investigating LA-RPV, the reported plasma and genital tract concentrations in 60 women and six men given intramuscular (IM) depot injections of three different doses of LA-RPV (300, 600, and 1200 mg) showed that RPV concentrations in females were between 26 and 77 % of plasma concentrations in cervico-vaginal fluid and between 45 and 379 % of plasma concentrations in cervicovaginal tissue, while in males, they were between 33 and >77 % of plasma concentration in rectal fluid and tissue. In a second study [45], LA-744 (200 mg/ml) was evaluated after abdominal SC (100 mg, 200 mg, and 400 mg) or gluteal IM (100 mg, 200 mg, 400 mg and 800 mg) administration. The highest doses for each route were split due to injection volume considerations. Due to the low solubility of the NPs and inherent low tissue perfusion of muscle, the mean absorption half-times ranged from 21 to 50 days as compared to 40 h following single dose oral administration. With the exception of the 100 mg doses, all treatment groups remained above the IC_{90} of wild-type HIV-1 for at least 6 months. In two additional cohorts, (400 mg and 2 x 200 mg IM) were studied in 4 males and 4 females. Median individual tissue:plasma drug concentration ratios ranged from 16 to 25% in the female genital tract and were 8% in rectal tissue in men suggesting that at the dose tested the formulation would fall short as a PrEP agent. Furthermore, a recent study conducted in rhesus macaques showed that two IM doses 1 month apart protected eight out of eight animals from multiple rectal exposures to simian/human immunodeficiency virus (SHIV), while all eight animals receiving placebo injections acquired infection [147-149].

Since all currently used ART regimens involve the administration of at least three drugs in combination, there is an urgent need for other LA/ER technologies to complement those in late stage development. Additionally, LA/ER technologies that do not require injection need to be developed. It is clear that high drug potency is a prerequisite for compatibility with the LA/ER

approach since it determines the plasma concentrations that need to be achieved (and sustained). Ultimately, dose is the limiting factor for LA/ER delivery because it directly influences the volume of the depot required to provide sufficient drug concentrations, which is limited by anatomical considerations as well as patient acceptability. However, release rate is also a key determinant of success since too fast a release rate will result in “dose dumping” where high initial concentrations that are rapidly cleared, whereas too slow a release rate will not provide sufficiently high plasma concentrations for therapeutic effect. A recent study employed physiologically-based pharmacokinetic modeling to determine which release rate / dose combinations would be required to provide either weekly or monthly therapeutic concentrations for a range of commonly used existing ART drugs [150]. Importantly, these data do not determine that the predicted dose/release characteristics are achievable, but they do set a benchmark to inform the target product profile for developing LA/ER medicines with other ART drugs. The National Institutes for Health have recently funded a Long-Acting/Extended Release Antiretroviral Resource Program (LEAP), which once launched will aim to foster further development of such medicines. LEAP will also provide services, which include a PBPK modelling core to help guide development of LA/ER drugs and/or regimens.

3.8. Future Perspectives, Gaps and Opportunities

The tripartite goals of preventing new HIV infections, achieving a functional cure and complete eradication have become even more important since ART transformed HIV infection into a chronically managed disease. In recent years, great strides have been made in understanding how novel DDS may benefit HIV therapy in a disease-specific manner. Central to this has been the explicit demonstration in pre-clinical species of pharmacologically beneficial behaviors. Indeed, some of these benefits have also been translated to studies in humans and this is true for PrEP and LA/ER development discussed in this review. However, there remain a significant number of unmet needs and this is particularly true for those technologies that are at early stages of

translation. In broad terms, considerations for successful future development can be divided into those that relate to the drug delivery system itself, as well as those that relate to the drug, pharmacological rationale and the ultimate clinical application.

While numerous benefits have been achieved and demonstrated pre-clinically, there remain significant challenges in terms of the intricacies of manufacture. The development of complex DDS such as NCs is challenging at the bench no less in scale for manufacture. Translation at all stages represents the biggest hurdle for large-scale fabrication, testing and manufacture of DDS. For many technologies, there is a current paucity of knowledge regarding how the physical properties and constituents of the DDS specifically relate to the pharmacological behavior. Drug loading potential will be a key determinant of success for many technologies because of its impact upon format size or volume required for injectable depot medicines. Moreover, many technologies are only compatible with drugs that exhibit specific physiochemical properties and this may pose challenges to holistic development of enabled-regimens consisting of drugs from different classes. For conventional oral medicines, the framework within which drugs are developed has been extensively researched over the past decades. This framework has resulted in the Biopharmaceutics Classification System (BCS) for oral drugs and a solid understanding of the chemical space that is optimal for oral drug delivery that is provided by Lipinski's rule of 5 (and variations thereof). However, there are gaps in knowledge that specifically relate to many newer DDS as well as the chemical compatibility of drugs with the DDS and with specific applications (e.g. LA/ER depot delivery).

One of the significant gaps in HIV/AIDS DDS research is targeting to sites of infection in order to achieve effective ART concentrations. Another significant gap is the ability to prolong ART effectiveness in order to reduce the frequency of administration and burden on patients. Classic sustained release technologies currently being utilized in LA/ER PrEP have proven the feasibility

of the approach. However, significant improvements are needed. This suggests a major opportunity for DD research – the marriage of targeting technologies and techniques to sustain not just the release of ART but, more importantly, the effect.

Since the overwhelming burden of HIV disease continues to fall upon individuals in resource-limited settings, there are societal implications that need to be considered if novel technologies are to impact significantly on the HIV pandemic. Some novel DDS challenge convention in terms of route of delivery, and consideration needs to be given to compatibility with existing global healthcare systems and acceptability of the approach to patients with different cultural backgrounds. Clearly, it is imperative that early technological development and selection of technologies for further development consider cost, and compatibility of the platform with sterile production of the medicine at scale.

3.9. Acknowledgements – Supported by the National Institutes of Health, National Institute of Allergy and Infectious Diseases Awards R37 AI051214, R01 AI117776 and R24 AI118397.

3.10. Figures

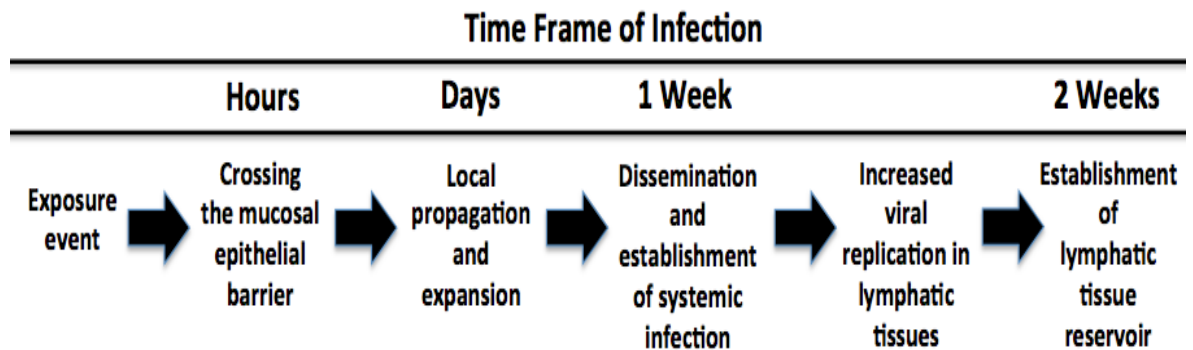


Figure 1. Approximate timeline for establishing HIV infection after vaginal exposure to HIV [3]. This timeline suggests a window of opportunity for PrEP therapy. Given the difficult logistics of diagnosing and initiating treatment immediately post transmission, PrEP delivers effective drug concentrations for at risk populations prior to exposure (adapted from [3]).

Name	MOA	Status	Source (Reference, trial number)
Tenofovir disoproxil fumarate (TDF)	RT inhibition	Approved 2012, Truvada	[32]
Emtricitabine, FTC	RT inhibition		
Tenofovir alafenamide (TAF, GS-7340)	RT inhibition	Investigational prodrug of TFV	[33]
Rilpivirine (TMC-278)	NNRT inhibition	Recruiting	[34]
Cabotegravir (GSK 744) (S/GSK1265744)	InST inhibition	Not yet recruiting	[35, 36]
Maraviroc	CCR5 antagonism	Ongoing trial	NCT01505114 [37]
Ciclopirox	TRAP	Recruiting	[38, 39]
Deferiprone			

Table 1. Recent drugs in use or development (MOA: mechanism of action; TRAP: therapeutic reclamation of apoptotic proficiency).

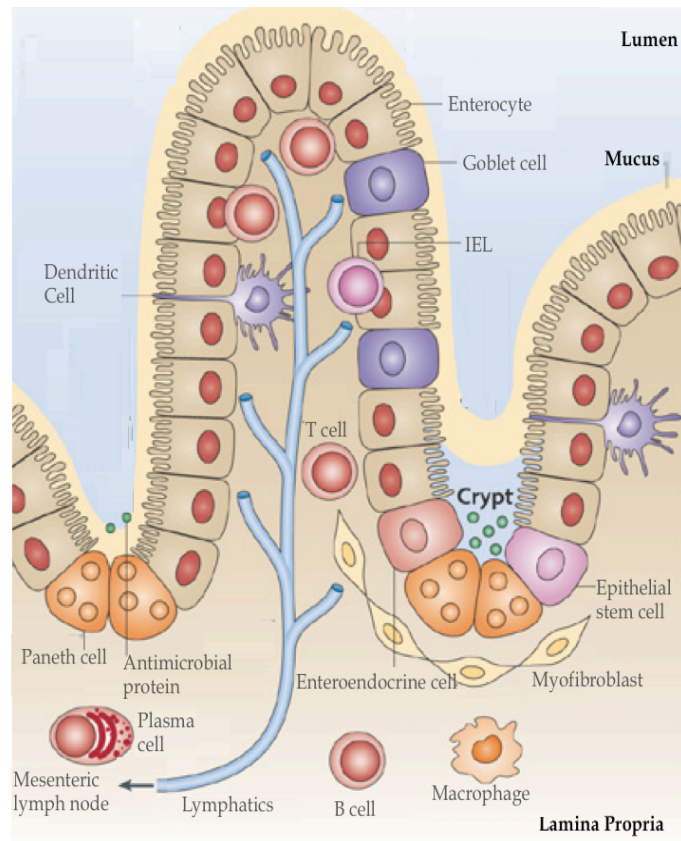


Figure 2. Colorectal Mucosal Barriers and HIV Transmission Pathway. A single epithelial layer provides a barrier between the intestinal lumen and the lamina propria. The cells most susceptible to/or responsible for propagating early HIV infection, $CD4^+$ T-cells, macrophages, dendritic cells, Langerhans cells and M-cells are located in the Lamina Propria. The lymphatics play an important role in the dissemination of HIV into the systemic circulation. (Image adapted from [79] with permission)

3.11. References

- [1] WHO [Internet].; 2015 [updated July 2015;]. Available from: <http://www.who.int/mediacentre/factsheets/fs360/en/>.
- [2] Tognotti E. The eradication of smallpox, a successful story for modern medicine and public health: What lessons for the future? *J Infect Dev Ctries*. 2010;4(5):264-266.
- [3] Haase AT. Targeting early infection to prevent HIV-1 mucosal transmission. *Nature*. 2010;464(7286):217-223.
- [4] Sáez-Cirión A, Bacchus C, Hocqueloux L, Avettand-Fenoel V, G, I., Lecuroux C, et al. Post-treatment HIV-1 controllers with a long-term virological remission after the interruption of early initiated antiretroviral therapy ANRS VISCONTI Study. *PLOS Pathog*. 2013;9(3):e1003211.
- [5] Salgado M, Rabi SA, O'Connell KA, Buckheit III RW, Bailey JR, Chaudhry AA, et al. Prolonged control of replication-competent dual-tropic human immunodeficiency virus-1 following cessation of highly active antiretroviral therapy. *Retrovirology*. 2011;8(97).
- [6] Buckheit Jr. RW, Watson KM, Morrow KM, Ham AS. Development of Topical Microbicides to Prevent the Sexual Transmission of HIV. *Antiviral Res*. 2010;85(1):142.
- [7] Garg A, Nuttall J, Romano J. The future of HIV microbicides: challenges and opportunities. *Antivir Chem & Chemother*. 2009;19(4):143-150.
- [8] Senise JF, Castelo A, Martinez M. Current treatment strategies, complications and considerations for the use of HIV antiretroviral therapy during pregnancy. *AIDS Rev*. 2011;13(4):198-213.
- [9] Tebit DM, Arts EJ. Tracking a century of global expansion and evolution of HIV to drive understanding and to combat disease. *Lancet Infect Dis*. 2011;11(1):45-56.
- [10] Gruell H, Klein F. Opening Fronts in HIV Vaccine Development: Tracking the development of broadly neutralizing antibodies. *Nat Med*. 2014;20(5):478-479.
- [11] Eisele E, Siliciano RF. Redefining the viral reservoirs that prevent HIV-1 eradication. *Immunity*. 2012;37(3):377-388.
- [12] Sarmati L, D'Ettoire G, Parisi SG, Andreoni M. HIV Replication at Low Copy Number and its Correlation with HIV Reservoir: A Clinical Perspective. *Curr HIV Res*. 2015;13(3):250-257.
- [13] Svicher V, Ceccherini-Silberstein F, Antinori A, Aquaro S, Perno CF. Understanding HIV compartments and reservoirs. *Curr HIV/AIDS Rep*. 2014;11(2):186-194.
- [14] Cory TJ, Schacker TW, Stevenson M, Fletcher CV. Overcoming pharmacologic sanctuaries. *Curr Opin HIV AIDS*. 2013;8(3):190-195.
- [15] Siewe B, Landay A. Key Concepts in the Early Immunology of HIV-1 Infection. *Curr Infect Dis Rep*. 2012;14(1):102-109.
- [16] Walker B, McMichael A. The T-cell response to HIV. *Cold Spring Harb Perspect Med*. 2012;2(11).
- [17] Veazey RS, Lackner AA. Getting to the guts of HIV pathogenesis. *J Exp Med*. 2004;200(6):697-700.
- [18] Cavarelli M, Scarlatti G. HIV-1 infection: the role of the gastrointestinal tract. *Am J Reprod Immunol*. 2014;71(6):537-542.
- [19] Assimakopoulos SF, Dimitropoulou D, Marangos M, Gogos CA. Intestinal barrier dysfunction in HIV infection: pathophysiology, clinical implications and potential therapies. *Infection*. 2014;42(6):951-959.
- [20] Santangelo PJ, Rogers KA, Zurla C, Blanchard EL, Gumber S, Strait K, et al. Whole-body immunoPET reveals active SIV dynamics in viremic and antiretroviral therapy-treated macaques. *Nat Methods*. 2015;12(5):427-432.
- [21] Tebit DM, Ndembu N, Weinberg A, Quinones-Mateu ME. Mucosal transmission of human immunodeficiency virus. *Curr HIV Res*. 2012;10(1):3-8.
- [22] Li Q, Estes JD, Schlievert PM, Duan L, Brosnahan AJ, Southern PJ, et al. Glycerol monolaurate prevents mucosal SIV transmission. *Nature*. 2009;458(7241):1034-1038.

- [23] FDA-Approved HIV Medicines [Internet].; 2015 [updated May 2015;]. Available from: <https://aidsinfo.nih.gov/education-materials/fact-sheets/21/58/fda-approved-hiv-medicines>.
- [24] Wong A. The HIV pipeline. *Nature Reviews Drug Discovery*. 2014;13:649-650.
- [25] Cox BD, Prosser AR, Sun Y, Li Z, Lee S, Huang MB, et al. Pyrazolo-Piperidines Exhibit Dual Inhibition of CCR5/CXCR5 HIV Entry and Reverse Transcriptase. *ACS Med Chem Lett*. 2015;6:753-757.
- [26] Chong H, Qui Z, Su Y, He Y. The N-terminal T-T Motif of a Third-Generation HIV-1 Fusion Inhibitor Is Not Required for Binding Affinity and Antiviral Activity. *J Med Chem*. 2015;Just Accepted Manuscript:1-43.
- [27] Gogtay JA, Malhotra G. Reformulation of existing antiretroviral drugs. *Curr Opin HIV AIDS*. 2013;8(6):550-555.
- [28] Falcon RW, Kakuda TN. Drug interactions between HIV protease inhibitors and acid-reducing agents. *Clin Pharmacokinet*. 2008;47(2):75-89.
- [29] Adams JL, Greener BN, Kashuba AD. Pharmacology of HIV integrase inhibitors. *Curr Opin HIV AIDS*. 2012;7(5):390-400.
- [30] Kakuda TN, Falcon RW. Effect of food and ranitidine on saquinavir pharmacokinetics and gastric pH in healthy volunteers. *Pharmacotherapy*. 2006;26(8):1060-1068.
- [31] Owen A. The impact of host pharmacogenetics on antiretroviral drug disposition. *Curr Infect Dis Rep*. 2006;8(5):401-408.
- [32] Press Announcements: FDA approves first drug for reducing the risk of sexually acquired HIV infection [Internet].; 2012 [updated July 2012;]. Available from: <http://www.fda.gov/NewsEvents/Newsroom/PressAnnouncements/ucm312210.htm>.
- [33] Callebaut C, Stepan G, Tian Y, Miller MD. *In Vitro* Virology Profile of Tenofovir Alafenamide, a Novel Oral Prodrug of Tenofovir with Improved Antiviral Activity Compared to Tenofovir Disoproxil. *Antimicrob Agents Chemother*. 2015;Accepted manuscript posted online 6 July 2015.
- [34] Jackson AG, Else LJ, Mesquita PM, Egan D, Back DJ, Karolia Z, et al. A compartmental pharmacokinetic evaluation of long-acting rilpivirine in HIV-negative volunteers for pre-exposure prophylaxis. *Clin Pharmacol Ther*. 2014;96(3):314-323.
- [35] Andrews CD, Heneine W. Cabotegravir long-acting for HIV prevention. *Curr Opin HIV AIDS*. 2015;10(4):258-263.
- [36] Pharmacokinetic Study of Cabotegravir Long-acting in Healthy Adult Volunteers [Internet].; 2015 [updated June 2015;]. Available from: <https://www.clinicaltrials.gov/ct2/show/NCT02478463>.
- [37] Evaluating the Safety and Tolerability of Antiretroviral Drug Regimens Used as Pre-Exposure Prophylaxis to Prevent HIV Infection in At-Risk Men Who Have Sex With Men and in At-Risk Women [Internet].; 2015 [updated August 2015;]. Available from: <https://clinicaltrials.gov/ct2/show/NCT01505114>.
- [38] Evaluation of the Safety, Efficacy, and Pharmacokinetics of Intravenous Deferiprone in HIV-Positive Subjects [Internet].; 2015 [updated July 2015;]. Available from: <https://clinicaltrials.gov/ct2/show/NCT02456558?term=deferiprone+hiv&rank=2>.
- [39] Hanauske-Abel H, Saxena D, Palumbo PE, Hanauske A, Luchessi AD, Cambiaghi TD, et al. Drug-Induced Reactivation of Apoptosis Abrogates HIV-1 Infection. *PLoS ONE*. 2013;8(9):e74414.
- [40] Friend D, Kiser PF. Assessment of topical microbicides to prevent HIV-1 transmission: Concepts, testing, lessons learned. *Antiviral Res*. 2013;99(3):391-400.
- [41] Karim SSA. Microbicides for the Prevention of HIV Infection. 2nd South African AIDS Conference in Durban, South Africa. 2005:30-40.
- [42] Mcgowan I. An Overview of Antiretroviral Pre-Exposure Prophylaxis of HIV Infection. *Am J Reprod Immunol*. 2014;71(6):624-630.

- [43] Omar RF, Bergeron MG. The future of microbicides. *International Journal of Infectious Diseases*. 2011;15:e656-e660.
- [44] Shattock RJ, Rosenberg Z. Microbicides: Topical Prevention against HIV. *Cold Spring Harb Perspect Med*. 2012;2(2):1-17.
- [45] Spreen WR, Margolis DA, Pottage JC. Long-acting injectable antiretrovirals for HIV treatment and prevention. *Curr Opin HIV AIDS*. 2013;8:565-571.
- [46] Thompson CG, Cohen MS, Kashuba ADM. Antiretroviral Pharmacology in Mucosal Tissues. *J Acquir Immune Defic Syndr*. 2013;63(0 2):S240-S247.
- [47] Hendrix CW. The clinical pharmacology of antiretrovirals for HIV prevention. *Curr Opin HIV AIDS*. 2012;7(6):498-504.
- [48] Tsai C, Follis KE, Sabo A, Beck TW, Grant RF, Bischofberger N, et al. Prevention of SIV Infection in Macaques by (R)-9-(2-Phosphonylmethoxypropyl)adenine. *Science*. 1995;270:1197-1199.
- [49] Gallant JE, Deresinski S. Tenofovir Disoproxil Fumarate. *Clin Infect Dis*. 2003;37(7):944-950.
- [50] Grant R, Lama JR, Anderson PL, McMahan V, Lui AY, Vargas L, et al. Preexposure Chemoprophylaxis for HIV Prevention in Men Who Have Sex with Men. *N Engl J Med*. 2010;363(27):2587-2599.
- [51] Donnell D, Baeten J, Bumpus N, Brantley J, Bangsberg D, Haberer J, et al. HIV Protective Efficacy and Correlates of Tenofovir Blood Concentrates in a Clinical Trial of PrEP for HIV Prevention. *J Acquir Immune Defic Syndr*. 2014;66(3):340-348.
- [52] Herold BC, Scordi-Bello I, Cheshenko N, Marcellino D, Dzuzelewski M, Francois F, et al. Mandelic Acid Condensation Polymer: Novel Candidate Microbicide for Prevention of Human Immunodeficiency Virus and Herpes Simplex Virus Entry. *J Virol*. 2002;76(22):11236-11244.
- [53] Gagné N, Cormier H, Omar R, Désormeaux A, Gourde P, Tremblay M, et al. Protective Effect of a Thermoreversible Gel Against the Toxicity of Nonoxynol-9. *Sexually Transmitted Diseases*. 1999;26(3):177-183.
- [54] Morrow KM, Underhill K, van den Berg, Jacob J., Vargas S, Rosen RK, Katz DF. User-Identified Gel Characteristics: A Qualitative Exploration of Perceived Product Efficacy of Topical Vaginal Microbicides. *Arch Sex Behav*. 2014;43:1459-1467.
- [55] Morrow KM, Fava JL, Rosen RK, Vargas S, Shaw JG, Kojic EM, et al. Designing Preclinical Perceptibility Measures to Evaluate Topical Vaginal Ge Formulations: Relating User Sensory Perceptions and Experiences to Formulaton Properties. *AIDS Res Hum Retroviruses*. 2014;30(1):78-91.
- [56] Nunes R, Sarmiento B, das Neves J. Formulation and delivery of anti-HIV rectal microbicides: Advances and challenges. *Journal of Controlled Release*. 2014(194):278-294.
- [57] Abdool Karim S, Baxter C. Microbicides for Prevention of HIV Infection: Clinical Efficacy Trials. In: *Current Topics in Microbiology and Immunology*. Springer-Verlag; 2014. p. 97-115.
- [58] Dezzutti CS, Rohan LC, Wang L, Uranker K, Shetler C, Cost M, et al. Reformulated tenofovir gel for use as a dual compartment microbicide. *J Antimicrob Chemother*. 2012;67:2139-2142.
- [59] Kiser PF, Johnson TJ, Clark JT. State of the Art in Intravaginal Ring Technology for Topical Prophylaxis of HIV Infection. *AIDS Rev*. 2012(14):62.
- [60] Singh O, Garg T, Rath G, Goyal AK. Microbicides for the Treatment of Sexually Transmitted HIV infections. *Journal of Pharmaceutics*. 2014;2014:1-18.
- [61] Abdool Karim Q, Abdool Karim SS, Frohlich J, Grobler A, Baxter C, Mansoor L, et al. Effectiveness and Safety of Tenofovir Gel, an Antiretroviral Microbicide, for the Prevention of HIV Infection in Women. *Science*. 2010;329(5996):1168-1174.
- [62] Haaland R, Evans-Strickfaden T, Holder A, Pau C, McNicholl J, Chaikummao S. UC781 microbicide gel retains anti-HIV activity in cervicovaginal lavage fluids collected following twice-daily vaginal application. *Antimicrob Agents Chemother*. 2012;56(7):3592-3596.

- [63] Nel A, Smythe S, Young K, Malcolm K, McCoy C, Rosenberg Z, et al. Safety and Pharmacokinetics of Dapivirine Delivery From Matrix and Reservoir Intravaginal Rings to HIV-Negative Women. *J Acquir Immune Defic Syndr*. 2009;51(4):416-423.
- [64] Nel A, Haazen W, Nuttall J, Romano J, Rosenberg Z, van Niekerk N. A safety and pharmacokinetic trial assessing delivery of dapivirine from a vaginal ring in healthy women. *AIDS*. 2014;28:1479-1487.
- [65] Nuttall JP, Thake DC, Lewis MG, Ferkany JW, Romano JW, Mitchnick MA. Concentrations of dapivirine in the rhesus macaque and rabbit following once daily intravaginal administration of a gel Formulation of [¹⁴C]dapivirine for 7 days. *Antimicrob Agents Chemother*. 2008;52(3):909-914.
- [66] Akil A, Devlin B, Cost M, Rohan LC. Increased Dapivirine Tissue Accumulation through Vaginal Film Codelivery of Dapivirine and Tenofovir. *Mol Pharmaceutics*. 2014;12:1533-1541.
- [67] Johnson TJ, Clark MR, Albright TH, Nebeker JS, Tuitupou AL, Clark JT, et al. A 90-Day Tenofovir Reservoir Intravaginal Ring for Mucosal HIV. *Antimicrobial Agents and Chemotherapy*. 2012;56(12):6272.
- [68] Boyd P, Desjardins D, Kumar S, Fetherston SM, Le-Grand R, Dereuddre-Bosquet N, et al. A Temperature-Monitoring Vaginal Ring for Measuring Adherence. *PLoS ONE*. 2015;10(5):1-19.
- [69] Nel AM, Mitchnick LB, Risha P, Muungo LTM, Norick PM. Acceptability of Vaginal Film, Soft Gel Capsule, and Tablet as Potential Microbicide Delivery Methods Among African Women. *Journal of Women's Health*. 2011;20(8):1207-1214.
- [70] Akil A, Agashe H, Dezzutti CS, Moncla BJ, Hillier SL, Devlin B, et al. Formulation and Characterization of Polymeric Films Containing Combinations of Antiretrovirals (ARVs) for HIV Prevention. *Pharm Res*. 2015;32:458-468.
- [71] Akil A, Parniak MA, Dezzutti CS, Moncla BJ, Cost M, Li M, et al. Development and Characterization of a Vaginal Film Containing Dapivirine, a Non-nucleoside Reverse Transcriptase Inhibitor (NNRTI), for Prevention of HIV-1 Sexual Transmission. *Drug Deliv Transl Res*. 2011;1(3):209-222.
- [72] Zhang W, Hu M, Shi Y, Gong T, Dezzutti CS, Moncla B, et al. Vaginal Microbicide Film Combinations of Two Reverse Transcriptase Inhibitors, EFdA and CSIC, for Prevention of HIV-1 Sexual Transmission. *Pharm Res*. 2015(DOI 10.1007/s11095-015-1678-2).
- [73] Antimisiaris SG, Mourtas S. Recent advances on anti-HIV vaginal delivery systems development. *Adv Drug Deliv Rev*. 2015(<http://dx.doi.org/10.1016/j.addr.2015.03.015>).
- [74] Chaowanachan T, Krogstad E, Ball C, Woodrow KA. Drug Synergy of Tenofovir and Nanoparticle-Based Antiretrovirals for HIV Prophylaxis. *PLoS ONE*. 2013;8(4):e61416.
- [75] das Neves J, Araújo F, Andrade F, Michiels J, Ariën KK, Vanham G, et al. In vitro and ex vivo evaluation of polymeric nanoparticles for vaginal and rectal delivery of the anti-HIV drug dapivirine. *Mol Pharm*. 2013;10(7):2793-2807.
- [76] Sharma P, Garg S. Pure drug and polymer based nanotechnologies for the improved solubility, stability, bioavailability and targeting of anti-HIV drugs. *Adv Drug Deliv Rev*. 2010;62(4-5):491-502.
- [77] das Neves J, Nunes R, Machado A, Sarmento B. Polymer-based nanocarriers for vaginal drug delivery. *Adv Drug Deliv Rev*. 2015(<http://dx.doi.org/10.1016/j.addr.2014.12.004>).
- [78] Hladik F, Hope TJ. HIV infection of the genital mucosa in women. *Curr HIV/AIDS Rep*. 2009;6(1):20-28.
- [79] Abreu MT. Toll-like receptor signalling in the intestinal epithelium: how bacterial recognition shapes intestinal function. *Nature Review Immunology*. 2010;10:131-144.
- [80] Hendrix CW, Fuchs EJ, Macura KJ, Lee LA, Parsons TL, Bakshi RP, et al. Quantitative Imaging and Sigmoidoscopy to Assess Distribution of Rectal Microbicide Surrogates. *Clinical Pharmacology & Therapeutics*. 2008;83(1):97-105.

- [81] Cao YJ, Caffo B, S., Fuchs EJ, Lee LA, Du Y, Li L, et al. Quantification of the spatial distribution of rectally applied surrogates for microbicide and semen in colon with SPECT and magnetic resonance imaging. *Br J Clin Pharmacol*. 2012;74(6):1013-1022.
- [82] Louissant NA, Nimmagadda S, Fuchs EJ, Bakshi RP, Cao Y, Lee LA, et al. Distribution of Cell-free and Cell-associated HIV surrogates in the Colon Following Simulated Receptive Anal Intercourse in Men who Have Sex with Men. *J Acquir Immune Defic Syndr*. 2012;59(1):10-17.
- [83] Carballo-Diéguez A, Exner T, Dolezal C, Pickard R, Lin P, Mayer KH. Rectal Microbicide Acceptability: Results of a Volume Escalation Trial. *Sexually Transmitted Diseases*. 2007;34(4):224-229.
- [84] Morrow KM, Hendrick C. Clinical Evaluation of Microbicide Formulations. *Antiviral Res*. 2010;88(Suppl 1):S40-S46.
- [85] Mgowan I, Dezzutti C. Rectal Microbicide Development. *Curr Top in Microbiol Immunol*. 2014;383:117-136.
- [86] Anton PA, Saunders T, Elliott J, Khanukhova E, Dennis R, Adler A, et al. First Phase 1 Double-Blind, Placebo-Controlled, Randomized Rectal Microbicide Trial Using UC781 Gel with a Novel Index of Ex Vivo Efficacy. *PLoS ONE*. 2011;6(9).
- [87] Anton PA, Cranston RD, Kashuba ADM, Hendrix CW, Bumpus N, Richardson-Harman N, et al. RMP-02/MTN-006: A Phase 1 Rectal Safety, Acceptability, Pharmacokinetic, and Pharmacodynamic Study of Tenofovir 1% Gel Compared with Oral Tenofovir Disoproxil Fumarate. *AIDS Res Hum Retroviruses*. 2012;28(11):1412-1421.
- [88] Mgowan I, Cranston RD, Duffill K, Siegel A, Engstrom JC, Nikiforov A, et al. A Phase 1 Randomized, Open Label, Rectal Safety, Acceptability, Pharmacokinetic, and Pharmacodynamic Study of Three Formulations of Tenofovir 1% Gel (the CHARM-01 Study). *PLoS ONE*. 2015;10(5):e0125363.
- [89] Telwatte S, Moore K, Johnson A, Tyssen D, Sterjovski J, Aldunate M, et al. Virucidal Activity of the Dendrimer Microbicide SPL7013 Against HIV-1. *Antiviral Res*. 2011;90(3):195.
- [90] das Neves J, Michiels J, Arien KK, Vanham G, Amiji M, Bahia MF, et al. Polymeric Nanoparticles Affect the Intracellular Delivery, Antiretroviral Activity and Cytotoxicity of the Microbicide Drug Candidate Dapivirine. *Pharm Res*. 2012(29):1468.
- [91] das Neves J, Araujo F, Andrade F, Michiels J, Arien KK, Vanham G, et al. *In Vitro* and *Ex Vivo* Evaluation of polymeric Nanoparticles for Vaginal and Rectal Delivery of Anti-HIV Drug Dapivirine. *Mol Pharmaceutics*. 2013;10:2793.
- [92] Sarmiento B, das Neves J. Nanosystem formulations for rectal microbicides: a call for more research. *Therapeutic Delivery*. 2012;3(1):1-4.
- [93] Ramana LN, Anand AR, Sethuranam S, Krishnan UM. Targeting strategies for delivery of anti-HIV drugs. *J Control Release*. 2014;192:271-283.
- [94] Wong HL, Chattopadhyay N, Wu XY, Bendayan R. Nanotechnology applications for improved delivery of antiretroviral drugs to the brain. *Adv Drug Deliv Rev*. 2010;62(4-5):503-517.
- [95] Gupta U, Jain NK. Non-polymeric nano-carriers in HIV/AIDS drug delivery and targeting. *Adv Drug Deliv Rev*. 2010;62(4-5):478-490.
- [96] Date AA, Destache CJ. A review of nanotechnological approaches for the prophylaxis of HIV/AIDS. *Biomaterials*. 2013;34(26):6202-6228.
- [97] das Neves J, Amiji MM, Bahia MF, Sarmiento B. Nanotechnology-based systems for the treatment and prevention of HIV/AIDS. *Adv Drug Deliv Rev*. 2010 62;4-5:458-477.
- [98] Ananworanich J, Schuetz A, Vandergeeten C, Sereti I, de Souza M, Rerknimitr R, et al. Impact of Multi-Targeted Antiretroviral Treatment on Gut T Cell Depletion and HIV Reservoir Seeding during Acute HIV Infection. *PLoS ONE*. 2012;7(3):e33948.
- [99] Ensign LM, Cone R, Hanes J. Oral drug delivery with polymeric nanoparticles: The gastrointestinal mucus barriers. *Adv Drug Deliv Rev*. 2012;64:557-570.

- [100] Willits RK, Saltzman WM. Synthetic polymers alter the structure of cervical mucus. *Biomaterials*. 2001;22:445-452.
- [101] Norris DA, Sinko PJ. Effect of size, surface charge, and hydrophobicity on the translocation of polystyrene microspheres through gastrointestinal mucin. *J Appl Polym Sci*. 1997;63(11):1481-1492.
- [102] Norris DA, Puri N, Sinko PJ. The effect of physical barriers and properties on the oral absorption of particulates. *Adv Drug Deliv Rev*. 1998;34(2-3):135-154.
- [103] Pridgen EM, Alexis F, Kuo TT, Levy-Nissenbaum E, Karnik R, Blumberg RS, et al. Transepithelial Transport of Fc-Targeted Nanoparticles by the Neonatal Fc Receptor for Oral Delivery. *Nanomedicine*. 2013;5(213):213ra167.
- [104] Porter CJH, Trevaskis NL, Charman WN. Lipids and lipid-based formulations: optimizing the oral delivery of lipophilic drugs. *Nature Reviews: Drug Discovery*. 2007;6:231-248.
- [105] Harde H, Das M, Jain S. Solid lipid nanoparticles: an oral bioavailability enhancer vehicle. *Expert Opinion on Drug Delivery*. 2011;8(11):1407-1424.
- [106] Aji Alex MR, Chacko AJ, Jose S, Souto EB. Lopinavir loaded solid lipid nanoparticles (SLN) for intestinal lymphatic targeting. *European Journal of Pharmaceutical Sciences: Official Journal of the European Federation for Pharmaceutical Sciences*. 2011;42(1-2):11-18.
- [107] Ravi PR, Vats R, Dalal V, Murthy AN. A hybrid design to optimize preparation of lopinavir loaded solid lipid nanoparticles and comparative pharmacokinetic evaluation with marketed lopinavir/ritonavir coformulation. *The Journal of Pharmacy and Pharmacology*. 2014;66(7):912-926.
- [108] Negi JS, Chattopadhyay P, Sharma AK, Ram V. Development of solid lipid nanoparticles (SLNs) of lopinavir using hot self nano-emulsification (SNE) technique. *European Journal of Pharmaceutical Sciences: Official Journal of the European Federation for Pharmaceutical Sciences*. 2013;48(1-2):231-239.
- [109] Bunjes H. Lipid nanoparticles for the delivery of poorly water-soluble drugs. *The Journal of pharmacy and pharmacology. The Journal of Pharmacy and Pharmacology*. 2010;62(11):1637-1645.
- [110] Chiappetta DA, Hocht C, Taira C, Sosnik A. Oral pharmacokinetics of the anti-HIV efavirenz encapsulated within polymeric micelles. *Biomaterials*. 2011;32(9):2379-2387.
- [111] McDonald TO, Giardiello M, Martin P, Siccardi M, Liptrott NJ, Smith D, et al. Antiretroviral solid drug nanoparticles with enhanced oral bioavailability: production, characterization, and in vitro-in vivo correlation^{br />}. *Advanced Healthcare Materials*. 2014;3(3):400-411.
- [112] Dembri A, Montisci MJ, Gantier JC, Chacun H, Ponchel G. Targeting of 3'-azido 3'-deoxythymidine (AZT)-loaded poly(isohexylcyanoacrylate) nanospheres to the gastrointestinal mucosa and associated lymphoid tissues. *Pharm Res*. 2001;18(4):467-473.
- [113] Kinman L, Brodie SJ, Tsai CC, Bui T, Larsen K, Schmidt A, et al. Lipid-drug association enhanced HIV-1 protease inhibitor indinavir localization in lymphoid tissues and viral load reduction: a proof of concept study in HIV-2287-infected macaques. *J Acquir Immune Defic Syndr*. 2003;34(4):387-397.
- [114] Kinman L, Bui T, Larsen K, Tsai CC, Anderson D, Morton WR, et al. Optimization of Lipid-Indinavir Complexes for Localization in Lymphoid Tissues of HIV-Infected Macaques. *J Acquir Immune Defic Syndr*. 2006;42(2):155-161.
- [115] Duan J, Freeling JP, Koehn J, Shu C, Ho RJ. Evaluation of atazanavir and darunavir interactions with lipids for developing pH-responsive anti-HIV drug combination nanoparticles. *J Pharm Sci*. 2014;103(8):2520-2529.
- [116] Freeling JP, Koehn J, Shu C, Sun J, Ho RJ. Long-acting three-drug combination anti-HIV nanoparticles enhance drug exposure in primate plasma and cells within lymph nodes and blood. *AIDS*. 2014;28(17):2625-2627.

- [117] Gunaseelan S, Gunaseelan K, Deshmukh M, Zhang X, Sinko PJ. Surface modifications of nanocarriers for effective intracellular delivery of anti-HIV drugs. *Adv Drug Deliv Rev.* 2010;62(4-5):518-531.
- [118] Zhou N, Luo Z, Luo J, Fan X, Cayabyab M, Hiraoka M, et al. Exploring the stereochemistry of CXCR4-peptide recognition and inhibiting HIV-1 entry with D-peptides derived from chemokines. *J Biol Chem.* 2002;277(20):17476-17485.
- [119] Xu Y, Duggineni S, Espitia S, Richman DD, An J, Huang Z. A synthetic bivalent ligand of CXCR4 inhibits HIV infection. *Biochem Biophys Res Commun.* 2013;435(4):646-650.
- [120] Tamamura H, Omagari A, Oishi S, Kanamoto T, Yamamoto N, Peiper SC, et al. Pharmacophore Identification of a Specific CXCR4 Inhibitor, T140, Leads to Development of Effective Anti-HIV Agents with Very High Selectivity Indexes. *Bioorg Med Chem Lett.* 2000;10:2633-2637.
- [121] Inokuchi E, Oishi S, Kubo T, Ohno H, Shimura K, Matsuoka M, et al. Potent CXCR4 Antagonists Containing Amidine Type Peptide Bond Isosteres. *ACS Med Chem Lett.* 2011;2:477-480.
- [122] Tamamis P, Floudas CA. Molecular recognition of CCR5 by an HIV-1 gp120 V3 loop. *PLoS ONE.* 2014;9(4):e95767.
- [123] Bellows ML, Taylor MS, Cole PA, Shen L, Siliciano RF, Fung HK, et al. Discovery of entry inhibitors for HIV-1 via a new de novo protein design framework. *Biophys J.* 2010;99(10):3445-3453.
- [124] Dutta T, Agashe HB, Garg M, Balakrishnan P, Kabra M. Poly (propyleneimine) dendrimer based nanocontainers for targeting of efavirenz to human monocytes/macrophages in vitro. *J Drug Target.* 2007;15(1):89-98.
- [125] Pooyan S, Qui B, Chan MM, Fong D, Sinko PJ, Leibowitz MJ, et al. Conjugates bearing multiple formyl-methionyl peptides display enhanced binding to but not activation of phagocytic cells. *Bioconj Chem.* 2002;13(2):216-223.
- [126] Chen P, Zhang X, Jia L, Prud'homme RK, Szekely Z, Sinko PJ. Optimal structural design of mannosylated nanocarriers for macrophage targeting. *J Control Release.* 2014;194:341-349.
- [127] D'Addio SM, Baldassano S, Shi L, Cheung L, Adamson DH, Bruzek M, et al. Optimization of cell receptor-specific targeting through multivalent surface decoration of polymeric nanocarriers. *J Control Release.* 2013;168(1):41-49.
- [128] Nowacek AS, Miller RL, McMillan J, Kanmogne G, Kanmogne M, Mosley RL, et al. NanoART synthesis, characterization, uptake, release and toxicology for human monocyte-macrophage drug delivery. *Nanomedicine (Lond).* 2009;4(8):903-917.
- [129] Magnani M, Rossi L, Fraternali A, Silvotti L, Quintavalla F, Piedimonte G, et al. Feline immunodeficiency virus infection of macrophages: in vitro and in vivo inhibition by dideoxycytidine-5'-triphosphate-loaded erythrocytes. *AIDS Res Hum Retroviruses.* 1994;10(9):1179-1186.
- [130] Dou H, Grotepas CB, McMillan JM, Destache CJ, Chaubal M, Werling J, et al. Macrophage delivery of nanoformulated antiretroviral drug to the brain in a murine model of neuroAIDS. *J Immunol.* 2009;183(1):661-669.
- [131] Martinez-Skinner AL, Veerubhotla RS, Liu H, Xiong H, Yu F, McMillan JM, et al. Functional proteome of macrophage carried nanoformulated antiretroviral therapy demonstrates enhanced particle carrying capacity. *J Proteome Res.* 2013;12(5):2282-2294.
- [132] Aouadi M, Tesz GJ, Nicoloso SM, Wang M, Chouinard M, Soto E, et al. Orally delivered siRNA targeting macrophage Map4k4 suppresses systemic inflammation. *Nature.* 2009;458(7242):1180-1184.
- [133] Steinbach JM. Protein and oligonucleotide delivery systems for vaginal microbicides against viral STIs. *Cell Mol Life Sci.* 2015;72:469-503.
- [134] Wang HB, Mo QH, Yang Z. HIV vaccine research: the challenge and the way forward. *J Immunol Res.* 2015;2015:503978.

- [135] Jardine J, Julien JP, Menis S, Ota T, Kalyuzhniy O, McGuire A, et al. Rational HIV immunogen design to target specific germline B cell receptors. *Science*. 2013;340(6133):711-716.
- [136] Hütter G, Nowak D, Mossner M, Ganepola S, Müßig A, Allers K, et al. Long-term control of HIV by CCR5 Delta32/Delta32 stem-cell transplantation. *N Engl J Med*. 2009;360(7):692-698.
- [137] Peterson CW, Younan P, Jerome KR, Kiem HP. Combinational anti-HIV gene therapy: using a multipronged approach to reach beyond HAART. *Gene Ther*. 2013;20(7):695-702.
- [138] Hu W, Kaminski R, Yang F, Zhang Y, Cosentino L, Li F, et al. RNA-directed gene editing specifically eradicates latent and prevents new HIV-1 infection. *Proc Natl Acad Sci U S A*. 2014;111(31):11461-11466.
- [139] Elliott JH, Wightman F, Solomon A, Ghneim K, Ahlers J, Cameron MJ, et al. Activation of HIV transcription with short-course vorinostat in HIV-infected patients on suppressive antiretroviral therapy. *PLOS Pathog*. 2014;10(10):e1004473.
- [140] Williams J, Sayles HR, Meza JL, Sayre P, Sandkovsky U, Gendelman HE, et al. Long-acting parenteral nanoformulated antiretroviral therapy: interest and attitudes of HIV-infected patients. *Nanomedicine (Lond)*. 2013;8:1807-1813.
- [141] Swindells S, Flexner C, Fletcher CV, Jacobson JM. The critical need for alternative antiretroviral formulations and obstacles to their development. *J Infect Dis*. 2011;204:669-674.
- [142] Adams CE, Fenton MKP, Quraishi S, David AS. Systematic meta-review of depot antipsychotic drugs for people with schizophrenia. *Brit J Psychiatry*. 2001;179:290-299.
- [143] Westhoff C. Depot-medroxyprogesterone acetate injection (Depo-Provera): a highly effective contraceptive option with proven long-term safety. *Contraception*. 2003;68:75-87.
- [144] Dolgin E. Long-acting HIV drugs advanced to overcome adherence challenge. *Nature Med*. 2014;20:323-324.
- [145] Flexner C, Saag M. The antiretroviral drug pipeline: prospects and implications for future treatment research. *Curr Opin HIV/AIDS*. 2013;8:572-578.
- [146] Jackson A, Else L, Tjia J, et al. Rilpivirine-LA formulation: pharmacokinetics in plasma, genital tract in HIV-females and rectum in males [Abstract no. 35]. 19th Conference on Retroviruses and Opportunistic Infections; Seattle WA. 2012.
- [147] Andrews CD, Spreen WR, Mohri H, Moss L, Ford S, Gettie A, et al. Long-acting integrase inhibitor protects macaques from intrarectal simian/human immunodeficiency virus. *Science*. 2014;343(6175):1151-1154.
- [148] Andrews CD, Yueh YL, Spreen WR, St Bernard L, Boente-Carrera M, Rodriguez K, et al. A long-acting integrase inhibitor protects female macaques from repeated high-dose intravaginal SHIV challenge. *Sci Transl Med*. 2015;7(270):270ra4.
- [149] Radzio J, Spreen W, Yueh YL, Mitchell J, Jenkins L, Garcia-Lerma JG, et al. The long-acting integrase inhibitor GSK744 protects macaques from repeated intravaginal SHIC challenge. *Sci Transl Med*. 2015;7(270):270ra5.
- [150] Rajoli RK, Back DJ, Rannard S, Freel Meyers CL, Flexner C, Owen A, et al. Physiologically Based Pharmacokinetic Modeling to Inform Development of Intramuscular Long-Acting Nanoformulations for HIV. *Clin Pharmacokinet*. 2015;54(6):639-650.

CHAPTER 4

Note: This chapter will be reproduced from the thesis for the following publication: Nelson, AG; Wang, H; Holloway, J; Zhang, X; Szekely, Z; Sinko, PJ. The Design, Characterization and Evaluation of Bac7-Labeled Nanoparticles as a Drug Delivery Platform for Colorectal HIV Pre-Exposure Prophylaxis (PrEP). *To be submitted to Journal of Controlled Release*.

The Design, Characterization and Evaluation of Bac7-Labeled Nanoparticles as a Drug Delivery Platform for Colorectal HIV Pre-Exposure Prophylaxis (PrEP)

4.1. Abstract

An ideal colorectal mucosal PrEP (mPrEP) would deliver antiretrovirals directly to the colorectal tissue, a critical site of early HIV infection. By achieving, and maintaining, effective mucosal drug concentrations, a mPrEP drug delivery system (DDS) would minimize the required dosing frequency and potential for systemic toxicity. The current work highlights a nanoparticle (NP) platform consisting of poly(caprolactone)–poly(ethylene glycol) (PCL-PEG) NPs labeled with a modified cell penetrating peptide (CPP), bactenecin7 (Bac7) to transport across mucus and epithelial barriers. Cellular uptake, and transport, was investigated in Caco-2 epithelial cell models *in vitro*. The ability of Bac7 NPs to traverse colorectal mucus to the epithelial cell layer was investigated in an *in situ* rat ligated intestinal loop model *in vivo*. Bac7 significantly increased NP transport (163.2% to 384.6%) across a Caco-2 epithelial cell monolayer compared to NPs without Bac7 labeling (i.e., plain NPs or 0% Bac7 NPs) after 18 hours. Flow cytometry and confocal microscopy demonstrated cytosolic delivery of NPs with significant uptake occurring through endosomal pathways. However, after 2 hours, Bac7 NPs showed a decrease in cell internalization compared with plain NPs. Results suggest a delay in uptake for Bac7 NPs due to initial electrostatic interactions and hydrogen bonding at the external cell surface. Bac7 NPs

were able to penetrate colorectal mucus in an *in situ* rat ligated intestinal loop model *in vivo*. NPs with 1% and 5% Bac7 ligand densities prompted a nearly 8-fold and 5-fold increase, respectively, in tissue association compared to plain NPs. This work establishes the feasibility of Bac7-labeled NPs for use in a mPrEP drug delivery approach. Further investigation is necessary to determine their potential in a long-acting PrEP platform.

4.2. Introduction

After more than three decades, the spread of HIV-1 remains a global pandemic. Despite the development of antiretroviral therapy (ART), one of the greatest achievements in therapeutic drug research, the Joint United Nations Programme on HIV/AIDS (UNAIDS) recently estimated that nearly 37 million people were living with HIV in 2016, with as many as 1.8 million new infections acquired that year and approximately one million mortalities [1-3]. Exposure to HIV through unprotected sexual activity remains the primary cause of transmission. The lower gastrointestinal tract, namely the distal colon and rectum, is a highly vulnerable target for HIV infection. Both men and women who engage in unprotected receptive anal intercourse (URAI) are at a significantly higher risk of contracting HIV from an infected partner than those who participate in unprotected vaginal intercourse (UVI). It is estimated that URAI results in 10-100 times more incidences per exposure than UVI [2, 4, 5]. According to the most recent data from the Center for Disease Control and Prevention, men who have sex with men (MSM) represent approximately 4% of the United States male population and yet accounted for 63% of all new HIV infections in 2010. This exposes a critical need for interventions to prevent viral transmission through this site of action [2, 4, 6].

The development of ART has slowed the spread of HIV, but there is still no cure or vaccine available [2]. Currently, the only FDA approved approach for HIV prevention is the systemic PrEP, Truvada. Truvada, raises toxicity concerns since the entire body is exposed to

antiretrovirals (ARVs) and relatively large dosages are required to achieve effective concentrations in mucosal tissues. Common adverse effects of long-term treatment include decreases in glomerular filtration rates and gastrointestinal discomfort with rare instances of renal tubular dysfunction (Fanconi syndrome) [7-9]. Additionally, original clinical trial data has reported oral PrEP to only be between 39 – 75% effective. Effectiveness becomes above 90% when adjusted to solely account for patients that took their medication consistently [2]. One of the major causes of variance is limited patient adherence largely due to the strict once-a-day oral dosing regimen. Therefore, a colorectal mucosal PrEP (mPrEP) DDS would address these concerns by delivering ARVs directly to the colorectal tissue to achieve higher mucosal drug concentrations lowering the necessary dosage and dosing frequency, and limiting systemic exposure [3, 10].

Intracellular drug delivery is a relatively daunting task. The cell membrane is impenetrable to most molecules that are not typically transported into living cells. The physiological function of the intestinal mucosa is to absorb nutrients from ingested material while preventing toxic particulates from translocating across the epithelial barrier into the systemic circulation. Therefore, the colorectal mucosa presents itself as a formidable barrier to NP penetration and translocation. Additionally, *in vivo*, NPs must successfully traverse two primary barriers in series. These include the mucus layer and the colorectal epithelial cells. Translocation is further complicated by the fact that these barriers are vastly different in their physicochemical properties. Thus, the goal of transporting NPs across the gut currently remains elusive due to a lack of known potentially exploitable mechanisms for barrier translocation. The development of a NP system capable of penetrating colorectal tissue and carrying a large drug-load would be widely beneficial to both the PrEP field and other areas of pharmaceutical research. Additionally, the penetrative

capabilities of Bac7 are not limited to colorectal cells and therefore findings from this study may be translatable to other topical delivery systems as well.

Cell-penetrating peptides (CPPs) have been utilized to facilitate the penetration of a variety of cargoes across cell membranes. One family of CPPs, the bactenecin family, stems from a proline/arginine rich family of antimicrobials. Bactenecin 7, a member of this family, is a 59-residue protein rich in cationic charged amino acids [11]. The CPP Bac7 (Scheme 1) is a modified fragment of the region 15-24 which harbors the cell-penetrating properties of the native protein, but not the microbial activity, that influence mammalian cells function [12].

Previous work conducted in the Sinko lab demonstrated the successful colorectal delivery and retention of PEG-amprenavir-Bac7 nanoconjugates as a proof-of-concept for a nano-based HIV mPrEP [3]. In summary, a colorectal mPrEP drug delivery system was engineered to increase antiretroviral concentrations and residence time in the mucosa after rectal administration. A 3.4 kDa model PEG nanoconjugate was covalently conjugated to the protease inhibitor amprenavir (APV) to slow down APV clearance from cells (APF). This resulted in a significant reduction in cellular uptake in Caco-2 cells *in vitro*. However, conjugation of Bac7 to fluorescently labeled PEG_{3.4kDa} conjugates (BPF) was shown to increase cell uptake with retention in tissue for 5 days after rectal dosing. These results showed the ability of a small (10 residue) peptide to deliver polymeric cargo to the cytosol of cells and into the lamina propria of a murine model *in vivo*. However, the conjugates provided a limited drug loading capacity (one single drug molecule could be chemically linked to each conjugate). This highlights the need to determine the ability of Bac7 to transport larger delivery systems capable of therapeutically relevant utility.

Here, the design, characterization, and evaluation of self-assembling polymeric NPs labeled with Bac7 is presented. NPs were capable of developing surface interactions with colonic cells to

enter, and translocate across, a cell monolayer *in vitro*. It is postulated that the conjugation of Bac7 will increase NP uptake into Caco-2 cells and facilitate transport across a Caco-2 model epithelial monolayer *in vitro*. Additionally, the ability of Bac7 NPs to perform *in vivo*, in the presence of colorectal mucus, was investigated. Within the gastrointestinal tract, mucus lines the luminal surface and serves as a barrier to protect the epithelium from exposure to foreign particles and the external environment. Mucus is a semipermeable layer of viscoelastic gel that selectively enables the exchange of nutrients, water, gases, hormones and other necessary biological components. It simultaneously prevents the translocation of most pathogens, and has shown to be a critical barrier to nanocarriers [13-15]. The hypothesis is that NPs of optimal architecture (i.e., having a dense PEG corona and optimal Bac7 ligand surface density) will successfully translocate across colorectal mucus to associate with the epithelial cell layer *in vivo*, was investigated. This work highlights the ability of a Bac7-labeled NP platform to traverse colorectal mucus *in vivo*, in a ligated intestinal loop murine model, and increase delivery to the colorectal mucosa.

4.3. Materials and Methods

4.3.1. Materials

Amino acids were purchased from Anaspec Inc. (Fremont, CA). Poly(ethylene oxide-b- ϵ -caprolactone) (*referred to as PCL-PEG in thesis*) (Catalog# P3130-EOCL) and functionalized-amino- ω -hydroxy terminated poly(ethylene glycol-b- ϵ -caprolactone) (*referred to as PCL-PEG-NH₂ in thesis*) (Catalog# P10288B-NH2EGCL) were purchased from Polymer Source (Montreal, Quebec, Canada). DL-alpha-Tocopherol (Vitamin E) (Lot# Q22B012) was obtained from Alfa Aesar (Tewksbury, MA). Tetrahydrofuran was purchased from Millipore Sigma (Lot# 56020). Fluorescein isothiocyanate isomer I (FITC) (Lot# 001521-2014-03) was obtained from Chem-Impex Int'l Inc. Maleic anhydride (95%, dry powder) (Lot# MKBC8270V), N,N-Dimethylformamide: anhydrous, 99.8% (Lot# SHBB8337V) and N,N-Diisopropylethylamine:

(Lot# 111K3081) were all purchased from Sigma Aldrich. Sieber TentaGel (Lot# BR151022) resin for peptide synthesis was purchased from EMD Millipore (Billerica, MA). The Caco-2 cell line was obtained from American Type Culture Collection (Rockville, MD) at passage 18. Diamidino-2-phenylindole dihydrochloride (DAPI) was purchased from Life Technologies Corp. (Carlsbad, CA). Dialysis tubing (MWCO 6000-8000) (Lot# 21-152-5) and LysoTrackerTM Deep Red were purchased from Fisher Scientific (Waltham, MA). Dulbecco's Modified Eagle Medium (DMEM) (1X) w/o phenol red (Lot # 1687980), DMEM (1X) w/ phenol red (Lot# 1860148), penicillin streptomycin (Lot# 1546518), Glutamax (100X) (Lot# 1646069), and 0.05% trypsin-EDTA (1X) (Lot# 1656932) were all obtained from Gibco (Waltham, MA). Heat inactivated fetal bovine serum (Lot# E13067) was purchased from Atlanta biological (Flowery Branch, GA) and Minimum Essential Medium (MEM) Non-Essential Amino Acids (100X) (Lot# 719461) was obtained from Quality biological (Gaithersburg, MD). 24-well plate format transwell inserts (1-micron pore size) and cell culture plates were purchased from Corning (Corning, NY). For molecular analysis, a Waters e2695 Alliance System (Milford, MA) high performance liquid chromatography (HPLC) was used complete with a photodiode array detector measuring ultraviolet absorption from 200-600 nm. The two part mobile phase gradient was one part (A) diH₂O with 0.05% TFA (v/v) and the remaining part (B) ACN with 0.05% TFA (v/v). A Waters Symmetry C18 column (Milford, MA) was used as the stationary phase. Additionally, electrospray ionization mass spectrometry (ESI-MS) was performed on a Finnegan LCQDuo (Thermo Finnegan, San Jose, CA).

4.3.2. Bac7 Molecular Modeling and *In Silico* Solubility Characterization

To evaluate the potential for Bac7 to orient towards the NP corona during nanofabrication, the log oil/water partition coefficient (LogP) and topographical polar surface area (TPSA) of Bac7 were determined using ChemDraw Professional 16.0 (Perkin Elmer, Waltham, MA) (Scheme 1) and Molinspiration Cheminformatics (Slovensky Grob, Slovak Republic) (Table 1). Both programs

have been widely used to report property calculations for organic molecules producing TPSA and LogP values that correlate well with experimental data [16]. LogP was determined as a function of molecular weight. TPSA was also calculated by a well-established methodology published by Ertl and colleagues [17]. Briefly, the sum of individual fragment polar areas, including those for O- and N- centered polar fragments, was calculated and used to determine the total polar surface area. The predicted molecular structure of Bac7 was modeled with the TASSER software (Ann Arbor, MI).

4.3.3 Bac7 Cell Penetrating Peptide Synthesis and Characterization

Fmoc solid-phase peptide synthesis was used to assemble the modified 15-24 residue fragment of Bac7 (Scheme 1) using a Nautilus 2400 automated peptide synthesizer. The CPP was synthesized on NovaSyn® TG Sieber resin to form the retro-inverso peptide sequence (N-acetyl-cg-p₁₅rplpfprpg₂₄-NH₂) with D-amino acids to confer resistance to proteolysis. The peptide was cleaved from the resin using trifluoroacetic acid (TFA), ethanedithiol, water, and triisopropylsilane (94/2.5/2.5/1, vol/vol). The product was analyzed using reverse phase HPLC (RT = 2.92 min) and characterized by MALDI-TOF-MS. The observed m/z was 1,334.6 Da for $\left[\frac{M+2H}{2}\right]^+$; the calculated m/z was 1,333.71 Da.

4.3.4 Bac7 Peptide Conjugation to PCL-PEG polymer

Prior to NP preparation, one molar equivalent of amino-functionalized copolymer poly(caprolactone)_{6.5kDa}-poly(ethylene glycol)_{5kDa} (PCL_{6.5kDa}-PEG_{5kDa}-NH₂) was reacted with 10 equivalents of maleic anhydride (MA) in 800 µl dimethylformamide (DMF). Five equivalents of N,N-Diisopropylethylamine (DIEA) was added as a base and the solution was allowed to stir on a magnetic plate for three hours. In relation to MA, 50% excess of Tentagel-amine resin was added to remove unreacted MA and the solution was left to stir for one hour. The sample was then

filtered to remove Tentagel. One equivalent of Bac7 peptide was added in an additional 200 μl of DMF and allowed to mix overnight (Scheme 2).

4.3.5 Fluorescent Dye Conjugation to PCL-PEG polymer

All NPs were labeled on the surface with 7% fluorescein isothiocyanate (FITC) for visualization by fluorescence microscopy and quantification. One equivalent of amino-functionalized copolymer ($\text{PCL}_{6.5\text{kDa}}\text{-PEG}_{5\text{kDa}}\text{-NH}_2$) was reacted with two equivalents of FITC in 800 μl DMF and DIEA was added as described above. The reaction was allowed to mix for three hours and quenched by 50% excess (in relation to FITC) Tentagel-amine resin followed by filtration.

4.3.6 Carboxylic Acid Conjugation to PCL-PEG polymer

The effect of NP net charge on transport was also investigated. To complete charge dependency studies, a carboxyl functional group was coupled to the PCL-PEG hydrophilic end. During NP preparation, PCL-PEG with carboxyl functional groups was added to the formulation to achieve twice the ligand density of Bac7. This was done to counterbalance its net cationic charge (+2). $\text{PCL}_{6.5\text{kDa}}\text{-PEG}_{5\text{kDa}}\text{-COOH}$ was synthesized by coupling $\text{PCL}_{6.5\text{kDa}}\text{-PEG}_{5\text{kDa}}\text{-NH}_2$ in excess succinic anhydride (two equivalents) in 800 μl DMF. Five equivalents of DIEA were also added. Contents were stirred for three hours and quenched with 50% excess Tentagel-amine resin. The solution was filtered after one hour to remove resin and stored at 4° C.

4.3.7 NP Synthesis and Characterization

Flash nanoprecipitation (FNP) uses rapid micromixing to impose high supersaturation and promote the precipitation and encapsulation of insoluble compounds within sterically stabilized NPs (Scheme 3) [18]. $\text{PCL}_{6.5\text{kDa}}\text{-PEG}_{5\text{kDa}}$ amphiphilic diblock copolymer was dissolved in THF at 15 mg/ml. Vitamin E was used as a hydrophobic encapsulating agent. Polymers were covalently conjugated to Bac7, or FITC, prior to FNP. The organic stream is comprised of polymer and

vitamin E dissolved in THF at a 1:1 mass ratio and sonicated for approximately 10 minutes. For each batch of NPs, one ml of the organic stream and one ml of de-ionized (DI) water were rapidly and evenly injected into a two-stream confined impingement jet mixer. Subsequent dilution occurred as the outlet stream was collected in 8 ml of additional DI water, totaling to 10 ml of NP suspensions with 10% THF. The NPs were vortexed and then dialyzed (molecular weight cutoff: 6000-8000 Da) in 4 liters of DI water to remove the remaining THF. After dialysis, 50 μ l of NP suspension was diluted in 500 μ l of DI water and added to a cuvette. NP sizes were determined on a Zeiss Nano ZS90 Zetasizer (Malvern Instruments, United Kingdom) by dynamic light scattering. NP diameters are reported.

4.3.8 Confocal Images of NPs

Confocal microscopy was used to determine NP internalization in human adenocarcinoma colonic (Caco-2) cells. At least one day before cell seeding, 4 wells of an 8-well Lab-Tek II chambered #1.5 German coverglass system was pre-coated with 500 μ l of 50 μ g/ml poly-D-lysine stock solution to increase cell attachment during subsequent seeding. After 24 hours, Caco-2 cells were seeded and grown until 50% confluence. Plain and 1% Bac7 labeled PCL_{6kDa}-PEG_{5kDa} NPs were diluted in 1X phenol red-free serum-free Dulbecco's Modified Eagle's Media (DMEM) and treated with 25X PBS to adjust osmolality to physiological conditions (290 mOsm/l). Samples were normalized by fluorescence to achieve 6 nM and 3 nM samples, respectively. One microliter of $\frac{1}{1000}$ X DAPI solution and 10 μ l of 1 μ M LysoTrackerTM Deep Red were added to each 1mL sample volume. Caco-2 cells were incubated at 37°C and 5% CO₂ for three hours with either plain NPs or 1% Bac7 NPs. After incubation, wells were washed three times with HBSS and then left to soak in 500 μ l HBSS to keep cells from drying out during the procedure. Fluorescence confocal imaging was performed using a Leica TSC SP2 laser scanning confocal microscope (Leica Microsystems CMS GmbH, Germany). Images were acquired at a 40x objective lens

magnification in the XYZ mode. Images were acquired in a sequential mode to eliminate emission light bleeding between filters. Approximately 10 scans in the z-plane were taken to cover the height of the cells (an expected $\sim 20\ \mu\text{m}$ for mature Caco-2 cells after 21 days)[19]. Individual image slices were acquired using the Leica companion software and stacked to determine NP internalization and localization within cells. DAPI intensity was adjusted for some images to ensure clear visibility of cell nuclei.

4.3.9 Cell Internalization of NPs in Caco-2 Cells Determined by Fluorescence-Activated Cell Sorting (FACS)

Cell internalization for plain NPs, 1% Bac7, 5% Bac7 and 5% Bac7 with 10% COOH NPs was determined by FACS to quantify relative cell uptake of NPs. Experiments were carried out in a 12-well tissue culture plate format. Caco-2 cells were seeded at $24,000\ \text{cells}/\text{cm}^2$ and cultured in complete DMEM with 10% FBS and grown to 80% confluence. Cells were treated with 15 nM samples of each NP in phenol red-free serum-free DMEM and incubated at $37^\circ\ \text{C}$ and 5% CO_2 for two hours. Three wells of control cells were incubated with DMEM only and used for gating parameter setup during FACS. Following incubation, wells were washed with Hank's Balanced Salt Solution (HBSS), trypsinized and washed again using centrifugation. Cells were finally collected in HBSS. Cells were stained with propidium iodide to remove dead cells from the program analysis. FACS was performed on a Gallios fluorescent-activated flow cytometer (Beckman Coulter, Indianapolis, IN). A series of gating events was applied to the samples. One event incorporated forward and side scattering, distinguishing unharmed cells from cellular debris. Another gating event was performed using forward scattering to separate single cells from doublet cells including those with cell-associated debris from dead cells. The final gating event was completed to select cells with FITC fluorescence above the background of unstained cells. Fluorescence intensity of at least 20,000 events was recorded for each sample.

4.3.10 Caco-2 Intestinal Epithelial Monolayer Translocation

Caco-2 cell monolayers have been extensively used as an *in vitro* model of the intestinal epithelial barrier over the last three decades [20, 21]. Caco-2 cells were grown in 10% fetal bovine serum (FBS) in DMEM and seeded in 24-well plate Transwell permeable inserts at a density of 1.5×10^4 cells/insert. Cells (passage number 40) were incubated at 37° C and 5% CO₂ for 28 days to form a mature epithelial monolayer. The extent of monolayer maturity was confirmed by morphological observation and measuring the trans-epithelial electric resistance (TEER) of each insert. TEER values for all experiments presented $\geq 500 \Omega \cdot \text{cm}^2$. For experiments, 15 nM samples of NPs of 0% (plain), 0.25%, 0.5%, 1%, 3%, 5% and 10% Bac7 surface coverage were prepared in phenol red-free DMEM without serum (A media) ($n \geq 4$ per NP). A 25x PBS solution was added to samples to maintain physiological osmolality and prevent cell toxicity. Samples were about 290 mOsm/L which is equivalent to physiological conditions. Samples (200 μl) were introduced to the apical side of the insert. Phenol red-free DMEM with 10% FBS (900 μl , B media) was added to the basolateral side of the monolayer within the chamber of the well plate, Plates were returned to incubate at 37° C for 18 hours. Following incubation, basolateral media was collected and transport was analyzed by fluorescence intensity. Fluorescence was read using a Tecan plate reader (Tecan Trading AG, Switzerland).

4.3.11 Investigation of NP Tissue Association in a Rat Ligated Intestinal Loop Model

The ligated intestinal loop model is a well-established method commonly used to measure the intestinal absorption properties of drugs [22]. Male Sprague-Dawley rats were fasted overnight ($n \geq 6$ rats per group). Rats were anesthetized with isoflurane, the abdominal region shaved and aseptically prepared with alternating betadine and isopropanol washes. The abdominal cavity was opened by a midline, longitudinal incision extending from the splenic flexure to the pelvis. Ligated sacs were prepared in the colon (distal to the cecum) and duodenum (directly distal to the stomach). Each portion was gently exposed and approximately five cm-long sacs were sectioned

off by tying each end with suture material. NP solutions (15 nM) were prepared in 6.5 pH PBS solutions at 290 mOsm/L. Samples were injected into sacs (100 μ l per cm or 500 μ l). After two hours, the rats were euthanized by diaphragm puncture and ligated sections were excised for analysis. Each sac was gently flushed with five ml of HBSS to remove the mucus layer and free NPs. The tissue was then sliced open through the lumen and the mucosa layer was gently scraped and collected. The mucosal samples were mechanically homogenized and then centrifuged at 5500 rpm for 30 minutes. The supernatant of each sample was collected and analyzed for fluorescence using a Tecan plate reader.

4.3.12. Statistical Analysis

GraphPad Prism version 6.0 (GraphPad Software, Inc., San Diego, CA) was used to perform all statistical and linear regression analysis. Results are represented by the mean and standard error of the mean (SEM). Statistical significance was determined by a 95% confidence interval ($p < 0.05$). One tailed or two-tailed, unpaired Student's t-tests were used to make comparisons between single groups assuming normal distribution and unequal or equal population measurements, respectively. A two-way analysis of variance (ANOVA) test was run on multiple group analysis. Tukey or Bonferroni post-hoc tests were applied to compare multiple groups following ANOVA, to further assess inter group significances.

4.4. Results

4.4.1. Characterization of Bac7 Peptide and Bac7-Labeled NPs

Bac7 was synthesized using solid phase peptide synthesis (Scheme 1) and modeled using I-TASSER modeling software (Ann Arbor, MI). The predicted coiled structure is shown in Figure 1. Bac7 was characterized by both reverse phase HPLC and electrospray mass spectrometry (Figures 2 and 3). Molecular properties were computed using pre-programmed software algorithms in ChemDraw Professional 16 and Molinspiration Cheminformatics Softwares.

Molecular weight (MW), exact mass, computational LogP, and TPSA as computed in ChemDraw are shown in Scheme 1. The reported molecular weight was 1334.61 and the exact mass was 1333.71. The reported theoretical LogP and TPSA are -2.026 and 472.14 Å², respectively. Theoretical LogP (miLogP), TPSA, and MW were determined in Molinspiration (Table 1). The calculated molecular weight was 1335.60. miLogP and TPSA were reported to be -5.21 and 466.33 Å², respectively. Successful synthesis, purification and characterization of Bac7 was confirmed by HPLC (Figure 2) and mass spectrometry (Figure 3). The purified peptide had a retention time of 2.92 min (Figure 2) and measured mass/charge (m/z) of 668.28 representing $\left[\frac{M+2H}{2}\right]^+$ (Figure 3).

4.4.2. Internalization of Bac7-labeled NPs in Caco-2 Cells

Caco-2 cells were grown until approximately 50% confluence. Less than 100% confluence was desired to avoid increased rigidity of the cell layer resulting in monolayer breakage and cell loss during wash steps. For both plain NPs and 1% Bac7 NPs, cellular internalization was observed by confocal microscopy after a three hour incubation period. Fluorescence intensity was markedly stronger in z-stacked images of cells treated with 1% Bac7 NPs showing greater NP presence (Figure 4, top). Lack of overlap between blue (DAPI) and green (NPs) fluorescence indicate NP localization within the cell cytoplasm. Cells were also treated with LysoTracker, an endosomal marker, which showed significant overlap with NPs indicating endosomal entrapment. To quantitate cell internalization for plain, 1% Bac7, 5% and 5% Bac7 with 10% COOH NPs, FACS was utilized. Mean arbitrary X-Mean fluorescence intensities were scaled and reported for each NP group (Figure 5). After two hours, cell internalization was seen for all NPs with an inverse correlation shown between cell uptake and Bac7 ligand density. Cell internalization was shown to decrease as Bac7 surface coverage increased from 0% to 5%. However, no significant differences were seen 5% Bac7 NPs with 10% COOH and plain NPs.

4.4.3 Effect of Ligand Density on Bac7 NP Transport Across Caco-2 Cell Monolayers

Figure 6 shows the transport of a series of Bac7-labeled NPs across Caco-2 cell monolayers over a period of 18 hours. NP transport across Caco-2 monolayers is shown for NPs with 0%, 0.25%, 0.5%, 1%, 3%, 5% and 10% Bac7 ligand surface density. Plain NPs resulted in a basal migration of approximately $0.4 \pm 0.2\%$ across the monolayer. Compared with plain NPs (control), a significant increase in transport is shown for all reported Bac7 densities. The greatest transport was shown for 0.25%, 0.5%, 5% and 10% Bac7 surface coverage with a ~ 4 -fold increase in transport when compared to plain NPs. NPs with 1% and 3% Bac7 surface densities showed about a 2-fold increase in transport compared to plain NPs. No significant differences were found between the Bac-7 labeled NP groups except between 0.5% Bac7 and 1% Bac7 NPs, which showed a 38% decrease for 1% Bac7 NPs. Cell monolayer integrity was assessed by measuring transepithelial electrical resistance (TEER) before and after each experiment. TEER values for all experiments was $\geq 500 \Omega \cdot \text{cm}^2$ before the experiments with a slight decrease in TEER ($\geq 470 \Omega \cdot \text{cm}^2$) after the experiment, suggesting that the monolayer maintained its integrity and there was no indication of NP cytotoxicity.

4.4.4. NPs Traverse Biological Barriers to Penetrate Colorectal Tissue *In Vivo*

A ligated intestinal loop model was used to investigate NP ability to translocate colorectal mucus and penetrate the epithelial cell layer *in situ*. Ligated loops were treated with NPs with 0%, 1%, 5%, and 10% Bac7 surface ligand densities. After two hours, a mean NP tissue association of 0.28 %/cm was observed for plain NPs in the colon (Figure 7). 1% Bac7 NPs showed an approximately 8-fold increase in mean NP tissue association (2.1%/cm) compared to plain NPs. 5% Bac7 NPs also showed a significant increase (5-fold) in tissue association (1.5 %/cm) compared to plain NPs. Similar results are shown in the duodenum with a ~ 2 -fold increase in NP

association with mucosal tissue for both 1% Bac7 and 5% Bac7 NPs. 10% Bac7 NPs showed no significant differences compared with plain NPs. NP tissue association was additionally quantitated in the presence of stool to determine fecal interference of NP delivery (Figure 8). Animals treated with 1% and 10% Bac7 surface coverage were separated into groups that had feces-free ligated sacs and those that had noticeable pieces of stool present. For 1% Bac7 NPs, significant differences were seen between empty sacs and those with stool present. No significant differences were found for 10% Bac7 NPs, which displayed baseline tissue association in both conditions.

4.4.5. NP Characterization and Mucosal Tissue Association after Ligand-Charge Balance *In Vivo*.

The effect of NP net charge on NP translocation across the intestinal mucus barrier *in vivo* was investigated. PCL_{6.5kDa}-PEG_{5kDa}-COOH was incorporated into NPs for charge dependent studies. NPs were labeled with 0, 1%, 5% Bac7. 5% Bac7 NPs were labeled with, or not labeled with, 10% COOH functional group to counterbalance the net (+2) cationic charge associated with Bac7. Surface zeta potentials show no significant differences between groups (Table 2). Additionally, there were no significant changes in size or polydispersity with the addition of Bac7 although a trend of decreasing size can be seen with increasing Bac7 surface density. NPs with 5% Bac7 and 10% COOH resulted in the smallest size which may potentially suggest surface interactions and tighter packing of molecules. NPs with 5% Bac7 surface coverage, with and without, 10% COOH were injected into ligated sacs in the colon and duodenum. After two hours, fluorescence analysis was performed to determine NP-tissue association. For both the colon and duodenum, no significant differences were found between treatment groups (Figure 9).

4.5. Discussion

The design and evaluation of a Bac7-labeled NP platform as a potential colorectal anti-HIV for mPrEP is demonstrated. Bac7 exhibits the capacity to transport large polymeric NPs across

intestinal cell membranes in a model cell barrier *in vitro*. The potential of Bac7 NPs to traverse the mucus layer *in vivo*, and achieve delivery to colorectal mucosal tissue was also determined.

Amphiphilic copolymers have gained attention over the past 30 years for their ability to self-assemble in aqueous environments forming micelle-like structures. They are able to enhance the solubility of hydrophobic agents and display good biocompatibility and biodegradability [23]. Placebo PCL-PEG NP sizes (data not shown) were tracked for two weeks following FNP and no significant changes were seen, which indicates acceptable NP stability. NP sizes and PDIs were reproducible over a series of runs thereby making PCL-PEG NPs an acceptable model nanocarrier for these studies.

Bac7 displays characteristics of both a hydrophobic and a hydrophilic nature that is a concern for its utility in FNP, a process that takes advantage of molecular polarity. During this process, NPs self-assemble so nonpolar molecules become encapsulated within the core and a stealth polar protective corona is formed. Organic molecules that may interact with the cell membrane, by hydrogen-bonding and electrostatic interactions, typically exhibit great difficulty traversing biological membrane like Caco-2 cells. In order to traverse a membrane, molecules need to exhibit the potential to break hydrogen bonds with its aqueous surroundings. Therefore, high hydrogen bonding potential is unfavorable and leads to low cell permeability [24]. The portion of Bac7 synthesized for this work P₁₅RPLPFPRPG₂₄ contains fragments of the original amphipathic full-length sequence that displays charged and hydrophobic clusters segregated into distinct regions. The selected sequence used (residues 15-24) contain the end tail of the highly cationic PR-rich repeat region (residues 15-16). The following c-terminus eight residue PX repeat sequence (residues 17- 24), comprised of a PX motif where X is either R, L, F or G, is considered the non-polar region. Overall, this 10-residue sequence has eliminated the charge cap (PR repeat residues) to form a truncated peptide with increased hydrophobicity. Bac7 is considered a

member of the Pro-rich family of CPPs with an approximate 50% proline composition[11]. Although Bac7 is considered a hydrophobic peptide fragment, two arginine residues are present and therefore it is expected to have similar properties to other Arg-rich CPPs. The arginine residues will impart polar characteristics to ensure Bac7 is not entrapped within the core of the NP during FNP.

Molinspiration Cheminformatics property algorithms were used to determine the TPSA and logP of Bac7. Chemdraw was also used as another well-accepted software for in silico determination of chemical properties. Both programs reported nearly identical TPSA values (472.14 Å² and 466.33Å² by Chemdraw and Molinspiration, respectively) suggesting high polarity. TPSA has been shown to have a strong correlation with a number of molecular compounds[17, 24, 25]. Calculated logP (cLogP) is the traditional coefficient used to determine the polarity of a molecule. LogP values computed by Chemdraw and Molinspiration were reported as -2.03 and -5.21 with respect to each program. Values indicate high aqueous solubility by Lipinski's Rule of 5 and general ADMET (absorption, distribution, metabolism, excretion and toxicity) Rules of Thumb outlined by Gleeson, et al [26, 27].

Confocal microscopy indicated cellular uptake for both plain NPs and 1% Bac7 NPs. Z-stacked images show a markedly stronger fluorescence intensity for cells treated with 1% Bac7 NPs indicating greater NP presence. Images show clear NP presence in the cell cytoplasm and no fluorescence overlap was shown for cell nuclei and NPs. Investigation of endosomal entrapment after three hours by LysoTracker reveals significant endosomal uptake of NPs. Multiple routes of cellular internalization for cationic CPPs and their delivery cargoes have been postulated and studied. In-depth studies have investigated uptake through endocytic pathways to elucidate intracellular trafficking within the endosomal compartment and the potential of these protein transduction domains to ensure release from the compartment [28]. It has been postulated that

endosome acidification and/or alterations of the endosomal lipid composition during maturation may facilitate CPP escape [28, 29]. Poly-arginine CPPs have been shown to enter cells through various endocytic pathways at lower concentrations (on the order of nanomolar to micromolar). Some fraction of these CPPs, and their delivery cargos, escape endosomal encapsulation and successfully deliver active transported molecules to target sites. However, escape from endosomes is inefficient. At higher concentrations ($\geq 10\mu\text{M}$), arginine-rich CPPs appear to bypass endocytosis and enter the cytosol directly [29]. To our knowledge, there are no reports of Bac7-facilitated cellular uptake of large cargo such as NPs. Mechanisms of uptake initiated by CPPs have been shown to differ for the various types of cargoes they may be attached to. Therefore, both endocytosis and direct cell-penetration may be responsible for cellular uptake, although endocytic processes may dominate for large cargoes [28, 30, 31]. Ligand density may also directly influence the mechanism of cellular uptake.

Further investigation of intracellular uptake by FACS demonstrated a decrease in internalization of Bac7 labeled NPs compared with plain NPs. Uptake then increased with the addition of a negatively charged succinic anhydride head group to balance out surface charge on 5% Bac7 NPs. Combined with the long term effectiveness of Bac7 NPs to translocate a cell monolayer, these results suggest a delay in cellular uptake for NPs labeled with Bac7. The guanidino group on arginine is capable of bidentate hydrogen bonding and forms ion-pairs with common H-bond-accepting cell surface moieties (e.g., sulfate, phosphate and carboxylate). These cell surface molecules are found in abundance on proteoglycans, phospholipids, and others. These chemical complexes are believed to promote accumulation of CPPs at the cell surface, a process ultimately leading to membrane migration at a rate proportional to membrane potential [28, 30, 31]. Recovery in uptake, with the addition of succinic anhydride to 5% Bac7 NPs, suggests the importance of surface charge on Bac7 intercellular interaction. Rothbard and colleagues [31] showed the importance of first-stage hydrogen bonding on CPP efficacy. They synthesized

octamers of mono and di-methylated arginines and showed that cellular uptake of methylated peptides was lower than the original octaarginine peptides with the guanidine function still intact. This was shown even though methylation was incorporated to increase guanidine basicity and function. These results further show that although charge is important, it is the function of the guanidinium group that is necessary for peptide utility in cell penetration[31].

Mueller and colleagues [32] compared the cellular uptake of 22 fluorochrome-tagged CPPs and found similar results showing predominantly surface adhesion at 30 minutes, for another member of the bactenecin sequence, Bac1-15 (FITC-RRIRPRPPLRPRP). Four different cell lines (Cos-7, HEK293, HeLa, MDCK) were incubated with Bac1-15 for 30 min at 37°C. Subsequently, the cells were washed twice with PBS and either lysed directly or treated with trypsin before lysis. Compared with cells that were not treated with trypsin, cells treated with trypsin showed a significant decrease in fluorescence intensity indicating very low Bac1-15 internalization after 30 min. No differences were seen between cell types. Bac1-15 translocation within cells was reported to be 1% cellular uptake. Similar results are shown for other popular CPPs including HIV-1 Tat-(48-60) (FITC-GRKKRRQRRPPQ) and Pep-1 (FITC-KETWWETWWTEWSQPKKRKY). It is important to note that FITC has been shown to result in protein binding and surface adhesion to cell surfaces potentially making it difficult to distinguish cell adhesion properties of the peptide independent of FITC surface interaction [33]. However, FITC does not display enhanced cell penetrative capabilities and is therefore not expected to alter membrane permeation [34].

Longer duration studies investigating NP translocation across a Caco-2 monolayer showed the ability of Bac7 to transport cargo into cells, and bypass, or escape endosomal entrapment resulting in transport of NPs to the basolateral compartment. Significant increases in transport were shown for Bac7-labeled NPs with ligand densities ranging from 0.25% to 10%. Ligand

density does not seem to have an effect on transport, with less transport for NPs of intermediate Bac7 surface coverage (1% and 3% densities). We postulate possible electrostatic surface interactions as a result of overlapping factors including charge balances and ligand distances between Bac7 ligands and FITC labeling. This may also support the hypothesis that ligand densities may promote different processes of cellular uptake. Ligand density may also influence NP escape following endosome entrapment. Further studies need to be completed to investigate this. Overall, *in vitro* investigation provides evidence of the utility of Bac7 to transport large polymeric NPs (approximately 40-60 nm) into Caco-2 cells and across a model epithelial cell barrier. This highlights its potential as an mPrEP strategy considering the importance of the lamina propria (anatomical site beneath the epithelium) in HIV infection. The lamina propria is the site within which majority of HIV target cells are found. These include the majority of the body's CD4+ T cells, dendritic cells, macrophages and other members of the innate immune system [2, 3].

Although promising results were seen *in vitro*, *in vitro-in vivo* data correlations are often poor for NP delivery systems, making it difficult to predict *in vivo* outcomes [35]. One of the major limitations of *in vitro* Caco-2 cell studies is the lack of a mucus barrier, a daunting hurdle for NP delivery to the gastrointestinal tract and other mucosal tissues. Mucin fibers, secreted by goblet cells, are cross-linked and entangled to form a mesh-like system. These fibers are highly flexible and coated with a complex and diverse arrangement of proteoglycans mostly tipped with a carboxyl or sulfate group creating a net negative charge. The flexible array of alternating regions in polarity allows for a variety of low-affinity hydrophilic and hydrophobic bonds to occur between the mucus gel and incoming particles. Additionally, spacing within the mesh range between 30-100 nm and may physically trap materials larger than the lower size cut-off.

Cationic termini are likely to adhere to mucus slowing or even preventing NP diffusion. On the other hand, neutral NPs may be highly hydrophobic, causing hydrophobic interactions resulting in reductions in diffusion as well. This highlights the intricacy of engineering nanocarriers to successfully traverse the mucus and epithelial cell barriers in series to deliver therapeutics when these two barriers are so vastly different in their physical properties [36]. Therefore, carrier surface chemistry plays a major role in NP interactions with mucus and its ability to traverse it. To determine the ability of Bac7 NPs to translocate across the mucus layer to reach the epithelial surface, a ligated intestinal loop model was utilized to measure the absorption of NPs with 0%, 1%, 5% and 10% Bac7 ligand surface densities in both the colon and the duodenum of mice. In both the colon and duodenum 1% and 5% Bac7 NPs showed significant tissue association compared with plain NPs showing the ability of Bac7 NPs to traverse mucus to penetrate the mucosal tissue. NPs with 10% Bac7 showed no significant differences compared with plain NPs indicating potential charge interactions along the way, or physical entrapment by peptide entanglement with the mesh. This suggests there is an optimal Bac7 ligand density range within which NPs are still able to travel across both layers. Similar results are shown in the duodenum, supporting previously reported non-cell specificity of Bac7 [28, 32]. The effect of net surface charge on NP translocation across the intestinal mucus barrier *in vivo* was also investigated, to determine if charge neutralization could help increase NP transport across mucus. PCL_{6.5kDa}-PEG_{5kDa}-COOH was incorporated into NPs for charge dependent studies. NPs labeled with 0, 1%, 5% Bac7 and 5% Bac7-10% COOH showed no significant differences in surface zeta potentials. Zeta potential reading reported near neutral voltages. Zeta potential, while commonly reported as a means of measuring surface charge, is only indicative of the nature of surface charge and the level of electrostatic stabilization. These results suggest that NPs were stabilized by electrostatic interactions with a near neutral surface potential comparing NP surface ionization with bulk ions present from the electric double layer to the slipping plane[37]. NPs with 5% Bac7 and 10% COOH resulted in the smallest size, which may indicate potential surface interactions and tighter

packing of molecules. NPs with 5% Bac7, showed similar levels of mucus translocation and tissue association *in situ* for groups with and without 10% COOH surface coverage. This suggests that a 5% Bac7 surface ligand density is not significantly impeded by electrostatic interaction with mucus.

To further evaluate the factors affecting NP absorption, the effect of feces on NP absorption within the colon was assessed. For 1% Bac7 NPs we found a significant decrease in measured NP absorption in the colon of animals that had stool present at the time of treatment. This finding is important to note since an ideal mPrEP will not require an individual to fast before use and will need to be effectively delivered in the presence of feces. Therefore, the selection of an appropriate delivery vehicle is critical. This also suggests that 1% Bac7 NPs result in greater effective tissue association than shown *in situ*.

These new findings differ from previous work showing 4-fold increase in Bac7-guided transport of a small PEG_{3.4kDa} nanoconjugate after two hours in Caco-2 cells [3]. No signs of delayed cellular internalization were seen due to peptide aggregation at the cell surface. The hypothesis is that this is due to the heavier burden large NPs impose on cell uptake. NP internalization appears to be more significantly guided by endocytic pathways that may result in slower uptake than the hypothesized direct penetration of Bac7-PEG nanoconjugates. Future research on Bac7 and Arg-rich CPPs may benefit from investigating the rate of cellular internalization and fate for various cargo sizes and shapes. NP tissue retention in colorectal mucosa should also be explored and optimized to identify the potential of this drug delivery strategy to be used in a long-acting PrEP application.

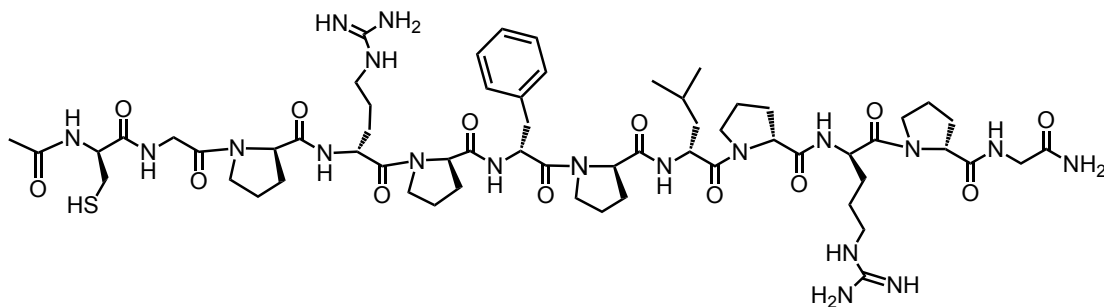
In summary, a NP drug delivery system to evade biological barriers and transport across colorectal monolayer as a mPrEP platform was designed and evaluated. The objective of this

work was to investigate the ability of Bac7 to transport large polymeric NPs across the mucus lining and cell barrier. While Truvada, an oral drug product and the only current FDA-approved PrEP, has substantiated the efficacy of PrEP, clinical trial effectiveness is dependent on patient compliance with a strict daily regimen and success rates have been variable. Mucosal strategies are needed to deliver, and maintain, effective concentrations of anti-HIV agents within colorectal mucosa, while limiting the dosage frequency and systemic toxicity to increase patient adherence. The current work aimed to evaluate a Bac7 NP strategy to penetrate the mucus lining and translocate across the colonic epithelial barrier. Bac7 was able to assist in the cellular uptake, and transport, of PCL-PEG NPs across a cell layer. This suggests the ability of Bac7 to transport NPs past the epithelium to the lamina propria, a highly vulnerable anatomical region for HIV infection, and therefore a critical site for prevention strategies. Bac7 is also capable of transporting NPs across mucus *in vivo* at optimal ligand densities. This work demonstrates the feasibility of Bac7-labeled NPs to be used as a mPrEP approach. Further work will need to be completed to determine its potential as a long-acting PrEP platform. This will include future work to investigate anti-HIV drug loading potentials and mucosal tissue retention *in vivo*.

4.6. Authors Contributions

Majority of work in this manuscript was completed by Nelson, AG with contributions of the listed co-authors as following: Wang, H assisted in the completion of *in vitro* cell studies and data analysis. Jennifer Holloway contributed in the design of animal studies and assisted in the completion of *in vivo* work. Szekely, Z and Zhang X were involved in planning. Sinko, P J supervised the project.

4.7. Figures



Formula	Molecular Weight	Exact Mass	CLogP	Topographical Polar Surface Area (TPSA)
C ₆₁ H ₉₅ N ₁₉ O ₁₃ S	1334.61	1333.71	-2.026	472.14

Scheme 1. Bac7 peptide synthesized in solid phase peptide synthesis. Molecular structure (N-Ac-Cys-Gly-Pro₁₅-Arg-Pro-Leu-Pro-Phe-Pro-Arg-Pro-Gly₂₄-NH₂) depicted in Chem Draw Professional 16.0 software. Molecular properties were computed using pre-programmed software algorithms. Calculated molecular weight, molecular mass, computational LogP, and Topographical Polar Surface Area are shown.

miLogP ^a	Topographical Polar Surface Area (TPSA) ^b	Molecular Weight (MW) ^c
-5.21	466.33	1335.60

Table 1. Molecular properties of Bac7 computed using pre-programmed Molinspiration software algorithms. Computational LogP, Topographical Polar Surface Area, and Molecular Weight are shown.

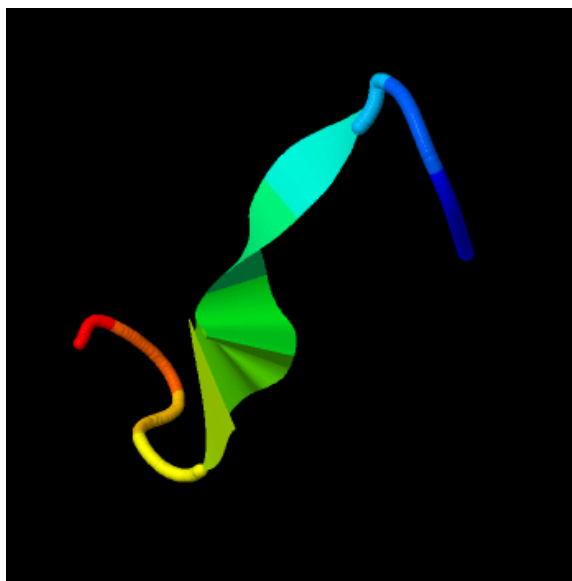


Figure 1. Predicted 3-D structure of Bac7 peptide recapitulated in TASSER Software. Bac7 molecular structure (N-Ac-Cys-Gly-Pro₁₅-Arg-Pro-Leu-Pro-Phe-Pro-Arg-Pro-Gly₂₄-NH₂) is shown. Figure shows the predicted coiled molecular structure.

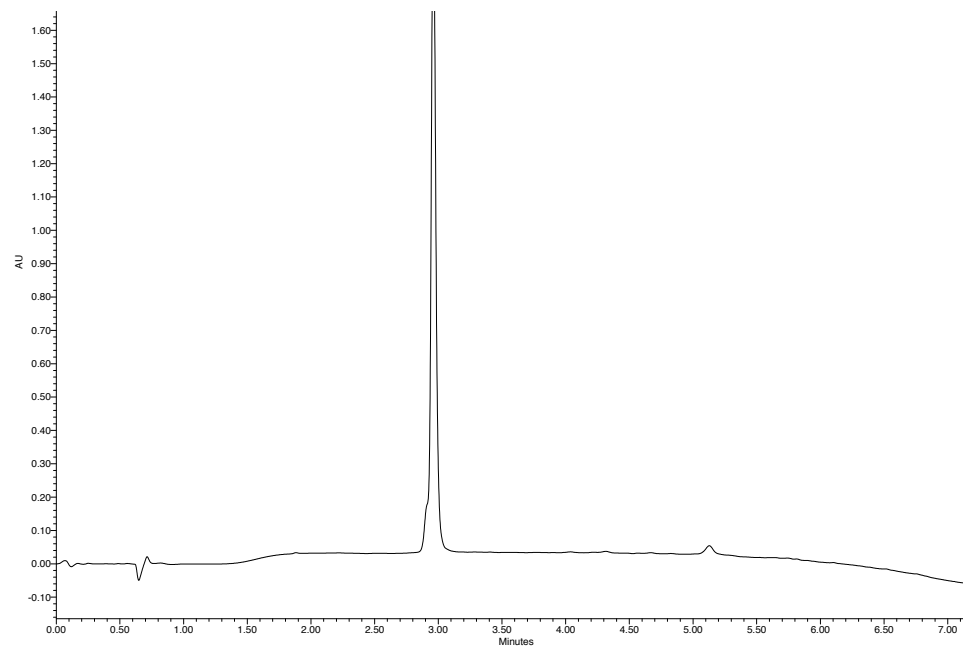


Figure 2. Characterization of Bac7 peptide by High Performance Liquid Chromatography (HPLC). Analytical HPLC chromatogram of purified peptide by ultraviolet (UV) detection. The compound had a retention time of 2.92 minutes.

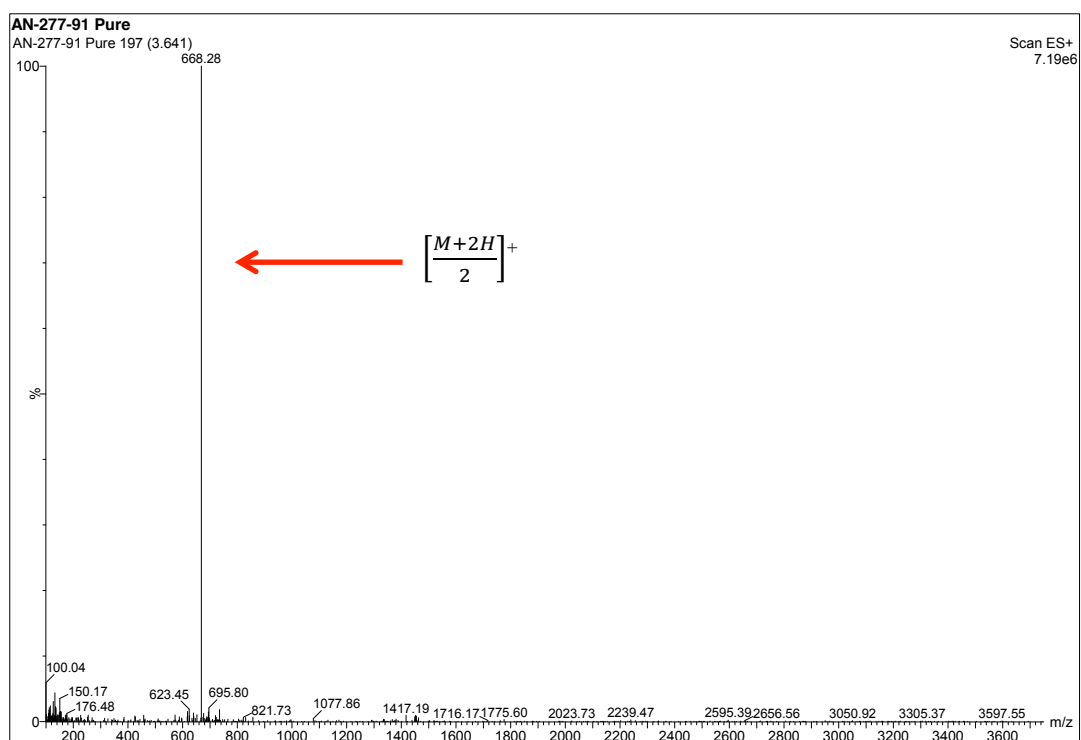
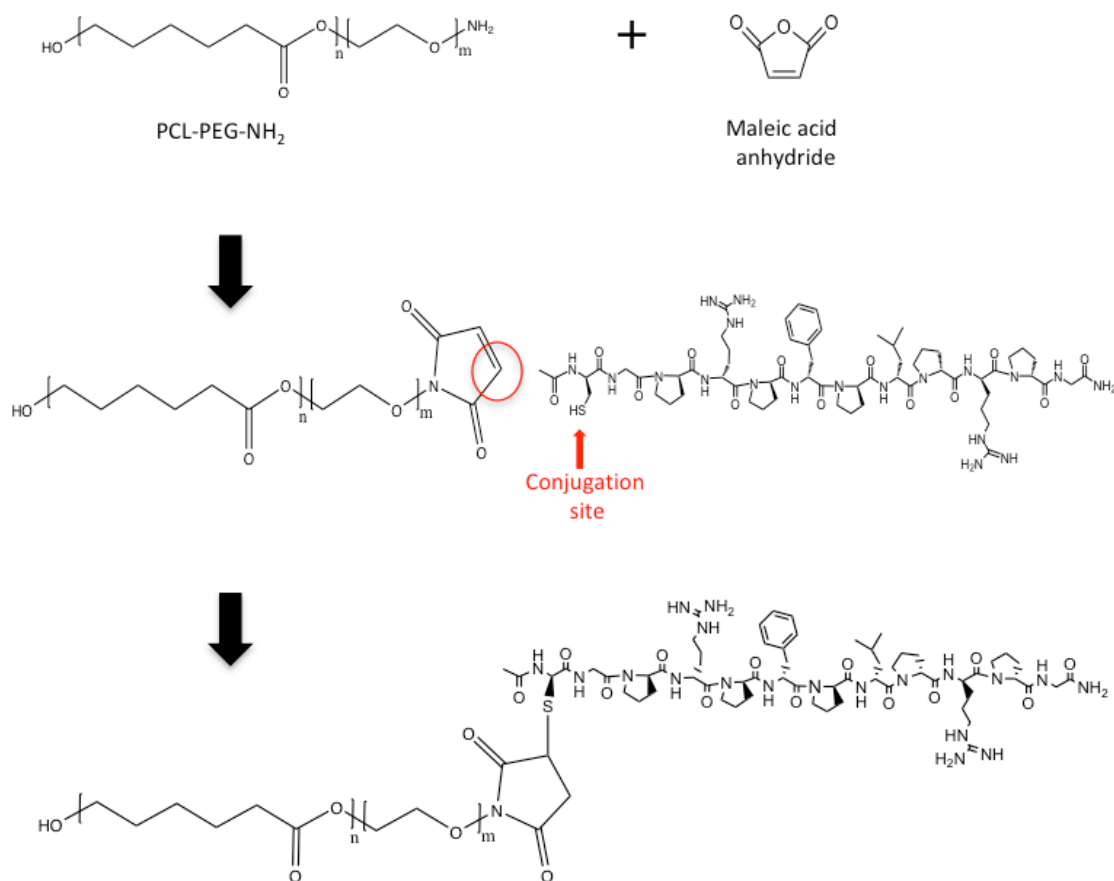
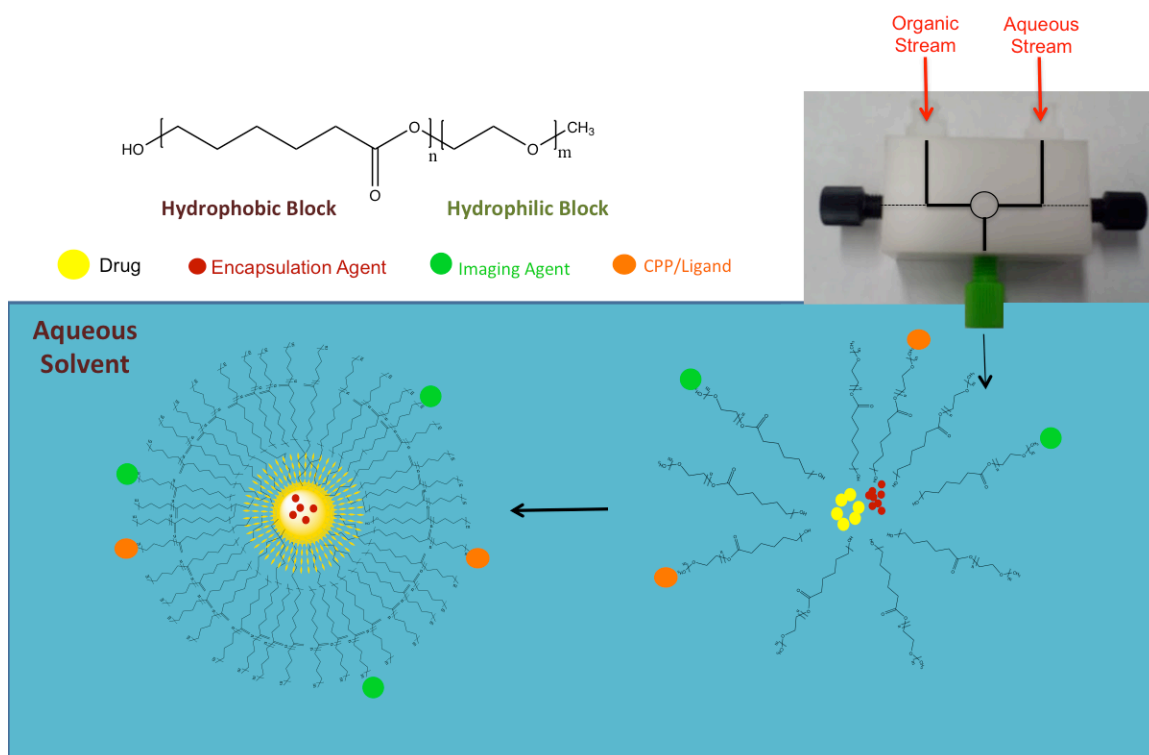


Figure 3. Characterization of Bac7 peptide by electrospray ionization-mass spectrometry (ESI-MS). ESI-MS spectrum of purified Bac7. The peak represents the $[m/z]$, $\left[\frac{M+2H}{2}\right]^+ = 668.2$, corresponding to the molecular ion of 1333.71 calculated by Chem Draw Professional 16.0.



Scheme 2. Schematic of PCL-PEG-Bac7 conjugation. Amino-functionalized polymer (PCL_{6.5kDa}-PEG_{5kDa}-NH₂) was reacted with maleic acid anhydride to form a PCL-PEG-Maleimide (Mal) functional polymer. The Mal-functionalized peptide was reacted with the n-acetyl-cysteine at the n-terminal end of Bac7 to form a final product of PCL-PEG-Bac7 via maleimide-thiol reaction (Michael's addition).



Scheme 3. Flash nanoprecipitation to fabricate NPs. Amphiphilic diblock copolymers form self-assembled NPs when exposed to aqueous environments. The addition of encapsulation agents (stabilizers) to the organic stream help to stabilize the structure. Polymers align themselves with the hydrophobic/lipophilic tails oriented within the core interacting directly with stabilizer and the hydrophilic tail surrounds the particle forming a protective corona shell to shield the non-polar additives. Additional lipophilic materials (drug, imaging agents, etc) may be easily encapsulated when of sufficient lipophilic nature. NPs, or polymeric building blocks, may be labeled with imaging agents, targeting ligands through chemical conjugation, after or prior to FNP, respectively.

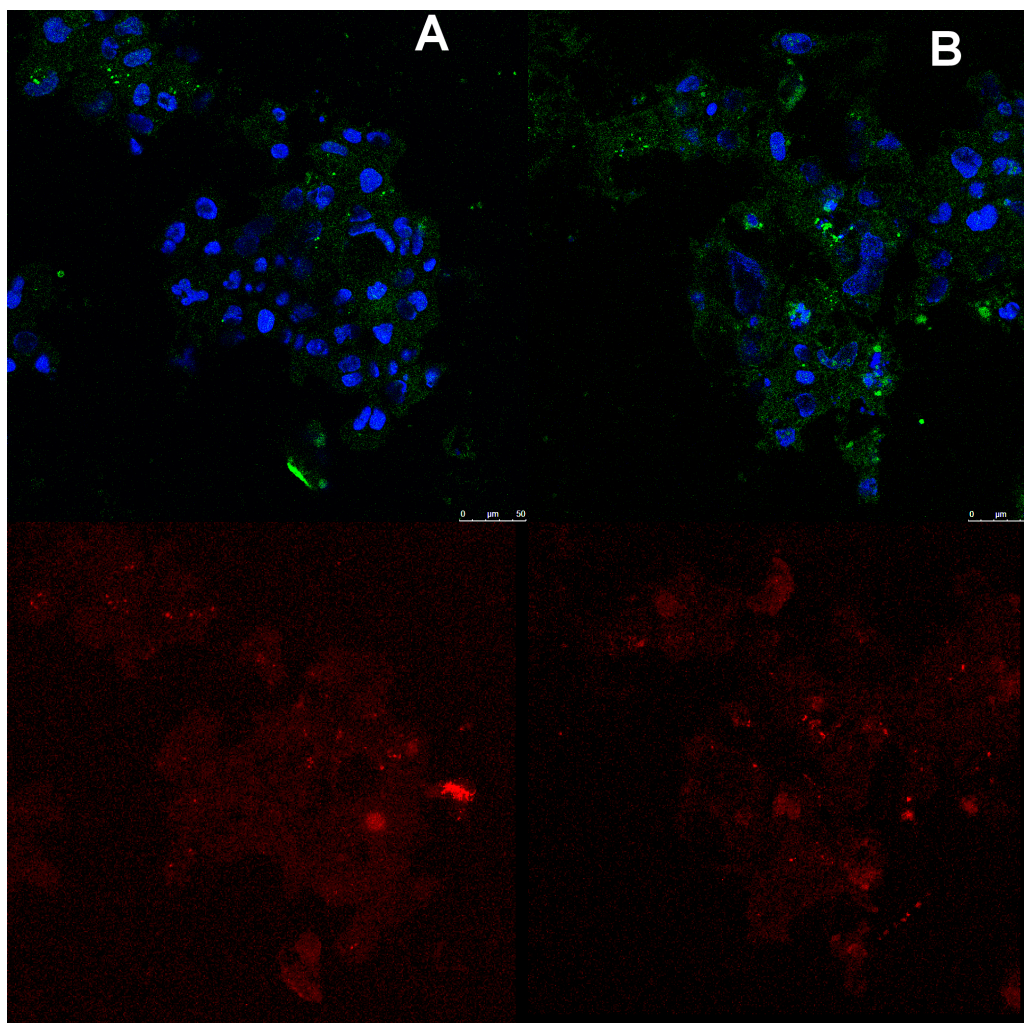


Figure 4. Confocal microscopy of plain and Bac7- labeled NPs. A. Plain NPs. B. Bac7 (1% surface coverage) NPs. Caco-2 cells were grown until about 50% confluence. Plain and Bac7 samples were prepared in serum-free phenol-red free DMEM. Samples were normalized by fluorescence for plain and Bac7 NP concentrations (6 nM and 3 nM, respectively). NPs are labeled with FITC to display a green fluorescence. DAPI nuclear stain shows cell nuclei in blue. Z-stacked images are shown for each. A significantly greater presence of green fluorescence can be seen for Bac7 labeled NPs showing greater presence of NPs with cell-penetrating ligand conjugation. Bottom images show Lysotracker staining for acidic compartments (ie. endosomes and lysosomes) indicating endosomal entrapment of a portion of both plain and 1% Bac7 NPs.

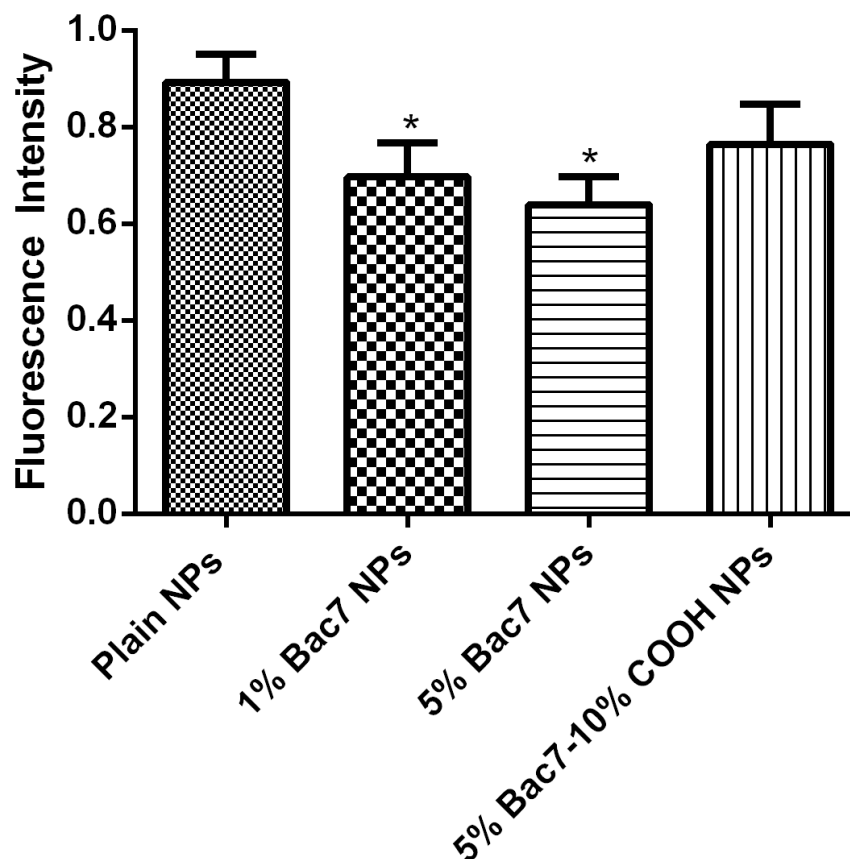


Figure 5. Cell internalization of NPs in Caco-2 cells after 2 hours incubation. Cell uptake and internalization for plain NPs, 1% Bac7, 5% Bac7 and 5% Bac7 with 10% COOH NPs was determined by FACS. Caco-2 cells were treated with samples of each NP in phenol red-free serum-free DMEM. Mean relative fluorescence intensity and standard deviation is reported for each NP group. Results show a decrease in internalization at 2 hours with increasing surface coverage of Bac7. An increase can be seen for NPs with 5% Bac7 and 10% COOH showing no significant difference in uptake compared with plain NPs (n=4) ($p < 0.05$, ANOVA) (* $p < 0.05$, compared with plain NPs by Student's t-test).

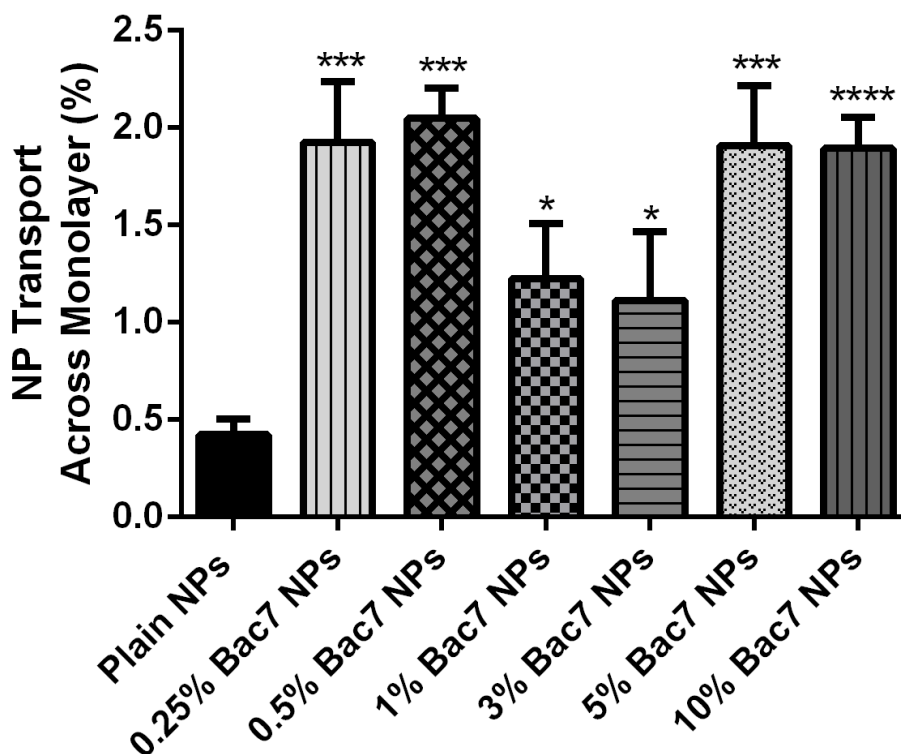


Figure 6. Translocation of NPs across Caco-2 intestinal monolayers. Caco-2 cells (passage number = 40) were grown for 28 days to form a monolayer as a model intestinal epithelium. Graph shows the transport of a series of Bac7-labeled NPs (0%, 0.25%, 0.5%, 1%, 3%, 5% and 10% Bac7 ligand density) across a model intestinal monolayer over 18 hours. Data shows NP transport presented as percent transport. Results show plain NPs result in a basal level of migration across the monolayer (0.42%). A significant increase in transport is shown for all Bac7 labeled ligand densities. The greatest transport was shown for 0.25%, 0.5%, 5% and 10% surface coverage with an approximately 4-fold increase in transport when compared to plain NPs. Ligand densities of 1% and 3% showed about a 2-fold increase in transport compared with plain NPs. Cell monolayer integrity was determined by transepithelial electrical resistance (TEER). TEER values for all experiments presented $\geq 500 \Omega \cdot \text{cm}^2$. Data shows the combination of two independent transport studies ($n > 6$). Mean and standard error of the mean is presented for each group (* $p < 0.05$, *** $p < 0.0005$, **** $p < 0.0001$).

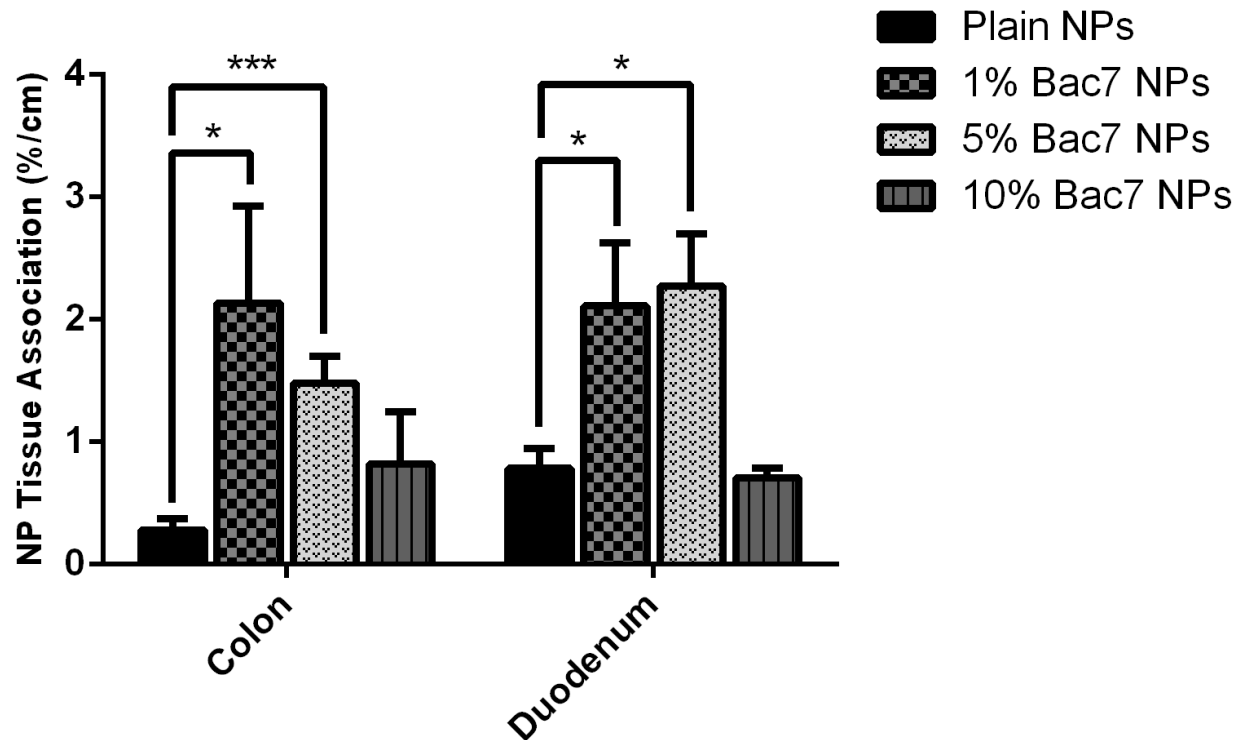


Figure 7. NP mucosal tissue association *in vivo* in Sprague-Dawley rats. Intestinal ligated loop model was used to investigate NP translocation through colorectal mucus to penetrate and associate with the mucosal tissue layer. NPs with 0%, 1%, 5%, and 10% Bac7 surface ligand densities were injected into 3-5 cm ligated sacs in the colon and duodenum and treated for 2 hours prior to tissue collection and analysis. NPs were fluorescently labeled with FITC. Mucosal tissue was scraped and fluorescence analysis was performed on processed samples. In the colon, there was an approximately 8-fold increase in NP tissue association for 1% Bac7 NPs compared with plain NPs. 5% Bac7 NPs also showed a significant increase of approximately 5 fold greater NP presence in the colon compared to plain NPs. Similar results are shown in the duodenum with a nearly 3-fold increase in NP association with mucosal tissue for 1%, and 5%, Bac7-labeled NPs. 10% Bac7 NPs showed no significant differences compared with plain NPs. Mean and standard error of the mean is presented for each group (n>6) , ***p<0.0005).

	Plain NPs	1% Bac7	5% Bac7	5% Bac7 10% COOH
Size (d.nm)	56.7±3.7	50.5±2.1	48.43±3.4	42.1±1.9
Polydispersity Index	0.13±0.01	0.14±0.06	0.17±0.03	0.20±0.05
Zeta Potential (mV)	-2.6±0.09	-3.8±0.37	-3.36±1.5	-2.34±1.9

Table 2. Effect of ligand type and density on NP properties. Size, polydispersity index (PDI) and zeta potential was determined for each group using a Zeiss Nano ZS90. NPs shown were labeled with 0, 1%, 5% Bac7. 5% Bac7 NPs were labeled with an additional 10% COOH functional group to counterbalance Bac7 cationic charges and determine the effect of NP net charge on translocation across a mucus barrier *in vivo*. Surface zeta potentials show no significant differences between groups. Data is presented in mean and standard deviation (N = 2) for each NP type. For most groups, no statistically significant differences were seen in size or polydispersity with the addition of Bac7, although a slight trend can be noticed suggesting a minor change in size as a result of increasing Bac7 surface density. NPs with 5% Bac7 and 10% COOH resulted in the smallest size and a significant decrease in size compared with plain NPs indicating potential surface interactions and tighter packing of fabrication materials. Experiment was repeated twice.

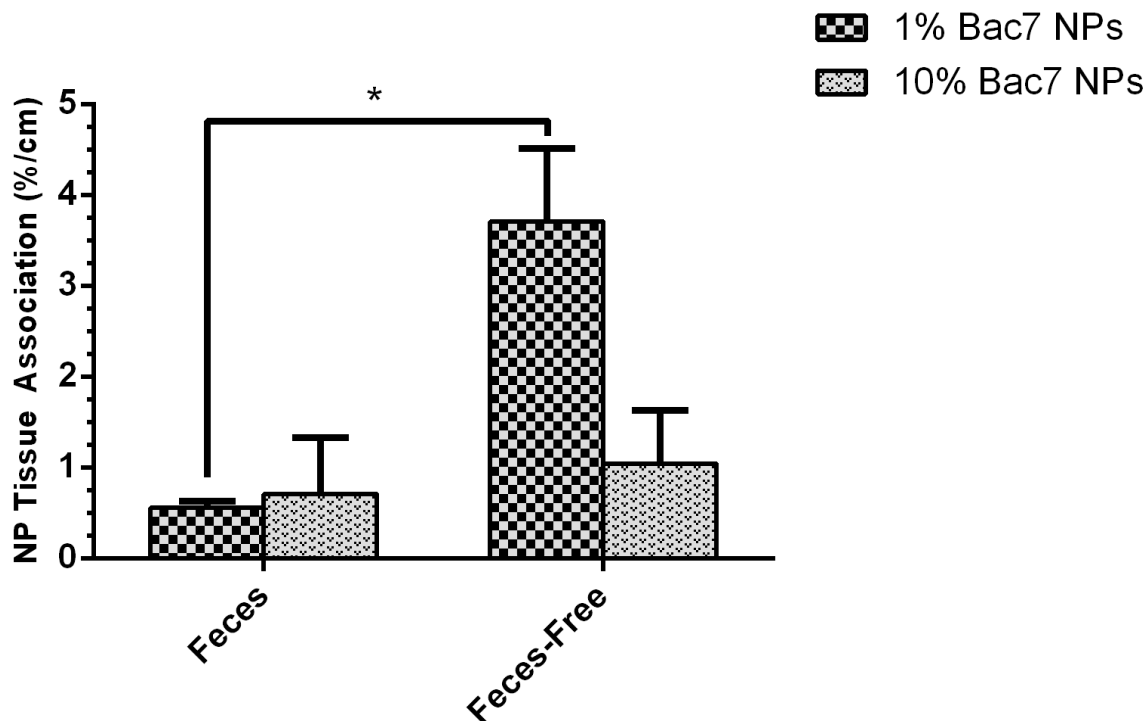


Figure 8. The effect of feces presence on NP tissue-interaction in the colon *in vivo* in Sprague-Dawley rats. NP tissue association was quantitated in the presence of stool to determine fecal interference of NP delivery to colonic mucosal tissue layer. Ligated sacs were treated with NPs with 1% and 10% Bac7 surface coverage ($N \geq 2$) for 2 hours prior to tissue collection and analysis. Mucosal tissue was scraped and fluorescence analysis was performed on processed samples to quantify NP tissue association. Significant differences were found for 1% Bac7 NP absorption in an empty colon vs colon with stool present ($*p < 0.05$). No significant differences were found for 10% Bac7 NPs.

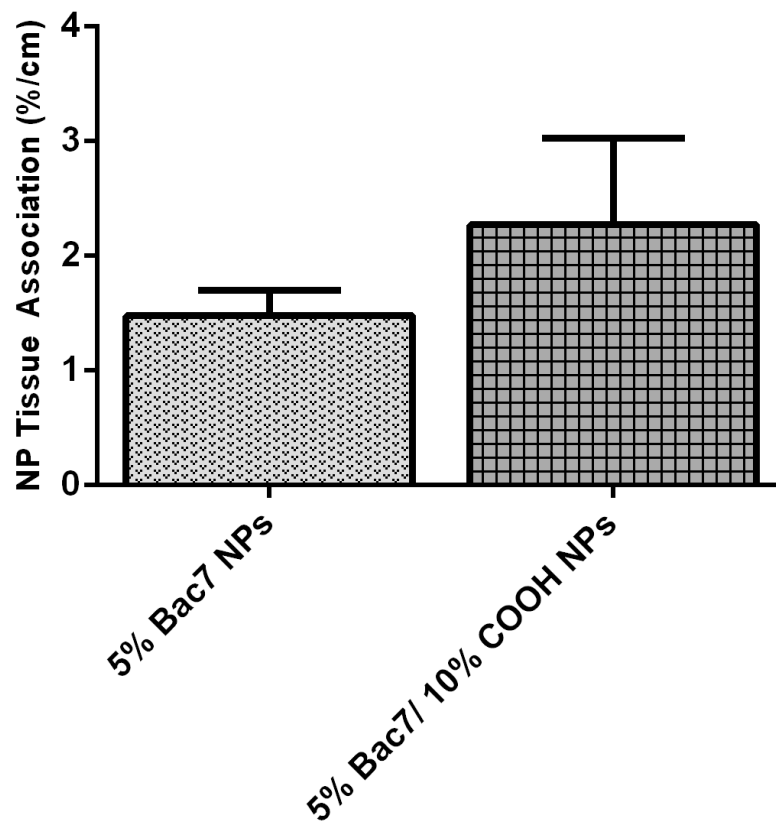


Figure 9. NP mucosal tissue association after NP ligand-charge balance *in vivo* in Sprague-Dawley rats. NPs with 5% Bac7 surface coverage, with and without, 10% COOH were injected into 3-5 cm ligated sacs in the colon and treated for 2 hours prior to tissue collection and analysis. COOH functional groups were added to NPs to counterbalance the net cationic charge (+2) associated with Bac7. Mucosal tissue was scraped and fluorescence analysis was performed on processed samples to determine NP presence. No significant differences were found between groups (N=6).

4.8. References

- [1] UNAIDS, Fact Sheet - Latest statistics on the status of the AIDS epidemic. 2018).
- [2] A.G. Nelson, X. Zhang, U. Ganapathi, Z. Szekely, C.W. Flexner, A. Owen, P.J. Sinko, Drug delivery strategies and systems for HIV/AIDS pre-exposure prophylaxis and treatment, *Journal of Controlled Release* 219 (2015) 669-680.
- [3] M. Samizadeh, X. Zhang, S. Gunaseelan, A.G. Nelson, M.S. Palombo, D.R. Myers, Y. Singh, U. Ganapathi, Z. Szekely, P.J. Sinko, Colorectal Delivery and Retention of PEG-Amprenavir-Bac7 Nanoconjugates - Proof of Concept for HIV Mucosal Pre-Exposure Prophylaxis, *Drug delivery and translational research* 6(1) (2016) 1-16.
- [4] F. Hladik, T.J. Hope, HIV infection of the genital mucosa in women, *Current HIV/AIDS Reports* 6(1) (2009) 20-28.
- [5] R.F. Baggaley, R.G. White, M.-C. Boily, HIV transmission risk through anal intercourse: systematic review, meta-analysis and implications for HIV prevention, *International Journal of Epidemiology* 39(4) (2010) 1048-1063.
- [6] A.E. Grulich, I. Zablotska, Commentary: Probability of HIV transmission through anal intercourse, *International Journal of Epidemiology* 39(4) (2010) 1064-1065.
- [7] A.M. Margolis, H. Heverling, P.A. Pham, A. Stolbach, A Review of the Toxicity of HIV Medications, *Journal of Medical Toxicology* 10(1) (2014) 26-39.
- [8] J.S. Young, J. Fux, C. A. Furrer, H. Bernasconi, E. Vernazza, P. Calmy, A. Cavassini, M. Weber, R. Bategay, M. Bucher, H. C. Renal function in patients with HIV starting therapy with tenofovir and either efavirenz, lopinavir or atazanavir, *AIDS* 26(5) (2012) 567-575.
- [9] G. Mathew, S.J. Knaus, Acquired Fanconi's Syndrome Associated with Tenofovir Therapy, *Journal of General Internal Medicine* 21(11) (2006) C3-C5.
- [10] R. Nunes, B. Sarmiento, J. das Neves, Formulation and delivery of anti-HIV rectal microbicides: Advances and challenges, *Journal of Controlled Release* 194 (2014) 278-294.
- [11] K. Sadler, K.D. Eom, J.-L. Yang, Y. Dimitrova, J.P. Tam, Translocating Proline-Rich Peptides from the Antimicrobial Peptide Bactenecin 7, *Biochemistry* 41(48) (2002) 14150-14157.
- [12] R.I. Dmitriev, H.M. Ropiak, D.V. Yashunsky, G.V. Ponomarev, A.V. Zhdanov, D.B. Papkovsky, Bactenecin 7 peptide fragment as a tool for intracellular delivery of a phosphorescent oxygen sensor, *FEBS Journal* 277(22) (2010) 4651-4661.
- [13] A. Ermund, A. Schütte, M.E.V. Johansson, J.K. Gustafsson, G.C. Hansson, Studies of mucus in mouse stomach, small intestine, and colon. I. Gastrointestinal mucus layers have different properties depending on location as well as over the Peyer's patches, *American Journal of Physiology - Gastrointestinal and Liver Physiology* 305(5) (2013) G341-G347.
- [14] S.K. Lai, Y.-Y. Wang, J. Hanes, Mucus-penetrating nanoparticles for drug and gene delivery to mucosal tissues, *Advanced drug delivery reviews* 61(2) (2009) 158-171.
- [15] M. Liu, J. Zhang, W. Shan, Y. Huang, Developments of mucus penetrating nanoparticles, *Asian Journal of Pharmaceutical Sciences* 10(4) (2015) 275-282.
- [16] S.M. D'Addio, W. Saad, S.M. Ansell, J.J. Squiers, D.H. Adamson, M. Herrera-Alonso, A.R. Wohl, T.R. Hoye, C.W. Macosko, L.D. Mayer, C. Vauthier, R.K. Prud'homme, Effects of block copolymer properties on nanocarrier protection from in vivo clearance, *Journal of Controlled Release* 162(1) (2012) 208-217.
- [17] P. Ertl, B. Rohde, P. Selzer, Fast Calculation of Molecular Polar Surface Area as a Sum of Fragment-Based Contributions and Its Application to the Prediction of Drug Transport Properties, *Journal of Medicinal Chemistry* 43(20) (2000) 3714-3717.
- [18] K.M. Pustulka, A.R. Wohl, H.S. Lee, A.R. Michel, J. Han, T.R. Hoye, A.V. McCormick, J. Panyam, C.W. Macosko, Flash Nanoprecipitation: Particle Structure and Stability, *Molecular Pharmaceutics* 10(11) (2013) 4367-4377.
- [19] G.H. Wilson, I.F.; Dix, C.J.; Williamson, I.; Shah, R.; Mackay, M.; Artursson, P., TRANSPORT AND PERMEABILITY PROPERTIES OF HUMAN CACO-2 CELLS: AN

- IN VITRO MODEL OF THE INTESTINAL EPITHELIAL CELL BARRIER, *Journal of Controlled Release* 11 (1990) 25-40.
- [20] Y. Sambuy, I. De Angelis, G. Ranaldi, M.L. Scarino, A. Stammati, F. Zucco, The Caco-2 cell line as a model of the intestinal barrier: influence of cell and culture-related factors on Caco-2 cell functional characteristics, *Cell Biology and Toxicology* 21(1) (2005) 1-26.
- [21] H.C.T. Yu, J. Sinko, P. J., Evidence for diminished functional expression of intestinal transporters in Caco-2 cell monolayers at high passages, *Pharm Res* 14(6) (1997) 757-62.
- [22] W. Liu, H. Pan, C. Zhang, L. Zhao, R. Zhao, Y. Zhu, W. Pan, Developments in Methods for Measuring the Intestinal Absorption of Nanoparticle-Bound Drugs, *International Journal of Molecular Sciences* 17(7) (2016) 1171.
- [23] R. Li, X. Li, L. Xie, D. Ding, Y. Hu, X. Qian, L. Yu, Y. Ding, X. Jiang, B. Liu, Preparation and evaluation of PEG-PCL nanoparticles for local tetradrine delivery, *International Journal of Pharmaceutics* 379(1) (2009) 158-166.
- [24] T.J. Hou, W. Zhang, K. Xia, X.B. Qiao, X.J. Xu, ADME Evaluation in Drug Discovery. 5. Correlation of Caco-2 Permeation with Simple Molecular Properties, *Journal of Chemical Information and Computer Sciences* 44(5) (2004) 1585-1600.
- [25] H.C. Van de Waterbeemd, G. Estimation of Caco-2 Cell Permeability using Calculated Molecular Descriptors, *Quant. Struct.-Act. Relat* 15 (1996) 480-490.
- [26] C.W. Lindsley, Lipophilicity, *Encyclopedia of Psychopharmacology*, Springer-Verlag Berlin Heidelberg, 2014.
- [27] M.P. Gleeson, Generation of a Set of Simple, Interpretable ADMET Rules of Thumb, *Journal of Medicinal Chemistry* 51(4) (2008) 817-834.
- [28] Ü. Langel, *Handbook of Cell-Penetrating Peptides*, Second Edition, Taylor & Francis Group, LLC, Boca Raton, FL, 2007.
- [29] K. Melikov, A. Hara, K. Yamoah, E. Zaitseva, E. Zaitsev, Leonid V. Chernomordik, Efficient entry of cell-penetrating peptide nona-arginine into adherent cells involves a transient increase in intracellular calcium, *Biochemical Journal* 471(Pt 2) (2015) 221-230.
- [30] S. Futaki, I. Nakase, Cell-Surface Interactions on Arginine-Rich Cell-Penetrating Peptides Allow for Multiplex Modes of Internalization, *Accounts of Chemical Research* 50(10) (2017) 2449-2456.
- [31] J.B. Rothbard, T.C. Jessop, R.S. Lewis, B.A. Murray, P.A. Wender, Role of Membrane Potential and Hydrogen Bonding in the Mechanism of Translocation of Guanidinium-Rich Peptides into Cells, *Journal of the American Chemical Society* 126(31) (2004) 9506-9507.
- [32] J. Mueller, I. Kretschmar, R. Volkmer, P. Boisguerin, Comparison of Cellular Uptake Using 22 CPPs in 4 Different Cell Lines, *Bioconjugate Chemistry* 19(12) (2008) 2363-2374.
- [33] L.-O. Andersson, A. Rehnström, D.L. Eaker, Studies on "Nonspecific" Binding, *European Journal of Biochemistry* 20(3) (1971) 371-380.
- [34] C.N. Carrigan, B. Imperiali, The engineering of membrane-permeable peptides, *Analytical Biochemistry* 341(2) (2005) 290-298.
- [35] P. Jain, R.S. Pawar, R.S. Pandey, J. Madan, S. Pawar, P.K. Lakshmi, M.S. Sudheesh, In-vitro in-vivo correlation (IVIVC) in nanomedicine: Is protein corona the missing link?, *Biotechnology Advances* 35(7) (2017) 889-904.
- [36] G. Aljayyousi, M. Abdulkarim, P. Griffiths, M. Gumbleton, Pharmaceutical Nanoparticles and the Mucin Biopolymer Barrier, *BioImpacts : BI* 2(4) (2012) 173-174.
- [37] S. Bhattacharjee, DLS and zeta potential – What they are and what they are not?, *Journal of Controlled Release* 235 (2016) 337-351.

CHAPTER 5

Note: Sections of this chapter will be reproduced from this thesis for the following publication:
Nelson, AG; Wang, H; Myers, DR; Holloway, J; Shike, Li; Szekely, Z; Sinko, P J. Formulation, Characterization and Evaluation of Rilpivirine-Loaded Bac7 Nanoparticles as a Long-Acting Platform for Colorectal HIV PrEP. *In preparation*.

Formulation, Characterization and Evaluation of Rilpivirine-Loaded Bac7 Nanoparticles as a Long-Acting Platform for Colorectal HIV PrEP

5.1. Abstract

Rilpivirine (RPV) is a highly potent non-nucleoside reverse transcriptase inhibitor (NNRTI) that has shown promising pre-clinical results when formulated as a long-acting nanosuspension. However, these suspensions require parenteral injections and may result in low patient adherence. A long-acting mucosal PrEP (mPrEP) drug delivery system (DDS) would provide a viable alternative to injectable options. Poly(ϵ -caprolactone) (PCL)-poly(ethylene glycol) (PEG) nanoparticles (NPs) fabricated by flash nanoprecipitation (FNP) successfully encapsulated the highly insoluble antiretroviral, RPV, resulting in high encapsulation efficiencies (85% to 98%) and moderate to high drug loadings (10.9 % to 17.7%). Extent of RPV release was modulated, by adjusting copolymer block sizes, to achieve 20% to 40% total cumulative release over 24 hours *in vitro*. Poly(lactide)_{6.3kDa}-PEG_{5kDa} (PLA-PEG) NPs resulted in a greater extent of release of 58% compared to 40% for PCL_{6kDa}-PEG_{5kDa}. However, PLA_{6.3kDa}-PEG_{5kDa} achieved an approximately 10% lower encapsulation efficiency and 1% decrease in drug loading compared with PCL_{6kDa}PEG_{5kDa}. In the colon, the inverso (I) Bac7 analog resulted in the greatest increase (142%) in tissue association compared with plain NPs. RPV concentrations, after 2-hour administration in an *in situ* rat model, were quantified and no significant differences were found between plain NPs

and Bac7 I NPs. A decreasing trend in free RPV, associated with the addition of Bac7, suggests strong tissue adsorption preventing total RPV quantitation of *in vivo* samples. Similar trends were shown in mouse intra-rectal studies. 24 hour RPV concentrations were below the limit of detection and unable to be quantified. Bac7 I NPs showed 3-fold greater mucosal tissue association compared with plain NPs (~1.7% and ~0.45%, respectively). Plain and Bac7 I NPs appear to be largely cleared from tissue after 24 hours. However, NPs are present past 48 hours at low levels. This work shows the feasibility of an RPV-loaded Bac7 NP platform to be used in an mPrEP. However, significant optimization is needed to further consider the feasibility of a polymeric NP DDS in a long-acting PrEP approach.

5.2. Introduction

HIV infection remains a major global health concern despite significant improvements in antiretroviral therapy (ART) and access to treatment. Without the prospect of an effective cure or vaccine in the clinical pipeline, prevention is considered the cornerstone of ending the HIV pandemic [1-3]. For high-risk populations, oral pre-exposure prophylaxis (PrEP) has shown to be highly effective at preventing HIV infection [4, 5]. Mathematical modeling of clinical trial data estimates up to 99% risk-reduction when optimal PrEP adherence is met. However, the real-world success of oral PrEP hinges on patient compliance with a strict daily regimen that has proven to be variable over a number of randomized clinical trials [5-7]. Therefore, PrEP alternatives to circumvent the need for less frequent dosing are starting to be explored. Long-acting and extended release formulations may improve adherence and confer longer durations of protection, avoiding the daily pressure and responsibility placed on individuals to remember to take a pill [5, 7, 8]. Parsons et al [6] conducted a study surveying 1071 MSM participants to determine preference in forms of PrEP. Nearly half of participants (46.0%) stated a strong preference for long-acting injectable PrEP over daily oral PrEP [4, 7].

Until recently, majority of clinical trial studies have involved regimens including tenofovir disoproxil fumarate. Alternative PrEP formulations are currently being explored incorporating new promising anti-HIV agents. RPV is a highly potent NNRTI that has shown promising pre-clinical results as a long-acting nanosuspension and is now currently undergoing clinical trial evaluation [9]. Rilpivirine-based approaches for rectal and vaginal HIV prophylaxis have reached efficacy levels of 75% to 100% in animal models following intramuscular administration [5, 10]. These approaches show promising extended release profiles with the potential to require infrequent dosing once every two to three months. However, these long-acting agents require parenteral injections via intravenous, intramuscular, or subcutaneous routes of administration. This raises novel adherence and safety challenges. Literature on injectable contraception reports high rates of nonadherence after the initial injection event. This suggests that even the availability of long-acting injectable PrEP formulations will not eliminate nonadherence concerns. A long-acting mPrEP, where antiretrovirals are delivered directly to the mucosal tissue would provide a viable alternative to injectable options. Although it is highly unlikely one strategy will result in universal acceptability, studies over a long history of contraceptive method development have shown that having a diverse array of options, to suit a range of user needs and preferences, can effectively enhance adherence [4, 7].

In the development of long-acting PrEP approaches, new delivery strategies to achieve target drug concentrations in mucosal tissues, while simultaneously avoiding cellular efflux and metabolism, are critical [11]. Previously, a proof-of-concept for a nano-based HIV mPrEP DDS showed the successful colorectal delivery, and retention, of a PEG_{3,4kDa} model nanoconjugate delivery system. This delivery system involved the conjugation of a modified fragment of the cell penetrating peptide, Bactenecin 7 (Bac7), to PEG conjugates. Bac7 was shown to increase cell uptake and be retained for 5 days after rectal administration in mice. The average epithelial cell

turnover rate in the colon is 2-3 days in rodents. [12]. Therefore retention that exceeds 2-3 days in a murine model indicates NP delivery to the lamina propria. However, these conjugates are incapable of achieving therapeutically relevant drug concentrations. The development of a Bac7 NP delivery system with higher drug loading, and the potential to achieve and sustain effective mucosal drug concentrations, would be a promising technology for use in a long-acting PrEP.

The benefits of NPs in drug delivery have been well-explored [13-15]. Their large surface areas significantly improve the dissolution and absorption of poorly soluble drugs, and allow for optimization. Surface properties may be modulated by functionalization or adjusting formulation parameters. However, the equipment required to formulate NPs is often costly and further increases drug product costs [16]. FNP is a simple, rapid, one-step and low-energy technique to prepare polymeric NPs within a controlled size range [17, 18]. Stable polymeric NPs with high loadings of hydrophobic compounds are easily achieved making FNP a convenient and cost-effective assembly method [19, 20].

In the current study, polymeric NPs, fabricated by FNP and capable of encapsulating the highly insoluble drug, RPV, are reported. It is hypothesized that drug loading and release can be tuned to sustain RPV release for a minimum of 24 hours, by modifying copolymer properties. *In vivo*, we assessed the delivery of RPV to colorectal tissue after *in situ*, or intra-rectal administration, in murine models. Our aim was to maintain NP levels for three days in mice, to surpass rodent epithelial turnover times [11, 21]. Finally, we assessed *in vitro* and *in vivo* results to determine the feasibility of this delivery platform to be applied to long-active applications for rectal HIV PrEP.

5.3. Materials and Methods

5.3.1. Materials

Amino acids were obtained from Anaspec Inc. (Fremont, CA). Poly(ethylene oxide-b- ϵ -caprolactone) (*referred to as PCL-PEG in thesis*) Mn:PEO(5000)-b-PCL(6000) (Sample# P3130-EOCL), Mn:PEO(5000)-b-PCL(3000) (Sample# P9737-EOCL), Mn:PEO(5000)-b-PCL(1600) (Sample# P7599-EOCL), Mn:PEO(2000)-b-PCL(8500) (Sample# P8849-EOCL), Mn:PEO(2000)-b-PCL(6000) (Sample# P9706-EOCL), Mn:PEO(2000)-b-PCL(2800) (Sample# P9820-EOCL), Poly(ethylene oxide-b- Lactide(DL form)) (*referred to as PLA-PEG in thesis*) Mn:PEO(5000)-b-PLA(6300) (Sample# P10901-EOLA) and functionalized-amino- ω -hydroxy terminated poly(ethylene glycol-b- ϵ -caprolactone) (*referred to as PCL-PEG-NH₂ in thesis*) (Sample# P10288B-NH2EGCL) were all purchased from Polymer Source (Montreal, Quebec, Canada). DL-alpha-Tocopherol (Vitamin E) (Lot# Q22B012) was purchased from Alfa Aesar (Tewksbury, MA). Tetrahydrofuran was purchased from Millipore Sigma (Lot# 56020). Fluorescein isothiocyanate isomer I (FITC) (Lot# 001521-2014-03) was acquired from Chem-Impex Int'l Inc. DL-alpha-Tocopherol succinate (Vitamin E succinate) (Lot# SLBH6145V), Anhydrous N,N-Dimethylformamide (Lot# SHBB8337V), N,N-Diisopropylethylamine: (Lot# 111K3081) and Pur-A-Lyzer™ Mini Dialysis Kits were all received from Sigma Aldrich (St. Louis, MO). Rilpivirine (Batch# FR158451601) was purchased from Carbosynth (San Diego, CA). Sieber TentaGel (Lot# BR151022) resin was obtained from EMD Millipore (Billerica, MA). Polysorbate 80 (Lot # 7086F) was obtained from ICN Biomedicals, Inc (Aurora, Ohio). Microcon Ultracel YM-10 ultrafiltration tubes (10,000 MWCO) (Lot # RBJN03841) were acquired from Millipore. Dialysis tubing (MWCO 6000-8000) (Lot# 21-152-5) was obtained from Fisher Scientific (Waltham, MA). Dulbecco's Modified Eagle Medium (DMEM) (1X): w/o phenol red (Lot # 1687980), DMEM (1X) w/ phenol red (Lot# 1860148), penicilin streptomycin (Lot #1546518), Glutamax (100X) (Lot # 1646069), and 0.05% trypsin-EDTA (1X) (Lot#1656932) were all ordered from Gibco (Waltham, MA) and Minimum Essential Medium (MEM) Non-Essential Amino Acids (100X) (Lot # 719461) was purchased from Quality biological (Gaithersburg, MD). For molecular analysis, a Waters e2695 Alliance System (Milford, MA)

high performance liquid chromatography (HPLC) was used complete with a photodiode array detector measuring ultraviolet absorption from 200-600 nm. The two part mobile phase gradient was one part (A) diH₂O with 0.05% TFA (v/v) and the remaining part (B) ACN with 0.05% TFA (v/v). A Waters Symmetry C18 column (Milford, MA) was used as the stationary phase. Additionally electrospray ionization mass spectrometry (ESI-MS) was performed on a Finnegan LCQDuo (Thermo Finnegan, San Jose, CA).

5.3.2. NP Preparation

Placebo NPs fabricated from a series of hydrophilic and hydrophobic block lengths (hydrophilic-hydrophobic MW block ratios) were formed. PCL-PEG amphiphilic diblock copolymers were dissolved in THF at a constant mass (7.5 mg/ml). A hydrophilic PEG block of 5kDa was matched with a 1.6 kDa, 3 kDa or 6 kDa PCL hydrophobic block, resulting in hydrophilic-hydrophobic block ratios of 3.13, 1.67 and 0.83 respectively (PCL_{1.8kDa}-PEG_{5kDa}, PCL_{3kDa}-PEG_{5kDa}, PCL_{6kDa}-PEG_{5kDa}). Alternatively, a PEG block of 2 kDa was paired with PCL blocks of 2.8 kDa, 6 kDa or 8.5 kDa to form hydrophilic-hydrophobic block ratios of 0.71, 0.33 or 0.24 respectively (PCL_{2.8kDa}-PEG_{2kDa}, PCL_{6kDa}-PEG_{2kDa}, and PCL_{8.5kDa}-PEG_{2kDa}). Vitamin E was incorporated, in a 1:1 mass ratio with polymer, as a core stabilizer. Immediately following FNP, the outlet stream was collected in DI water, totaling to 10 ml of NP solution with 10% THF. 50 µl of NP solution was diluted in 500 µl of DI water and NP sizes were immediately determined on a Zeiss Nano ZS90 Zetasizer.

5.3.3. Determination of RPV Solubility in Distilled Water, DMEM and 0.1% Tween 80/DMEM.

RPV solubility in distilled water (DI water), DMEM and 0.1% v/v Tween 80/DMEM (Tween/DMEM) was determined by adding excess RPV (1 mg/ml) in 1 ml of each medium and sonicating for 10 minutes. Samples were then incubated at 37°C for 1 or 7 days with constant

agitation on a rotational plate. Samples were filtered using a 0.2 μm poly(tetrafluoroethylene) filtration unit. The collected filtrate was directly analyzed by high performance liquid chromatography (HPLC).

5.3.4. RPV Drug Loading and Release from NPs

Drug loading and release characteristics of RPV were tuned and optimized during FNP. The hydrolysis rate within the NP core is dependent on the intrinsic bond stability, core pH and water concentration. Thus both drug loading and drug release may be tuned by altering the hydrophobicity of agents within the NP core. Series of formulations were tested using PCL-PEG NPs (not shown) resulting in the optimal encapsulation efficiency for RPV with 1:1 molar mass ratios of Vitamin E and Vitamin E succinate. This formulation was kept standard across all release studies.

PCL-PEG NPs of various hydrophobic and hydrophilic block ratios were fabricated as previously described. The only adjustment was a 1:1 molar ratio of Vitamin E (3.75 mg) and Vitamin E succinate (2.2 mg) was used as a hydrophobic stabilizer to efficiently encapsulate 1.5 mg of RPV in each batch of NPs. FNP was performed and NPs were immediately transferred to Millipore ultracentrifuge tubes (10 kDa MWCO) that were placed inside 1.5 ml microcentrifuge tubes. Samples were spun at 10,500 RPM for 20 minutes at 25°C. Liquid was collected from the tubes and diluted with DI water to the original sample volume. Supernatant that was filtered into the collection tubes was collected and 20 μl of filtered liquid was added to 100 μl of 1:1 ACN:DI water and analyzed by ESI-MS. Reported ESI-MS values were used to determine the amount of RPV unencapsulated within NPs. Simultaneously, 200 μl of NP samples was immediately pipetted into Pur-A-Lyzer dialysis tubes and placed in 8 ml glass vials filled with 4 mls of Tween 80/DMEM as the release medium. Vials were placed to rock in a heated rotational incubator at 37°C. At pre-determined time points, 100 μl of release media was collected and replaced with

fresh media to maintain sink conditions. Concentrations of RPV in release media were below the RPV solubility limit determined in Tween 80/DMEM.

Encapsulation efficiency was determined using the following equation:

$$\% \text{ Encapsulation Efficiency} = 100 * \frac{(\text{Total drug added} - \text{Free untrapped" drug})}{\text{Total drug added}}$$

Drug loading was also calculated as follows:

$$\% \text{ Drug Loading} = 100 * \frac{(\text{Total mass drug encapsulated})}{\text{Total mass NPs}}$$

5.3.5. Bac7 Cell Penetrating Peptide Synthesis

Three analogs of Bac7 were synthesized to compare their penetrative capabilities in the presence of *in vivo* proteolytic enzymes. Fmoc solid-phase peptide synthesis was used to complete the syntheses. A modified 15-24 residue fragment of the sequence was synthesized using a Nautilus 2400 automated peptide synthesizer. Analogs included wild-type (gly-pro₁₅-arg-pro-leu-pro-phe-pro-arg-pro-gly₂₄-NH₂) (wt, all l-amino acids), inverso (I, all d-amino acids), and retro-inverso (RI, all d-amino acids and reversed ordered) sequences (Scheme 1). The d-amino acid containing sequences were utilized to increase proteolytic stability. Peptides were conjugated with azide-PEG₄ for copper-free click chemistry conjugation. The peptide was cleaved from the NovaSyn® TG Sieber resin using trifluoroacetic acid (TFA), ethanedithiol, water, and triisopropylsilane in a 94/2.5/2.5/1 vol/vol/vol/vol ratio. The product was analyzed using reverse phase HPLC (RT =3.14 min) and characterized by ESI-MS. The observed $\left[\frac{M+2H}{2}\right]^+$ m/z was 732.47 Da (calculated exact mass =1,462.72 Da).

5.3.6. Bac7 Peptide Conjugation to PCL-PEG Polymer Prior to FNP, one molar equivalent of amino-functionalized copolymer (PCL_{6.5kDa}-PEG_{5kDa}-NH₂) was reacted with 25% excess dibenzocyclooctyl-poly(ethylene glycol)₅-N-hydroxysuccinimide (DBCO-PEG-NHS) in 500µl dimethylformamide (DMF). Six equivalents of N,N-Diisopropylethylamine (DIEA) was added as a base. The solution was mixed for four hours. 10 mg of Tentagel-amine resin was added to remove unreacted DBCO and allowed to stir for one hour. The sample was then filtered to remove Tentagel. One equivalent of Bac7 peptide was added to the solution in an additional 200 µl of DMF and stirred overnight.

5.3.7. Fluorescence Dye Conjugation to PCL-PEG Polymer

For quantification of NP *in situ* tissue association, fluorescein isothiocyanate (FITC) was conjugated to PCL-PEG polymer prior to FNP. FITC-labeled polymer accounted for 7% of NP polymer to achieve 7% surface ligand density. Briefly, one equivalent of amino-functionalized copolymer (PCL_{6.5kDa}-PEG_{5kDa}-NH₂) was reacted with two equivalents of FITC in 800 µl DMF. Four equivalents of DIEA were added. The reaction solution was stirred for three hours and quenched with 50% excess Tentagel-amine resin for one hour, followed by filtration.

5.3.8. Rat Intestinal Sac Ligation Model

PCL_{6kDa}-PEG_{5kDa} was used to fabricate NPs for all animal studies. Polymers were covalently conjugated with Bac7 CPP, or a fluorescein for quantification, prior to FNP. FITC labeling was used primarily for quantitation of placebo NPs (without RPV loaded). FNP was performed as described previously for placebo and RPV-loaded NPs with minor adjustments. For animal experiments, NP solutions were vortexed following FNP and then dialyzed (molecular weight cutoff: 6000-8000 Da) in 4 liters of DI water to remove the remaining THF. For animal studies, NPs were also fabricated at relative concentrations 2-fold higher than previous batches, to achieve tissue concentrations above the lower limit of detection by plate reader and LC/MS modalities.

For all *in situ* ligated loop studies, male Sprague-Dawley rats were fasted overnight ($n \geq 6$ rats per group). While anesthetized with isoflurane, the abdominal region of each rat was shaved and aseptically prepped. A longitudinal incision extending from the splenic flexure to the pelvis was applied to open the cavity. Sacs were prepared in the colon and duodenum. The duodenum was treated as a feces-free control and to compare NP transport in both the small and large intestines. Each sac was gently exposed and approximately 5-cm portions were tied off with suture material. In one study, animals were treated with Bac7-labeled NPs (wt, I, or RI) to determine tissue association in the presence of proteolytic enzymes, *in vivo*. All Bac7 NPs had a surface ligand density of 1% Bac7. Plain NPs were used as a control. Placebo NPs were fluorescently labeled with FITC. In separate studies, animals were treated with RPV-NP to quantitate RPV tissue amounts after treatment. NP solutions were prepared in 6.5 pH PBS at 290 mOsm/L. NPs (15 nM, 0.6 mg/ml RPV, 12% drug loading) with plain NPs, or Bac7 I (n=3), or 1.5 mM RPV nanosuspensions (positive control, n=2) in PEG 400 were injected into ligated sections (0.1ml per cm or 500 μ l). After 2 hours, animals were euthanized by diaphragm puncture and sacs were excised for analysis. Each sac was flushed with HBSS to remove the loose mucus layer and unabsorbed NPs. The tissue was then cut open along its longitude and the mucosa layer was gently scraped and collected in 400 μ l of HBSS. For fluorescence quantification, mucosal samples were mechanically homogenized and then centrifuged at 5500 rpm for 30 minutes at 4°C. The supernatant of each sample was collected and analyzed for fluorescence using a Tecan plate reader at Ex/Em of 485/535. Samples with RPV-loaded NPs were homogenized and treated with 1.4 ml of 5:1 ACN:H₂O for tissue precipitation. Samples were centrifuged at 5000 rpm for 10 min at 4°C and then analyzed by HPLC/MS to determine the concentration of RPV extracted.

5.3.9. *In Vivo* NP Retention Studies

NP retention and free RPV presence for up to 48 hours after intra-rectal dosing were investigated in male CD-1 mice. Anesthetized male CD-1 mice were dosed intra-rectally with enemas (200 μ l) of FITC-labeled placebo PCL-PEG NPs displaying Bac7 I. Plain NPs were used as a control. RPV-loaded (12 wt% drug loading) plain (control) NPs, or Bac7 I NPs (without FITC-labeling) was administered in a separate study to determine free RPV concentrations present in tissue. Following 2 hours, 24 hours, and 48 hours, mice were sacrificed by CO₂ euthanasia and necropsies were performed to remove intestinal tissue. Colorectal tissue was cut from below the ascending colon to the anus. The tissue was then flushed with 9 mLs of HBSS. The colon was then sliced longitudinally and the mucosal layer was gently scraped and collected. The uptake of placebo NPs into the colon after indicated time points was quantified by a fluorescence analysis. The uptake of RPV from RPV-containing NPs into the colon was measured using a Micromass ZQ-4000 mass spectrometer.

5.3.10. Validation of NP Surface Interactions and Fluorescence in Reaction Media

Potential surface interaction between FITC and FBS was investigated as an assessment of non-specific binding. Each NP was labeled with 7% FITC surface coverage as previously described. Bac7 ligand densities studied included 0% (plain), 1%, 5% and 10%. Placebo NPs were assembled by FNP and a mixture of 5:1 mass equivalent methyl- β -cyclodextrin: NP mass was made. Methyl- β -cyclodextrin was added to NP suspension as a lyoprotectant to assist NP resuspension following lyophilization. Liquid was flash frozen with liquid nitrogen and lyophilized for a minimum of 24 hours until a completely dry powder was formed. NP powders were weighted to acquire 2 nM NP samples that were transferred to microcentrifuge tubes. NP fluorescence was examined in pH-standardized culture media as described above. A range of pH values were tested (4.0, 5.0, 6.0, 7.0 and 8.0) using 1N HCl and 1N NaOH to make adjustments to

media. Samples were prepared by dissolving NPs in serum-treated, or serum-free, cell culture media and vortexing at high intensities for 30 seconds. This was followed by probe sonication Branson Sonifier 450 (Fischer Scientific, Pittsburgh, PA) (80% duty cycle and level 3 output) for a maximum of 60 seconds to disrupt aggregates and re-dissolve NPs. Fluorescein intensity was detected at excitation 485 and emission 535 in a Tecan plate reader.

5.3.11. Statistical Analysis

Graphpad Prism version 6.0 (GraphPad Software, Inc., San Diego, CA) was used to perform all statistical analysis for experiments. Results are represented by the mean and standard error of the mean (SEM). Statistical significance was determined by a 95% confidence interval ($p < 0.05$). Linear regression analysis was also performed using the GraphPad Prism Software for statistical analysis of curves and curve parameters. One tailed, unpaired Student's t-test assuming equal variances was used to compare individual groups. A two-way analysis of variance (ANOVA) test was run on multiple group analysis. Tukey or Bonferroni post-hoc tests were applied to compare multiple groups following ANOVA, to further assess inter group significances. F-tests were also applied sparingly for inter group analyses.

5.4. Results

5.4.1. Optimization of NP Hydrodynamic Diameter By Polymer Size Modifications

Copolymer hydrophilic and hydrophobic block lengths can be altered to fabricate a wide range of NP sizes. NP diameters, as measured by dynamic light scattering, ranged from 60-245 nm (Table 1). The effect of core:polymer ratio was consistent across all block copolymers, with a higher ratio of Vitamin E providing larger NPs, and a lower ratio of Vitamin E providing smaller NPs (data not shown). PCL_{6kDa}-PEG_{5kDa} with a 45% w/w PEG content and 0.83 hydrophilic-hydrophobic molecular block ratio resulted in the smallest NPs. PCL_{8.5kDa}-PEG_{2kDa} produced the

largest NPs with a 19% w/w PEG content and 0.24 hydrophilic-hydrophobic molecular block ratio. Hydrophilic-hydrophobic effect on NP size was determined by regression analysis for polymers with 2kDa and 5kDa PEG chains. A linear regression is shown for both data sets (Figure 1). PEG_{2kDa} polymers showed a negative regression with a correlation (R^2 value) of 0.99. PEG_{5kDa} polymers showed positive regression with a correlation of 0.98.

5.4.2. Rilpivirine Solubility in Release Media

Previously reported values for RPV solubility show it is practically insoluble in deionized (DI) water (< 0.1 mg/ml). More specifically, its solubility in water has ranged from 9.4×10^{-5} mg/ml to 20×10^{-5} mg/ml [22, 23]. We determined the solubility in DI water, DMEM (serum-free), and DMEM with 0.1% v/v Tween 80 (DMEM/Tween) (Figure 2). LC/MS values for RPV in water and DMEM were 5.7×10^{-6} mg/ml and 2.7×10^{-5} mg/ml, similar to previously reported data. Tween 80 significantly increased the dissolution of RPV resulting in approximately 4×10^{-3} mg/ml solubilized in DMEM/Tween. DMEM/Tween was chosen as the release medium for subsequent studies. RPV release studies were conducted at concentrations below the critical solubility and sink conditions were maintained throughout experiments.

5.4.3. Rilpivirine-NP Drug Loading and Characterization

Successful encapsulation of RPV within PCL-PEG NPs, of a range of molecular weight block combinations, was achieved by FNP. Salt formation with vitamin E succinate was found to control NP formation and increase stability compared with the vitamin E (non-salt) form. The non-salt form resulted in multiple peaks during dynamic light scattering showing inefficient drug encapsulation (data not reported). Size, polydispersity index, drug loadings and encapsulation efficiency is presented for each NP type in Table 1. Mean encapsulation efficiencies ranged from 85% to 98% with drug loadings about 10.9% to 17.7% of total NP mass (Table 2).

PLA_{6.5kDa}PEG_{5kDa} NPs resulted in the lowest encapsulation efficiency of 74% with drug loading of 9.8% (Figure 6).

5.4.4. Rilpivirine Release Kinetics

The release profile of RPV from NPs was studied for a series of polymers by dynamic dialysis. RPV release was quantified by measuring samples of release media over 24 hours by HPLC-MS. Maximum cumulative release was 32%, 23% and 41% for PCL_{1.6kDa}-PEG_{5kDa}, PCL_{3kDa}-PEG_{5kDa} and PCL_{6kDa}-PEG_{5kDa} NPs respectively (Figure 3). For the respective polymers, mean release rates were 0.5 µg/hr, 0.625 µg/hr and 0.56 µg/hr, over the first 8 hours. Samples of release media were acquired for up to 168 hours (7 days) with no significant changes in extent release after 24 hours. The maximum release for PCL_{2.8kDa}-PEG_{2kDa}, PCL_{6kDa}-PEG_{2kDa}, and PCL_{8.5kDa}-PEG_{2kDa} NPs was 43%, 24% and 20%, respectively, with mean release rates of 1.1 µg/hr, 0.55 µg/hr and 0.56 µg/hr over the beginning 8 hour duration (Figure 4). Average release rate for PLA_{6kDa}-PEG_{5kDa} NPs was 1.6 µg/hr for the first 8 hours and then a plateau in release at 58% is also seen (Figure 5). PLA_{6kDa}-PEG_{5kDa} resulted in a significantly lower, drug loading than comparable PCL-PEG NPs (Figure 6). First order release was observed for all NPs as shown by a linear regression in log % RPV remaining. A significant increase in release extent is shown as PCL block size decreases ($p < 0.05$), for polymers with 2 kDa MW PEG blocks. Modifying PCL block size from 8.5 kDa to 2.8 kDa, while PEG mass remained consistent, resulted in a greater than 2-fold increase in total percent cumulative release of RPV from formulated NPs. Inverted correlations between relative PCL block mass and release extent was shown for NPs with 5 kDa PEG chains. For these NPs, a 3 kDa PCL block resulted in lower total percent cumulative RPV release than that of a 6 kDa PCL block. Further decreasing the PCL block size to 1.6 kDa, resulted in intermediate levels of cumulative RPV release, between the previous two NP groups.

5.4.5. Ligated Loop Model-Analog Comparisons

An intestinal ligated loop model was used to investigate NP translocation through colorectal mucus to penetrate and associate with the mucosal tissue layer. Sacs were treated with plain NPs, NPs labeled with wt, I or RI Bac7 (Figure 7). In the colon, Bac7 I was found to result in the most significant increase (142%) in tissue association compared with plain NPs. However, in the duodenum, wt and RI Bac7 analogs showed significant increases in tissue association compared with plain NPs (81% and 93%, respectively). Plain NPs were used as a control. Bac7 I was chosen as the lead candidate to complete the remaining studies since colorectal delivery is the focus of this work.

5.4.6. Rilpivirine Tissue Extraction

For RPV-loaded NP studies, MS was used to measure RPV levels after tissue extraction. *A priori* validation tests confirmed our single-quadrupole, Micromass ZQ-4000 was sufficiently sensitive to determine RPV tissue concentrations as low as a single digit ng/mL level. Greater than 13% and 26% RPV tissue association is reported for Bac7 NPs and plain NPs, respectively, after 2 hours *in situ*. No significant differences were found in extracted RPV between plain NPs and Bac7 NPs (Figure 8). However, a trend is shown in which concentrations of extracted RPV decrease with the addition of Bac7. The decrease is likely due to strong association of Bac7 with tissue resulting in less RPV to extract after tissue precipitation for bioanalytical analysis. A similar trend is seen after analysis of mouse intra-rectal samples (Figure 9). The lowest amount of extracted RPV is shown for NPs labeled with both Bac7 and FITC. This can also be attributed to strong protein adsorption and unavailability of RPV bound within NPs, in the precipitated pellet. Intra-rectal RPV concentrations at the 24 hour time point were below our system's limit of detection and unable to be quantified. To investigate FITC non-specific binding potential with tissue protein, fluorescence intensity of FITC-labeled NPs for a group of representative Bac7 NPs was evaluated in the presence of FBS (Figure 10). For nearly all groups (plain, 1% Bac7, 5%

Bac7 or 10% Bac7 NPs), a significant decrease in fluorescence is seen when exposed to 10% FBS compared with serum-free control medium at pH values of 6, 7 and 8. At pH 4 and 5, after FITC is expected to become deionized, fluorescence is found to increase in the presence of FBS.

5.4.7. *In Vivo* NP Retention Studies

For NP retention studies after intra-rectal dosing of placebo NPs, Bac7 I NPs showed a greater than 3-fold increase in mucosal tissue association (~1.7% compared with ~0.45%) ($p < 0.05$) after two hours (Figure 11). NPs appear to be largely cleared from tissue by 24 hours. However, both plain and Bac7 NP presence is still above background up to 48 hours post administration indicating prolonged NP tissue concentrations. No significant differences were found between plain NPs and Bac7 NPs at 24- or 48-hour time points.

5.5. Discussion

An RPV-loaded NP platform was designed, characterized and assessed as a potential delivery system for a long-acting rectal mPrEP. Modeling of clinical trial data estimates up to 99% risk-reduction for the currently available oral PrEP, Truvada, when optimal adherence is met. However, efficacy hinges on patient compliance with a strict daily regimen and has proven to be variable over a number of randomized clinical trials[5-7]. Long-acting and extended release formulations may confer longer durations of protection, and improve adherence by avoiding the daily pressure and responsibility placed on the individual to remember to take a pill[5, 7, 8]. The development of a Bac7 NP delivery system with high drug loading, and the capability to achieve, and sustain, effective mucosal drug concentrations would be a promising technology to advance the long-acting PrEP field.

FNP was used as a simple, cost-effective technique to prepare placebo and RPV-loaded NPs with high loadings. Hydrophobic macromolecules are often used in FNP to reduce the activation

energy for nucleation and particle growth. They also have an effect on the nuclei number and thereby affect particle size. PCL homopolymers have been reported to drive nucleation in water [24]. The molecular weight was found to have a direct effect on NP size. Therefore, maintaining constant mass, higher molecular weight PCL chains were expected to produce larger NPs as a result of fewer nuclei available. In this study, placebo NPs resulted in similar trends for PCL-PEG copolymers with 2 kDa PEG chains. For this group of NPs, larger PCL chains imparted size increases. Glavas, et al. [25] previously investigated the effect of polymer block ratios, on NP size. They reported a similar hydrophilic-hydrophobic ratio range, as presented here, with copolymers comprised of 2 kDa MW PEG blocks. However, they reported that an increase in hydrophobic ratio resulted in a decrease in NP size. Therefore trends seen in our work are not uniform for all NP fabrication techniques or formulations. Glavas and colleagues prepared NPs by dissolution/evaporation method by which NPs are formed under different kinetic conditions than FNP. NPs formed by FNP result in uniform sizes caused by nonequilibrium quenching of unimers, which depends on the dimensions of the solvated amphiphilic block. Compared with traditional nucleation and growth of crystals, where NP size is dependent on initial concentrations, this is a fundamentally different process[26]. Additionally, we report an inverse correlation for PCL-PEG polymers with 5 kDa PEG compared with the 2 kDa PEG group. This makes it clear that correlations between hydrophilic-hydrophobic ratio and NP size may differ based on hydrophilic block size. We hypothesize that the hydrophobic core of placebo NPs expands at low PEG content (2kDa) due to relatively long PCL chains that dominate. This results in hydrodynamic expansion as the size of the PCL block is increased. When PEG content is relatively high (5kDa) and PEG chains dominate, PEG chains can extend outward increasing the space occupied by the corona. Future work should also be performed with a more extensive range of polymer block variations to see if linear correlations are seen at other ratios.

PCL_{6kDa}-PEG_{5kDa} was chosen as the model candidate to complete all subsequent *in vivo* studies due to ease of formulating NPs within the optimal size range (~40-60 nm) to achieve uninhibited diffusion across a mucus matrix. Saltzman et al. reported particles 30-60 nm were able to diffuse rapidly across samples of unstirred human cervical mucus [27, 28]. Mathematical modeling of solute behavior through hydrogel-like matrices exhibited the inhibition of mucus diffusion for particulates above 100nm[27, 29, 30]. Particles above 100 nm (200-500nm) with dense PEG coatings have been shown to avoid mesh entanglement and traverse the mucus barrier [27, 31]. However, Bac7 cationic charges may impose electrostatic interactions with surrounding mucus matrix. Therefore, it was important to keep particle sizes within a smaller range to avoid mucus interactions.

In precipitation processes such as FNP, the crystallinity and solubility of the active pharmaceutical ingredient (API) affect the formation and stability of nanostructures. Hydrophobic materials with logP values greater than 3.5 are generally formulated successfully into NPs, during FNP, because they are able to achieve sufficient supersaturation states and produce high nucleation rates, to control particle size. However, weakly hydrophobic or crystalline compounds form systems with low energy states that are inefficient to drive nucleation and lead to NP instability[19, 24]. RPV is classified as hydrophobic (experimental logP = 4.86, predicted value = 3.8)[23, 32] and crystalline[33], therefore *in situ* hydrophobic salt formation was implemented to successfully improve RPV stabilization [19]. This is a commonly used method for stabilizing drug loaded NPs. Previous Pinkerton, et al.[19] investigated, and substantiated, an assortment of salt formers capable of effectively encapsulating crystalline or weakly hydrophobic APIs. Salt formation is ideal for drug property modifications because it involves ionic interactions and therefore circumvents the need for FDA reapproval like conjugate prodrugs[19].

RPV-loaded NP size correlations with hydrophilic-hydrophobic block ratios are inconsistent with placebo trends showing the complexity of NP formation that is highly dependent upon formulation excipients. Encapsulation efficiency across PCL-PEG NPs ranged from 85% to 98% with high drug loadings between ~11% to 22%. All reported encapsulation efficiencies and drug loadings are considered moderate to high (EEs above 67% and DLs above 5%)[34] showing the ability of FNP to produce relatively high-loaded RPV NPs for drug delivery.

RPV release studies were performed in 0.1% v/v Tween 80/DMEM solution to model biological fluids and increase RPV dissolution. Tween 80 is frequently used in drug release studies for highly lipophilic drugs to maintain sink conditions[35, 36]. Studies were performed at pH 6.5 to model the environment of the lower gastrointestinal tract. The pH of the lumen in the proximal and distal colon ranges between 6-6.7 in healthy humans[37]. The results support our hypothesis that degree of drug release may be controlled by varying polymer block lengths and therefore can allow for modulation of drug delivery from PCL-PEG NPs. This was expected due to the common principles of drug release that state high molecular weight polymers have a low elastic moduli and are nondeformable[38]. However, only about a 20% increase in total cumulative release was shown by block modifications. PCL is a semi crystalline polymer. Polymer crystallinity is an important factor in drug release. Only amorphous regions are permeable and thereby provide access to water molecules and easy diffusion. A high degree of crystallinity results in slower drug release[38]. As an amorphous polymer alternative, we compared the release state of PLA_{6.3kDa}(DL Form)-PEG_{5kDa} NPs. While these NPs resulted in a greater total cumulative RPV release, we now faced alternative challenges with lower encapsulation efficiency and drug loading. Additionally, PLA-PEG NPs resulted in a more rapid burst release and even shorter release profiles was seen in comparison to PCL-PEG NPs.

For *in vivo* animal studies, Bac7 conjugation to polymer chains was performed using copper-free click chemistry instead of previously reported maleimide-thiol click linkage[39]. Thioether exchange with metabolites and proteins may potentially compromise linker stability and *in vivo* efficacy[40, 41]. For long-term PrEP, this would raise a critical concern. To mitigate this problem, we investigated the use of a DBCO-azido based click chemistry method as a potentially more stable alternative.

RPV tissue presence after RPV-loaded NP treatment was investigated in an *in situ* ligated loop study and intra-rectal mouse study. However, we were unsuccessful in quantifying the total RPV presence in mucosal tissue. For HPLC-MS, RPV must be isolated from tissue proteins to prevent contamination of the HPLC separation column. The quantified data suggest trapping of NPs, with Bac7 and FITC labeling, within tissue pellets during the protein precipitation step. The binding of charged surface moieties to tissue proteins likely causes this. Similar quantitation challenges, attributed to CPPs adhering to plasma proteins, have been reported by others[42-44]. Therefore, this highlights the need for future work in the development of new and simple bioanalytical methods to assess delivery system efficacy *in vivo*.

Theoretical calculations based on experimental results for percent *in situ* uptake predict the maximum RPV delivered from tissue-associated NPs to be approximately 0.5 nmol for plain NPs and approximately 1.1 nmol for Bac7 I NPs (values based on placebo tissue association). Our reported values for RPV extraction are unable to show complete RPV presence, however, they suggest a significant amount of RPV release from non-tissue associated NPs present within the sac lumen. These results support the potential of NP-based RPV delivery. RPV is classified by the biopharmaceutics class system as a class II drug having low aqueous solubility and high permeability[32]. Therefore delivery of RPV to epithelial tissue is still efficient if RPV is release from NP premature to tissue penetration. However, RPV loading in these polymeric NPs is still a

major concern. Similar trends in RPV extraction were seen for RPV-NP tissue association mouse studies and can also be attributed to ionic interactions between NPs and tissue proteins. In this study we also compared NPs with FITC surface labeling. Results suggest that even greater tissue association occurs for these NPs. This is also expected based on well-known non-specific binding between fluorescein and sera proteins[45, 46]. We investigated the interaction between FITC labeling and FBS by measuring the arbitrary fluorescence of NPs, with and without the presence of serum, to assess FITC binding. For all pH values where FITC is ionized, a significant decrease in fluorescence was shown indicating non-specific binding. An unexpected increase in fluorescence is seen at pH 4 and 5 where FITC is predominantly uncharged. At lower pH, the molecular confirmation of FITC and serum proteins is expected to be significantly different and may result in a more fluorescent FITC state. Additionally, as seen with *in situ* studies, extracted RPV values exceeded theoretical calculations of 0.14 nmol for plain NPs and 0.64 nmol for Bac7 I NPs. This suggests that RPV luminal delivery is achievable by intra-rectal dosing and not an artifact of the enclosed loop environment. Drug extraction complications, during *in vivo* analyses, highlight the need to develop more robust assessments of PrEP efficacy during early stages in development. The field of PrEP research relies heavily on animal models to assess treatment efficacy and derive preclinical data. Therefore, improving the evaluation of animal model systems will help ascertain the effectiveness of drug delivery systems for improved clinical outcomes [47, 48].

NP retention studies revealed majority clearance of Bac7 NPs at 24 hours. Both plain and Bac7 NPs were present in colorectal tissue for 48 hours, at low levels, suggesting minimal cellular internalization and potential transport into lamina propria. However, these low tissue concentrations show limitations in their potential to maintain therapeutically effective RPV concentrations within tissue. The cause for early clearance may be mucus shedding. Mucus is a viscoelastic barrier that is continuously secreted and shed, or digested and recycled. The

estimated turnover time of gastrointestinal mucus ranges from four to six hours in murine models[49]. Furthermore, the turnover rate is estimated to be even more rapid (about an hour) for the inner mucus of the distal colon in rodents[50, 51]. This makes it difficult for drugs and delivery systems to reach mucosal surfaces since they must travel “upstream” towards the epithelium and successfully penetrate the mucus lining before shedding occurs. It is common for mucus to adhere to particles along the way and be removed during shedding[50, 52]. High NP tissue presence after 2 hours show the level of dynamic transport within the colonic environment and the robustness of Bac7 NPs to reach the epithelial site. However, NPs may have been cleared from the epithelial surface before effective cellular internalization.

In summary, a RPV-loaded NP platform was designed, characterized and assessed as a potential delivery system in a long-acting colorectal mPrEP. This NP platform displayed relatively high drug loadings for polymeric NPs. Simple modulation of RPV release kinetics was achieved by adjusting polymer type and block size. However, this system suffers from overall poor RPV release. Sustained RPV release and NP retention were evaluated *in vitro* and *in vivo* showing the ability to successfully deliver RPV to colorectal tissue in rodent models. Plain NP and Bac7 NP presence was seen in tissue for over 48 hours at relatively low levels following significant tissue clearance after 2-hours post-administration. RPV tissue concentrations decreased below the MS limit of detection and were unable to be assessed at 24 hours. Low RPV tissue concentrations can be attributed to low cell uptake of NPs and incomplete RPV release from NPs. Additionally, further bioanalytical assay development is needed to accurately quantitate drug levels for delivery systems *in vivo*.

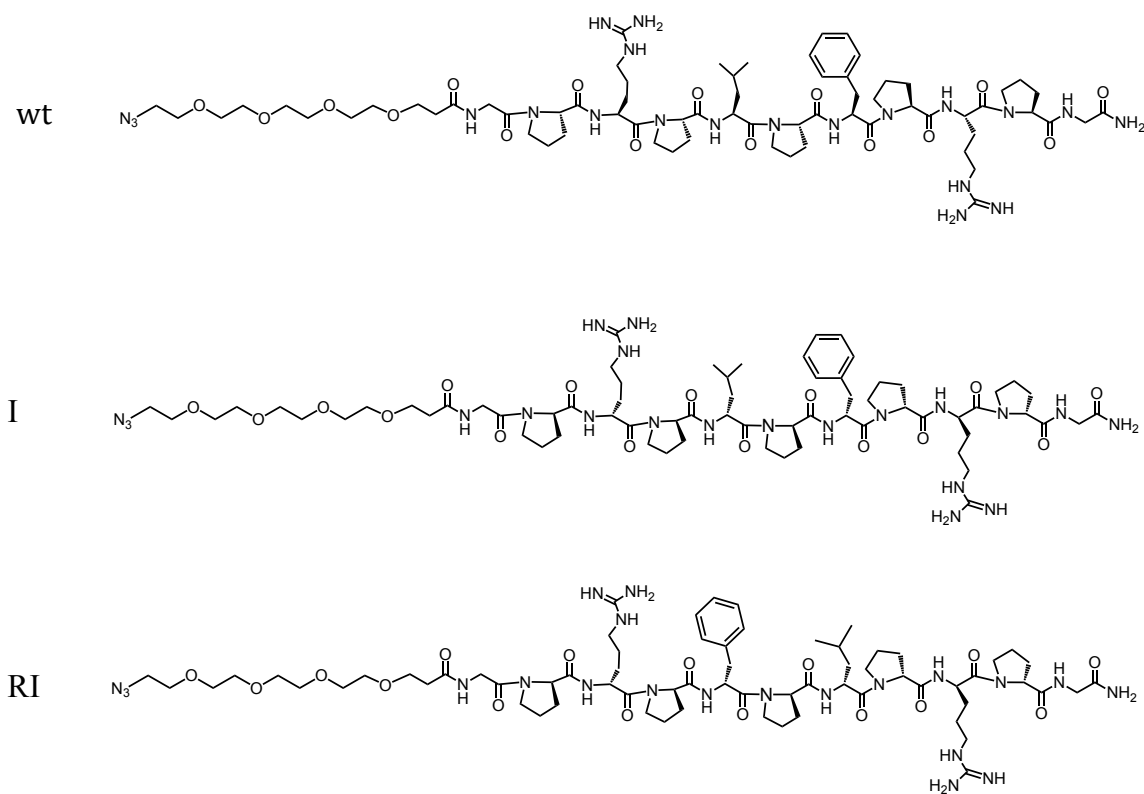
It is important to point out that normal epithelial turnover within the colon is 5-8 days in humans and 2-3 days in rodents[11, 21]. Thus for our PrEP platform, achieving 3 days in mice was considered sufficient as a one-week rodent equivalent to indicate extended NP retention. The

study was terminated after 48 hours due to low levels of NPs with no significant differences between plain NPs and Bac7 NPs. Compared with previous work successfully showing the 5-day retention of Bac7-PEG-FITC nanoconjugates, these results suggest that size, structure and functionalization play significant roles on platform retention. Future work needs to be completed to enhance NP properties and increase intracellular transport rates following mucus penetration. Additional drug delivery systems should also be explored to avoid rapid clearance, and to achieve the drug loading and release kinetics necessary to maintain therapeutically relevant drug concentrations in mucosal tissue.

5.6. Authors Contributions

Majority of work in this manuscript was completed by Nelson, AG with contributions of the listed co-authors as following: Wang, H assisted in the completion of *in vitro* drug release studies and data analysis. Myers, DR assisted with preliminary studies to develop framework for *in vitro* and *in vivo* work. Holloway, J and Shike, L contributed in the design of animal studies and assisted in the completion of *in vivo* work. Szekely, Z and Zhang X were involved in planning. Sinko, P J supervised the project.

5.7. Figures



Formula	Molecular Weight	Molecular Mass	CLogP	Topographical Polar Surface Area (TPSA)
C ₆₇ H ₁₀₇ N ₂₁ O ₁₆	1462.72	1461.82	-0.865	528.72

Scheme 1. Wild-type (wt), inverso (I) and retroinverso (RI) analogs of azido-PEG-linked Bac7 peptides synthesized by solid phase peptide synthesis. Molecular structure depicted in Chem Draw Professional 16.0 software. Molecular properties were computed using pre-programmed software algorithms. Calculated molecular weight, molecular mass, computational LogP, and Topographical Polar Surface Area are shown.

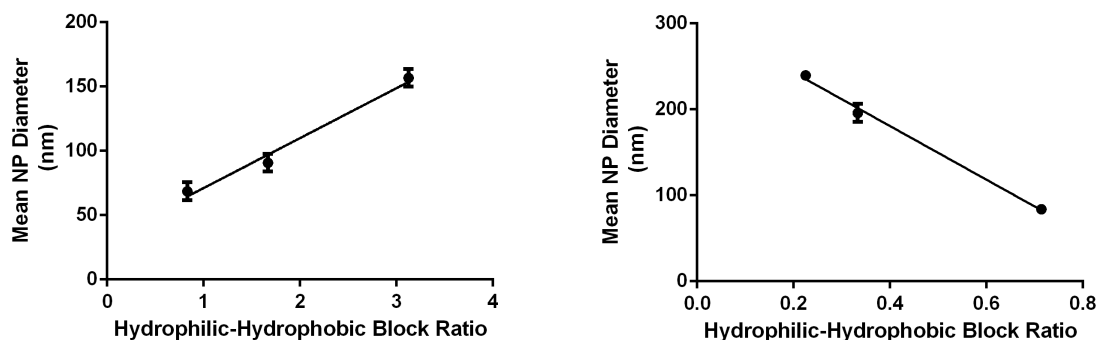


Figure 1. Left. NP size correlation with polymer hydrophilic-hydrophobic molecular weight block ratios for polymers with 5 kDa PEG. Placebo NPs were fabricated with 1:1 polymer: vitamin E mass ratio in FNP. Three different copolymers and hydrophilic-hydrophobic block ratios were used: PEG_{5kDa}-PCL_{1.6kDa} (3.13), PEG_{5kDa}-PCL_{3kDa} (1.66) , and PEG_{5kDa}-PCL_{6kDa} (0.83) ($n \geq 3$). **Right. NP size correlation with PCL-PEG hydrophilic-hydrophobic molecular weight block ratios for polymers with 2 kDa PEG.** Placebo NPs were fabricated with 1:1 polymer: vitamin E mass ratio in FNP. Three different copolymers and hydrophilic-hydrophobic block ratios were used: PEG_{2kDa}-PCL_{2.8kDa} (0.71), PEG_{2kDa}-PCL_{6kDa} (.33), and PEG_{2kDa}-PCL_{8.5kDa} (0.24) Mean NP sizes and standard error of the means are shown ($n \geq 3$).

	Diameter (nm)	Poly Dispersity Index (PDI)
PCL _{1.6kDa} -PEG _{5kDa}	156.7±6.9	0.09±0.01
PCL _{3kDa} -PEG _{5kDa}	90.7 ± 6.8	0.25±0.02
PCL _{6kDa} -PEG _{5kDa}	68.6 ± 7.0	0.31±0.21
PCL _{2.8kDa} -PEG _{2kDa}	84.0±2.2	0.13±0.00
PCL _{6kDa} -PEG _{2kDa}	196±10.4	0.17±0.01
PCL _{8.5kDa} -PEG _{2kDa}	239.7±5.7	0.13±0.01

Table 1. NP characterization of placebo NPs. The table shows NP characterization for placebo particles and RPV-loaded NPs following FNP. Mean and standard deviation shown (n = 4)

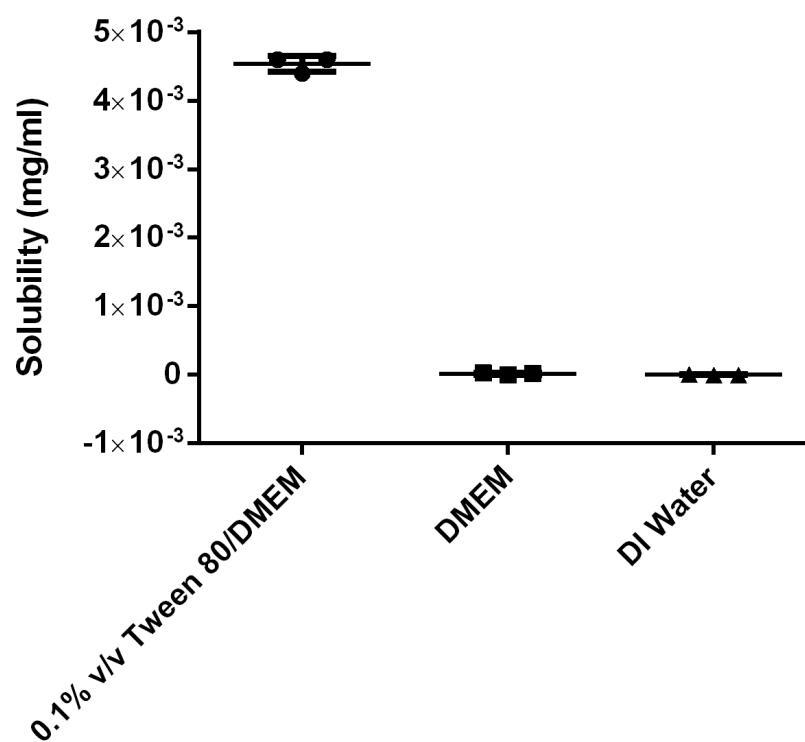


Figure 2. Measuring RPV solubility in 0.1% v/v Tween 80/DMEM, DMEM, and DI water. LC/MS values for RPV in water and media were 5.7×10^{-6} mg/ml and 2.7×10^{-5} mg/ml. Tween 80 significantly increased the solubility of RPV in DMEM to 4×10^{-3} mg/ml. Experiments were performed in triplicate. Individual sample solubilities are presented along with the group mean and standard deviation ($n=3$).

	Diameter (nm)	Poly Dispersity Index (PDI)	Drug Loading (%)	Encapsulation Efficiency (%)
PCL _{1.6kDa} -PEG _{5kDa}	105.1±7.5	0.20±0.06	10.9±0.3	85.4±2.6
PCL _{3kDa} -PEG _{5kDa}	54.3±11.4	0.25±0.06	13.3 ±2.3	98.0±0.9
PCL _{6kDa} -PEG _{5kDa}	57.4±9.4	0.32±0.07	10.7±0.5	85.9±4.2
PCL _{2.8kDa} -PEG _{2kDa}	112.3±0.14	0.19±0.05	22.4±11.7	91.4±4.0
PCL _{6kDa} -PEG _{2kDa}	199±31.8	0.19±0.00	17.7±3.4	90.5±0.9
PCL _{8.5kDa} -PEG _{2kDa}	165.4±45.3	0.16±0.01	13.0±3.9	92.3±2.5

Table 2. NP characterization of RPV-loaded NPs. The table shows NP characterization for placebo particles and RPV-loaded NPs following FNP. Mean and standard deviation shown (n = 3).

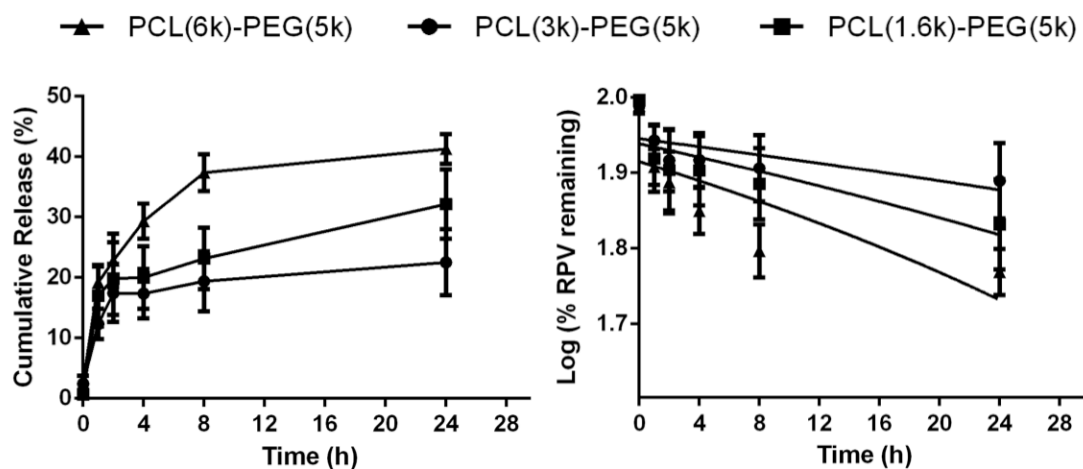


Figure 3. RPV release from PCL-PEG NPs with 5 kDa PEG coronas. Cumulative release of RPV in 0.1 v/v Tween 80 in serum-free DMEM. A first order release is shown for all NPs. Maximum cumulative release was 32%, 23% and 41% for PCL_{1.6kDa}-PEG_{5kDa}, PCL_{3kDa}-PEG_{5kDa} and PCL_{6kDa}-PEG_{5kDa}, respectively, with average release rates of 0.5 μ g/hr, 0.625 μ g/hr and 0.56 μ g/hr for the first 8 hours. All release rates plateaued by 24 hours. Samples were acquired for up to 7 days with no significant differences in release between days 2 and 7. Means and standard error of the means are shown (n=3).

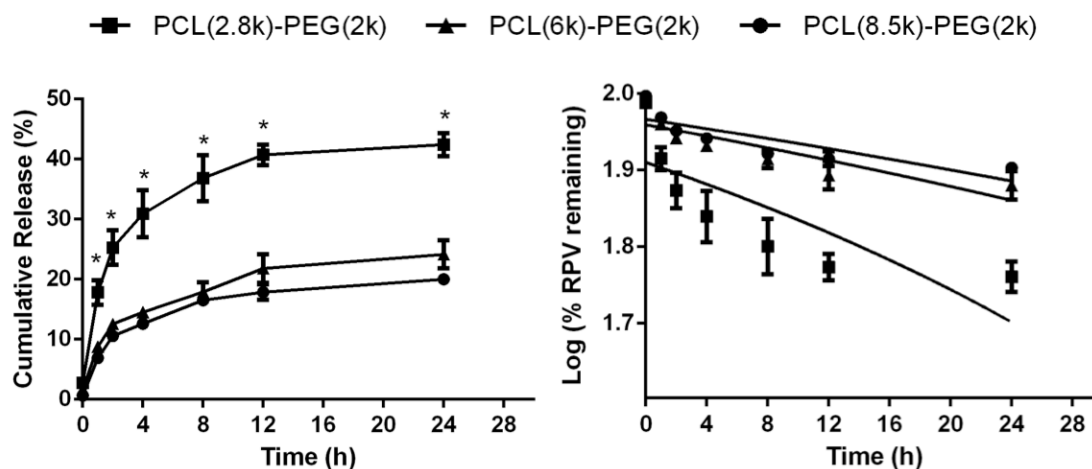


Figure 4. RPV release from PCL-PEG NPs with 2kDa PEG coronas. Cumulative release of RPV in 0.1 v/v Tween 80 in serum-free DMEM. Release for all NPs was first order as shown by a linear regression in log% RPV remaining. The maximum release for PCL_{2.8kDa}-PEG_{2kDa}, PCL_{6kDa}-PEG_{2kDa}, and PCL_{8.5kDa}-PEG_{2kDa} NPs was 43%, 24% and 20% for, respectively with mean release rates of 1.1 $\mu\text{g/hr}$, 0.55 $\mu\text{g/hr}$ and 0.56 $\mu\text{g/hr}$ for the first 8 hours. Release rates for all experiments plateaued by 24 hours. Samples were acquired for up to 7 days with no significant differences in release between days 2 and 7. A significant decrease in release rate is shown between groups with an increase in hydrophobic block length (* $p < 0.05$). Means and standard error of the means are shown ($n \geq 2$).

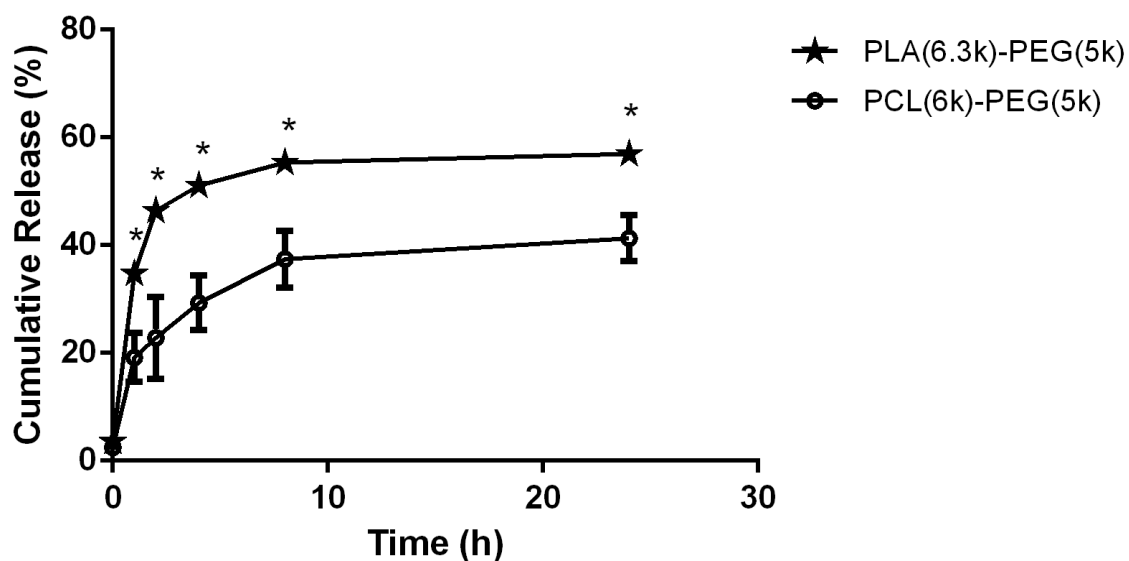


Figure 5. RPV release from PCL-PEG NPs and PLA-PEG NPs with comparable block weights. Cumulative release of RPV in 0.1 v/v Tween 80 in serum-free DMEM. With formulations resulting in a maximum release of 58% and 40% for PLA_{6kDa}-PEG_{5kDa} and PCL_{6kDa}-PEG_{5kDa}, respectively. An increase in RPV release is shown at all time points. Average release rates were 0.56 $\mu\text{g/hr}$ and 1.6 $\mu\text{g/hr}$ for PCL_{6kDa}-PEG_{5kDa} and PLA_{6kDa}-PEG_{5kDa}, respectively, for the first 8 hours. A plateau in release is reached for both polymers at 8 hours. Means and standard deviations are presented. Experiments were repeated at least twice (n=3) (*p<0.05).

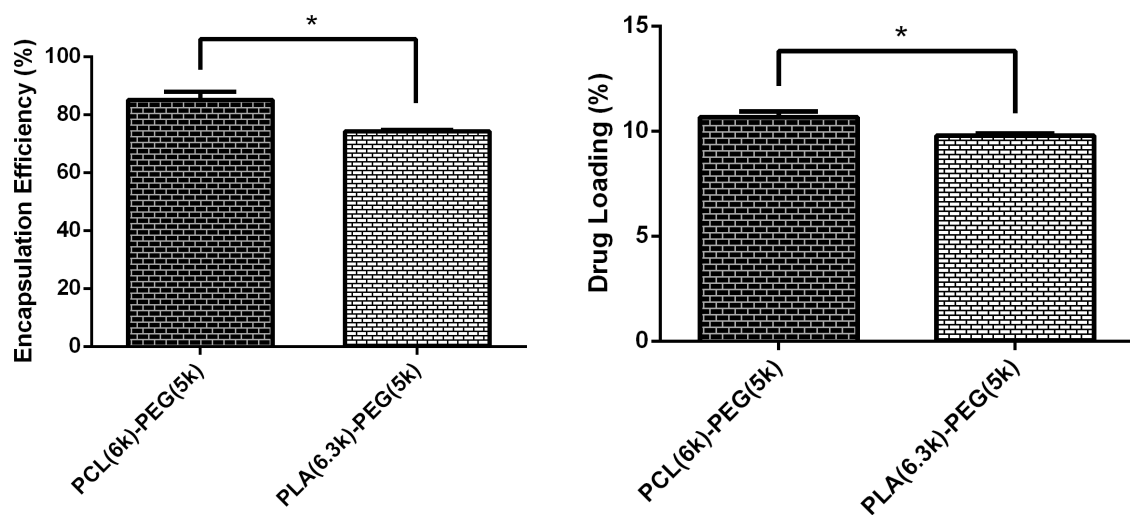


Figure 6. RPV-NP Characterization for PCL-PEG NPs and PLA-PEG NPs. Left. Percent of RPV encapsulated. PCL_{6kDa}-PEG_{5kDa} NPs and PLA_{6.3kDa}-PEG_{5kDa} NPs show a 85.9% and 74.3% mean encapsulation efficiency, respectively. **Right.** RPV loadings. PCL_{6kDa}-PEG_{5kDa} NPs and PLA_{6.3kDa}-PEG_{5kDa} NPs show a 10.7% and 9.8% mean drug loading, respectively. (N≥2) (*p<0.05).

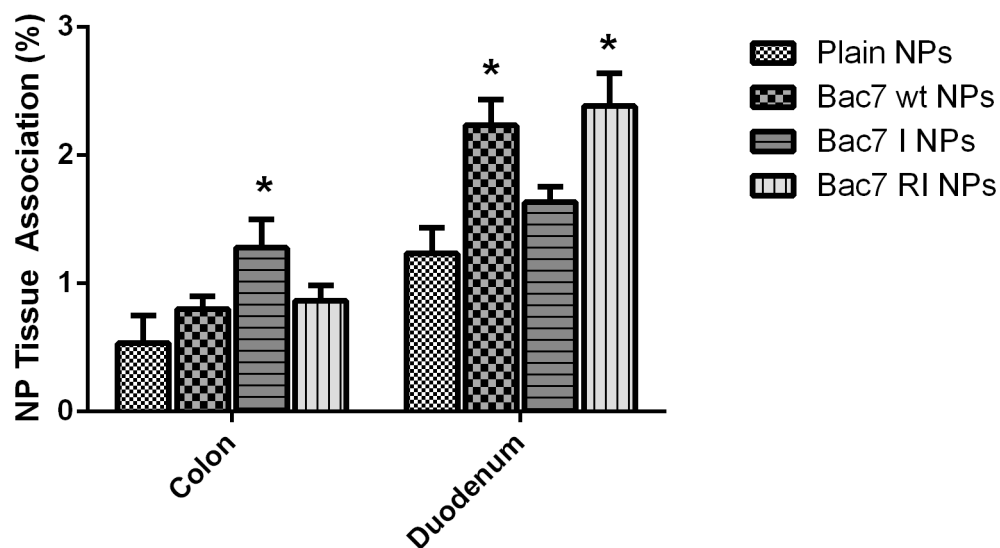


Figure 7. NP mucosal tissue association for wild-type (wt), inverso (I), and retroinverso (RI) Bac7 analogs *in vivo* in Sprague-Dawley rats. Intestinal ligated loop model was used to investigate NP translocation through colorectal mucus to associate with the epithelial layer. Plain NPs or NPs with wt, I or RI Bac7 were injected into 3-5 cm ligated sacs in the colon and duodenum and treated for 2 hours. NPs were fluorescently labeled with FITC. In the colon, Bac7 I was found to result in a significant increase (141.5%) in tissue association compared with plain NPs. However, in the duodenum, wt, and RI Bac7 analogs showed significant increases in tissue association compared with plain NPs (81% and 93% respectively). (n=6, *p<0.05).

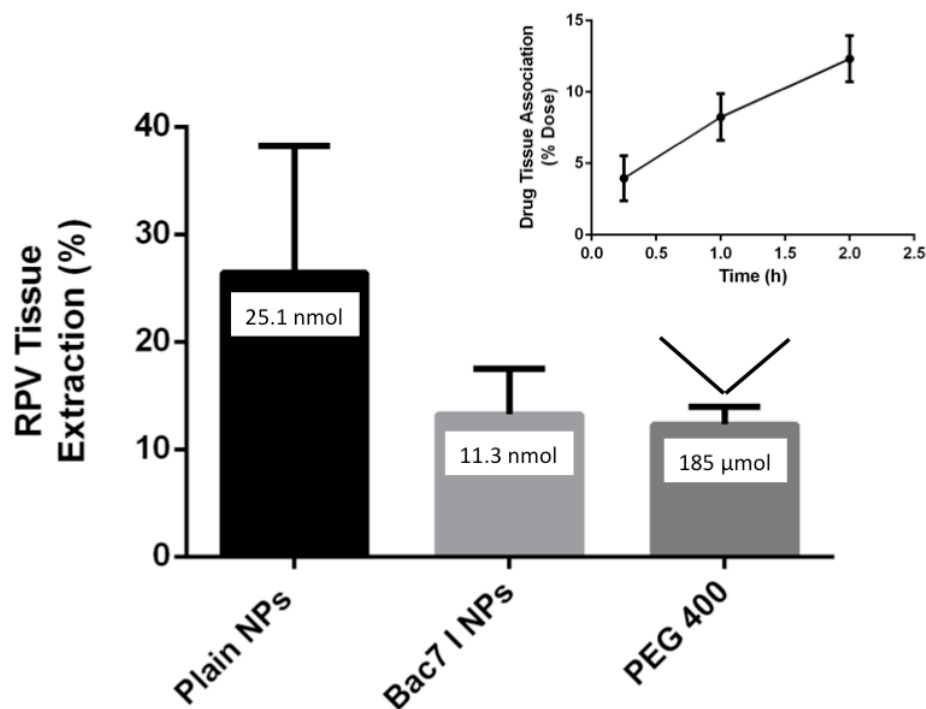


Figure 8. RPV extraction from colorectal tissue after *in situ* treatment with RPV-loaded NPs (RPV-NPs) and RPV nanosuspensions in PEG 400 *in vivo* in male Sprague-Dawley rats. Intestinal ligated loop model was used to investigate NP translocation through colorectal mucus to penetrate and associate with the mucosal tissue layer. Plain NPs, Bac7 I NPs (0.6 mg/ml RPV, 12% drug loading) (n=3) or 1.5 mM RPV nanosuspensions (positive control, n=2) in PEG 400, were injected into 3-5 cm ligated sacs in the colon and duodenum for 2 hours. Tissue drug concentrations were quantified and no significant differences were found in free RPV between plain NPs (25.1 nmol) and Bac7 I NPs (11.3 nmol). A trend is shown with a decrease in free RPV after tissue extraction with the addition of Bac7. The decrease can be attributed to a greater amount of RPV-NPs strongly associated with tissue thereby not available after tissue precipitation for bioanalytical analysis. Means and standard error of means are shown. Bar values indicate mean RPV amounts. Inset: RPV tissue association over 2-hour post dose for nanosuspensions.

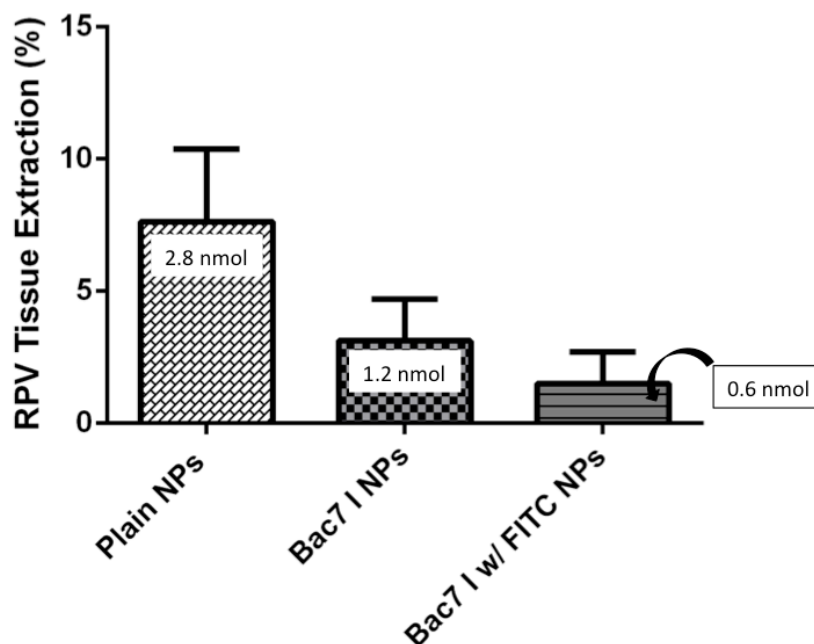


Figure 9. RPV extraction from colorectal tissue after intra-rectal treatment with RPV-loaded NPs and RPV nanosuspensions in PEG 400 *in vivo* in male CD-1 mice. Intestinal ligated loop model was used to investigate NP translocation through colorectal mucus to penetrate and associate with mucosal tissue layer. NPs (0.6 mg/ml RPV, 12% drug loading) with plain NPs, Bac7 I NPs or FITC-labeled Bac7 I NPs (n=3) were administered intra-rectally. Quantification of extracted RPV showed no significant differences between plain and Bac7 I NPs. A trend is shown with a decrease in free RPV after tissue extraction with the addition of Bac7. The decrease can be attributed to a greater amount of RPV-NP strongly associated with tissue thereby not available after tissue precipitation for bioanalytical analysis. Means and standard error of means are shown. RPV concentrations were below MS limit of detection by 24 hours and unable to be quantified.

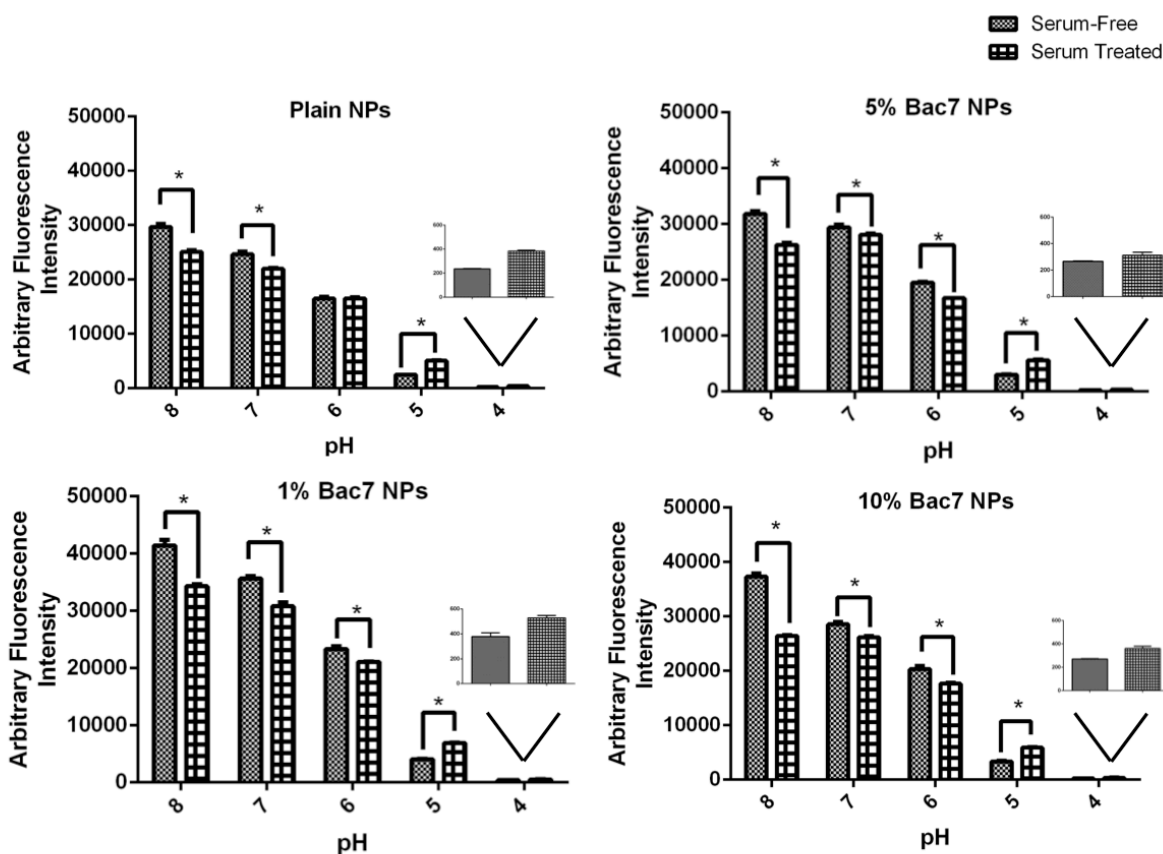


Figure 10. Interaction of covalently-conjugated FITC dye on NP corona with serum proteins. Fluorescence intensity of FITC-labeled NPs with 0%, 1%, 3%, 5% or 10% Bac7 surface coverage was measured as an indicator of the interaction of FITC ligand with fetal bovine serum proteins at pH 4, 5, 6, 7, and 8 (n=3). Each NP corona included a 7% FITC ligand density. FITC ionization profile shows ionization at above neutral pH (pH 7) and a loss of charge at lower pH (~pH 4). For all NP groups, a significant decrease in fluorescence is seen when exposed to 10% FBS compared with serum-free medium at pH 6, 7 and 8. At pH 4 and 5, after deionization of FITC, fluorescence increases in the presence of FBS. n=3, (*p<0.05). Inset: enlarged graph of pH 4 data.

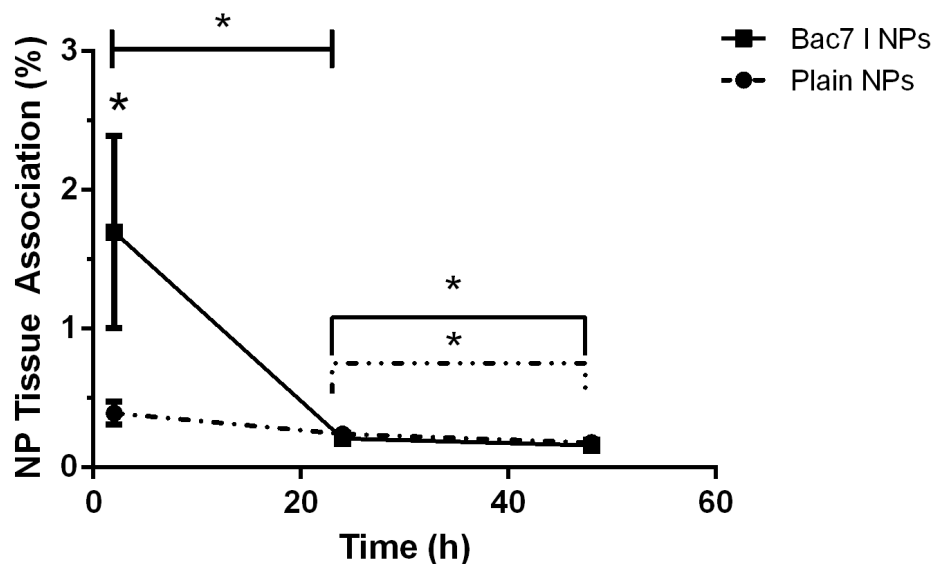


Figure 11. NP Tissue association of plain NPs and Bac7 I NPs over 48 hours *in vivo* in CD-1 mice. Mice were anesthetized and rectally treated with 200 μ l enemas containing 6.4 mg/ml plain or Bac7 I NPs for up to 48 hours. After 2 hours, Bac7 I NPs show 3-fold greater mucosal tissue association (~1.7% compared with ~0.45%). NPs appear to be largely cleared from tissue after 24 hours ($n \geq 3$). However, NP presence is still above background values at 48 hours indicating prolonged NP persistence. Values are present as the mean and SEM (* $p < 0.05$). Solid lines represent significance bars for Bac7 I NPs. Dotted lines show significance for plain NPs.

5.8. References

- [1] G.W. Huynh K, HIV, Prevention. <<https://www.ncbi.nlm.nih.gov/books/NBK470281/>>, 2017).
- [2] I. McGowan, An Overview of Antiretroviral Pre-Exposure Prophylaxis of HIV Infection, *American Journal of Reproductive Immunology* 71(6) (2014) 624-630.
- [3] R.J. Landovitz, R. Kofron, M. McCauley, The Promise and Pitfalls of Long Acting Injectable Agents for HIV Prevention, *Current opinion in HIV and AIDS* 11(1) (2016) 122-128.
- [4] J.M. Marrazzo, HIV Prevention: Opportunities and Challenges, *Topics in Antiviral Medicine* 24(4) (2016) 123-126.
- [5] R.P. Walensky, M.M. Jacobsen, L.-G. Bekker, R.A. Parker, R. Wood, S.C. Resch, N.K. Horstman, K.A. Freedberg, A.D. Paltiel, Potential Clinical and Economic Value of Long-Acting Preexposure Prophylaxis for South African Women at High-Risk for HIV Infection, *The Journal of Infectious Diseases* 213(10) (2016) 1523-1531.
- [6] J.T. Parsons, H.J. Rendina, T.H.F. Whitfield, C. Grov, Familiarity with and Preferences for Oral and Long-Acting Injectable HIV Pre-exposure Prophylaxis (PrEP) in a National Sample of Gay and Bisexual Men in the U.S, *AIDS and behavior* 20(7) (2016) 1390-1399.
- [7] G.J. Greene, G. Swann, A.J. Fought, A. Carballo-Diéguez, T.J. Hope, P.F. Kiser, B. Mustanski, R.T. D'Aquila, Preferences for Long-Acting Pre-exposure Prophylaxis (PrEP), Daily Oral PrEP, or Condoms for HIV Prevention Among U.S. Men Who Have Sex with Men, *AIDS and Behavior* 21(5) (2017) 1336-1349.
- [8] W.C. Goedel, J.A. Schneider, H.R. Hambrick, N.T. Kreski, J.G. Morganstein, S.H. Park, O. Mgbako, D.T. Duncan, Are Anal Sex Roles Associated with Preferences for Pre-Exposure Prophylaxis Administration Modalities Among Men Who Have Sex with Men?, *Archives of Sexual Behavior* (2017).
- [9] N.I.o.H.-U.S.N.L.o. Medicine, A Phase IIb Study to Evaluate a Long-Acting Intramuscular Regimen for Maintenance of Virologic Suppression (Following Induction With an Oral Regimen of GSK1265744 and Abacavir/Lamivudine) in Human Immunodeficiency Virus Type 1 (HIV-1) Infected, Antiretroviral Therapy-Naive Adult Subjects. <<https://clinicaltrials.gov/ct2/show/NCT02120352>>, 2014).
- [10] M. Kovarova, O.D. Council, A.A. Date, J.M. Long, T. Nochi, M. Belshan, A. Shibata, H. Vincent, C.E. Baker, W.O. Thayer, G. Kraus, S. Lachaud-Durand, P. Williams, C.J. Destache, J.V. Garcia, Correction: Nanoformulations of Rilpivirine for Topical Pericoital and Systemic Coitus-Independent Administration Efficiently Prevent HIV Transmission, *PLoS Pathogens* 11(10) (2015) e1005170.
- [11] A.G. Nelson, X. Zhang, U. Ganapathi, Z. Szekely, C.W. Flexner, A. Owen, P.J. Sinko, Drug delivery strategies and systems for HIV/AIDS pre-exposure prophylaxis and treatment, *Journal of Controlled Release* 219 (2015) 669-680.
- [12] M. Lipkin, *Proliferation and Differentiation of Normal and Diseased Gastrointestinal Cells*, Raven Press, New York, 1987.
- [13] E. Blanco, H. Shen, M. Ferrari, Principles of nanoparticle design for overcoming biological barriers to drug delivery, *Nature Biotechnology* 33 (2015) 941.
- [14] A.Z. Wilczewska, K. Niemirowicz, K.H. Markiewicz, H. Car, Nanoparticles as drug delivery systems, *Pharmacological Reports* 64(5) (2012) 1020-1037.
- [15] W.H. De Jong, P.J.A. Borm, Drug delivery and nanoparticles: Applications and hazards, *International Journal of Nanomedicine* 3(2) (2008) 133-149.
- [16] F. Notario-Pérez, R. Ruiz-Caro, M.-D. Veiga-Ochoa, Historical development of vaginal microbicides to prevent sexual transmission of HIV in women: from past failures to future hopes, *Drug Design, Development and Therapy* 11 (2017) 1767-1787.
- [17] Z.S. Zhang, L; Liu, R, Flash nanoprecipitation of polymer supported Pt colloids with tunable

- catalytic chromium reduction property, *Colloid and Polymer Science* 296 (2018) 327-333.
- [18] Y. Liu, Z. Tong, R.K. Prud'homme, Stabilized polymeric nanoparticles for controlled and efficient release of bifenthrin, *Pest Management Science* 64(8) (2008) 808-812.
- [19] N.M. Pinkerton, A. Grandeur, A. Fisch, J. Brozio, B.U. Riebesehl, R.K. Prud'homme, Formation of Stable Nanocarriers by in Situ Ion Pairing during Block-Copolymer-Directed Rapid Precipitation, *Molecular Pharmaceutics* 10(1) (2013) 319-328.
- [20] J. Han, Z. Zhu, H. Qian, A.R. Wohl, C.J. Beaman, T.R. Hoye, C.W. Macosko, A simple confined impingement jets mixer for flash nanoprecipitation, *Journal of Pharmaceutical Sciences* 101(10) (2012) 4018-4023.
- [21] M. Lipkin, *Proliferation and Differentiation of Normal and Diseased Gastrointestinal Cells*, New York.
- [22] T.M. Index, Rilpivirine. <<https://www.rsc.org/Merck-Index/monograph/m9619/rilpivirine?q=authorize>>, 2018 2018).
- [23] DrugBank, Rilpivirine. <<http://www.drugbank.ca/drugs/DB08864>>, 2013).
- [24] S.M. D'Addio, R.K. Prud'homme, Controlling drug nanoparticle formation by rapid precipitation, *Advanced Drug Delivery Reviews* 63(6) (2011) 417-426.
- [25] L. Glavas, P. Olsén, K. Odellius, A.-C. Albertsson, Achieving Micelle Control through Core Crystallinity, *Biomacromolecules* 14(11) (2013) 4150-4156.
- [26] B.K. Johnson, R.K. Prud'homme, Mechanism for Rapid Self-Assembly of Block Copolymer Nanoparticles, *Physical Review Letters* 91(11) (2003) 118302.
- [27] G. Aljayyousi, M. Abdulkarim, P. Griffiths, M. Gumbleton, Pharmaceutical Nanoparticles and the Mucin Biopolymer Barrier, *BioImpacts : BI* 2(4) (2012) 173-174.
- [28] W.M. Saltzman, M.L. Radomsky, K.J. Whaley, R.A. Cone, Antibody diffusion in human cervical mucus, *Biophysical Journal* 66(2 Pt 1) (1994) 508-515.
- [29] B. Amsden, Solute Diffusion within Hydrogels. Mechanisms and Models, *Macromolecules* 31(23) (1998) 8382-8395.
- [30] B. Amsden, An Obstruction-Scaling Model for Diffusion in Homogeneous Hydrogels, *Macromolecules* 32(3) (1999) 874-879.
- [31] S.K. Lai, D.E. Hanlon, S. Harrold, S.T. Man, Y.-Y. Wang, R. Cone, J. Hanes, Rapid transport of large polymeric nanoparticles in fresh undiluted human mucus, *Proceedings of the National Academy of Sciences* 104(5) (2007) 1482.
- [32] I. Usach, V. Melis, J.-E. Peris, Non-nucleoside reverse transcriptase inhibitors: a review on pharmacokinetics, pharmacodynamics, safety and tolerability, *Journal of the International AIDS Society* 16(1) (2013) 18567.
- [33] N.C.f.B. Information, Rilpivirine. <<https://pubchem.ncbi.nlm.nih.gov/compound/645116>>, 2006).
- [34] J. Xu, S. Zhang, A. Machado, S. Lecommandoux, O. Sandre, F. Gu, A. Colin, Controllable Microfluidic Production of Drug-Loaded PLGA Nanoparticles Using Partially Water-Miscible Mixed Solvent Microdroplets as a Precursor, *Scientific Reports* 7(1) (2017) 4794.
- [35] N. Sharma, P. Madan, S. Lin, Effect of process and formulation variables on the preparation of parenteral paclitaxel-loaded biodegradable polymeric nanoparticles: A co-surfactant study, *Asian Journal of Pharmaceutical Sciences* 11(3) (2016) 404-416.
- [36] Q. Wang, C. Li, T. Ren, S. Chen, X. Ye, H. Guo, H. He, Y. Zhang, T. Yin, X.-J. Liang, X. Tang, Poly(vinyl methyl ether/maleic anhydride)-Doped PEG-PLA Nanoparticles for Oral Paclitaxel Delivery To Improve Bioadhesive Efficiency, *Molecular Pharmaceutics* 14(10) (2017) 3598-3608.
- [37] S. Hua, E. Marks, J.J. Schneider, S. Keely, Advances in oral nano-delivery systems for colon targeted drug delivery in inflammatory bowel disease: Selective targeting to diseased versus healthy tissue, *Nanomedicine: Nanotechnology, Biology and Medicine* 11(5) (2015) 1117-1132.

- [38] N. Kamaly, B. Yameen, J. Wu, O.C. Farokhzad, Degradable Controlled-Release Polymers and Polymeric Nanoparticles: Mechanisms of Controlling Drug Release, *Chemical Reviews* 116(4) (2016) 2602-2663.
- [39] M. Samizadeh, X. Zhang, S. Gunaseelan, A.G. Nelson, M.S. Palombo, D.R. Myers, Y. Singh, U. Ganapathi, Z. Szekely, P.J. Sinko, Colorectal Delivery and Retention of PEG-Amprenavir-Bac7 Nanoconjugates - Proof of Concept for HIV Mucosal Pre-Exposure Prophylaxis, *Drug delivery and translational research* 6(1) (2016) 1-16.
- [40] S.D. Fontaine, R. Reid, L. Robinson, G.W. Ashley, D.V. Santi, Long-Term Stabilization of Maleimide–Thiol Conjugates, *Bioconjugate Chemistry* 26(1) (2015) 145-152.
- [41] J.T. Patterson, S. Asano, X. Li, C. Rader, C.F. Barbas, Improving the Serum Stability of Site-Specific Antibody Conjugates with Sulfone Linkers, *Bioconjugate Chemistry* 25(8) (2014) 1402-1407.
- [42] S.M.J. van Duijnhoven, M.S. Robillard, K. Nicolay, H. Gröll, In vivo biodistribution of radiolabeled MMP-2/9 activatable cell-penetrating peptide probes in tumor-bearing mice, *Contrast Media & Molecular Imaging* 10(1) (2015) 59-66.
- [43] M. Kosuge, T. Takeuchi, I. Nakase, A.T. Jones, S. Futaki, Cellular Internalization and Distribution of Arginine-Rich Peptides as a Function of Extracellular Peptide Concentration, Serum, and Plasma Membrane Associated Proteoglycans, *Bioconjugate Chemistry* 19(3) (2008) 656-664.
- [44] D. Sarko, B. Beijer, R.G. Boy, E.-M. Nothelfer, K. Leotta, M. Eisenhut, A. Altmann, U. Haberkorn, W. Mier, The Pharmacokinetics of Cell-Penetrating Peptides, *Molecular Pharmaceutics* 7(6) (2010) 2224-2231.
- [45] L.-O. Andersson, A. Rehnström, D.L. Eaker, Studies on “Nonspecific” Binding, *European Journal of Biochemistry* 20(3) (1971) 371-380.
- [46] J.H. Rockey, W. Li, J.F. Eccleston, Binding of fluorescein and carboxyfluorescein by human serum proteins: Significance of kinetic and equilibrium parameters of association in ocular fluorometric studies, *Experimental Eye Research* 37(5) (1983) 455-466.
- [47] J. Romano, A. Kashuba, S. Becker, J. Cummins, J. Turpin, F. Veronese, Pharmacokinetics and Pharmacodynamics in HIV Prevention; Current Status and Future Directions: A Summary of the DAIDS and BMGF Sponsored Think Tank on Pharmacokinetics (PK)/Pharmacodynamics (PD) in HIV Prevention, *AIDS Research and Human Retroviruses* 29(11) (2013) 1418-1427.
- [48] M. Veselinovic, K.-H. Yang, J. LeCureux, C. Sykes, L. Remling-Mulder, A.D.M. Kashuba, R. Akkina, HIV pre-exposure prophylaxis: Mucosal tissue drug distribution of RT inhibitor Tenofovir and entry inhibitor Maraviroc in a humanized mouse model, *Virology* 464–465 (2014) 253-263.
- [49] M. Boegh, H.M. Nielsen, Mucus as a Barrier to Drug Delivery – Understanding and Mimicking the Barrier Properties, *Basic & Clinical Pharmacology & Toxicology* 116(3) (2015) 179-186.
- [50] S.K. Lai, Y.-Y. Wang, J. Hanes, Mucus-penetrating nanoparticles for drug and gene delivery to mucosal tissues, *Advanced drug delivery reviews* 61(2) (2009) 158-171.
- [51] M.E.V. Johansson, Fast Renewal of the Distal Colonic Mucus Layers by the Surface Goblet Cells as Measured by *In Vivo* Labeling of Mucin Glycoproteins, *PLoS ONE* 7(7) (2012) e41009.
- [52] R.A. Cone, Barrier properties of mucus, *Advanced Drug Delivery Reviews* 61(2) (2009) 75-85.

CHAPTER 6

Summary of the Dissertation and Future Directions

6.1. Summary

The FDA approved drug product, Truvada, has substantiated the postulation of HIV pre-exposure prophylaxis (PrEP). However, although mathematically modeled to be 99% effective, real-world efficacy is highly dependent on patient adherence, which remains a critical challenge to address. Alternative PrEP options are being explored, with widespread focus on long-acting formulations to improve adherence, by offering longer durations of protection, and relinquishing users from the daily responsibility of adhering to medication. A long-acting colorectal mucosal PrEP (mPrEP) that would require only once-a-week dosing would be a promising option. To be successful, a drug delivery system (DDS) for mPrEP would need to deliver anti-HIV agents to the colorectal mucosa (a prime target of early HIV infection), lower the necessary dose and frequency, and minimize systemic exposure. Therefore a Bac7-labeled nanoparticle (NP) platform capable of transport across biological barriers (mucus lining and cell monolayer) was evaluated.

Bac7 increases NP transport across cells. Flow cytometry and confocal microscopy revealed cytosolic delivery of plain NPs and Bac7 NPs with a significant portion of uptake occurring through endosomal pathways. Bac7 labeled NPs with varied ligand densities (0.25% to 10%) resulted in a 163.2% to 384.6% increase in NP transport across a Caco-2 epithelial cell monolayer compared with plain NPs *in vitro*. This indicates that ligand density, within the indicated range is not a major factor in the extent of NP transport. Due to lower internalization of Bac7 NPs at 2 hours, results indicate a delay in uptake for Bac7 NPs likely due to initial electrostatic interactions and hydrogen bonding at the external cell surface. Bac7 NPs successfully traverse colorectal

mucus *in vivo* to reach the epithelial layer. 1% and 5% Bac7 ligand densities produced a nearly 8-fold and 5-fold increase in NP tissue association compared to plain NPs, respectively. NPs with a higher ligand density (10% Bac7) showed no significant differences in tissue association when compared with plain NPs. We attribute this to increased physicochemical interactions between Bac7 and the mucus mesh, hindering NP translocation. 1% Bac7 NPs were chosen as the lead candidate for further testing. This study established the feasibility of Bac7-labeled NPs to be used as a potential mPrEP approach.

Flash nanoprecipitation can achieve moderate to high drug loading of RPV in polymeric NPs and drug release can be modified. Flash nanoprecipitation encapsulation of rilpivirine (RPV), a crystalline and BCS Class II drug was assessed. Rilpivirine has shown promising pre-clinical results as a long-acting nanoparticle suspension. However, current formulations require parenteral injections and present a high-risk of patient nonadherence. Thus, an RPV-loaded NP mPrEP drug delivery system (DDS) would provide a viable alternative to currently explored injectable options. Successful RPV encapsulation, via salt formation, within PCL-PEG NPs resulted in high encapsulation efficiencies (85% to 98%), and moderate to high drug loadings (10.9% to 17.7%). Varying copolymer block sizes allowed for modification of RPV release rates. However, cumulative release over 24 hours was only modulated to achieve between 20% and 40% total release. Adjusting polymer block molecular weight ratios resulted in RPV-loaded NP size ranges from ~40 to 240 nm. PLA_{6.3kDa}-PEG_{5kDa} NPs resulted in a greater maximum release of 58% compared with 40% for PCL_{6kDa}-PEG_{5kDa}. However, PLA_{6.3kDa}-PEG_{5kDa} achieved an approximately 10% lower encapsulation efficiency and 1% decrease in drug loading compared with PCL_{6kDa}-PEG_{5kDa}. PCL_{6kDa}-PEG_{5kDa} NPs resulted in the most ideal sizes, for further *in vivo* evaluation, based on previously reported NP parameters needed to avoid mucus mesh entrapment.

PCL-PEG NPs successfully deliver RPV to colorectal tissue *in vivo*. The functionality of three Bac7 analogs (wild-type (wt), inverso (I), and retroinverso (RI) sequences) was evaluated *in vivo* in the presence of proteolytic enzymes. In the colon, the I Bac7 analog resulted in a 142% increase in tissue association compared with plain NPs. Therefore, the I Bac7 form was used for all remaining studies. NPs were evaluated *in vivo* to determine platform translocation across mucus and cells, to maintain prolonged tissue retention. Plain and Bac7 NPs resulted in 26% and 13% RPV tissue association in an *in situ* rat model, respectively, after 2 hours. No significant differences were found between plain NPs and Bac7 I NPs. However, similar trends were shown in mouse intra-rectal studies with a decreasing trend in extracted RPV, associated with the addition of Bac7. This suggests strong tissue adsorption of NPs preventing complete RPV quantitation. 24 hour RPV concentrations were below the limit of detection and unable to be quantified. Drug extraction complications, highlight the need for more robust bioanalytical assays, that are effective in separating both drug and nanoparticles from precipitated proteins, for HPLC analysis.

Bac7 NPs significantly cleared from tissue by 24-hours. NP retention, 2-hours after intra-rectal administration in mice, was also investigated. Bac7 I NPs showed 3-fold increase in mucosal tissue association compared with plain NPs (~1.7% and ~0.45%, respectively), similar to *in situ* study outcomes. Bac7 NPs appear to be largely cleared from tissue after 24 hours, although both plain NPs and Bac7 NPs are present in tissue past 48 hours at low levels. Therefore, this work shows the potential of an RPV-loaded Bac7 NP platform to be used in an mPrEP. Bac7 effectively increased NP and RPV residence time within the colon at 2 hours. However, cellular internalization of Bac7 labeled NPs appears to occur slowly, resulting in rapid clearance likely due to mucus shedding. The average epithelial cell turnover rate in the colon is 2-3 days in rodents. Therefore retention that exceeded 2-3 days in a murine model indicates NP delivery to

the lamina propria and is considered the rodent equivalent of a one-week duration. Significant mechanistic studies and kinetic optimization is still needed to further assess, and achieve, feasibility as a long-acting PrEP approach.

Dissertation Contribution to Science

The herein thesis, provided a framework to better understand NP transport across cells and mucus barriers guided by cell-penetrating peptides. It presents the development of rilpivirine-loaded NPs made by a simple NP fabrication process, FNP. The thesis demonstrates easy modulation of drug release through the systematic adjustment of polymer physical properties. It also highlights the challenges to data interpretation imposed by NP interactions with internal and external factors including the loaded drug, tissue of interest, and mucus.

6.2. Recommendations of future directions for this project include:

1. To investigate Bac7 internalization kinetics for NPs, nanoconjugates (branched), and novel nanostructures.
2. To develop more robust bioanalytical assays for nanoparticle extraction, along with drug extraction, during sample preparation. Special focus is needed for delivery systems with charged functionalized entities, which may form strong adhesion to sample proteins.
3. To determine RPV release kinetics at acidic (~4.5-5.0) pH ranges to evaluate release potential during endosomal entrapment.
4. To assess Bac7 mechanism of uptake *in vitro* by inhibiting various known transport pathways.

S1. SUPPLEMENTAL MATERIALS

Note: This section was reproduced for this dissertation from the following publication:

Samizadeh, M; Zhang, X; Gunaseelan, S; **Nelson, A**; Palombo, M; Myers, D; Singh, Y; Ganapathi, U; Szekely, Z; Sinko, P. Colorectal Delivery and Retention of PEG-Amprenavir-Bac7 Nanoconjugates-Proof of Concept for HIV Mucosal Pre-Exposure Prophylaxis (mPrEP). Drug Delivery and Translational Research. 6(1). 1-16. 2016 [1]

Colorectal Delivery and Retention of PEG-Amprenavir-Bac7 Nanoconjugates - Proof of Concept for HIV Mucosal Pre-Exposure Prophylaxis

S1.1. Abstract

Local delivery of anti-HIV drugs to the colorectal mucosa, a major site of HIV replication, and their retention within mucosal tissue would allow for a reduction in dose administered, reduced dosing frequency and minimal systemic exposure. The current report describes a mucosal Pre-Exposure Prophylaxis (mPrEP) strategy that utilizes nanocarrier conjugates (NC) consisting of poly(ethylene glycol) (PEG), amprenavir (APV) and a cell penetrating peptide (CPP; namely Bac7, a fragment derived from bactenecin 7). APV-PEG NCs with linear PEGs (2, 5, 10, and 30 kDa) exhibited reduced (52 - 21%) anti-HIV-1 protease (PR) activity as compared to free APV in an enzyme-based FRET assay. In MT-2 T-cells, APV-PEG_{3.4kDa}-FITC (APF) anti-HIV-1 activity was significantly reduced (160-fold, IC₅₀ = 8.064 mM) due to poor cell uptake whereas it was restored (IC₅₀ = 78.29 nM) and similar to APV (IC₅₀ = 50.29 nM) with the addition of Bac7 to the NC (i.e., APV-PEG_{3.4kDa}-Bac7, APB). Flow cytometry and confocal microscopy demonstrated Bac7-PEG_{3.4kDa}-FITC (BPF) uptake was two- and four-fold higher than APF in MT-2 T-cells and Caco-2 intestinal epithelial

cells, respectively. There was no detectable punctate fluorescence in either cell line suggesting that BPF directly enters the cytosol thus avoiding endosomal entrapment. After colorectal administration in mice, BPF mucosal concentrations were 21-fold higher than APF concentrations. BPF concentrations also remained constant for the 5 days of the study suggesting that (1) the NC's structural characteristics (i.e., the size of the PEG carrier and the presence of a CPP) significantly influenced tissue persistence and (2) the NCs were probably lodged in the lamina propria since the average rodent colon mucosal cell turnover time is 2-3 days. These encouraging results suggest that Bac7 functionalized NCs delivered locally to the colorectal mucosa may form drug delivery depots that are capable of sustaining colorectal drug concentrations. Although the exact mechanisms for tissue persistence are unclear and will require further study, these results provide proof-of-concept feasibility for mPrEP.

S1.2. Introduction

Eradicating HIV and preventing new infections remain formidable challenges despite enormous progress made during the past three decades in combating the HIV pandemic. There were more than 35 million people living with HIV in 2014, of whom 2.1 million were newly infected. This includes 50,000 new cases in the United States alone [2]. The majority of new HIV infections in the US each year occur in men who have sex with men (MSM) (63%) [3]. In the absence of an effective vaccine, multiple other prevention strategies including the use of condoms, microbicides and oral Pre-Exposure Prophylaxis (PrEP) and microbicide strategies have been evaluated but have had limited success [4]. CAPRISA 004, the first clinical trial to evaluate topical administration of the ARV drug tenofovir to the vaginal mucosa in a gel formulation, was somewhat effective (39%) in preventing HIV transmission [5],[6]. Since then, numerous microbicide or mixed microbicide/PrEP clinical trials (e.g., VOICE) have been conducted without success. Most of the focus has been

directed in the area of vaginal microbicides, some of which have advanced to phase 3 clinical trials before termination. To our knowledge, there have only been eight phase 1 clinical trials completed for rectal ARV microbicides; none of which have progressed to late-stage clinical testing according to clinicaltrials.gov. Unfortunately, technologies developed for vaginal delivery cannot be directly translated for rectal administration due to anatomical and luminal differences between the colorectum and vagina[7]. Whether considering rectal or vaginal prevention approaches, dosing and formulation acceptability remain significant concerns to patient adherence and clinical trial success[8]. Truvada[®], the first approved orally administered PrEP regimen, is a 300mg tenofovir disoproxil fumarate (TDF) and 200 mg emtricitabine (FTC) fixed dose combination product that demonstrated 75-90% effectiveness but requires strict patient adherence to the regimen. Since Truvada is administered orally every day, chronic systemic exposure to TDF/FTC increases the potential for toxicity and side effects. Treating HIV soon after mucosal transmission is likely to be more effective than treating at later stages due to viral vulnerability at the early stages of infection [9]. Dissemination of HIV to the secondary lymphatic tissues occurs once local viral expansion reaches a critical threshold level. This results in the establishment of chronic systemic HIV infection. Thus early intervention can limit viral expansion so the critical threshold for systemic viral dissemination is not reached. The window of opportunity to successfully intervene lasts about a week from the time of initial sexual exposure to HIV [9]. The vaginal and colorectal mucosae are considered early prevention sites for drug delivery due to their direct exposure to HIV. However, approaches for eliminating HIV at the early stages of infection should also consider the gut since, immediately post colorectal/vaginal transmission, massive viral replication and CD4⁺ T cell depletion occurs in the gut mucosa establishing it as a major reservoir site [10], [11]. The pivotal role of the gut in HIV replication and CD4⁺ T cell depletion persists thereafter at all subsequent stages of infection making it a prime target for eradication as well.

Clinical trial data suggests that topical application of ARV drugs by the vaginal and rectal routes is superior to the oral route in preventing sexual transmission of HIV-1 since the concentrations achieved in local tissues are significantly higher [12]. For example, tenofovir concentrations in vaginal tissue when administered as a vaginal gel (1%) are over 1000-fold higher than when administered orally [13],[14]. Drug concentrations after oral administration were found to be below what is believed to be the threshold of efficacy in clinical trials [15], [16], [12]. Although the ARV threshold concentrations in mucosal tissues for infection prevention have yet to be established, suboptimal concentrations of tenofovir, the main agent used in clinical trials, may have been achieved. An analysis of phase 1 trial results suggests that the concentration of tenofovir diphosphate, the metabolite of TDF, should be greater than 1000 fmol/mg. Unfortunately, vaginal concentrations in tissue after daily gel administration were about 1000 fmol/mg or just at the effective limit suggesting that current topical formulations operate within a thin margin of safety and missing one daily dose could result in the failure of protection [12]. It should be noted that TDF has a relatively long half-life (about 17 hours in serum), and this situation becomes further complicated when considering other ARVs, most of which are small molecule drugs and even more rapidly cleared from mucosal tissues[17]. More frequent administration may result in higher and more sustained mucosal drug concentrations but this regimen is likely to be too frequent to achieve sufficient patient adherence. Pre-clinical and clinical studies have established that polymer-drug conjugates that increase drug retention in the body result in reduced dosing frequency and improved patient adherence may offer a solution [18].

ARVs and drug carriers encounter multiple biological barriers in series as they attempt to reach their mucosal targets in the colon, gut, rectum and vagina. The first is the mucus layer, a viscoelastic gel consisting of interwoven glycoprotein fibers with water-filled spaces that is

tightly associated with the mucosal surface [19]. Translocation through mucus is size and charge dependent [20, 21]. Certain polymers such as poly(ethylene glycol) (PEG) and polyvinylpyrrolidone (PVP) as well as nanoparticles (NP) displaying short (~ 2 kDa) PEG polymers can penetrate the mucus layer [22, 23]. In addition to being a mechanical barrier, mucus can act as a carrier itself and deliver drugs and drug carriers past absorption sites since adherent mucus begins to flow distally under its own weight as additional mucus is secreted into the intestine [24, 25]. After crossing the mucus layer, a drug carrier must also penetrate the epithelial mucosal barrier to reach the lamina propria (LP) where HIV replication occurs. Cell penetrating peptides (CPP) conjugated to drug carriers have shown utility in enhancing cell uptake [26]. However, the commonly used Arg-rich family of CPPs is not a good choice as its prototype Tat CPP enters cells by endocytosis becoming trapped inside endosomes [27, 28]. On the other hand, the Pro-rich family of CPPs penetrate directly into the cytosol thus avoiding endosomal entrapment altogether [29]. One such example is a 10 residue CPP derived from the bactenecin 7 protein (Pro¹⁵-Arg-Pro-Leu-Pro-Phe-Pro-Arg-Pro-Gly²⁴-COOH). In fact, the membrane penetrating properties of this Pro-rich CPP are superior to Tat CPP [30]. A 12-residue derivative of this CPP, defined later as Bac7, is used in the current study.

A mucosal PrEP (mPrEP) strategy (i.e., where drug is administered and retained locally in mucosal tissues) could result in reductions in ARV doses administered and the resulting systemic exposure. In the current study, a mucosal PrEP strategy is proposed to achieve, sustain and retain effective mucosal ARV drug concentrations in colorectal tissues after local rather than systemic ARV exposure. The proposed delivery approach aims to sustain effective ARV concentrations by increasing ARV residence time in the LP after administration directly to the colorectal mucosa. In the current design, the PEG moiety of the CPP-drug-polymer nanocarrier conjugate (NC) enables mucosal retention while the Bac7 moiety enables mucosal penetration. The HIV-1 PR inhibitor amprenavir (APV, MW 505.6) was selected as a model ARV since it could be conjugated to the

NC *via* the amino functionality of the benzenesulfonamide moiety allowing it to retain its anti-HIV activity similar to enamino oxindole derivatives functionalized at the same amino group [31]. In addition to structural analogs of APV, the conjugation approach can also be applied to any ARV possessing an aromatic amino functional group such as tenofovir or emtricitabine. In the current study an mPrEP strategy employing CPP-drug-polymer conjugate is described and evaluated *in vitro* and *in vivo*.

S1.3. Materials and Methods

S1.3.1. Materials. Agenerase[®] capsules were obtained from GlaxoSmithKline (Research Triangle Park, NC). The mPEG_x-NHS derivatives (x= 2, 5, 10, and 30 kDa) were purchased from NOF America (White Plains, NY), FITC-PEG_{3.4kDa}-COOH and maleimide-PEG_{3.4kDa}-COOH from NANOCS (Burlington, MA), amino acids and Fluoresceine isothiocyanate (FITC) from AnaSpec Inc. (Fremont, CA), NovaSyn[®] TG Sieber resin from EMD Millipore (Billerica, MA) and 1-hydroxy-7-azabenzotriazole (HOAt) and 1-[Bis(dimethylamino)methylene]-1H-1,2,3-triazolo[4,5-b]pyridinium 3-oxid hexafluorophosphate (HATU) from GenScript (Piscataway, NJ). All other chemicals were purchased from Sigma-Aldrich (St. Louis, MO). Sephadex beads (LH-20 and LH-60) were obtained from Amersham Biosciences (Uppsala, Sweden). Dialysis membranes (MWCO, 1000 and 3000) and Microcon centrifugal filters (MWCO, 3000) were purchased from Cole-Parmer (Rancho Domingues, CA). Sensolyte 490 HIV-1 PR assay kit was purchased from Anaspec Inc. (Fremont, CA). The MT-2 cells were obtained from the NIH AIDS Research and Reference Reagent Program. Fetal bovine serum (FBS), phenol red-free RPMI Medium, penicillin/streptomycin 100x solution, tetramethylrhodamine dextran, diamidino-2-phenylindole dihydrochloride (DAPI) were purchased from Life Technologies Corp (Carlsbad, CA). Chambered coverglass (Lab-Tek[™] II) was purchased from Thermo Scientific (Waltham, MA).

Electrospray ionization mass spectrometry (ESI-MS) was performed on a Finnigan MAT TSQ 7000 and a Waters ZQ-4000. Mass spectrometry using matrix-assisted-laser-desorption-ionization time-of-flight (MALDI-TOF-MS) was carried out on ABI-MDS SCIEX 4800. UV and fluorescence were measured using a Tecan GENios multifunction microplate reader (MTX Lab Systems, Vienna, VA). Confocal imaging of MT2 cells was performed on a Leica TSC SP5 confocal microscope (Leica Microsystems CMS GmbH, Germany). HPLC analysis was carried on a Waters system (Milford, MA) equipped with UV and fluorescence detectors. The following reverse-phase (RP) C₁₈ HPLC columns were used: A - Waters (symmetry, 5 μ m, 4.6 x 150 mm, Milford, MA) or B - Agilent Technologies (3.5 μ m, 4.6 x 50 mm, Santa Clara, CA). Ultrahydrogel 250 (7.8 x 300 mm, 6 μ m) was used for size exclusion chromatography (Waters Corp., Milford, MA).

S1.3.2. Extraction of APV from Agenerase[®] capsules. The capsule shells were cut open with a sharp blade and contents containing APV and excipients, were mixed with distilled water resulting in crude APV as a white precipitate. The crude APV was purified on a silica column using an ethyl acetate/methanol gradient. The extracted APV was characterized using RP-HPLC (column A) and ESI-MS. Retention time (R_t) = 18 min; m/z was (calculated) 506.6 Da; observed, 506.74 Da for $[M+H]^+$.

S1.3.3. Preparation of APV-O-acetyl. APV (0.17 g, 0.34 mmol) was dissolved in N,N-dimethyl formamide (DMF, 3 mL) containing N,N-diisopropyl ethylamine (DIPEA, 2%). Acetic anhydride (0.125 mL, 1.32 mmol) was added drop wise into the solution. The reaction mixture was stirred at room temperature for 12 h. The crude product was purified on a silica column using a gradient of ethyl acetate/methanol. The pure product was obtained as off-white solid after evaporation on a rotary evaporator. The product was characterized using RP-HPLC (column B) and ESI-MS. R_t =

15 min; m/z values (calculated) were 570.2 Da and 1,117.5 Da, m/z values (observed) were 570.5 Da and 1117.4 Da for $[M+Na]^+$ and $[2M+Na]^+$ respectively.

S1.3.4. PEG_x-APV-O-acetyl and PEG_x-APV-OH. The mPEG_x-NHS (x = 2, 5, 10 or 30 kDa) polymers (0.01mmol) were reacted with APV-O-acetyl (0.03 mmol, 3 equiv) in DMF (4 mL) containing DIPEA (2%). The reaction mixtures were stirred at room temperature for 24 hr. The products were purified on Sephadex LH-20 (2 and 5 kDa conjugates) or Sephadex LH-60 column (10 and 30 kDa conjugates). The O-acetyl groups in PEG_x-APV-O-acetyl derivatives were removed by treating with HCl (0.1 N) at room temperature for 6 hr. The HCl was then neutralized with sodium bicarbonate and the solutions were lyophilized to obtain crude conjugates as white flakes. The conjugates were purified by size exclusion chromatography (SEC) on Waters Ultrahydrogel 250 column using water as mobile phase (flow rate: 0.8 ml/min) and characterized using MALDI-TOF-MS. The reaction yields were ~50% for all PEG conjugates. The retention times were: for the 2 kDa: R_t = 24 min, m/z observed 2,505.6 Da; 5 kDa: R_t = 23 min, m/z observed 5,625.6 Da; 10 kDa: R_t = 20 min, m/z observed 10,700.1 Da; 30 kDa: R_t = 17 min, m/z observed 31,098.7 Da.

S1.3.5. APV-PEG_{3.4kDa}-FITC (APF). An active ester of FITC-PEG_{3.4kDa}-COOH (0.03 mmol) was formed using 1-Ethyl-3-(3'-dimethylaminopropyl)carbodiimide (EDCI, 4 equiv., 0.12 mmol) and 1-hydroxy-7-azabenzotriazole (HOAt, 3 equiv., 0.09 mmol) in DMF (3 ml). After 2 min of activation, APV (2 equiv., 0.06 mmol) was added to the solution and the reaction mixture was stirred in dark at room temperature for 16 h. The conjugate was purified by dialysis (MWCO 3,000 Da) against water (3 × 2 L for 24 h) and lyophilized to obtain APF as yellow flakes. APF was quantified using a FITC standard curve and characterized by MALDI-TOF-MS. The m/z (calculated) was 4,705.6 Da and m/z (observed) was 4,800.9 Da for $[M+H]^+$.

S1.3.6. Bac7 Cell Penetrating Peptide. Bac7 (*N-Ac-Cys-Gly-Pro*¹⁵-Arg-Pro-Leu-Pro-Phe-Pro-Arg-Pro-Gly²⁴-COOH) is a modified Pro-rich CPP derived from bacterenecin 7 protein (residue 15-24) as described previously. Bac7 was synthesized on NovaSyn[®] TG Sieber resin using a Nautilus 2400 automated peptide synthesizer. Fmoc chemistry for solid-phase peptide synthesis (SPPS) was used to assemble the resin-bound Bac7. The peptide was cleaved from the resin using trifluoroacetic acid (TFA), ethanedithiol, water, and triisopropylsilane (94/2.5/2.5/1, vol/vol). The product was analyzed using RP-HPLC (Agilent 3.5 mm, 4.6 × 50 mm column, $R_t = 4$ min) and characterized by MALDI-TOF-MS. The m/z (calculated) was 1,333.71 Da and m/z (observed) was 1,334.6 Da for $[M+H]^+$.

S1.3.7. APV-PEG_{3,4kDa}-Bac7 (APB). The Bac7 peptide (0.01 mmol) was reacted with maleimide-PEG_{3,4kDa}-COOH (0.01 mmol, 1 equiv.) in DMF (0.5 mL). The reaction was monitored by measuring the reduction in free thiol groups using Ellman's assay at 0, 0.5, 1.0, 1.5, 2, and 4 h [32]. The reaction was ~85% complete in 4 h. The product was purified by dialysis (MWCO = 3000 Da) against water (3 x 2 L for 24 h). The Bac7-PEG_{3,4kDa}-COOH was characterized by MALDI-TOF-MS. The m/z (calculated) was 4,733.6 Da and m/z (observed) was 4,732.7 Da for $[M+H]^+$. In the next step, Bac7-PEG_{3,4kDa}-COOH (0.02 mmol) was reacted with APV (0.04 mmol, 2 equiv.) by a method similar to one described earlier. The product was purified by dialysis (MWCO, 3000 Da) and then lyophilized to obtain pure APB as white flakes. The conjugate was characterized by MALDI-TOF-MS. The m/z (calculated) was 5,219.9 Da and m/z (observed) was 5,459.5 Da for $[M+H]^+$.

S1.3.8. Bac7-PEG_{3,4kDa}-FITC (BPF). The maleimide-PEG_{3,4kDa}-FITC (0.01 mmol) was reacted with Bac7 (0.03 mmol, 3 equiv.) in dry DMF (0.5 mL). The reaction mixture was stirred in dark at room temperature. The product was purified by dialysis (MWCO, 3000 Da) and then

lyophilized to obtain BPF as yellow flakes. The product was characterized by MALDI-TOF/TOF MS. The m/z was (calculated) 4,710.6 Da and m/z was (observed) 4,806.3 Da for $[M+H]^+$.

S1.3.9. Preparation of Stable Fluorescein Isothiocyanate Analog. Due to the reactive nature of FITC, especially toward lysine side chains presented in proteins, a stable analogue fluoresceine thiourea (FTU), was synthesized and used as a negative fluorophore control for uptake experiments throughout the *in vitro* and *in vivo* experiments. FTU was prepared by reacting FITC with ammonium hydroxide in DMF-water (1/1, vol/vol) mixture. After evaporating the solvents and triturating the residue with cold ether, the desired product was obtained in 90% yield and over 95% purity. FTU was not used on APF and BPF since they were proven to be stable during the experiments.

S1.3.10. Stability of Amide Bonds in MT-2 CD4⁺ T-Cell Culture Medium Containing 10% Fetal Bovine Serum (FBS). MT-2 cells were maintained in RPMI medium supplemented with FBS (10%) and penicillin/streptomycin at 50 units/ml in a CO₂ incubator. APF and APB conjugates at 12- and 4-fold higher concentrations than their respective IC₅₀ values (96 μM and 350 nM) were exposed to serum-containing medium and the MT2 cells at 5×10^4 cells/ml under culture conditions for 5 days. The MT-2 cells were then removed by centrifugation. Each cell-free supernatant was filtered (Microcon, MWCO 3000 Da) to separate the cleaved APV from its conjugate. The filtrates were analyzed using MALDI-TOF MS.

S1.3.11. Cytotoxicity of NCs.

Cytotoxicities of the NCs were determined using a cell viability (MTT) assay [33]. MT-2 cells were plated in 96-well plates at 5×10^3 cells/well in triplicate in medium containing APB (0-350 nM), APF (0-11,000 nM) or APV (0-280 nM). The plates were cultured for 5 days. MTT was added to each well and the plates were incubated at 37 °C for 3 hr and absorbance was read at

570 nm. Cell viability (%) is reported as the absorbance ratio of NC-treated cells to untreated cells. The assays were performed at least three times.

S1.3.12. PR Inhibition Activity of PEG_x-APV-OH (x = 2, 5, 10, and 30 Da) in buffer. The PR inhibition activities of the NCs were measured using Sensolyte 490 HIV-1 PR assay kit (Anaspec Inc.) based on fluorescence resonance energy transfer (FRET) [34]. In a 96-well microplate, the HIV-1 PR FRET substrate (50 μ L) was pre-incubated with various concentrations (0, 0.5, 1.0, 2.0, 3.5 and 5.0 μ M) of unmodified APV (10 μ L) at 37 °C for 10 min, following the kit's protocol. HIV-1 PR solution (40 μ L) was then added to the wells (final volume 100 μ L/well, final APV concentration at 0 - 5 μ M). Fluorescence intensities were immediately measured on a Tecan microplate reader (I_{Ex}/I_{Em} = 360 nm/465 nm) at 2 min intervals until the readout was constant (~40 min). Identical experiments were performed for PEG_x-APV-OH NCs at an APV-equivalent concentration of 3.5 μ M. APV-O-acetyl and PEG_{10kDa}-APV-O-acetyl were used as negative controls.

S1.3.13. Anti-HIV-1 Activity of APB and APF in MT-2 CD4⁺ T Cells. The anti-HIV-1 activity was quantitatively determined *in vitro* using a syncytium count assay based on inhibition of HIV-1-induced cell syncytium formation [35]. Serial dilutions of APV, APF and APB in serum-containing RPMI medium (100 μ L/well) were prepared in 96-well tissue culture plates. MT-2 cells (5×10^4 cells/well) with or without the X-4 HIV-1 strain III_B at 0.03 multiplicity of infection (MOI) were added to the wells. Final concentrations were: APV, 0 - 560 nM; APF, 0 - 22,000 nM, and APB, 0 - 700 nM. After incubating the plates for 5 days at 37 °C, the viral-induced syncytia in each well were counted under a microscope. Each experiment was performed at least three times.

S1.3.14. Flow Cytometry. NC uptake was assessed using Caco-2 cells (American Type Culture Collection, ATCC). The cells were cultured in Dulbecco's Modified Eagle Medium supplemented with FBS (10%), non-essential amino acids at 1 x concentration (100 x stock solution from Invitrogen) and penicillin/streptomycin at 50 units/ml (the DMEM medium) until confluence was reached. The cells were then incubated with DMEM medium (control), DMEM medium containing 10 μ M APF, or DMEM medium containing 10 μ M BPF for 2hr. The cells were then trypsinized and washed with Hank's Balanced Salt Solution (HBSS) using centrifugation. The procedure was repeated without trypsinization in suspended MT-2 cells using serum-containing RPMI medium. NC uptake was quantified using flow cytometry (Gallios, Beckman Coulter). Fluorescence intensity was recorded for 5000 cell events for each NC. Each experiment was performed at least three times.

S1.3.15. Confocal Microscopy. MT-2 cells were incubated for 4 hr in RPMI medium containing the fluid phase endocytosis marker, tetramethyl rhodamine dextran (Rho Dex, 10 kDa, 30 μ g/mL), the nuclear marker diamidino-2-phenylindole (DAPI, 5 μ g/mL) and 10 μ M APF or BPF. The cells were then washed with PBS by centrifugation and were re-suspended in HBSS. The cells were transferred to a chambered coverglass pre-coated with poly-D-lysine hydrobromide and washed with PBS. A similar procedure was used for Caco-2 cells except that the cells were grown on chambered coverglass for three days after confluence was reached and a monolayer had formed. To compare fluorescence localization and intensity of the NCs within cells, imaging was performed using a Leica TSC SP5 confocal microscope (Leica Microsystems CMS GmbH, Germany). Z stack images were acquired in the XYZ mode with a 40 x objective. Cell surface fluorescence was not observed in the X-Y plane. Quantification of intracellular fluorescence was carried out using LAS AF Lite (Leica Software) on each confluent Caco-2 cell monolayer or un-zoomed Z-stack image of densely packed MT-2 cells. The Z-stack images were not subject to any editing and contained over 500 cells to ensure objectivity and statistical power.

S1.3.16. APF and BPF penetration into mouse colorectal mucosa

Male CD-1 mice were fasted overnight. Three dosing solutions consisting of 30 μ M APF, BPF or FTU (the stable form of the FITC-moiety in APF and BPF serving as a control) in HBSS were prepared and 200 μ l was administered rectally using a 1 ml syringe. The syringe was kept in place to serve as a rectal plug to prevent leakage of the dosed solution. The syringe was removed after 2 hr. At 2, 24, 48, 72 and 120 hr after dosing, mice were euthanized using CO₂, the colorectal segment was excised, washed and the mucosa scraped. The mucosal tissue from each mouse was placed into HBSS and homogenized by passing through a 20G needle 25 times followed by centrifugation at 4000 g for 30 min. The clear supernatant was collected for measurement of fluorescence. Mucosal tissue retention was represented as the amount of APF, BPF or FTU (fmol)/ tissue weight (mg).

S1.3.17. Statistical Analysis

Results are represented as the mean \pm standard deviation (SD). Statistical analyses were performed using GraphPad Prism Software, version 4.0.1 (GraphPad Software, Inc., San Diego, CA). One-way analysis of variance (One-way ANOVA) followed by Tukey's post hoc test was performed. Non-linear curve-fitting was performed by GraphPad Prism Software using the dose-response equation. Statistical significance was determined when $p < 0.05$.

S1.4. Results

S1.4.1. Synthesis and Characterization Studies. The free aliphatic hydroxyl moiety of APV was acetylated to obtain APV-O-acetyl. mPEG_x-NHS polymers (x = 2, 5, 10, 30 kDa, **Scheme 1**) were conjugated to APV-O-acetyl. APF was prepared as depicted in **Scheme 2A**. The APV-PEG NC containing Bac7 was also prepared and characterized (**Scheme 3**). Bac7 was synthesized

using Fmoc-based solid-phase peptide synthesis (SPPS) protocols (**Scheme 2B**). To obtain APV-PEG_{3.4kDa}-Bac7 (APB) NC, the maleimide-PEG_{3.4kDa}-COOH was coupled to the cysteine residue present on Bac7 via a stable thioether linkage. In the next step, Bac7-PEG_{3.4kDa}-COOH was coupled to APV via an amide bond using a procedure similar to one described for the synthesis of FITC-PEG_{3.4kDa}-APV. Bac7-PEG_{3.4kDa}-FITC (BPF) was obtained by coupling maleimide-PEG-FITC to the N-Ac-cysteine residue of Bac7 peptide *via* a thioether linkage (**Scheme 2C**).

All NCs were obtained in high purity ($\geq 90\%$, estimated using gel permeation chromatography). The NCs were characterized using MALDI-TOF mass spectrometry, and observed molecular weights were found to be in agreement with calculated values. The NCs exhibited significantly higher solubility in water than free APV.

S1.4.2. Stability of Amide Linkage. The goal of the current study was to develop a non-releasable APV-PEG NC with high anti-HIV-1 activity. Initially, the stability of the amide bond linking APV to PEG was assessed. The APV-PEG_x-OH ($x = 2, 5, 10, \text{ and } 30 \text{ kDa}$) NCs ($1 \mu\text{M}$) were incubated at 37°C in PBS (pH 7.4) for 24 h, and the released APV was monitored using RP-HPLC. All APV-PEG NCs were found to be stable with less than 2% degradation in PBS over the time course of the study. The stability of the amide bonds in the APF and APB NCs was also assessed in the presence of MT-2 cells and serum at ~ 12 - and 4-fold higher concentrations than their respective IC_{50} values ($96 \mu\text{M}$ and 350 nM). The two NCs were incubated at 37°C for 5 days. The cells were then removed by centrifugation and cell-free supernatants were centrifuged using a Microcon filter (MWCO 3000) to separate the released APV from the intact NC. The filtrates were analyzed in triplicate ($n=3$) for APV using an anti-HIV-1 functional assay (i.e., inhibition of syncytium formation of HIV-1 infected MT-2 cells). Less than 0.08% free APV was found in the filtrates suggesting that a negligible amount of APV was released. No trace of free

APV was found when the filtrate samples were subjected to MALDI TOF-MS. Thus, the amide bonds were stable during the period of exposure to MT-2 cells and serum in this study.

S1.4.3. Cytotoxicity Studies. The cytotoxicities of APF and APB NCs were assessed using the MTT cell viability assay. MT-2 cells were incubated with various concentrations of APF, APB, and APV at 37 °C for 5 days, and the untreated MT-2 cells were used as controls. Viability in cells treated with APF, APB, and APV exhibited no statistical difference in comparison to untreated cells, at the concentrations tested (data not shown). No significant cytotoxicity was observed for APF up to 96 µM and for APB up to 350 nM, which is 12- and 4-fold higher than their respective IC₅₀ values.

S1.4.4. Anti-HIV-1 PR activity of APV-PEG_x-OH NCs in buffer. The anti-HIV-1 PR activity of APV-PEG_x-OH NCs ($x = 2, 5, 10, \text{ and } 30 \text{ kDa}$) were measured in buffer using a FRET-based HIV-1 PR inhibition assay [34]. The method utilizes a quenched fluorogenic substrate, a HIV PR FRET peptide with the sequence: DABCYL-GABA-Ser-Gln-Asn-Tyr-Pro-Ile-Val-Gln-EDANS, where EDANS is the fluorophore and DABCYL is the quencher. In the absence of HIV-1 PR, the fluorescence of EDANS in the FRET peptide remains quenched, but when incubated with the recombinant HIV-1 PR at 37 °C, the peptide is cleaved leading to the recovery of fluorescence ($I_{\text{Ex}}/I_{\text{Em}} = 340\text{nm}/490 \text{ nm}$) (**Scheme 4**). However, in the presence of a PR inhibitor, like APV, the cleavage of the fluorogenic HIV-1 peptide substrate by HIV-1 PR is inhibited, leading to a decrease in fluorescence signal in a concentration-dependent manner.

APV activity was determined at various concentrations (0 – 5 µM) and is shown in **Figs. 1 & 2**. **Fig. 1** shows the time course of the fluorescence (F) from the FRET enzymatic reactions in the presence of various APV concentrations. **Fig. 2** shows plots of $\ln (F_{\infty} - F_t)$ against time, where F_{∞}

is the maximum fluorescence intensity (0 μM of APV), F_t is fluorescence intensity at time t (min) and $\ln (F_\infty - F_t)$ is the natural logarithm of F reduction at a given APV concentration and time. The plots of $\ln (F_\infty - F_t)$ values against time yielded straight lines (linear regression $R^2 \geq 0.9711$ for all concentrations). The slope of each line represents the rate of F reduction (i.e., the rate constant, k_{obs} , in min^{-1}) of a FRET substrate cleavage reaction. Linear regression yielded k_{obs} values (mean \pm s.d.) for 0 – 5 μM concentrations of APV as follows: -0.3027 (\pm 0.0234) for 0 μM , -0.2239 (\pm 0.0146) for 0.5 μM , -0.1638 (\pm 0.0080) for 1.0 μM , -0.0890 (\pm 0.0049) for 2.0 μM , -0.05704 (\pm 0.0014) for 3.5 μM and -0.03766 (\pm 0.0019) for 5.0 μM .

Since APV loses some activity after being linked to PEG, pilot experiments were carried out to determine a concentration that was optimal for comparing APV activity to $\text{PEG}_x\text{-APV-OH NCs}$ ($x = 2, 5, 10,$ and 30 kDa) and the respective negative controls (APV-O-acetyl and $\text{PEG}_{10\text{kDa}}\text{-APV-O-acetyl}$). The free -OH group on APV, which is necessary for anti-HIV activity, was blocked using acetylation for the two negative controls. The largest decrease in F (**Fig. 1**) was observed in the presence of 3.5 and 5 mM APV even though there was no significant difference between the two concentrations ($p > 0.05$). Therefore, the comparison was made at 3.5 mM APV. HIV-1 PR inhibition activity is defined as the negative reciprocal of the rate constant [$-(1/k_{\text{obs}})$]. In **Fig. 3**, plots of [$-(1/k_{\text{obs}})$] derived from Fig. 2 versus APV concentrations are shown. APV activity increases linearly with increasing concentration. Regression analysis of the data indicates a straight line ($R^2 = 0.9858$). Therefore, **Fig. 3** was used as a standard curve to determine the apparent APV concentration (APV_{app}) for NCs. The APV_{app} value is derived for an APV NC at 3.5 μM by referring to a concentration of APV in **Fig. 3** that has the same $-(1/k_{\text{obs}})$ value as the APV conjugate.

Fig. 4 shows the natural log of fluorescence reduction ($\ln(F_\infty - F_t)$) versus time (R^2 values ≥ 0.9773) for 3.5 μM APV and 3.5 μM -equivalent concentrations of various PEG NCs, applying the same mathematical treatment to the experimental data as described previously. The k_{obs} values were then converted to $[-(1/k_{\text{obs}})]$ and the latter values were converted to their APV_{app} values using **Fig. 3** (cf. **Table 1**). **Fig. 5** shows the relative HIV-1 PR inhibition activity represented by the APV_{app} values relative to the activity of APV. The APV reference value is taken as being 100% potent. The figure shows that the PEG_x-APV-OH NCs prepared using 2- and 5-kDa PEGs exhibited 53% and 51% of APV potency, whereas NCs prepared using 10- and 30-kDa PEGs exhibited 34 and 24% of APV potency, respectively. The two negative controls were nearly inactive (9% and 8% of free APV potency). Thus, NCs prepared using smaller-sized PEGs retained half of APV potency compared to the reference, whereas the larger-sized PEG NCs suffered a greater loss in potency. Therefore, for the initial evaluation of the PrEP strategy (i.e., mucosal retention) the PEG size selected for PEG_x-APV-OH NCs was 2 - 5 kDa.

S1.4.5. PEG conjugation ablated anti-HIV-1 activity in T-cells while further conjugation with Bac7 restored activity. As indicated in **Fig. 5**, PEG_x-APV-OH ($x = 2 - 5$ kDa) NCs retained half of APV's ability to inhibit HIV-1 PR when tested with the FRET-based assay in buffer. However, their activity in suppressing HIV-1 replication in MT-2 T-cells was very low, suggesting that the PEG_x-APV-OH was unable to enter cells efficiently. To address the issue of low cell penetration, another NC, APV-PEG_{3.4kDa}-Bac7 (APB) was synthesized by conjugating PEG_{3.4kDa}-APV to Bac7, as described earlier (**Scheme 3**).

The anti-HIV-1 activity of APF and APB NCs were investigated in human CD4⁺ MT-2 T-cells infected with an HIV-1 X-4 strain, III_B. Infection of the cells with enveloped HIV-1 virus leads to the formation of syncytia (cells fusing together to form large multinuclear cells). The anti-HIV-1 activities were assessed by scoring the reduction in syncytia formation in infected cells in the

presence of the NCs. Other anti-HIV-1 assays such as reducing in viral p24 capsid protein production and cell viability were performed, but the well-to-well variability in the results was greater than the syncytium assay. Therefore, the syncytium assay was adopted for these studies. Statistical analysis was conducted after normalization of treatment groups to untreated wells (**Fig. 6**). The APF NC exhibited greater than a 160-fold decrease in activity ($IC_{50} = 8064$ nM) compared to APV ($IC_{50} = 50.29$ nM) suggesting that PEG_{3.4kDa}-APV-OH was unable to access HIV-1 PR located in the cytosol. APV-PEG_{3.4kDa}-Bac7 exhibited anti-HIV-1 activity ($IC_{50} = 78.29$ nM) that was similar to free APV ($p > 0.05$). Incorporation of Bac7 in the NC, therefore, effectively overcame the lack of cell permeability observed with PEG_{3.4kDa}-APV-OH. Since current results demonstrate that the amide bonds linking APV to PEG are stable under the conditions used in these studies, the observed anti-HIV-1 activity was due to intact APB.

S1.4.6. Flow Cytometry and confocal microscopy. To study the intracellular fate of APB, a fluorescein-labeled analog, FITC-PEG_{3.4kDa}-Bac7 (BPF) was synthesized by replacing APV with a surrogate fluorescent molecule, FITC. While APB contained 10.5% (w/w) APV, BPF contained 8.1% (w/w) FITC. Thus, both have the same PEG_{3.4kDa}-Bac7 component that constitutes a comparable ~ 90% of total weight. (**Scheme 2C**). Flow cytometry and confocal microscopy were performed in human Caco-2 and MT-2 cells to compare the extent of uptake of APF and BPF into representative mucosal epithelial cells and target T cells, respectively.

For flow cytometry, Caco-2 cells or MT-2 cells were incubated with the culture medium containing no NC (control), 10 μ M APF or 10 μ M BPF. **Fig. 7** shows the total cell-associated BPF fluorescence intensity in Caco-2 cells was 4.1 fold higher than APF and 2.0 fold higher in MT-2 cells, which is consistent with the superior anti-HIV-1 activity of APB over APF in MT-2 cells. The intracellular uptake of the APF and BPF was also investigated using confocal microscopy (**Fig. 8 and 9**). Significantly less intracellular fluorescence was observed in MT-2

cells as compared to Caco-2 cells (image not shown) consistent with the flow cytometry data. The observed fluorescence was exclusively intracellular since no cell surface fluorescence was observed in the XY-plane. **Fig. 8** shows that the intracellular fluorescence intensity of BPF in Caco-2 cells was 3.5-fold higher than APF and 2.0-fold higher in MT-2 cells, consistent with the flow cytometry and in vitro anti-HIV-1 activity results. Note that the absolute total cell-associated fluorescent intensities of APF and BPF were 3- and 6-fold higher in Caco-2 cells than in MT-2 cells, respectively, suggesting Caco-2 cells have higher uptake capacity than MT-2 cells. Because of the low absolute fluorescence levels of APF and BPF in MT-2 cells, clear ascertainment of punctate (vesicular) vs. diffuse (cytosolic/nuclear) localization was not possible. In **Fig. 9**, a 2.47x-zoomed, blue/green/red merged image of Caco-2 cells from a middle section of its Z-stack is shown. No punctate orange color resulting from co-localization of FITC and Rho-Dex (the fluid endocytosis marker) was observed. The undetectable BPF in intracellular endosomes/lysosomes (no orange color) and detectable BPF as the intracellular green fluorescence are mostly due to the cytosolic localization of the NC. Combined with the anti-HIV-1 activities of APF and APB in MT-2 cells, confocal microscopy suggests that APF did not efficiently enter the cells, while APB entered the cytosol efficiently without being trapped in endosomes. The results also suggest that the main mechanism responsible for Bac7-assisted cell entry of the PEG-APV NC is either direct translocation across the plasma membrane, or endocytosis followed by very efficient endosomal escape.

S1.4.7. NC penetration and retention in mouse colorectal mucosa. The FTU mucosal tissue concentration was negligible at 2 h and 1 d suggesting that no uptake occurred or possibly that systemic absorption was rapid and FTU was completely cleared from the tissue (**Fig. 10**). APF (i.e., the NC without the Bac7) concentrations were low during the entire study. BPF tissue concentrations were significantly higher and also persisted for the 5 days of the study. This time period exceeded the typical epithelial turnover time in mice (2-3 days) suggesting BPF transport

and retention in the lamina propria of the colorectal mucosa. The average BPF tissue concentration on Day 5 was 124 fmol/mg, or 2.1% of the initial dose. On Day 5, the BPF tissue concentration was 21-fold higher than APF demonstrating the importance of Bac7 in promoting colorectal mucosal uptake.

S1.5. Discussion

A drug delivery strategy incorporating CPP-ARV drug-polymer nanocarrier conjugates was designed and evaluated in the current study. The goal was to sustain ARV drug concentrations in the colorectal mucosa by increasing ARV residence time in the submucosa. Oral or parenteral PrEP dose forms are at various stages of development with Truvada representing the only PrEP drug product approved to date. While there are distinct advantages to maintaining constant plasma ARV drug concentrations, there are also significant limitations such as patient adherence to chronic dosage regimens and therapy-limiting side effects due to constant systemic ARV exposure. In order to address this, long acting/extended release (LA/ER) treatments for PrEP are being proposed and evaluated that will result in infrequent dosing with long dosing intervals making administration convenient for patients resulting in improved adherence. Two formulations, a LA/ER injectable Non-nucleoside Reverse Transcriptase Inhibitor (NNRTI) rilpivirine (LA-RPV) and an HIV Integrase Strand Transfer Inhibitor (InSTI), LA/ER injectable cabotegravir (LA-744), have been developed and are currently undergoing clinical testing [36-38]. Although these and similar technologies will address patient adherence issues, the clinical implications of chronic systemic ARV exposure remain unknown. Progress has been made in local/topical delivery of ARVs to the vaginal and colorectal mucosae [39, 40]. These topical products, also known as microbicides, deliver ARVs through the rectum or vagina and act in the lumen or in the respective mucosal tissues. However, given the nature of ARVs they are rapidly cleared from tissue and require frequent dosing. Intravaginal films and rings have demonstrated the ability to deliver ARVs vaginally for prolonged periods but require the chronic presence of

the dose form in the vagina [41, 42]. In the current study, a colorectal mucosal approach is proposed that we refer to as mucosal PrEP (mPrEP) since the site of retention (i.e., depot) is not located in the rectal or vaginal lumen and the ARV does not enter the tissue from the systemic circulation.

In the current study, the concept of prolonging tissue ARV exposure by reducing ARV elimination rather than sustaining its release is evaluated. However, the approach can be applied to other nanocarriers such as nanoparticles that could deliver drug for prolonged periods. The HIV-1 PR inhibitor APV was selected as a model ARV since it could be conjugated to the NC *via* the amino functionality of the benzenesulfonamide moiety allowing it to retain anti-HIV activity [31]. APV inhibits the vast majority of clinical HIV mutants by binding to the more conservative protein (enzyme) backbone than the variable amino acid side-chains. Although APV is no longer a first line treatment for HIV infection, it serves well as a model ARV since the approach can also be applied to darunavir (DRV, Prezista), a widely used potent analog that has the same amino and hydroxyl functional groups, as well [43]. The set of APV derivatives studied includes controls such as APV-OAc (an O-acetylated compound with the hydroxyl function blocked preventing binding to HIV PR) and PEG_{10kDa}-APV-OAc (a N-conjugated and O-acetylated analog to study the PEG-conjugation effect with a blocked hydroxyl function). Conjugation of PEG polymers to drugs has been extensively investigated with the objective of increasing drug retention in the body. In each of these cases; however, the conjugate is inactive and the drug must be released in order to exert its therapeutic effect [18]. In essence, the PEG polymer conjugate forms a blood circulating depot that slowly releases drug thus prolonging body exposure to the drug and dramatically reducing dosing frequency. The influence of PEG size on the anti-HIV-1 activity of APV was investigated first. The PEG_x-APV-OH NCs were prepared using 2, 5, 10 and 30 kDa PEGs and anti-HIV-1 PR activity was measured in buffer using FRET-based PR inhibition assay. It was observed that APV retained about half of its original anti-HIV PR activity for PEGs up to 5

kDa in size. In another experiment, fluorescently labeled 3.4 kDa PEG APF NC exhibited a 160-fold reduction in anti-HIV-1 activity in human CD4⁺ MT-2 T-cells ($IC_{50} = 8.064 \mu\text{M}$) compared to free APV ($IC_{50} = 50.29 \text{ nM}$), suggesting that poor cell penetration may be responsible as the PEG-conjugated APV needs to enter cells to exert its anti-HIV-1 activity. Therefore the PEG size suitable for the proposed mPrEP strategy was found to be relatively small (2 – 5 kDa) as opposed to the large size (~ 30 kDa) of PEG used for current FDA-approved, intravenously administered drugs based on the following rationale. First, the size is far above the ~ 0.4 kDa threshold below which acute PEG toxicity has been observed [44], but much smaller than the size ($\geq 30 \text{ kDa}$) at which PEG ends up accumulating in lysosomes [45],[46], reminiscent of a “lysosomal storage disease” [47]. Second, PEG-conjugation has been reported to make a P-glycoprotein (P-gp)-substrate circumvent P-gp-mediated efflux [48], [49], [50],[51]. Third, NPs densely coated with lower molecular weight PEGs (2 - 5 kDa) have been reported to traverse the human cervicovaginal mucus barrier [52] since it appears to mimic the surface of viruses that can easily pass through human mucus linings. The surface of these viruses feature charge neutrality and lack a hydrophobic patch [53].

CPPs have been widely used to facilitate intracellular drug delivery and hundreds have been investigated to date [26, 54]. The most frequently studied class of CPPs is the Arg-rich category, of which Tat CPP is the prototype. However, Arg-rich CPPs tend to enter cells by endocytosis becoming trapped endosomes especially when they are conjugated to polymers such as PEG [55-57]. Few endosomal escape schemes have been developed [57] and some even require radical changes such as the introduction of primary amino groups in the polymer moiety. There are other CPPs, such as the Pro-rich CPPs, which includes Bac7, that apparently enter cells in an endocytosis-independent manner [29, 30]. It is noteworthy that in a side-by-side comparison with the Arg-rich prototypic Tat CPP, Bac7 was found in the cytosol while Tat CPP was trapped in endosomes [30]. Intracellular delivery to the cytosol/nucleus compartment is important for the

proposed mPrEP strategy as most current ARV drugs target the intracellular compartment as opposed to the vesicular (endosome/lysosome/endoplasmic-reticulum) compartment that is topologically equivalent to the extracellular space.

BPF intracellular fluorescence intensity in Caco-2 cells, a human *in vitro* intestinal mucosal epithelial model, was significantly greater than APF, which lacked Bac7, and was diffuse as well indicating direct cellular entry of BPF (**Fig. 7-9**). This in direct contrast to a study that reported after conjugation to a 1.3 kDa linear PEG, PEG-TAT entered CHO-K1 cells by endocytosis, was trapped in endosomes and was unable to reach the cytosol [55]. It is remarkable that Bac7, a short 10 amino acid peptide, is able to deliver a polymeric cargo into the cytosol with almost the same efficiency as a 29-residue chimeric CPP that consisted of a 11-residue TAT CPP and a 18-residue membrane disrupting peptide [56]. In that study, the membrane-disrupting peptide was apparently used to facilitate endosomal escape.

Further supporting the observation of direct cell entry were the current HIV results. Bac7 covalently linked to PEG_{3.4kDa}-APV (i.e., APB NC) showed anti-HIV-1 potency ($IC_{50} = 78.29$ nM) close to free APV ($IC_{50} = 50.29$ nM) in MT-2 T-cells, a model representative of HIV target T cells. These results also suggest very efficient cellular (cytosolic) entry of APB. Since APB differs from APF mainly by the presence of covalently attached Bac7, the promising outcomes with this NC suggest that Bac7 is able to completely negate the inability of PEG to penetrate the plasma cell membrane.

In colorectal mPrEP, the most important anatomic site is the lamina propria located beneath the epithelium in the submucosa. This is because the majority of HIV target CD4⁺ cells required for HIV transmission (e.g., T cells, dendritic cells and macrophages) are found in the LP. In addition, the establishment of infected founder cells and their expansion and subsequent spreading to

systemic sites takes place in the LP [9]. Another reason for establishing persistent drug concentrations in the LP rather than the epithelial cells is the relatively short turnover time of colonic epithelial cells in rodents (2-3 days) and humans (3-8 days) [58]. Once the cells slough off, the drug would have to be administered once again to re-establish effective anti-HIV local concentrations. On the other hand, if the NCs are retained in the LP, it would not be subjected to clearance by epithelial cell removal. As seen in **Fig. 10**, the BPF signal is significantly higher than APF and persists for the entire 5-day study. BPF residence significantly exceeded mouse epithelial turnover suggesting that the NC translocated across the epithelial cell layer and was retained in the LP. This is especially suitable for HIV drug delivery to the intestinal mucosa, which is the critical anatomic site for CD4⁺ T cell depletion, viral replication and persistence [59, 60]. Although not yet evaluated, this technology could be applied to particulate carriers such as NPs whereby they form a traditional sustained release drug delivery depot. Even though the diffusion of particulate carriers across intestinal mucus barriers is known to be size and charge dependent, the NC evaluated in the current study is relatively small and was able to traverse the mucus barrier [20, 21]. Interestingly, the PEG size utilized for the current NC was also found to be optimal for facilitating NP translocation across the mucus layer [52].

The current approach can be applied to structurally similar compounds of APV such as DRV. In addition, several other ARVs have amino groups that are compatible with the chemical derivatization process presented in this study. Examples include the active pharmaceutical ingredients (APIs) of Truvada, tenofovir and emtricitabine, which are widely used in HIV PreP. Although these APIs are completely structurally different from APV or DRV, their aromatic amino functional groups can be used to make peptide or carbamate linked conjugates as shown in patents describing prodrugs for TNF and FTC [61, 62]. The single or multivalent drug conjugation strategy will allow us to develop combination treatments using several ARVs for mPreP.

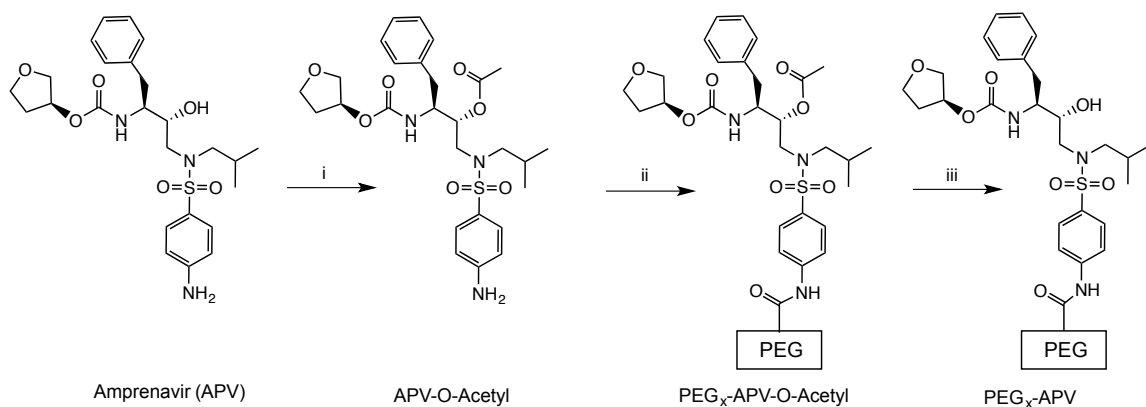
In summary, a colorectal mPrEP drug delivery strategy incorporating CPP-ARV-polymer NCs was designed and evaluated in the current study. The goal was to attain and prolong ARV concentrations in the colorectal mucosa by increasing ARV residence time in the submucosa after rectal administration. Current ARVs like APV are small molecule drugs that, after entering the submucosa, are quickly cleared from the tissue into the blood circulation. To overcome rapid drug clearance from the tissue, frequent administration is required. Truvada, the only currently FDA-approved product for PrEP, is given orally every day resulting in chronic systemic drug concentrations in order to maintain effective TDF and FTC concentrations at strategic sites. While Truvada is considered a major breakthrough in the field since it firmly establishes the concept of PrEP, improvements are needed to reduce dosing frequency to increase patient adherence and reduce systemic exposure in order to reduce the potential for therapy limiting side-effects. The current mPrEP strategy aimed to increase APV colorectal mucosal tissue residence time thereby effectively retaining ARVs locally in the tissues resulting in lower systemic exposure. APV was covalently conjugated to PEG to slow its removal from cells, which significantly reduced its uptake into cells. Further conjugation to Bac7 enabled cell uptake and a near complete restoration of anti-HIV activity. For this study the readily available ARV amprenavir was utilized as a model drug. However, the approach can be applied to the newer and much more potent close structural analog darunavir as well as tenofovir and emtricitabine. Applying the technology to vaginal delivery would require a modification of the approach to accommodate the thicker vaginal mucosa as well as the different luminal environment. While colorectal mPrEP proof-of-concept/feasibility was established in this study, several challenges remain including the development of suitable and patient friendly rectal dose forms to deliver the NCs to the colorectal mucosa.

S1.6. ACKNOWLEDGEMENTS

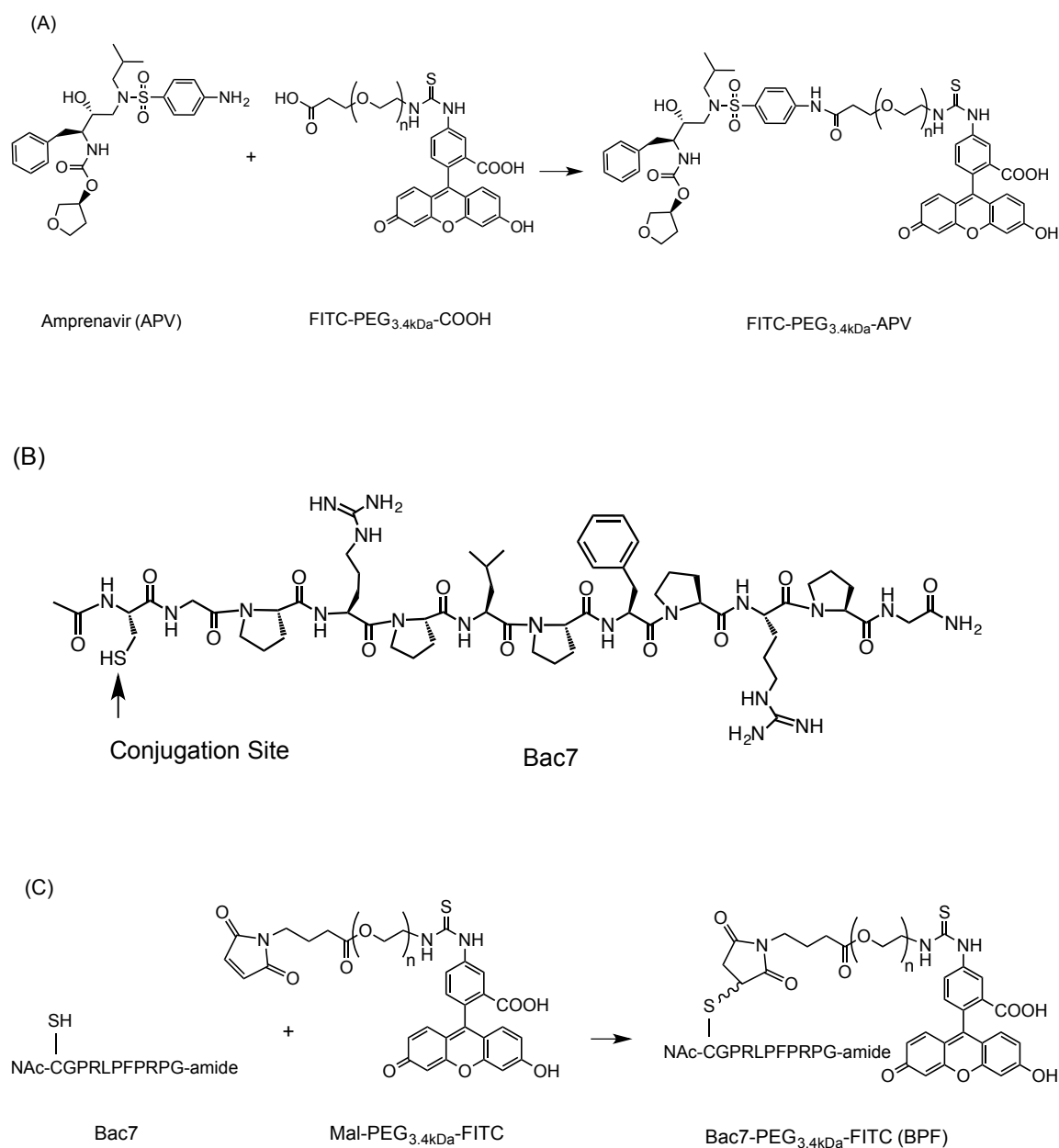
Financial support from NIH MERIT AI51214, AI117776 and the Parke-Davis Endowed Chair in Pharmaceutics and Drug Delivery is gratefully acknowledged. Flow cytometry/Cell sorting CORE facility at Rutgers, The State University of New Jersey is acknowledged for performing flow cytometry and confocal microscopy. The human CD4⁺ MT-2 T-cells were obtained from Dr. Douglas Richman, courtesy the NIH AIDS research and reference program, division of AIDS, NIAID (NIH cat # 237). A fellowship from the American Foundation for Pharmaceutical Education to M. Palombo is also acknowledged.

All institutional and national guidelines for the care and use of laboratory animals were followed.

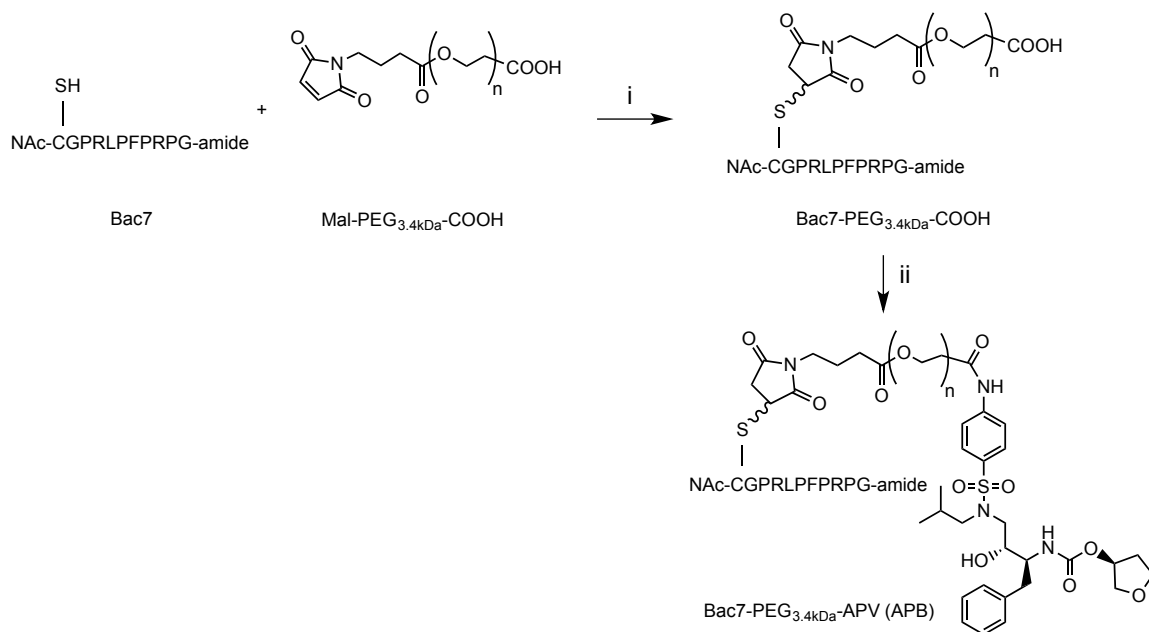
S1.7. Figures



Scheme 1. Synthesis of PEG_x-APV-O-acetyl and PEG_x-APV-OH nanocarrier conjugates. Reagents and conditions: (i) DMF, DIPEA, acetic anhydride, room temperature, 12 h; (ii) DMF, DIPEA, mPEG_x-NHS ($x = 2, 5, 10, 30$ kDa), room temperature, 24 h; and (iii) 0.1 N HCl, neutralized with NaHCO₃.



Scheme 2. Synthesis of fluorescein-labeled APV-PEG (APF) and Bac7 CPP-PEG NCs (BPF): (A) APV-PEG_{3.4kDa}-FITC; (B) Structure of Bac7 analog; and (C) Bac7 CPP-PEG_{3.4kDa}-FITC. Reagents and conditions: (i) DMF containing EDCI and HOAt, room temperature, 16 h; and (ii) DMF, room temperature, 4 h. PEG-fluorescein is linked to APV *via* an amide bond and to Bac7 *via* a thioether bond.



Scheme 3. Synthesis of APV-PEG_{3.4kDa}-Bac7 CPP (APB). The cell penetrating peptide, Bac7, was linked to maleimide-PEG_{3.4kDa}-COOH via a thioether bond. APV was linked to Bac7 CPP-PEG_{3.4kDa}-COOH via an amide bond. Reagents and conditions: (i) DMF, room temperature, 4 h. (ii) DMF containing WSC and HOAt, room temperature, 16 h.

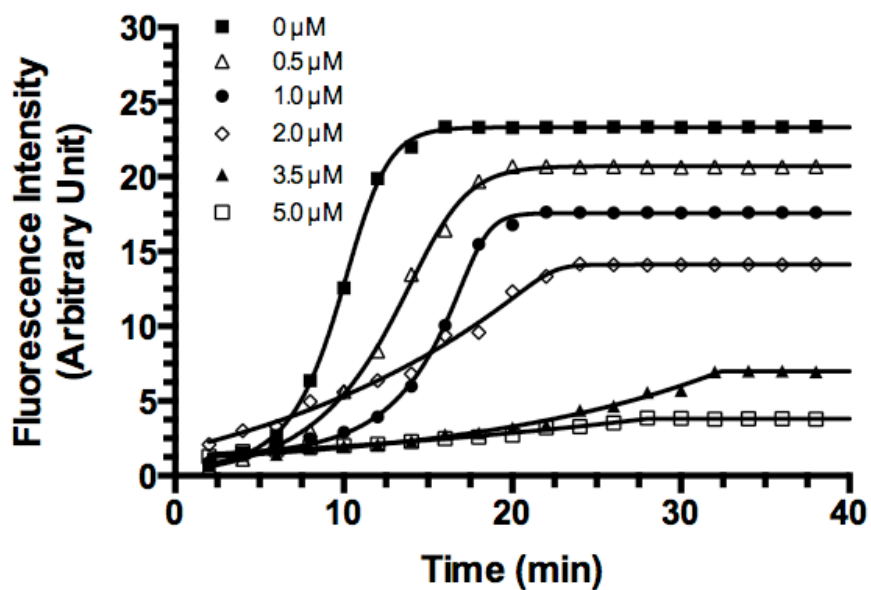


Figure 1. Cleavage kinetics of HIV-1 PR FRET peptide substrate ($5.0 \mu\text{M}$) by recombinant HIV-1 PR (35.2 nM) at $37 \text{ }^\circ\text{C}$ in the assay buffer in the presence of different APV concentrations ($0\text{--}5.0 \mu\text{M}$). All measurements were performed in triplicate and reported as mean \pm SD ($n = 3$). The effect of APV $3.5 \mu\text{M}$ and $5.0 \mu\text{M}$ was not significantly different ($p > 0.05$).

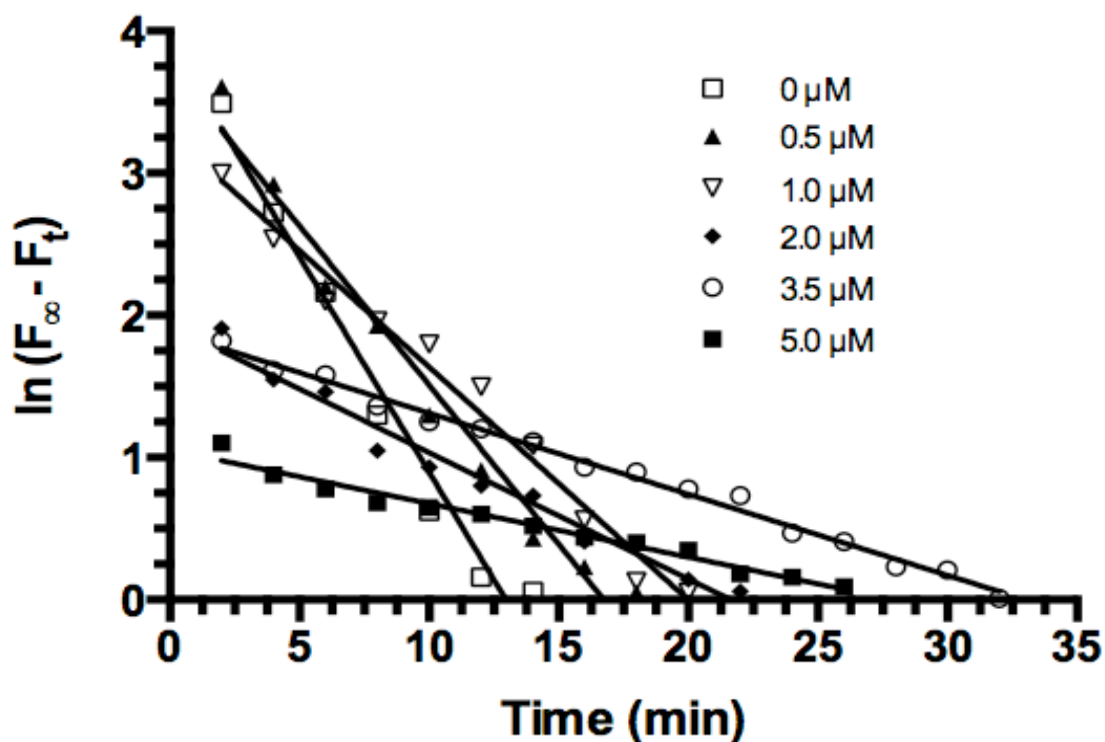


Figure 2. Plots of $\ln(F_{\infty} - F_t)$ vs. time for APV (0-5 μM). The plots were prepared using the data obtained from Figure 1. F_{∞} is the maximum fluorescence intensity (0 μM of APV) and F_t is fluorescence intensity at time t (min). Linear regression analysis yielded straight lines ($R^2 \geq 0.9711$) and the slope of each line yields the rate constant (k_{obs} , min^{-1}). k_{obs} values: $-0.3027 (\pm 0.02341)$ for 0 μM , $-0.2239 (\pm 0.01459)$ for 0.5 μM , $-0.1638 (\pm 0.007995)$ for 1.0 μM , $-0.0890 (\pm 0.004938)$ for 2.0 μM , $-0.05704 (\pm 0.00144)$ for 3.5 μM , and $-0.03766 (\pm 0.00191)$ for 5.0 μM .

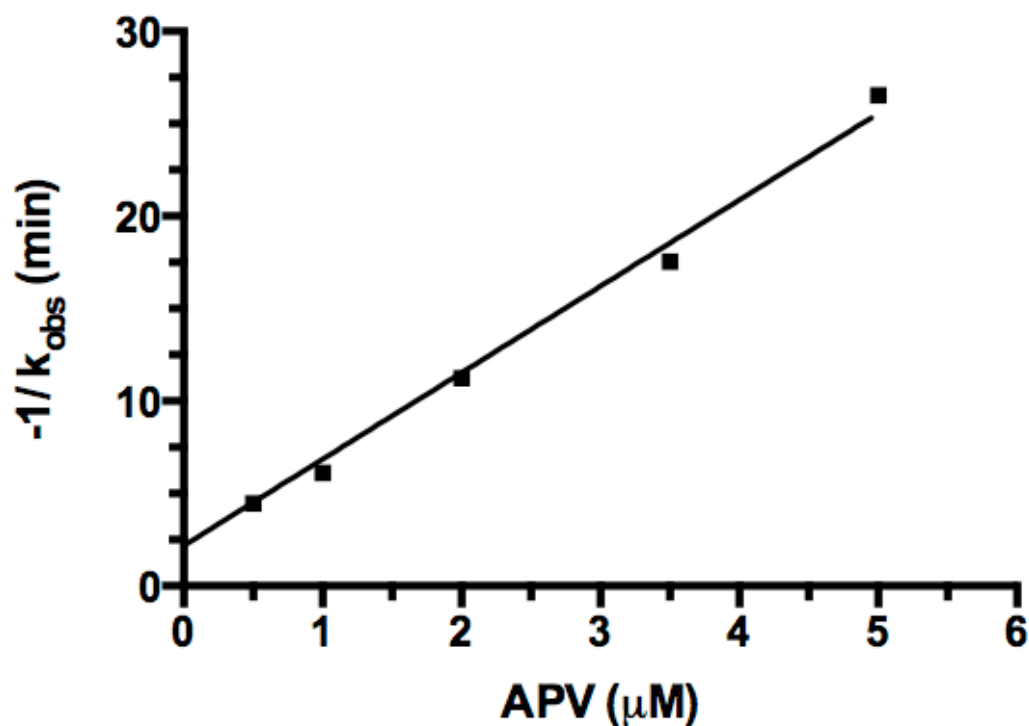


Figure 3. Plot of negative reciprocal of observed rate constant ($-1/k_{\text{obs}}$) vs. APV concentrations. The $-1/k_{\text{obs}}$ value increased with APV concentration in a linear manner ($R^2 = 0.9858$), which reflects the anti-HIV-1 PR activity of APV or an APV-PEG NC. This figure was used to derive the apparent APV concentration (APV_{app}) values for APV and each APV-PEG NC, all at $3.5 \mu\text{M}$. The APV_{app} value was used as an indicator of anti-HIV-1 PR potency to compare APV with different APV-NCs (cf. Table 1).

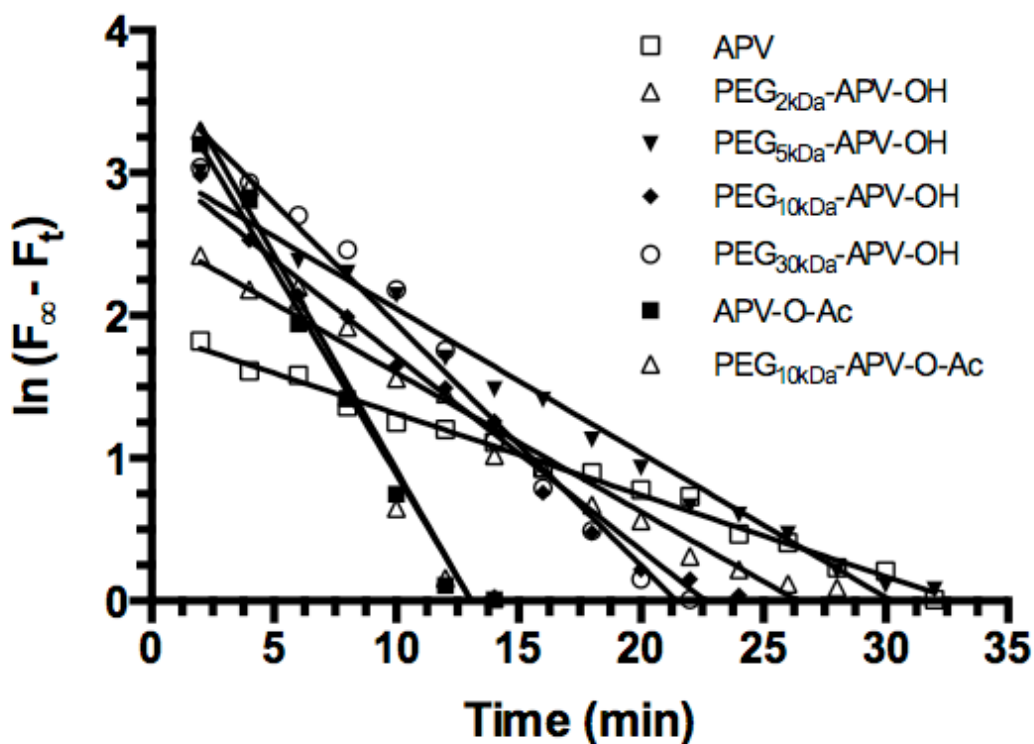


Figure 4. Plots of $\ln (F_{\infty} - F_t)$ vs. time for APV, PEG-APV NCs and the two negative controls, all at $3.5 \mu\text{M}$ APV-equivalent concentrations. Linear regression analysis yielded straight lines ($R^2 \geq 0.9655$) and the slope of each line yields the rate constant (k_{obs} , min^{-1}). The k_{obs} values are: $-0.05704 (\pm 0.001439)$ for APV, $-0.09743 (\pm 0.004131)$ for $\text{PEG}_{2\text{kDa}}\text{-APV-OH}$, $-0.1011 (\pm 0.003616)$ for $\text{PEG}_{5\text{kDa}}\text{-APV-OH}$, $-0.1358 (\pm 0.005545)$ for $\text{PEG}_{10\text{kDa}}\text{-APV-OH}$, $-0.1695 (\pm 0.008027)$ for $\text{PEG}_{30\text{kDa}}\text{-APV-OH}$, $-0.2886 (\pm 0.01815)$ for APV-O-Ac, and $-0.3013 (\pm 0.02051)$ for $\text{PEG}_{10\text{kDa}}\text{-APV-O-Ac}$. The k_{obs} values were converted to $[-1/(k_{\text{obs}} \pm \text{s.d.})]$ that were fitted into the linear regression equation derived from Fig. 3 to yield the apparent APV concentration (APV_{app}) values for APV and APV-PEG NCs. APV_{app} values (mM): $3.288 (\pm 0.095)$ for APV, $1.737 (\pm 0.093)$ for $\text{PEG}_{2\text{kDa}}\text{-APV-OH}$, $1.678 (\pm 0.109)$ for $\text{PEG}_{5\text{kDa}}\text{-APV-OH}$, $1.117 (\pm 0.064)$ for $\text{PEG}_{10\text{kDa}}\text{-APV-OH}$, $0.804 (\pm 0.060)$ for $\text{PEG}_{30\text{kDa}}\text{-APV-OH}$, $0.285 (\pm 0.047)$ for APV-O-Ac, and $0.254 (\pm 0.049)$ for $\text{PEG}_{10\text{kDa}}\text{-APV-O-Ac}$.

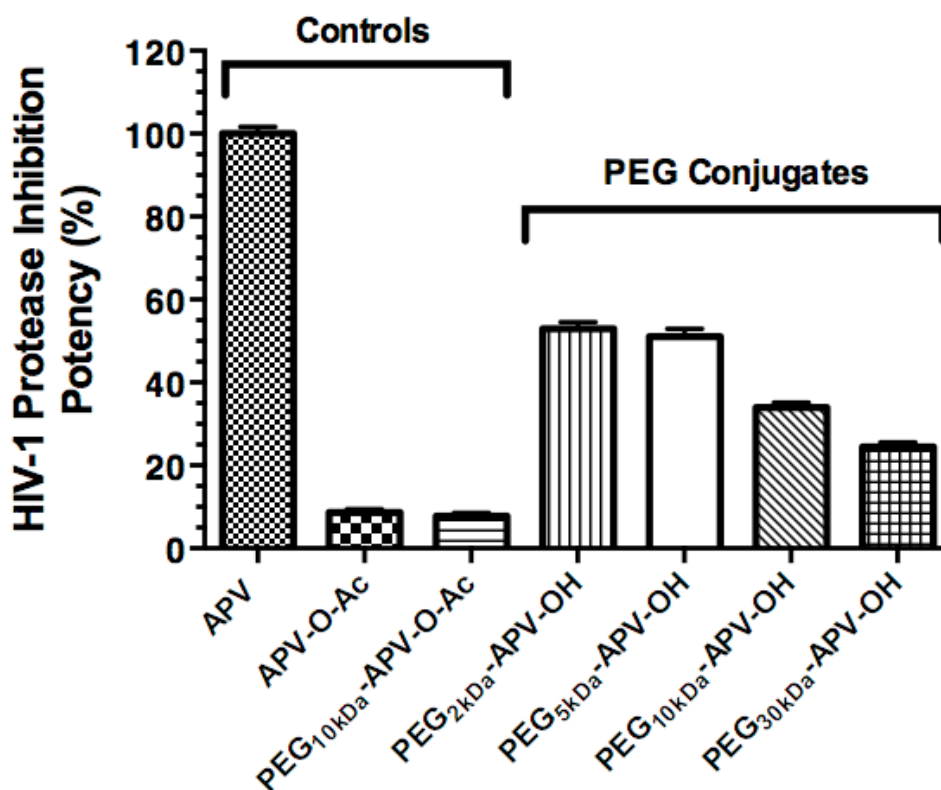


Figure 5. Effect of PEG size on the HIV-1 PR inhibition potency of APV-PEG NCs. All NCs were tested at APV-equivalent concentration of $3.5 \mu\text{M}$. The potencies expressed as the apparent APV concentrations (APV_{app}) derived from Fig. 3 and 4 were referenced to the potency of APV (the APV reference being 100% potent). One-way ANOVA analysis followed by Tukey multiple comparison test were performed. Except for the comparison between PEG_{2kDa}-APV-OH and PEG_{5kDa}-APV-OH and between the two negative controls (APV-O-Ac and PEG_{10kDa}-APV-O-Ac) ($p > 0.05$), all other pair-wise comparisons were highly statistically different ($p < 0.01$). Specifically, each NC's potency differed from that of either the positive control or either one of the two negative controls ($p < 0.01$) and the potency of PEG_{2kDa}-APV-OH/PEG_{5kDa}-APV-OH differed from either that of PEG_{10kDa}-APV-OH or that of PEG_{30kDa}-APV-OH ($p < 0.01$).

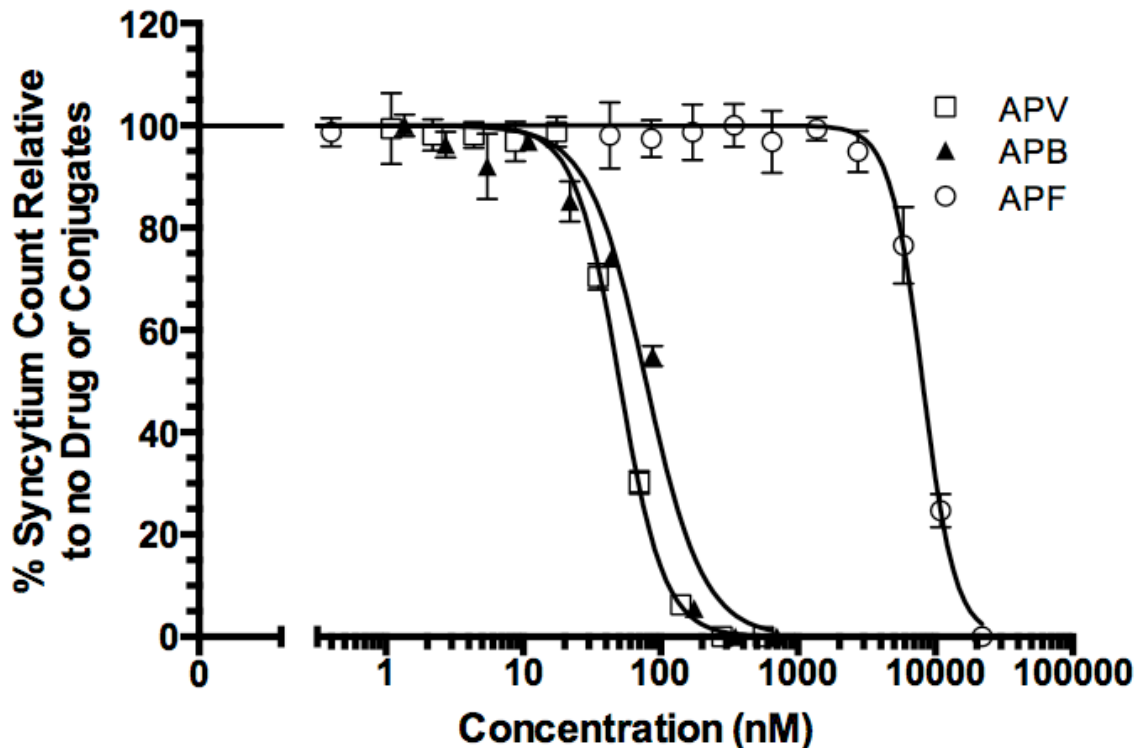


Figure 6. Anti-HIV-1 activity of APV-PEG_{3.4kDa}- Bac7 CPP (APB), APV-PEG_{3.4kDa}-FITC (APF) and free APV. The anti-HIV-1 activity was determined by the inhibition of syncytium formation in HIV-1 infected MT-2 T-cells and expressed as % of syncytium count of no treatment. Non-linear curve-fitting using the dose-response equation was used to determine the IC₅₀ values. The R² values of the curve fitting are 0.9672 for APV, 0.9067 for APF and 0.9511 for APB. APF activity (IC₅₀ = 8064 nM) was significantly lower than APV (IC₅₀ = 50.29 nM) (p<0.001). Further conjugation with Bac7 CPP (i.e., the APB NC, IC₅₀ = 78.29 nM) almost completely restored APV activity with no significant difference in IC₅₀ values (p>0.05). Data are reported as mean ± SD of three independent experiments.

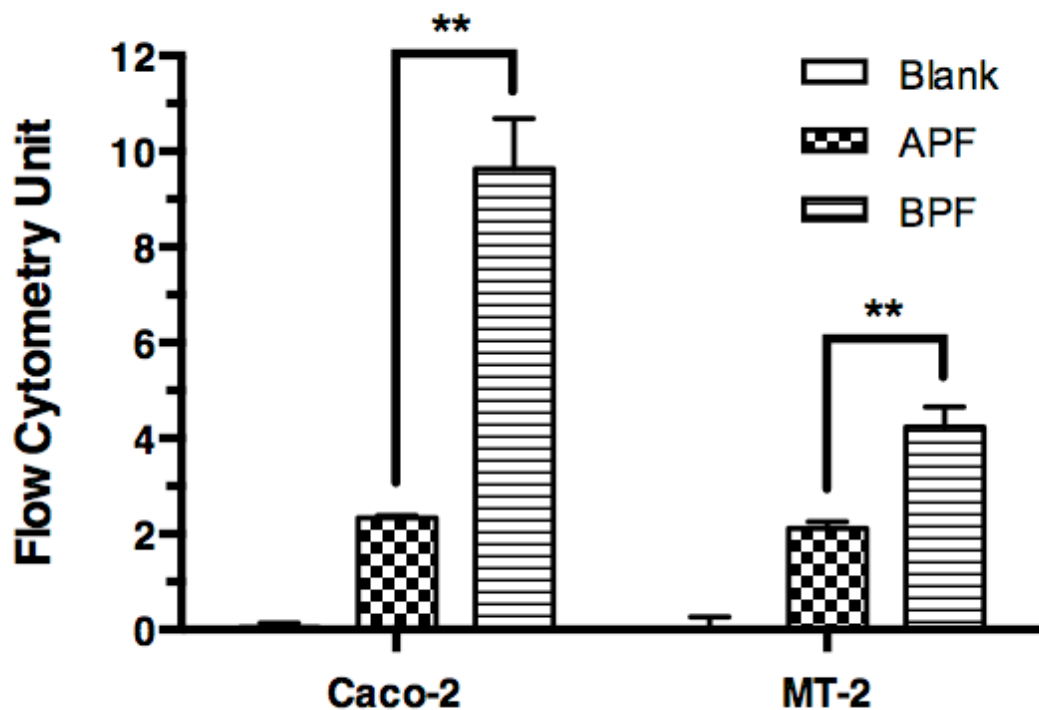


Figure 7. Total cell-associated fluorescence levels of NCs in Caco-2 and MT-2 cells as measured by flow cytometry. Caco-2 cells and MT2 cells were incubated with medium (Blank), 10 μM of APF, or 10 μM BPF for 2 h and washed before flow cytometry. The total cell-associated fluorescence levels are mean \pm s.d. of at least of two independent experiments. One-way ANOVA analysis followed by Tukey multiple comparison test were performed. The symbol “**” indicates that the fluorescence level of BPF in both cell types was significantly higher than that of APF ($p < 0.01$).

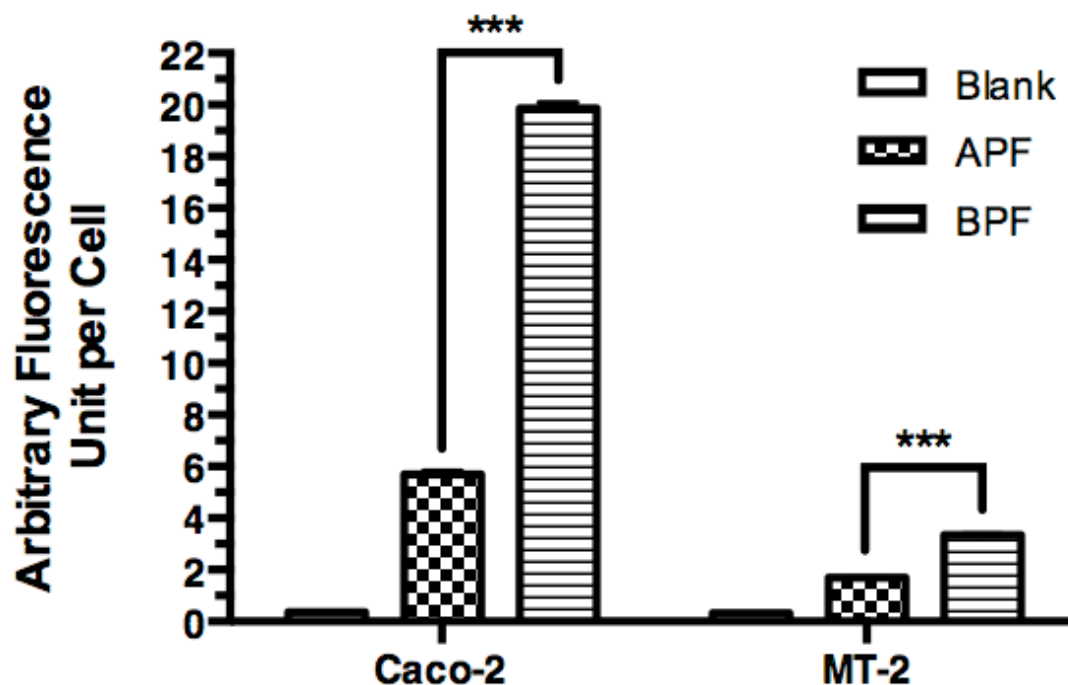


Figure 8. Intracellular levels of NCs in Caco-2 cells and MT-2 T-cells as measured by confocal microscopy. Caco-2 cells and MT-2 cells were incubated with medium (Blank), 10 μ M of APF, or 10 μ M BPF for 4 h and washed before confocal microscopy. A 40 \times objective was used for the acquisition of Z-stack of images in the XYZ mode for each treatment. Quantification of intracellular fluorescence levels used LAS AF Lite (Leica Software) on non-edited entire stacks of images (sections) that contained more than 500 cells per stack. Each value is the mean \pm s.d. of fluorescence of an entire stack of 13 to 17 sections. One-way ANOVA analysis followed by Tukey multiple comparison test were performed. The symbol *** indicates that the fluorescence level of BPF in both cell types was significantly higher than that of APF ($p < 0.0001$).

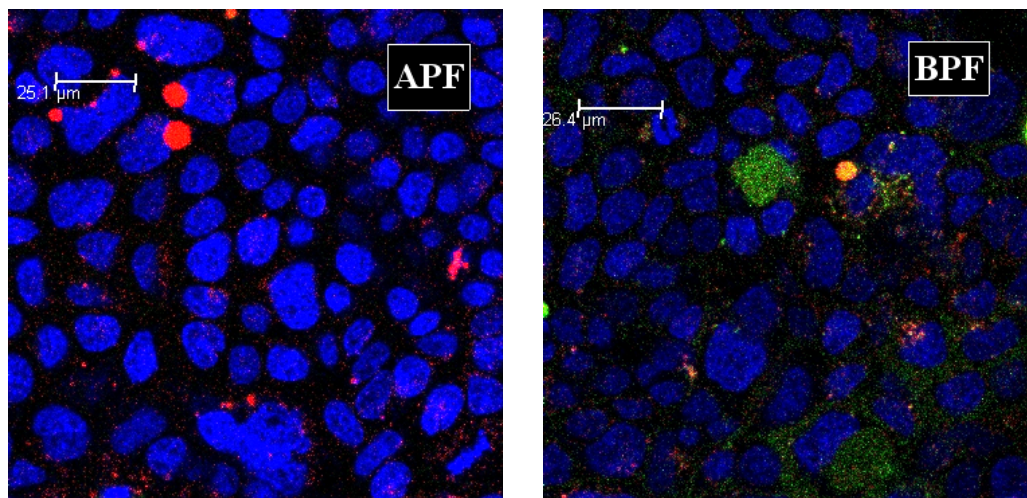


Figure 9. Confocal microscopic images of Caco-2 cells incubated with APF (left) or BPF (right) at 2.47 x magnification. Caco-2 cells three days after confluence were treated as described in Fig. 8. A middle section in a stack is shown. Each image was merged from three separate blue, green and red images of the same field. Two features are clear. The first is the sharp contrast between lack of green intracellular fluorescence in APF-treated cells (APF) and significant green intracellular fluorescence in BPF-treated cells (BPF). The second one is lack of co-localization of green and red fluorescence in the BPF image, indicating that most intracellular green fluorescence was located in the cytosol/nucleus compartment. Note in the APF image there are a few blobs of red fluorescence at the upper-left corner that are likely to be artifacts of cell debris.

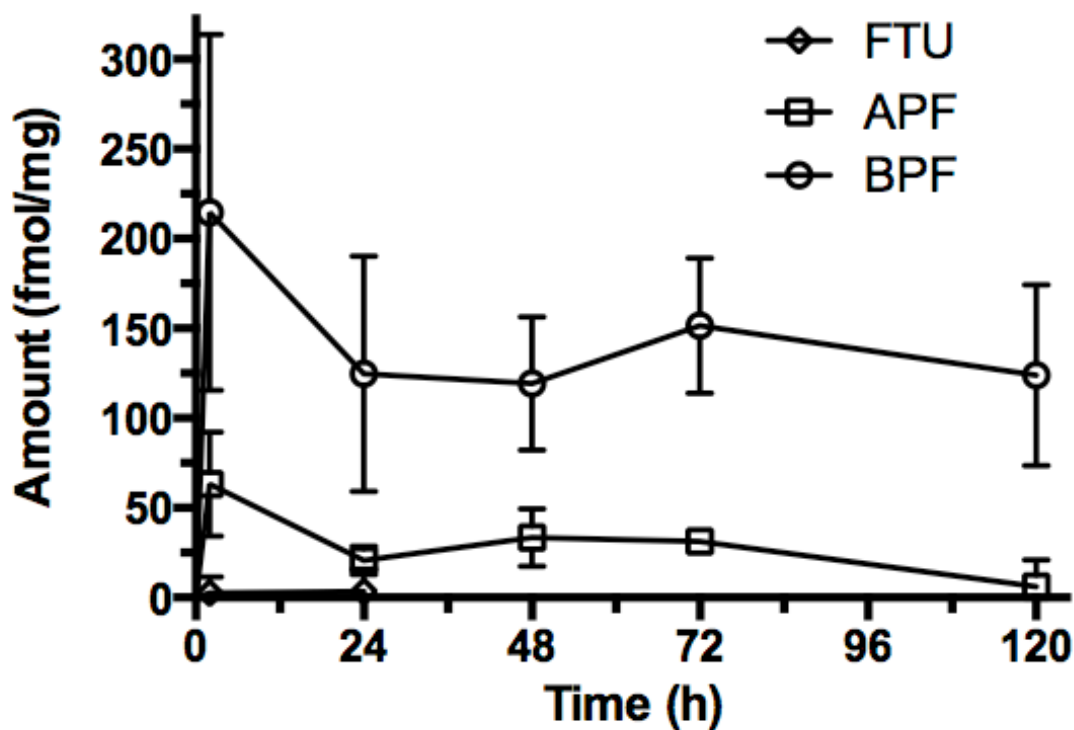


Figure 10. Retention of PEG-conjugated and Bac7 CPP-conjugated BPF in mouse colorectal mucosa. Mice treated with 200 μ l enema containing 30 μ M FTU, APF or BPF for 2h. Colorectal mucosa tissue was scrapped, homogenized, spun and the fluorescence of the supernatant was quantified, converted to fmole, normalized by mucosa tissue weight. Tissue retention was examined for up to 5 days, BPF is greater than APF at all time points (One way ANOVA $p < 0.05$, $n = 4$).

Compound^a	Mean Rate Constant* (k_{obs}, min⁻¹)	APV_{app} (μM)	HIV-1 PR Inhibition Activity (%)
Free APV (positive control)	-0.057	3.30	100
PEG _{2kDa} -APV-OH	-0.097	1.73	53
PEG _{5kDa} -APV-OH	-0.101	1.68	51
PEG _{10kDa} -APV-OH	-0.136	1.12	34
PEG _{30kDa} -APV-OH	-0.170	0.80	24
APV-O-acetyl (negative control)	-0.289	0.28	9
PEG _{10kDa} -APV-O-acetyl (negative control)	-0.301	0.25	8

Table 1. HIV-1 PR inhibition activity of APV-PEG NCs

^a All APV compounds tested in the PR inhibition assay contained 3.5 μ M APV equivalents.

*The k_{obs} in absence of any inhibitor is -0.303 min⁻¹.

S1.8. References

- [1] M. Samizadeh, X. Zhang, S. Gunaseelan, A.G. Nelson, M.S. Palombo, D.R. Myers, Y. Singh, U. Ganapathi, Z. Szekely, P.J. Sinko, Colorectal delivery and retention of PEG-Amprenavir-Bac7 nanoconjugates—proof of concept for HIV mucosal pre-exposure prophylaxis, *Drug Delivery and Translational Research* 6(1) (2015) 1-16.
- [2] W.A.F. Sheet, Fact sheet N°360. <<http://www.who.int/mediacentre/factsheets/fs360/en/>>, 2015 (accessed July 28.2015).
- [3] G. Mutua, E. Sanders, P. Mugo, O. Anzala, J.E. Haberer, D. Bangsberg, B. Barin, J.F. Rooney, D. Mark, P. Chetty, P. Fast, F.H. Priddy, Safety and adherence to intermittent pre-exposure prophylaxis (PrEP) for HIV-1 in African men who have sex with men and female sex workers, *PloS one* 7(4) (2012).
- [4] Q.A. Karim, S.S.A. Karim, J.A. Frohlich, A.C. Grobler, C. Baxter, L.E. Mansoor, A.B.M. Kharsany, S. Sibeko, K.P. Mlisana, Z. Omar, T.N. Gengiah, S. Maarschalk, N. Arulappan, M. Mlotshwa, L. Morris, D. Taylor, Effectiveness and safety of tenofovir gel, an antiretroviral microbicide, for the prevention of HIV infection in women, *Science* 329(5996) (2010) 1168-1174.
- [5] M.C. Thigpen, P.M. Kebaabetswe, L.A. Paxton, D.K. Smith, C.E. Rose, T.M. Segolodi, F.L. Henderson, S.R. Pathak, F.A. Soud, K.L. Chillag, R. Mutanhaurwa, L.I. Chirwa, M. Kasonde, D. Abebe, E. Buliva, R.J. Gvetadze, S. Johnson, T. Sukalac, V.T. Thomas, C. Hart, J.A. Johnson, C.K. Malotte, C.W. Hendrix, J.T. Brooks, Antiretroviral preexposure prophylaxis for heterosexual HIV transmission in Botswana, *The New England journal of medicine* 367(5) (2012) 423-34.
- [6] J.M. Baeten, D. Donnell, P. Ndase, N.R. Mugo, J.D. Campbell, J. Wangisi, J.W. Tappero, E.A. Bukusi, C.R. Cohen, E. Katabira, A. Ronald, E. Tumwesigye, E. Were, K.H. Fife, J. Kiarie, C. Farquhar, G. John-Stewart, A. Kacia, J. Odoyo, A. Mucunguzi, E. Nakku-Joloba, R.

- Twesigye, K. Ngure, C. Apaka, H. Tamoo, F. Gabona, A. Mujugira, D. Panteleeff, K.K. Thomas, L. Kidoguchi, M. Krows, J. Revall, S. Morrison, H. Haugen, M. Emmanuel-Ogier, L. Ondrejcek, R.W. Coombs, L. Frenkel, C. Hendrix, N.N. Bumpus, D. Bangsberg, J.E. Haberer, W.S. Stevens, J.R. Lingappa, C. Celum, Antiretroviral prophylaxis for HIV prevention in heterosexual men and women, *The New England journal of medicine* 367(5) (2012) 399-410.
- [7] X.Z. Antoinette G. Nelson, Usha Ganapathi, Zoltan Szekely, Charles W. Flexner, Andrew Owen, Patrick J. Sinko, Drug delivery strategies and systems for HIV/AIDS pre-exposure prophylaxis and treatment, *Journal of Controlled Release* 219 (2015) 669-680.
- [8] A.G. Nelson, X. Zhang, U. Ganapathi, Z. Szekely, C.W. Flexner, A. Owen, P.J. Sinko, Drug delivery strategies and systems for HIV/AIDS pre-exposure prophylaxis and treatment, *Journal of Controlled Release* 219 (2015) 669-680.
- [9] A.T. Haase, Targeting early infection to prevent HIV-1 mucosal transmission, *Nature* 464(7286) (2010) 217-223.
- [10] R.S. Veazey, A.A. Lackner, Getting to the guts of HIV pathogenesis, *The Journal of experimental medicine* 200(6) (2004) 697-700.
- [11] S. Yukl, J.K. Wong, Blood and guts and HIV: preferential HIV persistence in GI mucosa, *The Journal of infectious diseases* 197(5) (2008) 640-2.
- [12] S.S. Karim, A.D. Kashuba, L. Werner, Q.A. Karim, Drug concentrations after topical and oral antiretroviral pre-exposure prophylaxis: implications for HIV prevention in women, *Lancet* 378(9787) (2011) 279-81.
- [13] K.B. Patterson, H.A. Prince, E. Kraft, A.J. Jenkins, N.J. Shaheen, J.F. Rooney, M.S. Cohen, A.D. Kashuba, Penetration of tenofovir and emtricitabine in mucosal tissues: implications for prevention of HIV-1 transmission, *Science translational medicine* 3(112) (2011) 112re4.
- [14] J.L. Schwartz, W. Rountree, A.D. Kashuba, V. Brache, M.D. Creinin, A. Poindexter, B.P. Kearney, A multi-compartment, single and multiple dose pharmacokinetic study of the vaginal candidate microbicide 1% tenofovir gel, *PloS one* 6(10) (2011) e25974.

- [15] L.M. Ferguson, L.C. Rohan, The importance of the vaginal delivery route for antiretrovirals in HIV prevention, *Therapeutic Delivery* 2(12) (2011) 1535-1550.
- [16] C.W. Hendrix, B.A. Chen, V. Guddera, C. Hoesley, J. Justman, C. Nakabiito, R. Salata, L. Soto-Torres, K. Patterson, A.M. Minnis, S. Gandham, K. Gomez, B.A. Richardson, N.N. Bumpus, MTN-001: Randomized Pharmacokinetic Cross-Over Study Comparing Tenofovir Vaginal Gel and Oral Tablets in Vaginal Tissue and Other Compartments, *PLoS ONE* 8(1) (2013).
- [17] R. Hazra, F.M. Balis, A.N. Tullio, E. DeCarlo, C.J. Worrell, S.M. Steinberg, J.F. Flaherty, K. Yale, M. Poblenz, B.P. Kearney, L. Zhong, D.F. Coakley, S. Blanche, J.L. Bresson, J.A. Zuckerman, S.L. Zeichner, Single-Dose and Steady-State Pharmacokinetics of Tenofovir Disoproxil Fumarate in Human Immunodeficiency Virus-Infected Children, *Antimicrobial Agents and Chemotherapy* 48(1) (2004) 124-129.
- [18] A. Kolate, D. Baradia, S. Patil, I. Vhora, G. Kore, A. Misra, PEG - A versatile conjugating ligand for drugs and drug delivery systems, *Journal of Controlled Release* 192 (2014) 67-81.
- [19] A. Allen, Structure of gastrointestinal mucus glycoproteins and the viscous and gel-forming properties of mucus, *British Medical Bulletin* 34(1) (1978) 28-33.
- [20] D.A. Norris, N. Puri, P.J. Sinko, The effect of physical barriers and properties on the oral absorption of particulates, *Advanced Drug Delivery Reviews* 34(2-3) (1998) 135-154.
- [21] D.A. Norris, P.J. Sinko, Effect of size, surface charge, and hydrophobicity on the translocation of polystyrene microspheres through gastrointestinal mucin, *Journal of Applied Polymer Science* 63(11) (1997) 1481-1492.
- [22] L.M. Ensign, R. Cone, J. Hanes, Oral drug delivery with polymeric nanoparticles: The gastrointestinal mucus barriers, *Advanced Drug Delivery Reviews* 64(6) (2012) 557-570.
- [23] R.K. Willits, W.M. Saltzman, Synthetic polymers alter the structure of cervical mucus, *Biomaterials* 22(5) (2001) 445-452.

- [24] A. Silberberg, F.A. Meyer, Structure and function of mucus, *Advances in Experimental Medicine and Biology* 144 (1982) 53-74.
- [25] A. Silberberg, Meyer, F. A. , Structure and function of mucus, Plenum Press, New York, 1982.
- [26] J.D. Ramsey, N.H. Flynn, Cell-penetrating peptides transport therapeutics into cells, *Pharmacology and Therapeutics* (2015).
- [27] X. Zhang, Y. Jin, M.R. Plummer, S. Pooyan, S. Gunaseelan, P.J. Sinko, Endocytosis and membrane potential are required for HeLa cell uptake of R.I.-CKTat9, a retro-inverso tat cell penetrating peptide, *Molecular Pharmaceutics* 6(3) (2009) 836-848.
- [28] R. Brock, The uptake of arginine-rich cell-penetrating peptides: Putting the puzzle together, *Bioconjugate Chemistry* 25(5) (2014) 863-868.
- [29] S. Pujals, E. Giralt, Proline-rich, amphipathic cell-penetrating peptides, *Advanced Drug Delivery Reviews* 60(4-5) (2008) 473-484.
- [30] K. Sadler, K.D. Eom, J.L. Yang, Y. Dimitrova, J.P. Tam, Translocating proline-rich peptides from the antimicrobial peptide bactenecin 7, *Biochemistry* 41(48) (2002) 14150-14157.
- [31] M. Eissenstat, T. Guerassina, S. Gulnik, E. Afonina, A.M. Silva, D. Ludtke, H. Yokoe, B. Yu, J. Erickson, Enamino-oxindole HIV protease inhibitors, *Bioorganic and Medicinal Chemistry Letters* 22(15) (2012) 5078-5083.
- [32] G.L. Ellman, A colorimetric method for determining low concentrations of mercaptans, *Arch Biochem Biophys* 74(2) (1958) 443-50.
- [33] T. Mosmann, Rapid colorimetric assay for cellular growth and survival: Application to proliferation and cytotoxicity assays, *Journal of Immunological Methods* 65(1-2) (1983) 55-63.
- [34] E.D. Matayoshi, G.T. Wang, G.A. Krafft, J. Erickson, Novel fluorogenic substrates for assaying retroviral proteases by resonance energy transfer, *Science* 247(4945) (1990) 954-958.
- [35] P.L. Nara, W.C. Hatch, N.M. Dunlop, W.G. Robey, L.O. Arthur, M.A. Gonda, P.J. Fischinger, Simple, rapid, quantitative, syncytium-forming microassay for the detection of human

immunodeficiency virus neutralizing antibody, *AIDS Res Hum Retroviruses* 3(3) (1987) 283-302.

[36] W.R. Spreen, D.A. Margolis, J.C. Pottage, Long-acting injectable antiretrovirals for HIV treatment and prevention, *Current Opinion in HIV and AIDS* 8(6) (2013) 565-571.

[37] C. Flexner, M. Saag, The antiretroviral drug pipeline: Prospects and implications for future treatment research, *Current Opinion in HIV and AIDS* 8(6) (2013) 572-578.

[38] E. Dolgin, Long-acting HIV drugs advanced to overcome adherence challenge, *Nature medicine* 20(4) (2014) 323-324.

[39] D.R. Friend, P.F. Kiser, Assessment of topical microbicides to prevent HIV-1 transmission: Concepts, testing, lessons learned, *Antiviral Research* 99(3) (2013) 391-400.

[40] A.B. Garg, J. Nuttall, J. Romano, The future of HIV microbicides: Challenges and opportunities, *Antiviral Chemistry and Chemotherapy* 19(4) (2009) 143-150.

[41] J.M. Smith, P. Srinivasan, R.S. Teller, Y. Lo, C.T. Dinh, P.F. Kiser, B.C. Herold, Tenofovir Disoproxil Fumarate Intravaginal Ring Protects High Dose Depot Medroxyprogesterone Acetate Treated Macaques from Multiple SHIV Exposures, *Journal of Acquired Immune Deficiency Syndromes* (2014).

[42] W. Zhang, M. Hu, Y. Shi, T. Gong, C.S. Dezzutti, B. Moncla, S.G. Sarafianos, M.A. Parniak, L.C. Rohan, Vaginal Microbicide Film Combinations of Two Reverse Transcriptase Inhibitors, EFdA and CSIC, for the Prevention of HIV-1 Sexual Transmission, *Pharmaceutical Research* 32(9) (2015) 2960-2972.

[43] E.D. Deeks, Darunavir: A review of its use in the management of HIV-1 infection, *Drugs* 74(1) (2014) 99-125.

[44] D.A. Herold, K. Keil, D.E. Bruns, Oxidation of polyethylene glycols by alcohol dehydrogenase, *Biochemical Pharmacology* 38(1) (1989) 73-76.

- [45] A. Bendele, J. Seely, C. Richey, G. Sennello, G. Shopp, Short communication: Renal tubular vacuolation in animals treated with polyethylene-glycol-conjugated proteins, *Toxicological Sciences* 42(2) (1998) 152-157.
- [46] W.S. Cho, M. Cho, J. Jeong, M. Choi, H.Y. Cho, B.S. Han, S.H. Kim, H.O. Kim, Y.T. Lim, B.H. Chung, J. Jeong, Acute toxicity and pharmacokinetics of 13 nm-sized PEG-coated gold nanoparticles, *Toxicology and Applied Pharmacology* 236(1) (2009) 16-24.
- [47] R. Duncan, S.C.W. Richardson, Endocytosis and intracellular trafficking as gateways for nanomedicine delivery: Opportunities and challenges, *Molecular Pharmaceutics* 9(9) (2012) 2380-2402.
- [48] B.M. Johnson, W.N. Charman, C.J.H. Porter, An in vitro examination of the impact of polyethylene glycol 400, Pluronic P85, and vitamin E d- α -tocopheryl polyethylene glycol 1000 succinate on P-glycoprotein efflux and enterocyte-based metabolism in excised rat intestine, *AAPS PharmSci* 4(4) (2002).
- [49] Q. Shen, Y. Lin, T. Handa, M. Doi, M. Sugie, K. Wakayama, N. Okada, T. Fujita, A. Yamamoto, Modulation of intestinal P-glycoprotein function by polyethylene glycols and their derivatives by in vitro transport and in situ absorption studies, *International Journal of Pharmaceutics* 313(1-2) (2006) 49-56.
- [50] E.D. Hugger, K.L. Audus, R.T. Borchardt, Effects of poly(ethylene glycol) on efflux transporter activity in Caco-2 cell monolayers, *Journal of Pharmaceutical Sciences* 91(9) (2002) 1980-1990.
- [51] J.S. Choi, B.W. Jo, Enhanced paclitaxel bioavailability after oral administration of pegylated paclitaxel prodrug for oral delivery in rats, *International Journal of Pharmaceutics* 280(1-2) (2004) 221-227.
- [52] Y.Y. Wang, S.K. Lai, J.S. Suk, A. Pace, R. Cone, J. Hanes, Addressing the PEG mucoadhesivity paradox to engineer nanoparticles that "slip" through the human mucus barrier, *Angewandte Chemie - International Edition* 47(50) (2008) 9726-9729.

- [53] S.S. Olmsted, J.L. Padgett, A.I. Yudin, K.J. Whaley, T.R. Moench, R.A. Cone, Diffusion of macromolecules and virus-like particles in human cervical mucus, *Biophysical Journal* 81(4) (2001) 1930-1937.
- [54] F. Milletti, Cell-penetrating peptides: Classes, origin, and current landscape, *Drug Discovery Today* 17(15-16) (2012) 850-860.
- [55] A.E. Ziegler, J. Seelig, Contributions of glycosaminoglycan binding and clustering to the biological uptake of the nonamphipathic cell-penetrating peptide WR 9, *Biochemistry* 50(21) (2011) 4650-4664.
- [56] F. Salomone, F. Cardarelli, M. Di Luca, C. Boccardi, R. Nifosi, G. Bardi, L. Di Bari, M. Serresi, F. Beltram, A novel chimeric cell-penetrating peptide with membrane-disruptive properties for efficient endosomal escape, *Journal of Controlled Release* 163(3) (2012) 293-303.
- [57] A. El-Sayed, S. Futaki, H. Harashima, Delivery of macromolecules using arginine-rich cell-penetrating peptides: Ways to overcome endosomal entrapment, *AAPS Journal* 11(1) (2009) 13-22.
- [58] M. Lipkin, *Proliferation and Differentiation of Normal and Diseased Gastrointestinal Cells*, Raven Press, New York, 1987.
- [59] R.S. Veazey, A.A. Lackner, Getting to the guts of HIV pathogenesis, *Journal of Experimental Medicine* 200(6) (2004) 697-700.
- [60] S. Yukl, J.K. Wong, Blood and guts and HIV: Preferential HIV persistence in GI mucosa, *Journal of Infectious Diseases* 197(5) (2008) 640-642.
- [61] W. Zhang, *Preparation of L-nucleoside derivatives as antiviral agents*, China, 2004.
- [62] S.Z. Mingyan Zhao, *Preparation of acyclic nucleotides as antiviral agents*, China, 2007, p. 15.